

## **UC Irvine**

### **UC Irvine Electronic Theses and Dissertations**

#### **Title**

Cyclopropenones for biomolecule labeling and assembly

#### **Permalink**

<https://escholarship.org/uc/item/7rq427p7>

#### **Author**

Row, Roy David

#### **Publication Date**

2018

Peer reviewed|Thesis/dissertation

UNIVERSITY OF CALIFORNIA, IRVINE

Cyclopropenones for biomolecule labeling and assembly

DISSERTATION

submitted in partial satisfaction of the requirements for the degree of

DOCTOR OF PHILOSOPHY

in Chemistry

by

Roy David Row

Dissertation Committee:  
Professor Jennifer A. Prescher, Chair  
Professor Christopher D. Vanderwal  
Professor Gregory A. Weiss

2018

Chapter 1 © American Chemical Society  
Chapter 2 © American Chemical Society  
All other materials © 2018 Roy David Row

## **DEDICATION**

To my wife Rachel, and  
my daughters Scarlet and Violet.

## TABLE OF CONTENTS

	Page
LIST OF FIGURES	iv
LIST OF SCHEMES	vi
LIST OF TABLES	vii
ACKNOWLEDGEMENTS	viii
CURRICULUM VITAE	ix
ABSTRACT OF THE DISSERTATION	xi
CHAPTER 1: Constructing new bioorthogonal reagents and reactions	1
CHAPTER 2: Cyclopropenones for metabolic targeting and sequential bioorthogonal labeling	31
CHAPTER 3: A Cyclopropenethione-phosphine ligation for rapid bioorthogonal labeling	89
CHAPTER 4: Chemically triggered crosslinking with bioorthogonal cyclopropenones	117
APPENDIX A: NMR spectra for Chapter 2	147
APPENDIX B: NMR spectra for Chapters 3 and 4	213

## LIST OF FIGURES

	Page
Figure 1-1. Bioorthogonal chemistries react reliably and with high specificity in complex environments.	2
Figure 1-2. Popular bioorthogonal motifs found in natural products.	4
Figure 1-3. Bioorthogonal reagents come in all shapes and sizes.	6
Figure 1-4. Genetic code expansion with bioorthogonal functional groups.	8
Figure 1-5. Bioorthogonal reagents can be tuned for downstream applications.	10
Figure 1-6. Cyclopropene isomers exhibit unique reactivity profiles.	12
Figure 1-7. Mutually orthogonal reactions enable simultaneous tagging of multiple biomolecules.	13
Figure 1-8. Examples of bioorthogonal chemistries that exploit distinct reaction mechanisms.	14
Figure 1-9. The cyclopropenone-phosphine ligation.	15
Figure 2-1. The bioorthogonal chemical reporter strategy.	31
Figure 2-2. Triaryl phosphines react with cyclopropenones to form ketene-ylides.	33
Figure 2-3. Cyclopropenone LUMO energies calculated using density functional theory (DFT).	35
Figure 2-4. Kinetic experiments to analyze cyclopropenone and phosphine reactivity.	37
Figure 2-5. Reaction plots used to calculate second order rate constants between cyclopropenone <b>2.3b</b> and phosphines <b>2.11–2.13</b> and <b>2.15–2.17</b> .	39
Figure 2-6. Reaction plots used to calculate second order rate constants between cyclopropenone <b>2.8</b> and phosphines <b>2.13</b> , <b>2.14</b> , and <b>2.18</b> .	40
Figure 2-7. Phosphine <b>2.12</b> was observed to react with two equivalents of cyclopropenone <b>2.8</b> .	40
Figure 2-8. Hydrogen bonding enhances cyclopropenone reactivity.	42

Figure 2-9. Hydrogen bond activation of cyclopropenone <b>2.3b</b> was assessed by measuring rates in the presence of phenol	42
Figure 2-10. Cyclopropenones can be used for recombinant protein production.	44
Figure 2-11. Fluorescence measurements comparing incorporation of <b>2.24b</b> with PyIRS mutant G1-RS and the PyIRS-Y306T.	46
Figure 2-12. Possible base-promoted cleavage of carbamate <b>2.24b</b> .	46
Figure 2-13. ESI-MS of amber codon interrupted GFP.	47
Figure 2-14. <b>GFP-Cpo</b> can be labeled with phosphine-biotin <b>2.25</b> in a time and dose dependent manner.	48
Figure 3-1. Bioorthogonal ligations of cyclopropenones and cyclopropenethiones.	90
Figure 3-2. Cyclopropenethiones are stable to L-glutathione (GSH) at physiological pH	92
Figure 3-3. Rate comparison of compounds <b>3.2d</b> and <b>3.3d</b> .	94
Figure 3-4. Hydrogen bond activation.	97
Figure 3-5. LC-MS plots of CpS-phosphine ligations.	98
Figure 3-6. Mass spectrometry analysis of functionalized lysozyme.	99
Figure 3-7. Cyclopropenethione conjugates are readily ligated <i>in vitro</i> and in cell lysate.	100
Figure 3-8. <b>Lys-Phos</b> is stable for up to 7 days.	101
Figure 4-1. Chemically activated crosslinking with cyclopropenones.	118
Figure 4-2. Split luciferase model system.	121
Figure 4-3. LC-MS characterization of smallbit peptides <b>4.2–4.4</b> .	122
Figure 4-4. Smallbit dissociation constants.	123
Figure 4-5. Covalent crosslinking is possible through activation and subsequent trapping of cyclopropenones.	124
Figure 4-6. Crosslinking time course and mutant largebit analysis.	126
Figure 4-7. Trypsin digest of crosslinked Nluc.	127
Figure 4-8. Crosslinking is affinity-dependant.	128
Figure 4-9. Cyclopropenone-bearing lysine analog <b>4.6</b> can be genetically encoded into proteins.	129

## LIST OF SCHEMES

	Page
Scheme 2-1. Synthesis of model cyclopropenones.	34
Scheme 2-2. Synthesis of a cyclopropenone-functionalized amino acid.	43
Scheme 2-3. Sequential Cyclopropenone-Phosphine and Traceless Staudinger Ligations.	49
Scheme 3-1. Synthesis of model cyclopropenethiones.	91
Scheme 3-2. Thionoester product formation.	93
Scheme 3-3. Cyclopropenethiones exhibit faster ligation rates than analogous cyclopropenones.	94
Scheme 3-4. Phosphine <b>3.8</b> can react with more than one equivalent of <b>3.3d</b> to form multiple products.	96
Scheme 4-1. Solid-phase peptide synthesis (SPPS) of CpO-containing smallbit peptides.	122



## LIST OF TABLES

	Page
Table 2-1. Cyclopropenone stability.	36
Table 3-1. Cyclopropenethione reactivity with phosphine probes.	96
Table 4-1. Apparent $K_D$ values for largebit and peptides <b>4.2–4.4</b> .	123

## ACKNOWLEDGMENTS

I would first like to thank my research advisor, Prof. Jennifer Prescher. Working in her lab has been an amazing experience. I've learned so much from her, and wouldn't have been able to do any of this without her mentorship and guidance. Jenn has set an example that has inspired me during my entire time in the lab, and the lessons I've learned from her will stay with me throughout my career. I can't say it enough – thank you Jenn!

I would also like to thank all the members of the Prescher lab, past and present. They have been a great group to work with, and I'm grateful for all of the training, advice, editing, and great discussions that they have provided. There are several people that I'd like to thank in particular. I'm very grateful for the training, mentorship, and guidance that Hui-Wen Shih provided during my first year in the lab. She taught me the basics of synthesis, brought me up to speed on the projects, and helped me find my place in the lab. She also started the work with cyclopropenones, which set the stage for all that I have done in the lab. I would also like to thank Sean Nguyen for being a fantastic person to work with, chat with, and collaborate with on projects. Sean is an amazing scientist, and his input during research discussions has been invaluable. Sean has also been a great friend, and I will really miss him! I'd also like to thank Zi Yao for many valuable suggestions and comments that were very helpful in my projects. He has also been fun to work with, and I'll miss his special brand of humor. I also want to thank Colin Rathbun for many great conversations. They were always fun and helpful! Zach Reinert was also a great help to me, and I'm grateful for his friendship. He was always ready to lend an ear if I needed to vent, to give a second opinion on experiments, and to lighten things up with his humor. I'd like to thank Krysten Jones for training in molecular biology techniques. She was also fun to chat with, and I'm grateful for all of her input. Zane Long has been a blast to work with as well. He has been a pleasure to train and mentor, and I'm very proud of him. I'm excited to see watch his career unfold! Tyler Heiss has also been a lot of fun to work with. We've had many great discussions, and I'm excited for the new directions that he is taking with his work. Drew Ferreira has also been great to work with over the last months. We've had a lot of fun discussions and it's been exciting to have him join the bioorthogonal subgroup. I would also like to thank the other members of the Prescher lab for many great discussions, and for being a fun and friendly group of people to work with. I also want to give a special thanks to Tyler Albin, who has been a friend and colleague throughout both undergraduate and graduate school. It's been great to have someone to do spectroscopy homework with, stress about advancement with, and share (or brew) a beer with. I also want to thank Prof. John Antos for getting me involved in research as an undergraduate. He was a blast to work with, and has continued to give me valuable career advice. Prof. Ryan Mehl has also given me lots of valuable career advice and training, and he has been a great collaborator.

During my time at UCI, I have made extensive use of the facilities. This wouldn't have been possible without the hard work of Phillip Denison, Ben Katz, Felix Grun, and John Greaves. I'm grateful to them for keeping the facilities up and running, for all of the training, and for providing experimental advice. In particular, Ben Katz has spent a great deal of time helping with protein experiments. I've learned a lot from him and I'm grateful for his time and training.

Last, but far from least, I want to thank my wife Rachel and my daughters Scarlet and Violet. Without Rachel's incredible patience, hard work, and emotional support, I could never have done this. I consider any successes that I have had to be as much hers as mine, and I am forever grateful for her dedication to me and to our family throughout this period of our lives. Also, my daughters have been a continuous source of joy and inspiration during my time in graduate school. I'm very proud of them!

## CURRICULUM VITAE

### Roy David Row

#### Education and Training

---

**University of California, Irvine**, Irvine, CA 2014 – 2018  
*Ph.D.*, Chemistry

**Western Washington University**, Bellingham, WA 2012 – 2014  
*B.S.*, Biochemistry  
Graduated *cum laude* with honors in Chemistry

**Whatcom Community College**, Bellingham WA 2010 – 2011  
*A.S.*, Arts and Sciences  
Graduated with honors

#### Research Experience

---

**University of California, Irvine**, Irvine CA 2014 – 2018  
Graduate Research  
Advisor: Professor Jennifer A. Prescher

**Western Washington University**, Bellingham, WA 2013 – 2014  
Undergraduate Research  
Advisor: Professor John M. Antos

#### Honors and Awards

---

2018 Genentech Graduate Research Award  
2016 NSF GRFP Fellowship  
2015 Michael Gebel Award (UCI)  
2015 NSF GRFP Honorable Mention  
2014 Sherwood Rowland Fellowship (UCI)  
2014 Sea-Bong Chang Award for Outstanding Biochemistry Students (WWU)  
2013 Barbara-French Duzan Award (WWU)  
2013 Phillips 66 Summer Research Fellowship (WWU)

#### Publications

---

Row, R. David; Ferreira, Andrew J.; Prescher, Jennifer A. Chemically triggered crosslinking with bioorthogonal cyclopropenones, *manuscript in preparation*.

Row, R. David; Prescher, Jennifer A. A cyclopropenethione-phosphine ligation for rapid bioorthogonal labeling, *manuscript submitted*.

Row, R. David; Prescher, Jennifer A. Constructing New Bioorthogonal Reagents and Reactions, *Acc. Chem. Res.* **2018**, *51*, 1073–1081.

Nikghalb, Keyvan; Horvath, Nicholas M.; Prelesnik, Jesse; Banks, Orion; Filipov, Pavel; Row, R. David; Roark, Travis J.; Antos, John M. Expanding the Scope of Sortase-Mediated Ligations Using Sortase Homologs, *ChemBioChem*, **2018**, *19*, 185–195.

Row, R. David; Shih, Hui-Wen; Alexander, Austin T.; Mehl, Ryan A.; Prescher, Jennifer A. Cyclopropenones For Metabolic Targeting and Sequential Bioorthogonal Labeling, *J. Am. Chem. Soc.* **2017**, *139*, 7370–7375.

Row, R. David; Prescher, Jennifer A. Tetrazine Marks the Spot. *ACS Cent. Sci.* **2016**, *2*, 493–494.

Row, R. David; Roark, Travis J.; Philip, Marina C.; Perkins, Lorena L.; Antos, John M. Enhancing the Efficiency of Sortase-Mediated Ligations Through Nickel-Peptide Complex Formation. *Chem. Comm.* **2015**, *51*, 12548–12551.

## Presentations

---

### Poster Presentations:

*Bioorthogonal cyclopropenones for site-specific targeting of intracellular proteins* 2017  
Gordon Research Conference (GRC):  
High Throughput Chemistry & Chemical Biology, Andover NH

*Cyclopropenones are stable bioorthogonal chemical reporters* 2016  
National Meeting of the American Chemical Society (ACS), San Diego CA

### Oral Presentations:

*Cyclopropenones for bioorthogonal labeling and assembly* 2018  
ACS Division of Organic Chemistry Graduate Research Symposium  
Indiana University, Bloomington IN

*Cyclopropenones for bioorthogonal labeling and assembly* 2018  
Genentech Graduate Student Symposium, San Francisco CA

*Stable cyclopropenones for bioorthogonal labeling* 2017  
Graduate Symposium, UCI, Irvine CA

*Cyclopropenones for intracellular tagging and dual bioorthogonal labeling* 2017  
Vertex Day, UCI Dept. of Pharm. Sci., Irvine CA

*Blocking the reversibility of sortase-mediated transpeptidation* 2014  
WWU Chemistry Department Honors Seminar, Bellingham WA

# ABSTRACT OF THE DISSERTATION

Cyclopropenones for biomolecule labeling and assembly

By

Roy David Row

Doctor of Philosophy in Chemistry

University of California, Irvine, 2018

Professor Jennifer A. Prescher, Chair

Bioorthogonal chemistries are widely used to image and profile biomolecules in their native environments. While many bioorthogonal reactions have been reported in recent years, most cannot be used inside cells owing to reagent instabilities. Additionally, there are few reactions that can be used concurrently for multi-component labeling. Many of the most popular bioorthogonal reagents exhibit significant cross-reactivities. To address these limitations, I developed new classes of bioorthogonal reagents, including cyclopropenones, cyclopropenethiones, and functionalized phosphines.

In Chapter 1, I introduce the overall strategy involved in designing and optimizing new bioorthogonal reagents. I also highlight some of the current needs in bioorthogonal reactivity and recent advances that have been made in these areas. In Chapter 2, I describe the optimization of bioorthogonal cyclopropenones for use in intracellular environments. I synthesized a panel of disubstituted cyclopropenones and identified scaffolds that are inert to thiols and other biological nucleophiles. These substituted

cyclopropenones react efficiently with a wide array of functionalized phosphines to form covalent adducts. I further developed cyclopropenone amino acids that can be used for recombinant protein production and labeling applications. Chapter 3 showcases the investigation of cyclopropenethiones as more rapidly reacting heteroanalogs of cyclopropenones. Cyclopropenethione-phosphine ligations proceed at markedly improved rates, and cyclopropenethiones are suitable for use in complex biological environments. Finally, in Chapter 4, I discuss the use of cyclopropenones as chemically activatable protein crosslinkers. Using a model split protein system, I demonstrated that cyclopropenones can serve as electrophilic traps to form covalent adducts between interacting biomolecules.

Overall, this thesis describes the optimization of cyclopropenones, cyclopropenethiones, and phosphines for use in biological environments. The stability and highly tunable nature of these reagents make them useful for a wide range of applications, including protein conjugation, cellular imaging, and biomolecule trapping. The unique reactivity of these reagents also presents new opportunities for multicomponent labeling. Based on their biocompatibility and versatility, I anticipate that the cyclopropenone and cyclopropenethione will be broadly adopted for applications in cells and living systems.

# Chapter 1: Constructing new bioorthogonal reagents and reactions

Adapted from published work: Row, R. D.; Prescher, J. A. *Acc. Chem. Res.* **2018**, *51*, 1073–1081.

## 1.1 Introduction

Over the past 20 years, bioorthogonal chemistries have become a mainstay of chemical biology. These transformations are routinely used to target individual biomolecules with imaging agents or other probes, even in live cells and organisms. Key to their success are functional groups that react reliably and selectively in complex settings (Figure 1-1). Considering the breadth of functionality present in cells and tissues, the demands on bioorthogonal reactions are enormous [1, 2]. The reagents must tolerate aqueous environments and large concentrations of cellular nucleophiles. While remaining inert to their surroundings, the functional groups must also react robustly with one another to provide stable adducts. Despite these stringent criteria, transformations have been identified that are well recognized as being bioorthogonal. Many have been used for decades to tag proteins and other biomolecules [3], profile active enzymes [4, 5], and identify drug targets [6, 7]. More recent advances in bioorthogonal reactions are enabling new pursuits in drug delivery [8, 9], genetic code expansion [10, 11], and protein activation [12-16].

Even with its impressive résumé, the field of bioorthogonal chemistry is not without limitation. Few reagents can be used in the harshest cellular confines and in conjunction with the smallest biomolecules [17]. Furthermore, many of the most popular bioorthogonal reagents cross-react with one another and thus cannot be employed concurrently [18]. These and other drawbacks continue to inspire new explorations for

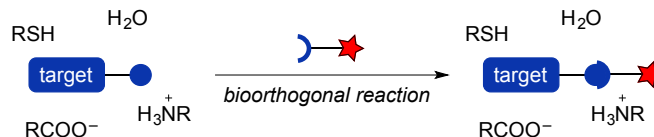


**Figure 1-1.** Bioorthogonal chemistries comprise reagents (blue circle and arc) that react reliably and with high specificity in complex environments. These reactions enable target biomolecules to be covalently ligated with fluorophores, affinity tags, or other probes (red star).

chemistries with potential biological utility. The Prescher lab has focused on constructing reagents that are small in size, highly stable, and tunable – features that can facilitate their widespread adoption. This chapter highlights the development of three recent bioorthogonal functional groups: cyclopropenes, triazines, and cyclopropenones. These motifs can also be used together in live cells, enabling multicomponent imaging and other multiplexed analyses. The work is presented against a backdrop of design considerations for new bioorthogonal reactions. These principles can guide the continued pursuit of useful chemistries.

How many bioorthogonal reactions are ultimately necessary? A strong case for hundreds can be made, based on analogy to other classes of synthetic organic transformations. Dozens of distinct methods exist to construct amides and other key bonds, each having its pros and cons. The approach selected is dictated by the individual experiment. Similar parallels exist in bioorthogonal chemistry. Each transformation has its strengths and weaknesses, with no single reaction type being suitable for all applications. In some cases, the fastest-reacting probes are necessary; in others, slower, but more selective reagents should be employed. Some reagents exhibit background reactivities with cellular nucleophiles and other instabilities, hindering *in vivo* applications. Such liabilities can often be mitigated via steric and



electronic tuning, and dozens of examples exist among the major classes of bioorthogonal ligations. The time invested to fine-tune and optimize bioorthogonal scaffolds is often critical to their long-term success. Thus, it is important to appreciate the bioorthogonal “workbench” just as much as the tools in the toolbox.

## 1.2 Laying the foundation

At the outset of new reaction development, it is important to tackle a fundamental question: what does it mean to be bioorthogonal? Quite literally, bioorthogonal reagents and transformations are orthogonal to (i.e., independent of) biology. Thus, in the strictest sense, the functional groups must not be present in living systems. This type of “bioorthogonality” is rarely (if ever) achieved, as many of the classic motifs have precedence in microbial natural products and other metabolites. “Bioorthogonal”, in practice, tends to be more loosely applied to reagents that *minimally interfere* with the system under study. Even with this broader definition, perfect compatibility can be difficult to achieve. Nearly all bioorthogonal reagents have liabilities in certain cellular environments [1]. Such drawbacks do not necessarily lessen the impact of a given probe, but can provide motivation to optimize and develop new reactions that address the inherent shortcomings.

Our work to build better bioorthogonal reactions (via the latter definition) has often been inspired by nature. The diversity of chemical functionality present in natural products and other metabolites is immense (Figure 1-2). Many of the motifs are not found in higher eukaryotes, making them “bioorthogonal” in a heterologous context. The groups also possess some degree of stability in cellular environments, owing to their

presence in living systems. Thus, they can be ideal starting points for new reaction development and eventual translation *in vivo*. One of the best examples of a naturally occurring bioorthogonal functional group is the terminal alkyne [19, 20]. Alkynes comprise numerous small molecule metabolites (often as part of diyne or poly-yne scaffolds) in sponges and other organisms. The stability and unique reactivities of this functional group have rendered it one of the most widely used labels in all of bioorthogonal chemistry.

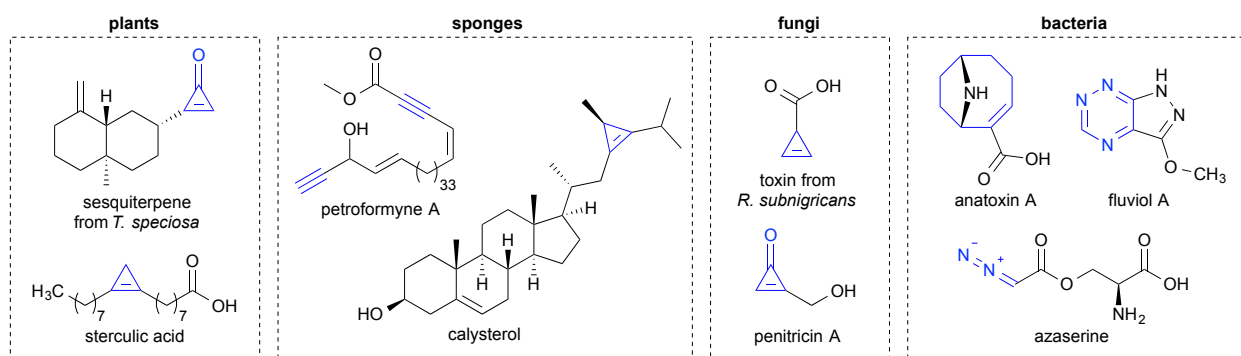


**Figure 1-2.** Many popular bioorthogonal motifs (blue) are found in natural products. The functional groups highlighted here have been repurposed for selective tagging reactions in heterologous environments.

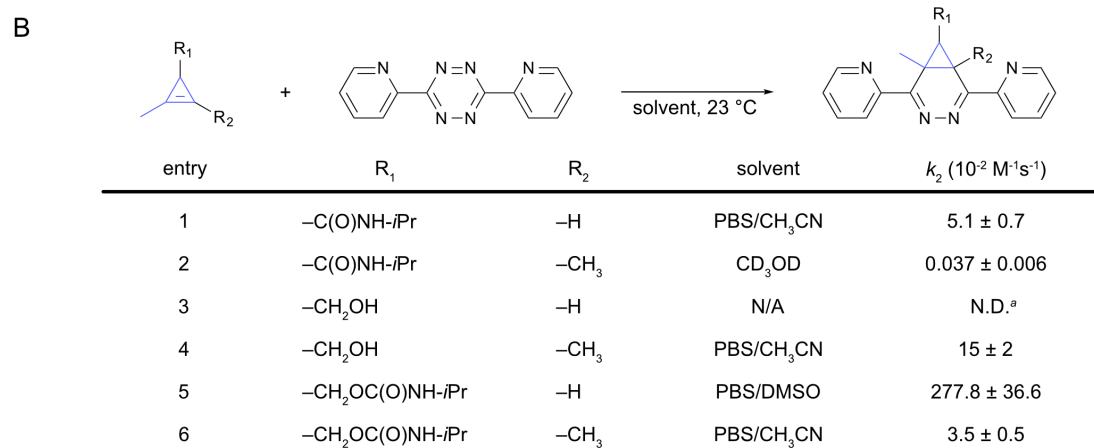
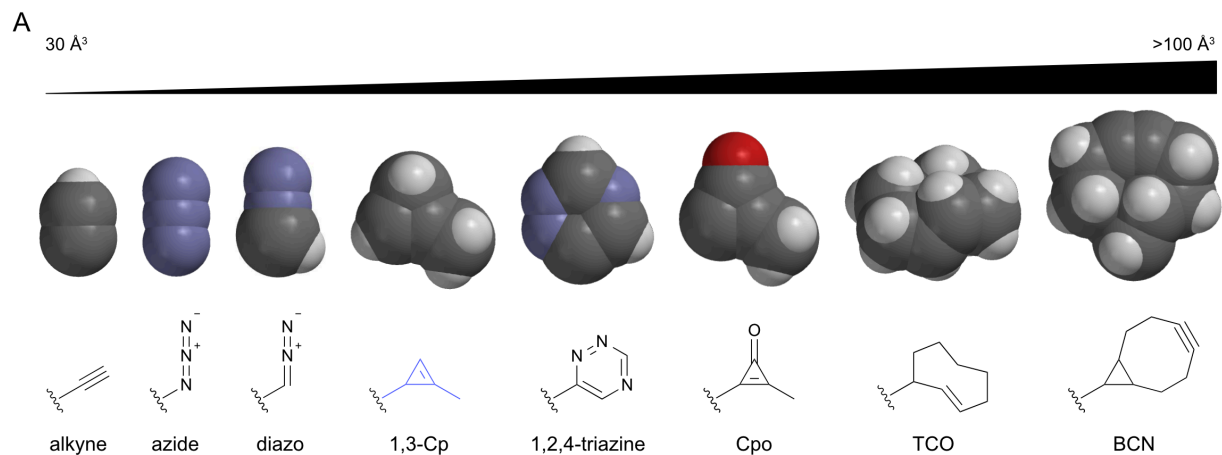
Our group took additional cues from nature in developing selective chemistries with cyclopropenes [21-26], triazines [27-29], and cyclopropenones [30-33]. All three motifs are found in natural product structures, suggesting that they were suitable starting points for probe development. Indeed, the native scaffolds inspired our initial choices of model scaffolds to prepare. Further optimization to tune stabilities and reactivities was guided by physical organic chemistry principles and computation

(described below). It is anticipated that continued mining of natural product structures will uncover new functionality and reaction platforms to pursue.

### **1.3 Filling the voids**

Many applications of bioorthogonal chemistry involve profiling or visualizing small targets, including metabolites and drugs. In these cases, there is a clear need for functional groups that minimally perturb the systems under study. Even with proteins and larger targets, it is often desirable to use small tags to preserve native functions and interactions. When steric considerations are important, the azide and terminal alkyne have long dominated as the bioorthogonal reagents of choice (Figure 1-3). Comprising just a few atoms, these groups have been ubiquitously employed in chemical biology. Both are well tolerated in biological systems and can be readily detected via copper-catalyzed azide–alkyne cycloaddition (CuAAC) [34]. The azide and alkyne are also quite “user friendly”. Many popular azido- and alkynyl-functionalized probes are commercially available or otherwise easily constructed. Consequently, they have found widespread application in bioconjugation, materials chemistry, drug discovery, and many other areas [34]. Limitations of CuAAC in cellular environments also drove numerous efforts to improve the scope and biocompatibility of azide–alkyne cycloadditions [34, 35].

Inspired by the versatility of small and stable reagents, the Prescher lab set its sights initially on cyclopropenes as candidate bioorthogonal reagents. As noted earlier, cyclopropenes are found in some natural products, suggesting compatibility with living systems. While slightly larger than both azides and alkynes, cyclopropenes are the



<sup>a</sup>Rates not measured due to cyclopropene instability

**Figure 1-3.** Bioorthogonal reagents come in all shapes and sizes. (A) Sample probes are shown, arranged by approximate size. Volumes were estimated using atomic radii measurements in Spartan. (B) Cyclopropenes can be tuned for reaction with tetrazines. Minimally substituted cyclopropenes exhibit the fastest rates.

smallest of the isolable strained alkenes. This class of reactants includes the venerable *trans*-cyclooctene (TCO), a motif that has emerged as a powerful and versatile addition to the bioorthogonal toolkit. Strained alkenes react with tetrazines via inverse electron-demand Diels–Alder (IED-DA) reactions, exhibiting remarkably fast kinetics [36-39]. The TCO–tetrazine ligation is unrivaled in its reaction speed. Such rapid reactivity has enabled applications in rodent models and other large organisms – settings where only minimal reaction times and reagent concentrations are tolerated.

While TCO is routinely used for IED-DA reactions, it is roughly double the size of a standard cyclopropene (Figure 1-3A), making it less attractive for some applications. The Prescher lab was motivated to examine the utility of the smaller strained alkene for bioorthogonal labeling. In early work, David Patterson synthesized a small panel of substituted cyclopropenes (Figure 1-3B) [21]. Methyl-substituted scaffolds were found to be stable in a variety of biological environments, even in the presence of common nucleophiles. The reactivities of the probes with various tetrazines were also measured, and the fastest reactions were observed with the least sterically congested cyclopropenes. Complementary studies were performed by the Devaraj group [40, 41]. Rapid reactions were also observed in more polar solvents and with cyclopropenes having reduced electron-withdrawing character at C-3, consistent with the inverse electron-demand of the cycloaddition.

Cyclopropene–tetrazine reaction rates are markedly slower than the corresponding ligations with TCO. Nonetheless, the reaction has been applied in numerous biomolecule tagging experiments, including protein and nucleic acid

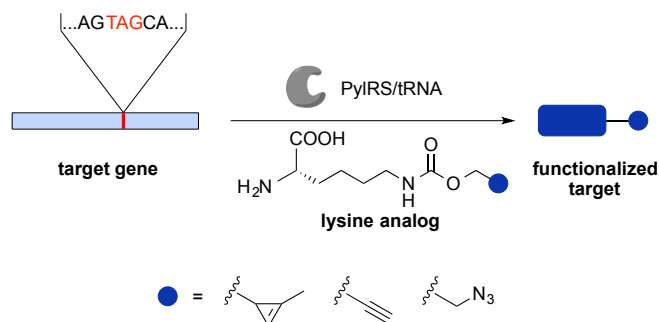


**Figure 1-4.** Genetic code expansion with bioorthogonal functional groups. Using an orthogonal AARS/tRNA pair, ncAAs can be site-specifically incorporated into proteins of interest. A variety of small bioorthogonal motifs (including cyclopropenes) have been installed via the pyrrolysine synthetase (PyIRS) machinery.

visualization [42-45], cell surface labeling [46, 47], and *in vivo* proteomics [48, 49]. Importantly, the small size of the cyclopropene has enabled experiments that would be difficult to achieve with larger motifs. One poignant example includes metabolic targeting of cellular glycans with functionalized monosaccharides. The enzymes involved in glycan biosyntheses can be quite stringent, allowing only minimally perturbed scaffolds to be processed. The fact that cyclopropene sugars were metabolized on par with analogous azido substrates is a testament to the potential broad utility of the new bioorthogonal reagent [21, 46, 50].

The small size of the cyclopropenes has also been a boon to genetic code expansion efforts. This powerful technology enables noncanonical amino acids (ncAAs) to be site-specifically installed into target proteins in response to a stop codon (Figure 1-4) [3]. The key step involves an orthogonal aminoacyl-tRNA synthetase (AARS) that charges the ncAA onto a cognate tRNA. The tRNA is similarly orthogonal to the cell's endogenous machinery. To identify an appropriate AARS/tRNA pair, large libraries of

mutants must typically be screened and extensive optimization for use in mammalian cells must be performed [51, 52]. Interestingly, ncAAs bearing cyclopropene motifs can be efficiently processed by a native pyrrolysine AARS from archaeobacteria, without the need for additional mutagenesis [48, 53, 54]. This feature has enabled cyclopropenes to be immediately applied in a variety of contexts, including cell-specific proteome labeling in flies and mouse brain tissue [48, 55]. More recent work has capitalized on cyclopropene ncAAs for dual protein labeling experiments [56, 57].

#### 1.4 Hammering out the details

Understanding the stability and reactivity profiles of bioorthogonal reagents is critical to their successful application *in vitro*, in cells, and *in vivo*. Such analyses are often aided by detailed investigations of reaction mechanism and substituent effects. Ideally, these studies provide insight on how to tune scaffolds for desired reaction speeds, biocompatibilities, or other parameters. In our work, a deep dive into reaction mechanism has been best exemplified in studies of the other half of the IED-DA reaction: the electron-deficient diene. To date, tetrazines have dominated in this role. Tetrazines react robustly with cyclopropenes, TCO, and a variety of other strained dienophiles. Like other families of bioorthogonal reagents, tetrazines have been tuned to achieve desired levels of reactivity (Figure 1-5). Electron-withdrawing substituents at the 3 or 6 positions lower tetrazine LUMO energies and increase reaction rates [58]. Steric effects can also play a role in tetrazine reactivity, with less encumbered scaffolds displaying the fastest rates. Improvements in speed, though, often come at the expense

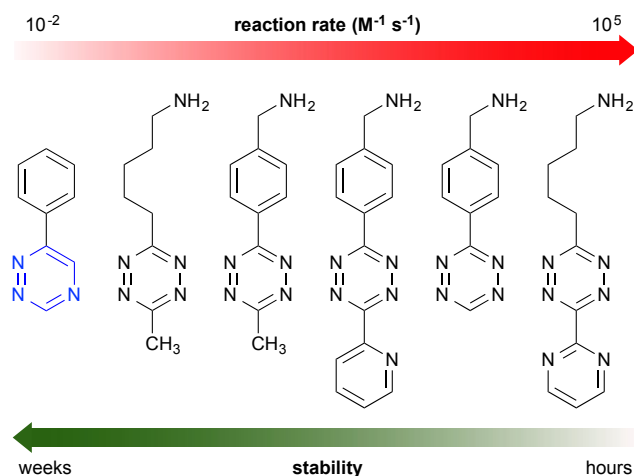


**Figure 1-5.** Bioorthogonal reagents can be tuned for downstream applications. A panel of tetrazine and triazine motifs have been developed that exhibit a wide range of stabilities and reactivities.

of stability. For many applications, this is a fair trade, but for others it is desirable to minimize background labeling.

The need for additional tuning inspired a search for new dienes. To this end, the Prescher lab was drawn to triazine scaffolds. 1,2,4-Triazines have been identified in microbial natural products and pigments, suggesting that they are stable in physiological environments. Density functional theory (DFT) calculations performed by the Houk group [27] further suggested that 1,2,4-triazines would exhibit enhanced stability relative to tetrazines yet retain reactivity with TCO (Figure 1-5). Based on these observations, it was hypothesized that triazines would be good candidates for bioorthogonal reaction development. David Kamber synthesized a small panel of triazine probes and found them to be highly stable in aqueous conditions and to cellular thiols. Importantly, they were still reactive with dienophiles such as TCO and some strained alkynes [27, 59]. Because triazines require fewer substituents than analogous tetrazines for long-term



stability, they can leave a smaller footprint. These features were capitalized on to showcase the utility of triazines for recombinant protein production [27]. The long incubation times required in this process are not compatible with many tetrazines and other bioorthogonal scaffolds. Triazines have also found recent application in labeling nucleic acids [60], and further tuning has identified fluorogenic analogs [61].

The increase in stability gained with triazines comes at the expense of decreased reaction rates. Modifications to the triazine core (e.g., electron-withdrawing substituents) can recover some reactivity, and even small modifications were found to have dramatic impacts [27]. Further calculations predicted that 1,2,4-triazines would be nonreactive with other strained alkenes, including cyclopropenes and norbornene. These results were verified experimentally and set the stage for mutually orthogonal reaction development [27, 62].

Mechanistic studies and computational analyses further enabled efficient reagent tuning in the case of the cyclopropenes. Initial investigations revealed that cyclopropene–tetrazine reactions occur from the least hindered face of the cyclopropene. The adducts can undergo additional rearrangements to produce mixtures of diastereomers [21]. Computational analyses predicted that the addition of a single methyl group at C-3 would be sufficient to impede tetrazine reactivity (Figure 1-6A) [63]. The methyl substituent was predicted to engender a steric clash that could control cycloaddition preference. Indeed, 3,3-disubstituted cyclopropenes (**3,3-Cp**) were refractory to tetrazine ligation, while their 1,3-disubstituted counterparts (**1,3-Cp**) reacted robustly. Both scaffolds were readily ligated with less sterically encumbered 1,3-dipoles (e.g., nitrile imines). The unique reactivity profiles of the isomeric cyclopropenes

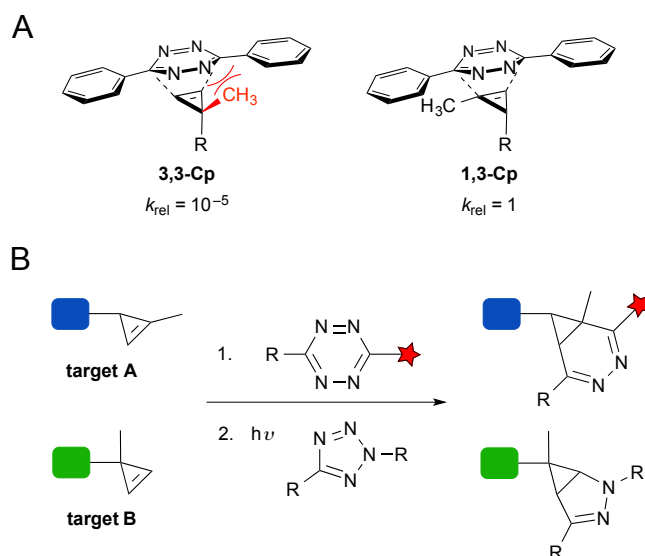


**Figure 1-6.** Cyclopropene isomers exhibit unique reactivity profiles. (A) Predicted transition states indicated a steric clash in the reaction of a 3,3-disubstituted cyclopropene (**3,3-Cp**) with 3,6-diphenyltetrazine [63]. The unfavorable interaction was predicted to markedly diminish the reaction rate compared to the 1,3-disubstituted isomer (**1,3-Cp**). (B) The unique reactivities of **1,3-Cp** and **3,3-Cp** enabled tandem labeling of distinct biomolecules.

enabled tandem labeling of biomolecules in a single pot (Figure 1-6B). Recent work by the Lin group has uncovered a more strained 3,3-disubstituted cyclopropene that can be effectively ligated with tetrazines, suggesting that even more finely tuned reagent pairs will be uncovered [53].

### 1.5 Thinking outside the (tool)box

As the number of bioorthogonal tools continues to expand, their application to multicomponent labeling becomes feasible. Such studies require reactions that are not only bioorthogonal but also *orthogonal to one another*. The challenges in this context are immense, considering the number of potential side products (Figure 1-7).

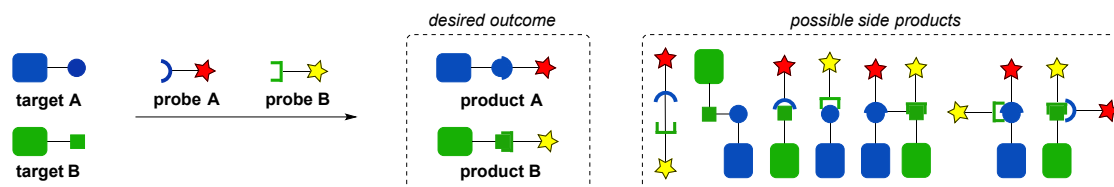


**Figure 1-7.** Mutually orthogonal reactions enable simultaneous tagging of multiple biomolecules. The reagents and products in such transformations must exhibit no off-target or cross-reactivities. Even in the simplest case (two targets, A and B) the number of undesirable reactions that must be avoided is large.

Additionally, most bioorthogonal reactions, and nearly all reported in recent years, comprise cycloadditions [1]. Many of the underlying reagents are incompatible with one another and cannot be used concurrently [18, 64]. In some cases, differences in rate can be exploited for sequential labeling. However, such strategies often require the removal of excess reagents from the first reaction, before the second can be initiated. Our initial work with isomeric cyclopropenes [63] (described above) enabled tandem labeling, but only with sequential reagent addition.

A potentially more general approach to developing mutually orthogonal reactions involves focusing on transformations that operate via distinct mechanisms (Figure 1-8). In early work, our lab showed that the cyclopropene–tetrazine ligation is compatible with azide–alkyne cycloadditions. These reactions were used to simultaneously tag cell surface glycans for downstream imaging applications [46]. The compatible ligations have also enabled concurrent labeling of multiple bacterial targets [65]. In recent years, additional orthogonal reactions have been reported that promise to bolster multiparameter imaging and other applications [18, 62, 66-69].

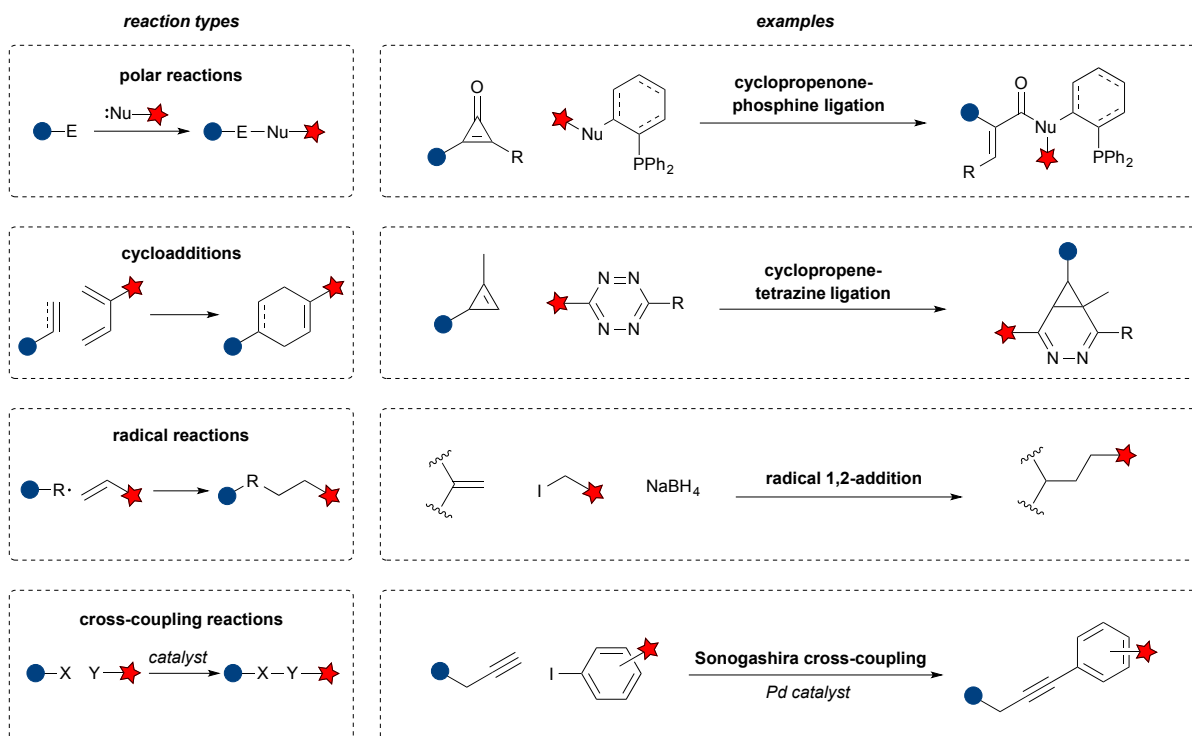


**Figure 1-8.** Examples of bioorthogonal chemistries that exploit distinct reaction mechanisms.

Our lab has also begun examining polar reactions – chemistries that are likely compatible with existing bioorthogonal ligations based on their unique mechanisms. In one area, we have been exploring the reaction between cyclopropenones and bioorthogonal phosphines [30, 70]. Monosubstituted cyclopropenones are found in some natural products (Figure 1-2), suggesting that they are suitable candidates for biocompatible reaction development [31, 33]. We synthesized a panel of cyclopropenones and analyzed their stabilities in aqueous solution and in the presence of cellular nucleophiles [70]. The most stable scaffolds were structurally similar to bioorthogonal cyclopropenes, yet exhibited unique manifolds of reactivity.

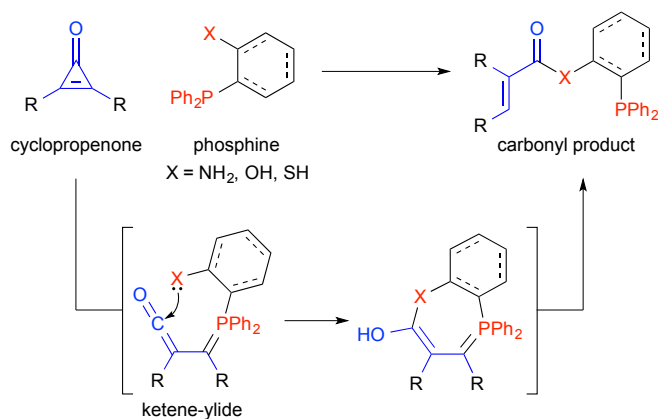


**Figure 1-9.** The cyclopropenone–phosphine ligation. Cyclopropenones react with phosphines to generate ketene–ylide intermediates. The ketenes are subject to intramolecular trapping by pendant nucleophiles. Subsequent protonation and elimination steps provide carbonyl products.

Cyclopropenones react with phosphines to generate ketene–ylides; these intermediates can be trapped by pendant nucleophiles on the phosphine probe (Figure 1-9). We demonstrated that the ligation can be performed on model proteins *in vitro* and in cell lysate. The cyclopropenone–phosphine reaction also holds promise for multicomponent labeling, as the reagents are not expected to interfere in common bioorthogonal cycloadditions. Indeed, preliminary work in our lab has shown that cyclopropenones and phosphines are compatible with tetrazines, cyclopropenes, and TCO.

Ongoing work in the field has also revealed new platforms for “orthogonal bioorthogonal” labeling. Davis and others have demonstrated that radical reactions can be employed for bioconjugation reactions [71, 72]. Other transformations that are garnering attention include metal-catalyzed ligations [73-76] and bioorthogonal cleavage reactions [12]. It should also be noted that many bioorthogonal chemistries can be

triggered with light or other exogenous stimuli, enabling spatiotemporal control of reactivity [45, 77].

## **1.6 Paving the way for new discoveries**

The application of bioorthogonal reactions to diverse problems has not only revealed new and often unanticipated discoveries but also driven the development of new tools and synthetic methods [78]. For example, bioorthogonal transformations have been used to expediently prepare diverse libraries of complex molecules [79]. Mild methods to affix azides and other bioorthogonal motifs to complex drugs and natural products have also been reported [80, 81]. Systematic efforts to tune and optimize biocompatible reactions will continue to provide probes with novel capabilities; these tools, in turn, will spur new advances. This iterative cycle of tool development and discovery will expand as the field grows. We are still in the midst of establishing a fleet of sensitive, selective reagents that will bolster chemistries in living systems and thus enable new research directions.

As the number of bioorthogonal reagents and their spectrum of reactivities grows, new challenges are emerging. The sheer number of possible reagents and conditions can be daunting to the non-specialist. Unlike other areas of organic chemistry, where organized catalogs of reaction conditions exist, there is no comparable “Larock book” of bioorthogonal transformations. Tool users must wade through an ever expanding and complex body of literature to identify reagents best suited for their applications. Thus, knowing which probes to select for a given experiment remains difficult. Additionally, while numerous chemical tools have been

developed in recent years, their transition to the broader scientific community (and widespread adoption) have often been quite sluggish. This is due, in part, to limited probe accessibilities. Many of the best reagents for a given application are not commercially available or require complex syntheses. Renewed efforts to develop more accessible probes will ease the transition of these reactions from the hands of the toolmaker to the tool user.

There is also an ongoing need to fill gaps along the continuums of reactivity and stability. Few reagents meet the strict requirements for use in living animals. Such probes must often be both exquisitely stable and potently reactive with complementary functionality. Further advances in reagent design will likely address this challenge and broaden the scope of possible applications. Along the way, probes that fall short of the bar for *in vivo* work will likely be useful in other contexts. Already, many reagents that are insufficiently stable for intracellular application have found utility in antibody–drug conjugate formation and materials research [82]. Recent developments in methionine labeling [83], cysteine conjugations [84], and carbonyl ligations [85-87] are also addressing the need for diverse chemical transformations.

## **1.7 Introduction to the thesis**

Bioorthogonal chemistries have become indispensable tools for modern chemical biology research. These reactions enable biomolecules to be studied in real time and in their native environments. Despite decades of achievements in crafting biocompatible reagents and reactions, limitations remain. Only a few probes are suitable for use in intracellular labeling experiments. Even fewer are small enough to traverse native

biosynthetic pathways. Many popular probes also cross-react with one another, limiting applications in multicomponent studies. We and others have been addressing these challenges by focusing on small and stable reagents that react via unique mechanisms.

Crafting new bioorthogonal reactions is not trivial, but successful examples can illuminate some guiding principles. In many cases, new transformations have been inspired by natural product structures. Such scaffolds often comprise unique functional groups that, when used in heterologous hosts, exhibit bioorthogonal character. These naturally occurring motifs thus offer advantageous starting points for developing new reactions. Further optimization can be achieved via classic physical organic studies or computational analyses. Together, these approaches can reveal unanticipated modes of reactivity and guide new reaction development. Embracing a spectrum of reactivity will encourage the development and application of new reactions without the unrealistic constraints of a one-size-fits-all transformation. Reactions that operate via distinct mechanistic pathways will further enable simultaneous labeling of multiple targets. As new biological questions continue to emerge, the demand for new probes will grow. Efforts to expand the collection of bioorthogonal tools will not only enable new pursuits in biology but also push the frontiers of chemistry.

This thesis will discuss the development and optimization of one class of bioorthogonal reactions. The Prescher lab previously introduced a ligation between cyclopropenones and phosphines for *in vitro* bioconjugations [30]. In Chapter 2, cyclopropenone stability was improved and their rate of reactivity with phosphines was investigated. Cyclopropenones were also genetically encoded into model proteins, demonstrating their compatibility with cells. To further optimize the cyclopropenone



scaffold, heteroanalogs were investigated. In Chapter 3, cyclopropenethiones were also found to be viable bioorthogonal reporters. Their reaction rates with phosphines are significantly increased relative to cyclopropenones, and they are stable enough for use in complex biological environments. The unique reactivity profile of the cyclopropenethione also opens up new opportunities for tandem labeling with cyclopropenones. Finally, in Chapter 4, cyclopropenones were investigated as chemically activatable crosslinkers for capturing biomolecular interactions. Together, these chemistries expand the currently available bioorthogonal toolset.

## 1.8 References

1. D. M. Patterson, L. A. Nazarova, J. A. Prescher. Finding the right (bioorthogonal) chemistry. *ACS Chem. Biol.* **2014**, *9*, 592–605.
2. J. A. Prescher, C. R. Bertozzi. Chemistry in living systems. *Nat. Chem. Biol.* **2005**, *1*, 13–21.
3. K. Lang, J. W. Chin. Cellular incorporation of unnatural amino acids and bioorthogonal labeling of proteins. *Chem. Rev.* **2014**, *114*, 4764–4806.
4. L. I. Willems, W. A. van der Linden, N. Li, K.-Y. Li, N. Liu, S. Hoogendoorn, G. A. van der Marel, B. I. Florea, H. S. Overkleeft. Bioorthogonal chemistry: Applications in activity-based protein profiling. *Acc. Chem. Res.* **2011**, *44*, 718–729.
5. D. K. Nomura, M. M. Dix, B. F. Cravatt. Activity-based protein profiling for biochemical pathway discovery in cancer. *Nat. Rev. Cancer* **2010**, *10*, 630–638.

6. K. S. Yang, G. Budin, C. Tassa, O. Kister, R. Weissleder. Bioorthogonal approach to identify unsuspected drug targets in live cells. *Angew. Chem. Int. Ed.* **2013**, *52*, 10593–10597.
7. A. Rutkowska, D. W. Thomson, J. Vappiani, T. Werner, K. M. Mueller, L. Dittus, J. Krause, M. Muelbaier, G. Bergamini, M. Bantscheff. A modular probe strategy for drug localization, target identification and target occupancy measurement on single cell level. *ACS Chem. Biol.* **2016**, *11*, 2541–2550.
8. R. M. Versteegen, R. Rossin, W. ten Hoeve, H. M. Janssen, M. S. Robillard. Click to release: Instantaneous doxorubicin elimination upon tetrazine ligation. *Angew. Chem. Int. Ed.* **2013**, *52*, 14112–14116.
9. J. M. Mejia Oneto, I. Khan, L. Seebald, M. Royzen. In vivo bioorthogonal chemistry enables local hydrogel and systemic pro-drug to treat soft tissue sarcoma. *ACS Cent. Sci.* **2016**, *2*, 476–482.
10. S. E. Stone, W. S. Glenn, G. D. Hamblin, D. A. Tirrell. Cell-selective proteomics for biological discovery. *Curr. Opin. Chem. Biol.* **2017**, *36*, 50–57.
11. B. Alvarez-Castelao, C. T. Schanzenbächer, C. Hanus, C. Glock, S. T. Dieck, A. R. Dörrbaum, I. Bartnik, B. Nassim-Assir, E. Ciirdaeva, A. Mueller, D. C. Dieterich, D. A. Tirrell, J. D. Langer, E. M. Schuman. Cell-type-specific metabolic labeling of nascent proteomes *in vivo*. *Nat. Biotechnol.* **2017**, *35*, 1196–1201.
12. J. Li, P. R. Chen. Development and application of bond cleavage reactions in bioorthogonal chemistry. *Nat. Chem. Biol.* **2016**, *12*, 129–137.

13. X. Fan, F. L. Yun Ge, Y. Yang, G. Zhang, W. S. C. Ngai, S. Z. Zhi Lin, J. Wang, J. Zhao, J. Li, P. R. Chen. Optimized tetrazine derivatives for rapid bioorthogonal decaging in living cells. *Angew. Chem. Int. Ed.* **2016**, *55*, 14046–14050.
14. G. Zhang, J. Li, R. Xie, X. Fan, Y. Liu, S. Zheng, Y. Ge, P. R. Chen. Bioorthogonal chemical activation of kinases in living systems. *ACS Cent. Sci.* **2016**, *2*, 325–331.
15. T. Völker, E. Meggers. Transition-metal-mediated uncaging in living human cells – an emerging alternative to photolabile protecting groups. *Curr. Opin. Chem. Biol.* **2015**, *25*, 48–54.
16. J. Li, J. Yu, J. Zhao, J. Wang, S. Zheng, S. Lin, L. Chen, M. Yang, S. Jia, X. Zhang, P. R. Chen. Palladium-triggered deprotection chemistry for protein activation in living cells. *Nat. Chem.* **2014**, *6*, 352–361.
17. H. E. Murrey, J. C. Judkins, C. W. am Ende, T. E. Ballard, Y. Fang, K. Riccardi, L. Di, E. R. Guilmette, J. W. Schwartz, J. M. Fox, D. S. Johnson. Systematic evaluation of bioorthogonal reactions in live cells with clickable HaloTag ligands: Implications for intracellular imaging. *J. Am. Chem. Soc.* **2015**, *137*, 11461–11475.
18. D. M. Patterson, J. A. Prescher. Orthogonal bioorthogonal chemistries. *Curr. Opin. Chem. Biol.* **2015**, *28*, 141–149.
19. Q.-Y. Chai, Z. Yang, H.-W. Lin, B.-N. Han. Alkynyl-containing peptides of marine origin: A review. *Mar. Drugs* **2016**, *14*, 216.

20. G. Cimino, A. De Giulio, S. De Rosa, V. Di Marzo. High molecular weight polyacetylenes from *Petrosia ficiformis*: Further structural analysis and biological activity. *Tetrahedron Lett.* **1989**, *30*, 3563–3566.
21. D. M. Patterson, L. A. Nazarova, B. Xie, D. N. Kamber, J. A. Prescher. Functionalized cyclopropenes as bioorthogonal chemical reporters. *J. Am. Chem. Soc.* **2012**, *134*, 18638–18643.
22. M. Matsuura, Y. Saikawa, K. Inui, K. Nakae, M. Igarashi, K. Hashimoto, M. Nakata. Identification of the toxic trigger in mushroom poisoning. *Nat. Chem. Biol.* **2009**, *5*, 465–467.
23. E. Fattorusso, S. Magno, L. Mayol, C. Satacroce, D. Sica. Calysterol: A C29 cyclopropene-containing marine sterol from the sponge *Calyx nicaensis*. *Tetrahedron* **1975**, *31*, 1715–1716.
24. G. A. Doss, C. Djerassi. Sterols in marine invertebrates. 60. Isolation and structure elucidation of four new steroidal cyclopropenes from the sponge *Calyx podatypa*. *J. Am. Chem. Soc.* **1988**, *110*, 8124–8128.
25. M. K. Pasha, F. Ahmad. Analysis of triacylglycerols containing cyclopropene fatty acids in *Sterculia foetida* (Linn.) seed lipids. *J. Agric. Food Chem.* **1992**, *40*, 626–629.
26. R. A. Zoeller, R. Wood. Effects of cyclopropene fatty acids on the lipid composition of the Morris hepatoma 7288C. *Lipids* **1984**, *19*, 529–538.
27. D. N. Kamber, Y. Liang, R. J. Blizzard, F. Liu, R. A. Mehl, K. N. Houk, J. A. Prescher. 1,2,4-Triazines are versatile bioorthogonal reagents. *J. Am. Chem. Soc.* **2015**, *137*, 8388–8391.

28. V. V. Smirnov, E. A. Kiprianova, A. D. Garagulya, S. E. Esipov, S. A. Dovjenko. Fluviols, bicyclic nitrogen-rich antibiotics produced by *Pseudomonas fluorescens*. *FEMS Microbiol. Lett.* **1997**, *153*, 357–361.
29. H. J. Lindner, G. Schaden. Pyrazolo[4.3-e]as-triazin, ein neues heterocyclisches system aus *Pseudomonas fluorescens* var. *pseudoiodinum*. *Chem. Ber.* **1972**, *105*, 1949–1955.
30. H.-W. Shih, J. A. Prescher. A bioorthogonal ligation of cyclopropenones mediated by triarylphosphines. *J. Am. Chem. Soc.* **2015**, *137*, 10036–10039.
31. H. Kogen, T. Kiho, K. Tago, S. Miyamoto, T. Fujioka, N. Otsuka, K. Suzuki-Konagai, T. Ogita. Alutacenoic acids A and B, rare naturally occurring cyclopropenone derivatives isolated from fungi: Potent non-peptide Factor XIIIa inhibitors. *J. Am. Chem. Soc.* **2000**, *122*, 1842–1843.
32. T. Okuda, K. Yokose, T. Furumai, H. B. Maruyama. Penitricin, a new class of antibiotic produced by *Penicillium aculearum* I. Isolation and characterization. *J. Antibiot.* **1984**, *37*, 718–722.
33. F. Bohlmann, J. Jakupovic, L. Müller, A. Schusser. Naturally occurring cyclopropenone derivatives. *Angew. Chem. Int. Ed.* **1981**, *3*, 292–293.
34. M. Meldal, C. W. Tornøe. Cu-catalyzed azide–alkyne cycloaddition. *Chem. Rev.* **2008**, *108*, 2952–3015.
35. J. C. Jewett, C. R. Bertozzi. Cu-free click cycloaddition reactions in chemical biology. *Chem. Soc. Rev.* **2010**, *39*, 1272–1279.

36. M. L. Blackman, M. Royzen, J. M. Fox. Tetrazine ligation: Fast bioconjugation based on inverse-electron-demand Diels–Alder reactivity. *J. Am. Chem. Soc.* **2008**, *130*, 13518–13519.
37. M. T. Taylor, M. L. Blackman, O. Dmitrenko, J. M. Fox. Design and synthesis of highly reactive dienophiles for the tetrazine–*trans*-cyclooctene ligation. *J. Am. Chem. Soc.* **2011**, *133*, 9646–9649.
38. W. D. Lambert, S. L. Scinto, O. Dmitrenko, S. J. Boyd, R. Magboo, R. A. Mehl, J. W. Chin, J. M. Fox, S. Wallace. Computationally guided discovery of a reactive, hydrophilic *trans*-5-oxocene dienophile for bioorthogonal labeling. *Org. Biomol. Chem.* **2017**, *15*, 6640–6644.
39. R. J. Blizzard, D. R. Backus, W. Brown, C. G. Bazewicz, Y. Li, R. A. Mehl. Ideal bioorthogonal reactions using a site-specifically encoded tetrazine amino acid. *J. Am. Chem. Soc.* **2015**, *137*, 10044–10047.
40. J. Yang, J. Šečková, C. M. Cole, N. K. Devaraj. Live-cell imaging of cyclopropene tags with fluorogenic tetrazine cycloadditions. *Angew. Chem. Int. Ed.* **2012**, *51*, 7476–7479.
41. J. Yang, Y. Liang, J. Šečková, K. N. Houk, N. K. Devaraj. Synthesis and reactivity comparisons of 1-methyl-3-substituted cyclopropene mini-tags for tetrazine bioorthogonal reactions. *Chem. Eur. J.* **2014**, *20*, 3365–3375.
42. A. Sachdeva, K. Wang, T. Elliott, J. W. Chin. Concerted, rapid, quantitative, and site-specific dual labeling of proteins. *J. Am. Chem. Soc.* **2014**, *136*, 7785–7788.

43. H. Wu, B. T. Cisneros, C. M. Cole, N. K. Devaraj. Bioorthogonal tetrazine-mediated transfer reactions facilitate reaction turnover in nucleic acid-templated detection of microRNA. *J. Am. Chem. Soc.* **2014**, *136*, 17942–17945.
44. F. Eggert, S. Kath-Schorr. A cyclopropene-modified nucleotide for site-specific RNA labeling using genetic alphabet expansion transcription. *Chem. Commun.* **2016**, *52*, 7284–7287.
45. Z. Yu, Y. Pan, Z. Wang, J. Wang, Q. Lin. Genetically encoded cyclopropene directs rapid, photoclick-chemistry-mediated protein labeling in mammalian cells. *Angew. Chem. Int. Ed.* **2012**, *51*, 10600–10604.
46. D. M. Patterson, K. A. Jones, J. A. Prescher. Improved cyclopropene reporters for probing protein glycosylation. *Mol. BioSyst.* **2014**, *10*, 1693–1697.
47. A.-K. Späte, H. Bußkamp, A. Niederwieser, V. F. Schart, A. Marx, V. Wittmann. Rapid labeling of metabolically engineered cell-surface glycoconjugates with a carbamate-linked cyclopropene reporter. *Bioconjugate Chem.* **2014**, *25*, 147–154.
48. T. S. Elliott, F. M. Townsley, A. Bianco, R. J. Ernst, A. Sachdeva, S. J. E. A. Elsässer, L. Davis, K. Lang, R. Pisa, S. Greiss, K. S. Lilley, J. W. Chin. Proteome labeling and protein identification in specific tissues and at specific developmental stages in an animal. *Nat. Biotechnol.* **2014**, *32*, 465–472.
49. T. S. Elliott, A. Bianco, F. M. Townsley, S. D. Fried, J. W. Chin. Tagging and enriching proteins enables cell-specific proteomics. *Cell Chemical Biology* **2016**, *23*, 805–815.

50. J. M. J. M. Ravasco, C. M. Monteiro, A. F. Trindade. Cyclopropenes: A new tool for the study of biological systems. *Org. Chem. Front.* **2017**, *4*, 1167–1198.
51. J. W. Chin. Expanding and reprogramming the genetic code of cells and animals. *Annu. Rev. Biochem.* **2014**, *83*, 379–408.
52. J. Xie, P. G. Schultz. An expanding genetic code. *Methods* **2005**, *36*, 227–238.
53. C. P. Ramil, M. Dong, P. An, T. M. Lewandowski, Z. Yu, L. J. Miller, Q. Lin. Spirohexene-tetrazine ligation enables bioorthogonal labeling of class B G protein-coupled receptors in live cells. *J. Am. Chem. Soc.* **2017**, *139*, 13376–13386.
54. T. Peng, H. C. Hang. Site-specific bioorthogonal labeling for fluorescence imaging of intracellular proteins in living cells. *J. Am. Chem. Soc.* **2016**, *138*, 14423–14433.
55. R. J. Ernst, T. P. Krogager, E. S. Maywood, R. Zanchi, V. Beránek, T. S. Elliott, N. P. Barry, M. H. Hastings, J. W. Chin. Genetic code expansion in the mouse brain. *Nat. Chem. Biol.* **2016**, *12*, 776–778.
56. Y. Zheng, P. S. Addy, R. Mukherjee, A. Chatterjee. Defining the current scope and limitations of dual noncanonical amino acid mutagenesis in mammalian cells. *Chem. Sci.* **2017**, *8*, 7211–7217.
57. Y. Zheng, R. Mukherjee, M. A. Chin, P. Igo, M. J. Gilgenast, A. Chatterjee. Expanding the scope of single and dual noncanonical amino acid mutagenesis in mammalian cells using orthogonal polyspecific leucyl-tRNA synthetases. *Biochemistry* **2017**, *57*, 441–445.



58. M. R. Karver, R. Weissleder, S. A. Hilderbrand. Synthesis and evaluation of a series of 1,2,4,5-tetrazines for bioorthogonal conjugation. *Bioconjugate Chem.* **2011**, *22*, 2263–2270.
59. K. A. Horner, N. M. Valette, M. E. Webb. Strain-promoted reaction of 1,2,4-triazines with bicyclononynes. *Chem. Eur. J.* **2015**, *21*, 14376–14381.
60. K. Peewasan, H.-A. Wagenknecht. 1,2,4-Triazine-modified 2'-deoxyuridine triphosphate for efficient bioorthogonal fluorescent labeling of DNA. *ChemBioChem* **2017**, *18*, 1473–1476.
61. S. J. Siegl, R. Dzijak, A. Vázquez, R. Pohl, M. Vrabel. The discovery of pyridinium 1,2,4-triazines with enhanced performance in bioconjugation reactions. *Chem. Sci.* **2017**, *8*, 3593–3598.
62. F. Liu, Y. Liang, K. N. Houk. Bioorthogonal cycloadditions: Computational analysis with the distortion/interaction model and predictions of reactivities. *Acc. Chem. Res.* **2017**, *50*, 2297–2308.
63. D. N. Kamber, L. A. Nazarova, Y. Liang, S. A. Lopez, D. M. Patterson, H.-W. Shih, K. N. Houk, J. A. Prescher. Isomeric cyclopropenes exhibit unique bioorthogonal reactivities. *J. Am. Chem. Soc.* **2013**, *135*, 13680–13683.
64. H.-W. Shih, D. N. Kamber, J. A. Prescher. Building better bioorthogonal reactions. *Curr. Opin. Chem. Biol.* **2014**, *21*, 103–111.
65. J. E. Hudak, D. Alvarez, A. Skelly, U. H. von Andrian, D. L. Kasper. Illuminating vital surface molecules of symbionts in health and disease. *Nat. Microbiol.* **2017**, *2*, 17099.

66. A. R. Sherratt, M. Chigrinova, D. A. MacKenzie, N. K. Rastogi, M. T. M. Ouattara, A. T. Pezacki, J. P. Pezacki. Dual strain-promoted alkyne–nitronc cycloadditions for simultaneous labeling of bacterial peptidoglycans. *Bioconjugate Chem.* **2016**, *27*, 1222–1226.
67. M. K. Narayanam, Y. Liang, K. N. Houk, J. M. Murphy. Discovery of new mutually orthogonal bioorthogonal cycloaddition pairs through computational screening. *Chem. Sci.* **2016**, *7*, 1257–1261.
68. M. R. Aronoff, B. Gold, R. T. Raines. 1,3-Dipolar cycloadditions of diazo compounds in the presence of azides. *Org. Lett.* **2016**, *18*, 1538–1541.
69. S. Eising, F. Lelivelt, K. M. Bongers. Vinylboronic acids as fast reacting, synthetically accessible, and stable bioorthogonal reactants in the Carboni–Lindsey reaction. *Angew. Chem. Int. Ed.* **2016**, *55*, 12243–12247.
70. R. D. Row, H.-W. Shih, A. T. Alexander, R. A. Mehl, J. A. Prescher. Cyclopropanones for metabolic targeting and sequential bioorthogonal labeling. *J. Am. Chem. Soc.* **2017**, *139*, 7370–7375.
71. T. H. Wright, B. J. Bower, J. M. Chalker, G. J. L. Bernardes, R. Wiewiora, W.-L. Ng, R. Raj, S. Faulkner, M. R. J. Vallée, A. Phanumartwiwath, O. D. Coleman, M.-L. Thézénas, M. Khan, S. R. G. Galan, L. Lercher, M. W. Schombs, S. Gerstberger, M. E. Palm-Espling, A. J. Baldwin, B. M. Kessler, T. D. W. Claridge, S. Mohammed, B. G. Davis. Posttranslational mutagenesis: A chemical strategy for exploring protein side-chain diversity. *Science* **2016**, *354*, aag1465-1–11.

72. A. Yang, S. Ha, J. Ahn, R. Kim, S. Kim, Y. Lee, J. Kim, D. Söll, H.-Y. Lee, H.-S. Park. A chemical biology route to site-specific authentic protein modifications. *Science* **2016**, *354*, 623–626.
73. J. M. Chalker, C. S. C. Wood, B. G. Davis. A convenient catalyst for aqueous and protein Suzuki–Miyaura cross-coupling. *J. Am. Chem. Soc.* **2009**, *131*, 16346–16347.
74. J. Willwacher, R. Raj, S. Mohammed, B. G. Davis. Selective metal-site-guided arylation of proteins. *J. Am. Chem. Soc.* **2016**, *138*, 8678–8681.
75. N. Li, C. P. Ramil, R. K. V. Lim, Q. Lin. A genetically encoded alkyne directs palladium-mediated protein labeling on live mammalian cell surface. *ACS Chem. Biol.* **2015**, *10*, 379–384.
76. E. V. Vinogradova, C. Zhang, A. M. Spokoiny, B. L. Pentelute, S. L. Buchwald. Organometallic palladium reagents for cysteine bioconjugation. *Nature* **2015**, *526*, 687–691.
77. A. A. Poloukhine, N. E. Mbua, M. A. Wolfert, G.-J. Boons, V. V. Popik. Selective labeling of living cells by a photo-triggered click reaction. *J. Am. Chem. Soc.* **2009**, *131*, 15769–15776.
78. J. M. Lopchuk, K. Fjelbye, Y. Kawamata, L. R. Malins, C.-M. Pan, R. Gianatassio, J. Wang, L. Prieto, J. Bradow, T. A. Brandt, M. R. Collins, J. Elleraas, J. Ewanicki, W. Farrell, O. O. Fadeyi, G. M. Gallego, J. J. Mousseau, R. Oliver, N. W. Sach, J. K. Smith, J. E. Spangler, H. Zhu, J. Zhu, P. S. Baran. Strain-release heteroatom functionalization: Development, scope, and stereospecificity. *J. Am. Chem. Soc.* **2017**, *139*, 3209–3226.

79. P. Thirumurugan, D. Matosiuk, K. Jozwiak. Click chemistry for drug development and diverse chemical–biology applications. *Chem. Rev.* **2013**, *113*, 4905–4979.
80. A. Sharma, J. F. Hartwig. Metal-catalysed azidation of tertiary C–H bonds suitable for late-stage functionalization. *Nature* **2015**, *517*, 600–604.
81. R. R. Karimov, A. Sharma, J. F. Hartwig. Late stage azidation of complex molecules. *ACS Cent. Sci.* **2016**, *2*, 715–724.
82. A. Beck, L. Goetsch, C. Dumontet, N. Corvaia. Strategies and challenges for the next generation of antibody–drug conjugates. *Nat. Rev. Drug Discov.* **2017**, *16*, 315–337.
83. S. Lin, X. Yang, S. Jia, A. M. Weeks, M. Hornsby, P. S. Lee, R. V. Nichiporuk, A. T. Lavarone, J. A. Wells, F. D. Toste, C. J. Chang. Redox-based reagents for chemoselective methionine bioconjugation. *Science* **2017**, *355*, 597–602.
84. C. Zhang, M. Welborn, T. Zhu, N. J. Yang, M. S. Santos, T. V. Voorhis, B. L. Pentelute.  $\pi$ -Clamp-mediated cysteine conjugation. *Nat. Chem.* **2016**, *8*, 120–128.
85. D. K. Kölmel, E. T. Kool. Oximes and hydrazones in bioconjugation: Mechanism and catalysis. *Chem. Rev.* **2017**, *117*, 10358–10376.
86. P. Schmidt, C. Stress, D. Gillingham. Boronic acids facilitate rapid oxime condensations at neutral pH. *Chem. Sci.* **2015**, *6*, 3329–3333.
87. J. W. Bode. Chemical protein synthesis with the  $\alpha$ -ketoacid–hydroxylamine ligation. *Acc. Chem. Res.* **2017**, *50*, 2104–2115.

## Chapter 2: Cyclopropenones for metabolic targeting and sequential bioorthogonal labeling

Adapted from published work: Row, R. D.; Shih, H.-W.; Alexander, A. T.; Mehl, R. A.; Prescher, J. A. J. *Am. Chem. Soc.* **2017**, *139*, 7370–7375.

### 2.1 Introduction

The bioorthogonal chemical reporter strategy ranks among the most powerful and popular methods for labeling biomolecules in their native environments (Figure 2-1) [1, 2]. This strategy exploits cellular enzymes to incorporate non-natural metabolites (endowed with unique chemical functional groups, i.e. “reporters”) into target biomolecules. In a second step, the reporters are selectively ligated with complementary functional groups bearing detectable probes. Depending on the nature of the probe, this two-step approach can be used to visualize and isolate a broad range of biomolecules, including glycans [2-4], lipid metabolites [5, 6], and proteins [7]. Recent applications have uncovered new functional roles for post-translational modifications [8, 9], mechanisms of cell wall assembly [10, 11], and cell-specific proteomes [12, 13].

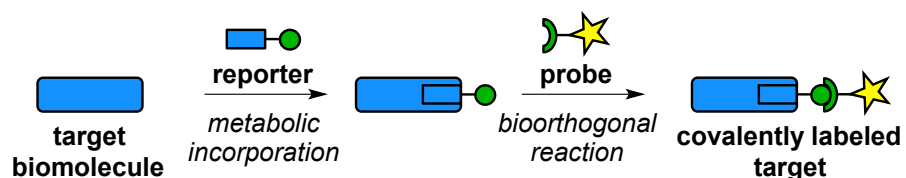


**Figure 2-1.** The bioorthogonal chemical reporter strategy. First, a non-natural precursor (small rectangle) bearing a chemical reporter (circle) is metabolically introduced into a target biomolecule (large rectangle). In a second step, the chemical reporter can be covalently labeled with a complementary chemical probe (arc) via a bioorthogonal reaction.

While the bioorthogonal chemical reporter strategy continues to reveal new facets of biology, limitations remain. Many of the requisite reagents are not completely inert to cysteine or other biological nucleophiles in cells and tissues. Some scaffolds are also too large to traverse cellular metabolic pathways. Another limitation is that several bioorthogonal reagents cross-react with one another [14-16], precluding multicomponent labeling experiments. Thus, despite decades of work on bioorthogonal reaction development, few reactions can be used reliably – and in combination – in living systems.

To address these limitations, the Prescher lab is identifying more stable and small reporters for cellular use. Included in this group are cyclopropenes [17, 18] and triazines [19]. These motifs are small enough to target a variety of biomolecules in cells, and can be selectively detected via biocompatible cycloadditions. More recently, we turned our attention to cyclopropenones. These motifs are also small and thus appealing for general use. Cyclopropenones are found in some natural products [20-22], underscoring their biocompatibility and potential metabolic stability. They are also robustly reactive with triaryl phosphines [23, 24], reagents that have been used extensively for bioorthogonal Staudinger ligations [4, 25]. The cyclopropenone–phosphine reaction proceeds through a ketene-ylide [23]; this intermediate can be trapped by a variety of nucleophiles (Figure 2-2). When the nucleophile is attached to the phosphine itself, tethered adducts are formed.

Hui-Wen Shih previously showed that the unique features of monosubstituted cyclopropenones could be exploited for biomolecule labeling in aqueous conditions [23]. The motifs were appended to model proteins *in vitro* and selectively targeted with

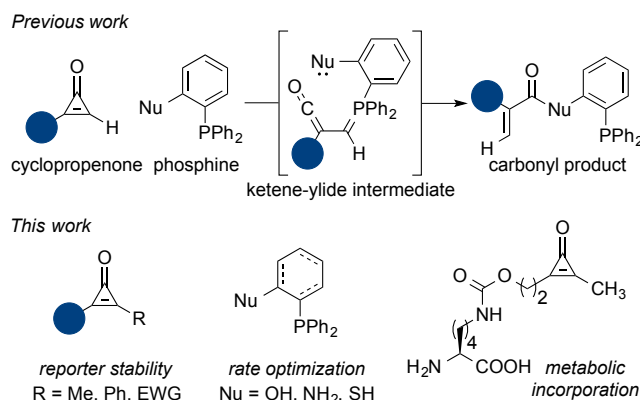
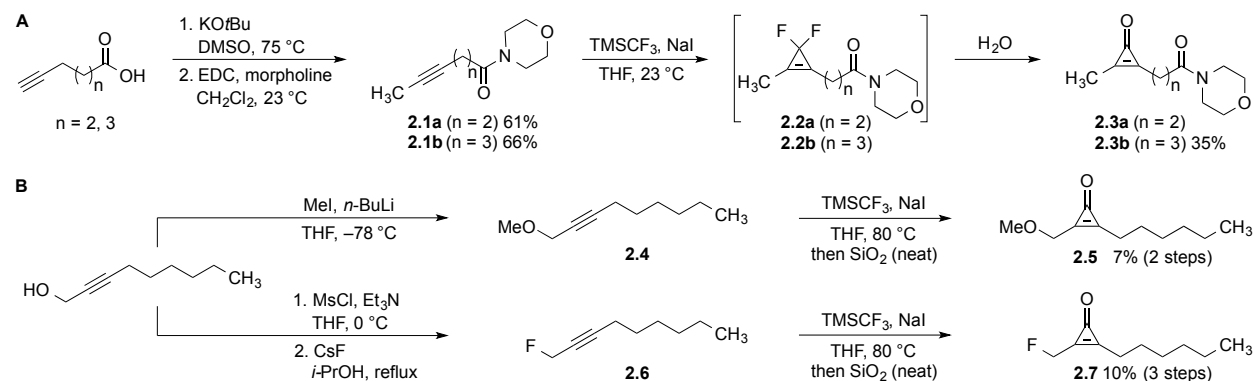


**Figure 2-2.** Previous work in our lab demonstrated that triaryl phosphines react efficiently with cyclopropenones to form ketene-ylides. These intermediates can be trapped via tethered nucleophiles to afford stable adducts. In this work, cyclopropenone stability, reactivity, and cellular use were investigated.

phosphine-fluorophore conjugates [23]. While the monosubstituted cyclopropenones were observed to react robustly with phosphines, they were susceptible to reaction with cysteine and other biological thiols at pH > 7. Such side reactivity limits their utility for intracellular imaging and other applications.

To optimize the cyclopropenones for intracellular use, we aimed to identify scaffolds with improved stability (Figure 2-2). We focused on disubstituted cyclopropenones for this purpose, as previous observations by our lab and others suggested that these reagents were less prone to thiol attack [23, 26, 27]. As improved stability often comes at the expense of rapid reactivity, we also investigated a panel of phosphine reagents to tune the kinetics of the ligation. Cyclopropenones with improved stability were identified, along with phosphines with markedly improved reaction rates. These motifs are suitable for intracellular work and, based on the unique products formed, can be used for sequential labeling experiments.

## Scheme 2-1. Synthesis of model cyclopropenones.

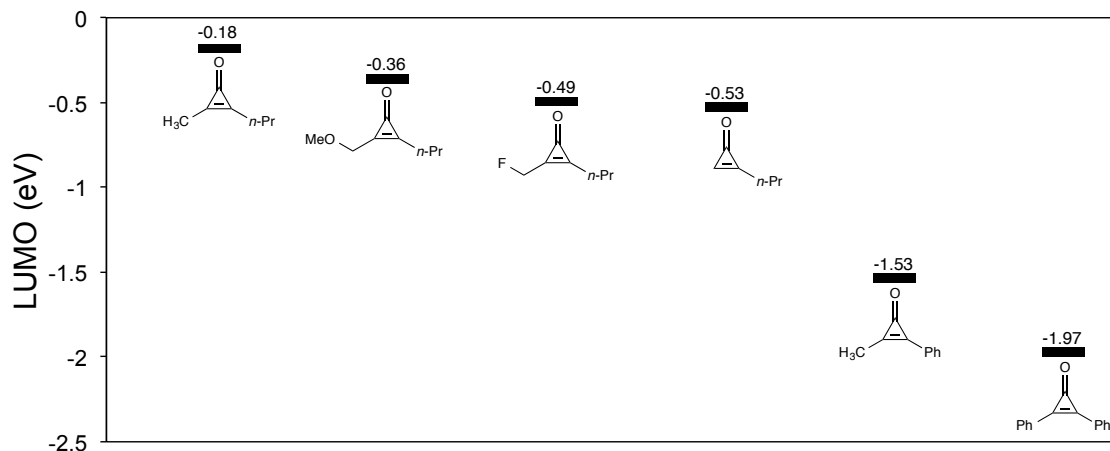


## 2.2 Results and discussion

We observed that monosubstituted cyclopropenones, while robustly reactive with phosphines, are susceptible to background reactions with thiols in cellular environments. To identify more stable cyclopropenones, we synthesized a panel of disubstituted variants bearing either alkyl or aryl appendages (Scheme 2-1). Many of these scaffolds possessed higher LUMO energies (Figure 2-3) and extra steric bulk to mitigate against thiol attack. As bulky substituents would also likely impede phosphine addition, cyclopropenones with electron-withdrawing character were also included to more precisely “tune” the reactivity. Density functional theory (DFT) calculations (Figure 2-3) suggested that cyclopropenones bearing methoxymethyl or monofluoromethyl groups (as in compounds **2.5** or **2.7**) might provide the appropriate balance between thiol stability and phosphine reactivity. The LUMO energies for these compounds fell between those of the dialkyl (**2.3a,b**) and monoalkyl (**2.8**) scaffolds.

The desired cyclopropenones were prepared via a common route involving difluorocarbene addition to alkyne precursors (Scheme 2-1) [23]. To access the water-



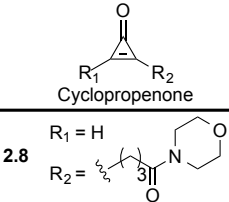
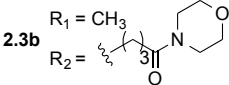


**Figure 2-3.** Cyclopropenone LUMO energies calculated using density functional theory (DFT). Calculations were performed with Spartan Student Edition, using the B3LYP level of theory and the basis set 6-31G\*.

soluble cyclopropenones **2.3a** and **2.3b** (Scheme 2-1A), 5-hexynoic acid and 6-heptynoic acid were first isomerized and amidated. The resulting alkynes were then reacted with difluorocarbene (following the procedure of Olah *et al.*) [28] to form **2.2a,b**. These intermediates spontaneously hydrolyzed to the corresponding cyclopropenones (**2.3a,b**) upon aqueous workup. The yield of **2.3a** was quite low (<10%), as this compound was unstable. By contrast, cyclopropenone **2.3b** was isolated in reasonable yield and was stable to concentration. These observed differences may be attributed to the shortened tether in compound **2.2a** and undesirable intramolecular reactivity [29].

The remaining cyclopropenones were prepared in a similar fashion (Scheme 2-1B). In brief, methoxymethyl cyclopropenone **2.5** was accessed by methylating 2-nonyn-1-ol prior to forming the difluorocyclopropene. Interestingly, this intermediate did not hydrolyze to the corresponding cyclopropenone upon aqueous workup. Complete conversion was only realized upon prolonged exposure to silica gel. To access the

**Table 2-1.** Cyclopropenone stability.

Cyclopropenone	Conditions	$t_{1/2}$ (h)	
		- Cys	+ Cys
 <b>2.8</b> $R_1 = \text{H}$ $R_2 = \text{CH}_2\text{CH}_2\text{C}(=\text{O})\text{N}(\text{CH}_2\text{CH}_2)_2\text{O}$	<i>d</i> -PBS pH 7.4, 37 °C	N.R.*	< 0.2
<b>2.5</b> $R_1 = \text{CH}_2\text{OCH}_3$ $R_2 = \text{hexyl}$	20% CD <sub>3</sub> CN / <i>d</i> -PBS pH 7.4, 37 °C	N.R.	~1.5
<b>2.7</b> $R_1 = \text{CH}_2\text{F}$ $R_2 = \text{hexyl}$	20% CD <sub>3</sub> CN / <i>d</i> -PBS pH 7.4, 37 °C	N.R.	< 0.2
<b>2.9</b> $R_1 = \text{CH}_3$ $R_2 = \text{Ph}$	20% CD <sub>3</sub> CN / <i>d</i> -PBS pH 7.4, 23 °C	N.R.	~12.5
<b>2.10</b> $R_1 = \text{Ph}$ $R_2 = \text{Ph}$	20% CD <sub>3</sub> CN / <i>d</i> -PBS pH 7.4, 23 °C	3 d*	< 0.2
 <b>2.3b</b> $R_1 = \text{CH}_3$ $R_2 = \text{CH}_2\text{CH}_2\text{C}(=\text{O})\text{N}(\text{CH}_2\text{CH}_2)_2\text{O}$	<i>d</i> -PBS pH 7.4–8.4, 37 °C	N.R.	N.R.

\*As reported in ref. 23

fluorinated cyclopropenone **2.7**, 2-nonyn-1-ol was first mesylated. Subsequent S<sub>N</sub>2 displacement provided scaffold **2.6**, which was ultimately converted to the cyclopropenone **2.7** as previously described.

With the desired cyclopropenones in hand, we monitored their stabilities under physiological conditions. Phenyl-substituted cyclopropenones **2.9** and **2.10** were included for comparison. All compounds were dissolved in phosphate-buffered solutions (pH 7.4) and analyzed via NMR spectroscopy (Table 2-1). After 1 week, most of the cyclopropenones showed no signs of degradation (see Appendix A), even at elevated temperatures. One exception was diphenylcyclopropenone **2.10**, which is known to be photolytically unstable [23, 30]. We also examined cyclopropenone stabilities in the

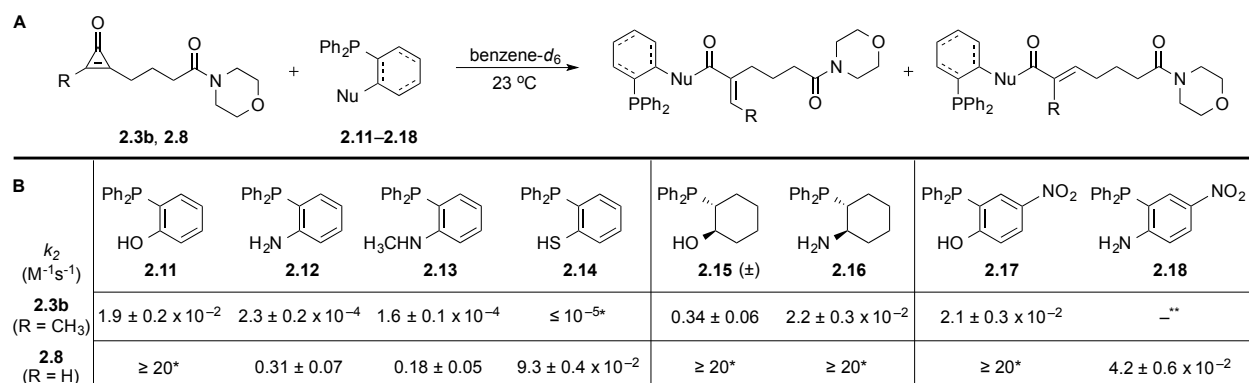


**Figure 2-4.** Kinetic experiments to analyze cyclopropenone and phosphine reactivity. (A) Reactions were performed in benzene-*d*<sub>6</sub> and monitored via NMR. Two products were formed, corresponding to phosphine addition at either side of the cyclopropenone ring. (B) Second-order rate constants for reactions between mono- and disubstituted cyclopropenones and a panel of phosphine probes. Errors are given as the standard deviation for *n* = 3 experiments. For **2.12**, **2.16**, and **2.18**, multiple addition products were observed late in the reactions (Figure 2-7). \*Reactions were too fast or too slow to measure via NMR. \*\*Upon mixing **2.3b** and **2.18**, an unidentified precipitate formed, preventing accurate rate measurements.

presence of thiols. The compounds were incubated with L-cysteine or L-glutathione and monitored at room temperature or at 37 °C (see Appendix A). While the methoxymethyl (**2.5**) and monofluoromethyl (**2.7**) cyclopropenones were stable in aqueous solution, they reacted rapidly with cysteine (see Appendix A), making their use in cellular contexts impractical. The half-lives of most cyclopropenone scaffolds, in general, were <12 h. However, cyclopropenone **2.3b** remained inert to cysteine over a 24-h period, even at elevated pH (see Appendix A) and temperature. Similar trends were observed with glutathione (see Appendix A). These data suggested that the dialkyl-substituted scaffold was an excellent candidate for *in cellulo* work.

Encouraged by the enhanced stability of **2.3b**, we proceeded to investigate its reactivity with a panel of phosphines (Figure 2-4). The panel included triaryl phosphines bearing tethered nucleophiles, such as alcohols (**2.11**), amines (**2.12**, **2.13**), and thiols (**2.14**), along with alkyl phosphine variants (**2.15**, **2.16**). Some of these probes (**2.11–2.13**) were previously shown to react with cyclopropenones and efficiently trap ketene-ylide intermediates [23]. These phosphines also had the potential to afford a variety of covalent linkages (e.g., esters, amides, and thioesters) for biomolecule derivatization. We hypothesized that scaffolds with more electron-donating substituents would boost phosphine nucleophilicity and thus increase reaction rates. Similarly, alkyl phosphine probes were expected to provide enhanced reactivity.

When cyclopropenones **2.3b** and **2.8** were treated with the phosphine panel, the expected trends in reactivity were observed. Reactions with the disubstituted scaffold (**2.3b**) proceeded more slowly than reactions with the monosubstituted analogue **2.8** (Figures 2-4, 2-5, and 2-6). Increased reaction rates were achieved with cyclohexyl phosphines **2.15** and **2.16** compared to their triaryl counterparts **2.11–2.13**. It should be noted that the enhanced nucleophilicity of **2.15** and **2.16** also renders these phosphines more susceptible to oxidation. However, only minimal levels of oxidation were observed in ligations performed with the cyclohexyl variants (<5% observed by NMR). The unusual stability of phosphine **2.16** has been previously reported [31], and related scaffolds are known to be stable [32], suggesting their feasibility in biological experiments.

A surprising observation was made upon treating cyclopropenone **2.3b** with phosphine phenol **2.11**. These reactions were ~100 times faster than reactions with the

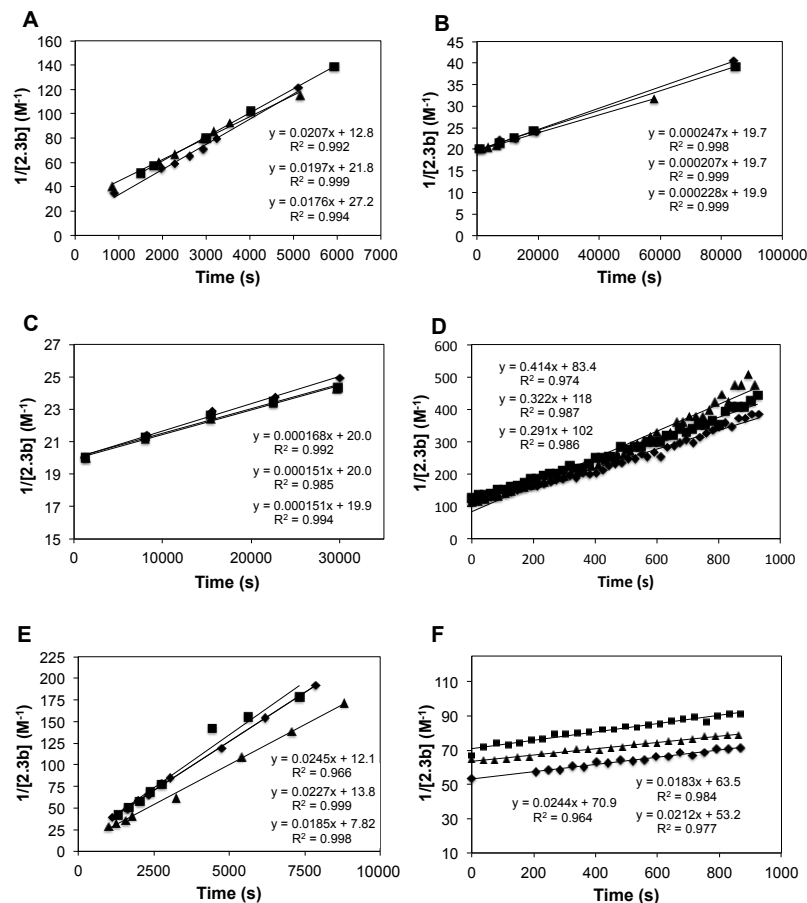


**Figure 2-5.** Reaction plots used to calculate second-order rate constants between cyclopropanone **2.3b** and phosphines **2.11–2.13** and **2.15–2.17**. Each panel shows  $n = 3$  separate experiments. The plots were generated by monitoring reactions between: A) **2.3b** (50 mM) and **2.11** (50 mM). B) **2.3b** (50 mM) and **2.12** (50 mM). C) **2.3b** (50 mM) and **2.13** (50 mM). D) **2.3b** (10 mM) and **2.15** (10 mM). E) **2.3b** (50 mM) and **2.16** (50 mM). F) **2.3b** (20 mM) and **2.17** (20 mM).

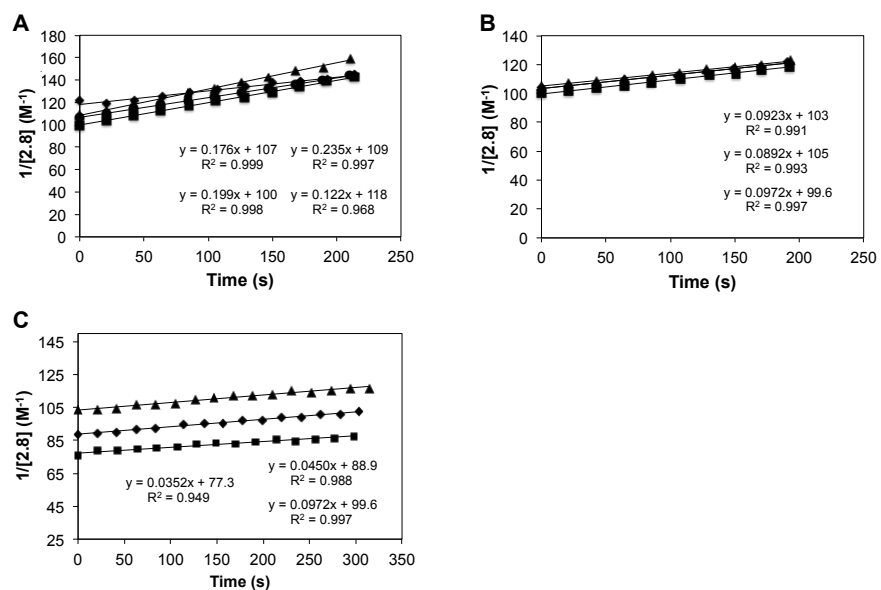


**Figure 2-6.** Reaction plots used to calculate second order rate constants between cyclopropanone **2.8** and phosphines **2.13**, **2.14**, and **2.18**. Each panel shows at least  $n = 3$  separate experiments. The plots were generated by monitoring reactions between: A) **2.8** (10 mM) and **2.13** (10 mM). B) **2.8** (10 mM) and **2.14** (10 mM). C) **2.8** (10 mM) and **2.18** (10 mM).

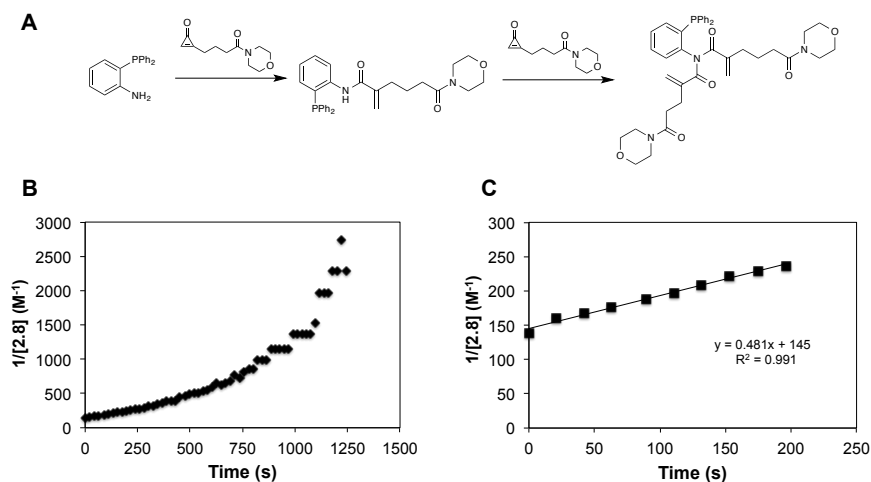


**Figure 2-7.** Phosphine **2.12** was observed to react with two equivalents of cyclopropanone **2.8**. A) Reaction scheme for the double addition. B) Deviation from linearity observed for **2.8** (10 mM) and **2.12** (10 mM) when rate data were plotted for a second order reaction. C) Early time points were used to estimate the second order rate constant for the reaction between **2.12** and **2.8**.

corresponding anilines (**2.12**, **2.13**). Similar trends were observed with cyclohexyl phosphines **2.15** and **2.16**. One possible explanation for the rate differential is that phosphines **2.11** and **2.15** activate the cyclopropanone for attack via an intermolecular hydrogen bond (Figure 2-8A). Dialkylcyclopropanones are known to readily form hydrogen bonds with phenol [33]. The pKa values (in DMSO) for phenol (pKa = 18) [34] and aniline (pKa = 31) [35] further suggest that **2.11** should be a better hydrogen bond donor than **2.12** and **2.13**. Indeed, when **2.11** was reacted with **2.3b**, the rate increased with additional equivalents of exogenous phenol (Figures 2-8B and 2-9). We further measured rates with phosphines **2.17** and **2.18**. These scaffolds comprise hydrogen bond donors and *para*-nitro groups. We hypothesized that these phosphines would provide increased reaction rates as a result of stronger hydrogen bonding. However, the rate of the reaction between **2.17** and **2.3b** was nearly identical to that of **2.11** and **2.3b**. One potential explanation is that the rate increase achieved by lowering the pKa of **2.17** is offset by a decrease in phosphine nucleophilicity (due to the electron-withdrawing nitro group). For aniline phosphine **2.18**, a noticeable decrease in rate was observed. Phosphine **2.18** does not likely provide for a strong hydrogen bond. The pKa values for phenol and *p*-nitroaniline (18.0 and 20.9, respectively) support this hypothesis [34, 35].

To showcase the stability and reactivity of the dialkyl cyclopropanone scaffold, we investigated its use for intracellular biomolecule labeling. We aimed to site-specifically target proteins with cyclopropanones via genetic code expansion. Toward this end, we synthesized a noncanonical amino acid for *in cellulo* experiments (Scheme 2-2). Briefly, 3-pentyn-1-ol was protected with tetrahydropyran (THP) to afford **2.19**. The alkyne was then subjected to the aforementioned carbene insertion and hydrolysis

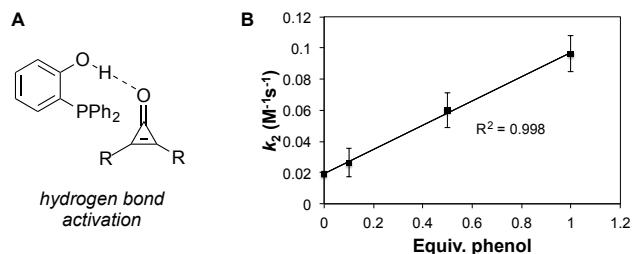


**Figure 2-8.** Hydrogen bonding enhances cyclopropenone reactivity. A) Hydrogen bonding can position the phosphorus atom near the vinyl carbon. B) Reaction rates between **2.3b** and **2.11** increase with additional equivalents of phenol.

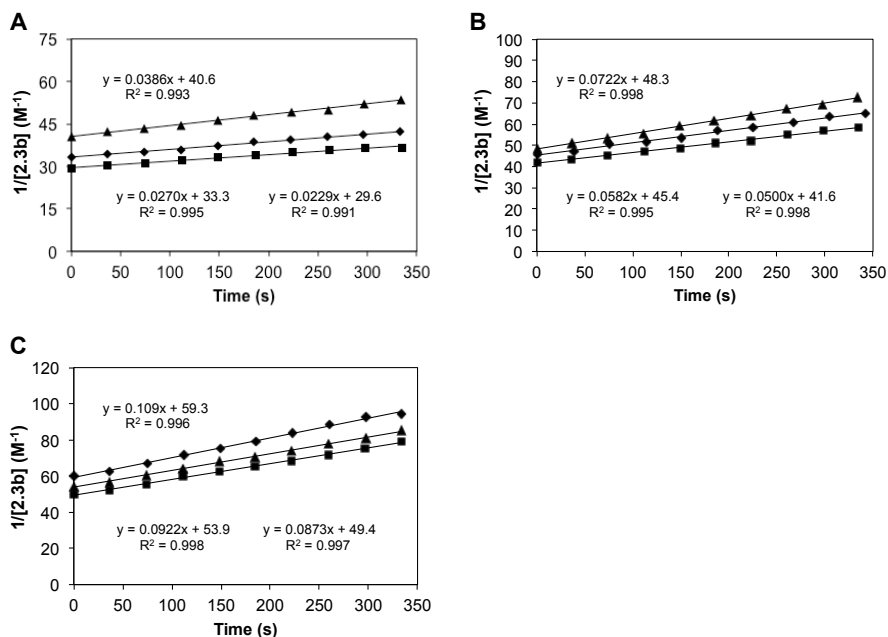
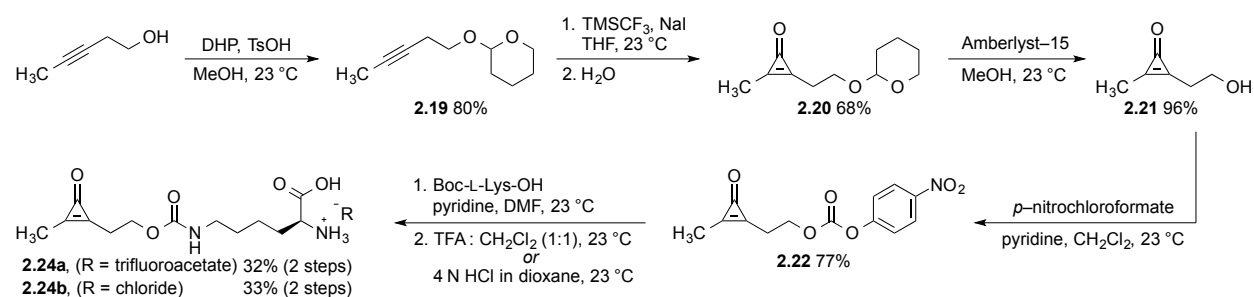


**Figure 2-9.** Hydrogen bond activation of cyclopropenone **2.3b** was assessed by measuring rates in the presence of phenol. Cyclopropenone **2.3b** (50 mM) and phosphine **2.11** (50 mM) were incubated with phenol (5, 25, or 50 mM). Each panel shows  $n = 3$  separate experiments. Reactions were monitored by  $^1H$  NMR with: A) 0.1 equivalents (5 mM), B) 0.5 equivalents (25 mM), or C) 1.0 equivalents (50 mM) phenol.



**Scheme 2-2.** Synthesis of a cyclopropenone-functionalized amino acid.



sequence to provide **2.20**. The acid-labile THP group was removed to give alcohol **2.21**. This intermediate was then appended to Boc-L-lysine. To remove the Boc group and liberate the desired amino acid, compound **2.23** was initially subjected to trifluoroacetic acid (TFA). The isolated trifluoroacetate salt (**2.24a**) exhibited significant toxicity in bacteria, likely due to cellular interference from the TFA counterion [36]. Subsequent deprotections were carried out using hydrochloric acid in dioxane. The chloride salt (**2.24b**) was compatible with cells (data not shown). Importantly, the cyclopropenone amino acids were also stable in physiological buffers and in the presence of cysteine (see Appendix A).

With the amino acid in hand, we needed to identify an appropriate noncanonical aminoacyl-tRNA synthetase (ncAA-RS)/tRNA pair for genetic incorporation. The ncAA-RS/tRNA pair is responsible for installing the unnatural amino acid in response to a single codon (in this case, TAG, the amber stop codon). Frequently, a compatible ncAA-RS can be identified via screening of existing synthetase libraries that have been previously selected for structurally similar ncAAs. When successful, this strategy of using permissive ncAA-RSs avoids the need for evolving a new mutant from wild-type

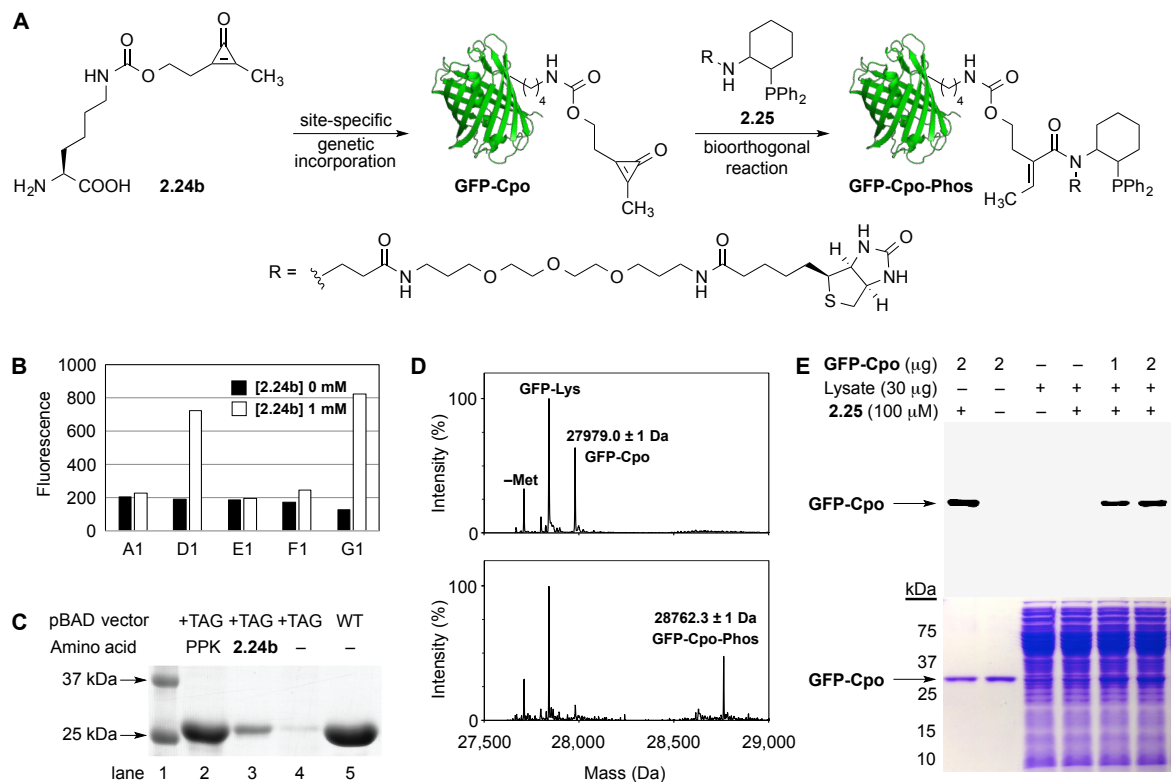


**Figure 2-10.** Cyclopropenones can be used for recombinant protein production. (A) Overall strategy for incorporating noncanonical amino acid **2.24b** into GFP via amber codon suppression. **GFP-Cpo** was targeted with phosphine probe **2.25**. (B) A library of PylRS mutants was screened to identify synthetases compatible with **2.24b**. (C) **GFP-Cpo** was expressed in the presence of **2.24b**. Minimal GFP expression was observed in the absence of **2.24b**. (D) ESI-Q-TOF mass spectrometry analysis of the genetic incorporation and reactivity of cyclopropenone **2.24b**. Reactions between **GFP-Cpo** (30 μM) and phosphine **2.25** (500 μM) were performed in PBS (pH 7) at 37 °C. Quantitative conversion was observed. (E) The cyclopropenone– phosphine ligation enables sensitive imaging in complex mixtures. Bacterial cell lysate containing **GFP-Cpo** (1–2 μg) was treated with phosphine-biotin **2.25** (100 μM) for 1 h at 37 °C. Covalent adducts were detected via Western blot with avidin staining (above). Protein loading was assessed with Coomassie staining (below).

AARSs. We used such existing libraries to identify ncAA-RS mutants that were permissive to the cyclopropanone amino acid **2.24b** (Figure 2-10B).

We screened a panel of 96 previously selected pyrrolysine *Methanosarcina barkeri* amino acyl-tRNA synthetases/(Mb)tRNA<sub>CUA</sub> pairs (ncAA-PylRS/tRNA) for permissivity toward **2.24b**, while maintaining their fidelity against native amino acids [19, 37]. Two PylRS/tRNA pairs that had been previously selected for photoprotected lysine (PPK) and photoprotected ornithine (PPO) derivatives were able to incorporate **2.24b** (Figure 2-10B). It is important to note that the two PylRS/tRNA mutants (D1 and G1) harbor Cys at the active site, highlighting again the biocompatibility of the cyclopropanone motif.

While the efficiency of incorporation was low compared to other ncAA-PylRS/tRNA pairs, G1-RS was capable of incorporating **2.24b** in response to an amber codon-disrupted GFP gene (GFP-150-TAG), resulting in expression of **GFP-Cpo** (Figure 2-10B and 2-10-C, lane 3). We also found that only a single mutation (Y306T) in G1-RS was necessary to facilitate **2.24b** incorporation and GFP-Cpo production (Figure 2-11). In all cases, minimal GFP was translated when **2.24b** was withheld (Figure 2-10C, lane 4). To verify that **2.24b** was stable in complex media and could be incorporated into recombinant proteins, we compared the masses of **GFP-Cpo** to **GFP-WT** and **GFP-PPK** using ESI-Q-TOF mass analysis. Native GFP (**GFP-WT**) exhibited the expected mass of  $27828.9 \pm 1$  Da and **GFP-Cpo** showed the expected mass increase to  $27979.0 \pm 1$  Da, verifying that **2.24b** is installed at a single site (Figure 2-10D). Lysine incorporation was also detected in the **GFP-Cpo** sample, perhaps due to

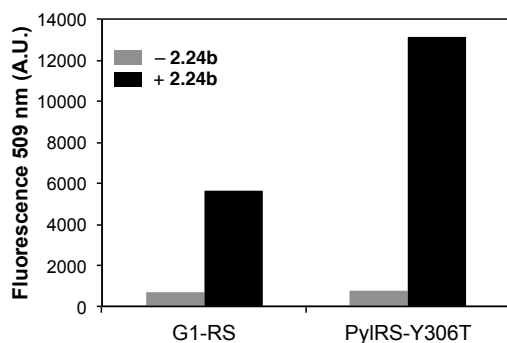


**Figure 2-11.** Fluorescence measurements comparing incorporation of **2.24b** with PyIRS mutant G1-RS and the PyIRS-Y306T. TOP10 cells expressing GFP-150-TAG and G1-RS or PyIRS-Y306T were incubated in AIM with **2.24b** (0 or 1 mM) for 48 h. Note that the PyIRS-Y306T mutant originates from *M. mazei*, while the G1-RS mutant is from *M. barkeri* (residue numbering is different in these mutants).

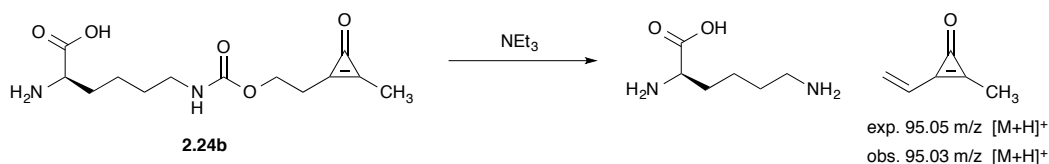


**Figure 2-12.** Possible base-promoted cleavage of carbamate **2.24b**. When aqueous solutions of **2.24** were treated with triethylamine, cleavage products were observed via mass spectrometry.

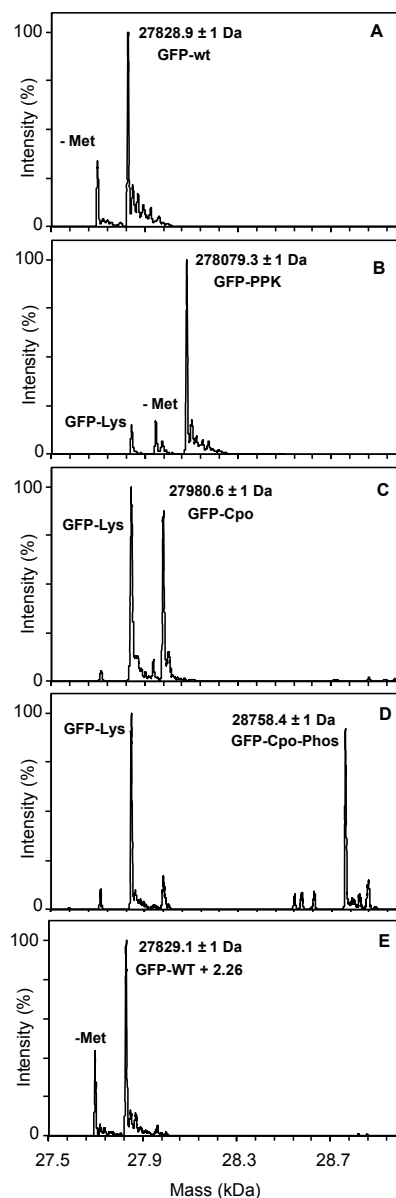


**Figure 2-13.** ESI-MS of amber codon interrupted GFP. A) ESI-MS of **GFP-WT** conforms to the expected mass, showing a single major peak at  $27828.9 \pm 1$  Da (expected mass 27827.3). B) ESI-MS of **GFP-PPK** shows a major peak at  $28079.3 \pm 1$  Da (expected mass 28079.3 Da) and a minor peak at  $27946.8 \pm 1$  Da (**GFP-Lys** expected mass 27841.4 Da) which could result from lysine incorporation or photodeprotection of **GFP-PPK**. C) ESI-MS of **GFP-Cpo** contains two major peaks; one with a mass of  $27842.3 \pm 1$  Da (**GFP-Lys** has an expected mass of 27841.4 Da), and the second with a mass of  $27980.6 \pm 1$  Da (**GFP-Cpo** has an expected mass 27978.5 Da). D) ESI-MS of **GFP-Cpo-Phos** shows two major peaks; one matching the unreacted **GFP-Lys** (expected mass 27841.4 Da) and the second major peak showing a mass of  $28758.4 \pm 1$  Da (expected mass of **GFP-Cpo-Phos** is 28757.5 Da). E) ESI-MS of the reaction containing **GFP-WT + 2.26** was used as a negative control during the reaction and has a mass of  $27829.1 \pm 1$  Da and conforms to the expected mass of 27827.3 Da for unreacted **GFP-WT**. Each sample showed a small secondary peak at -131 Da indicating cleavage of N-terminal methionines.

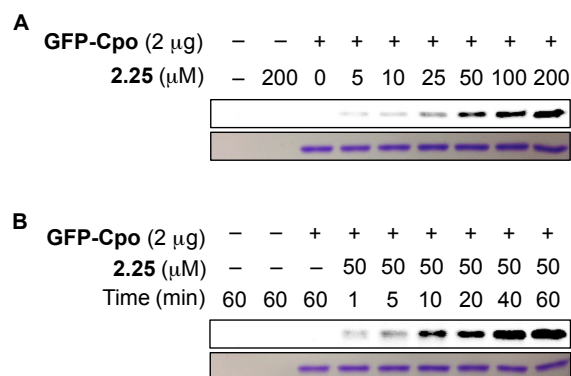
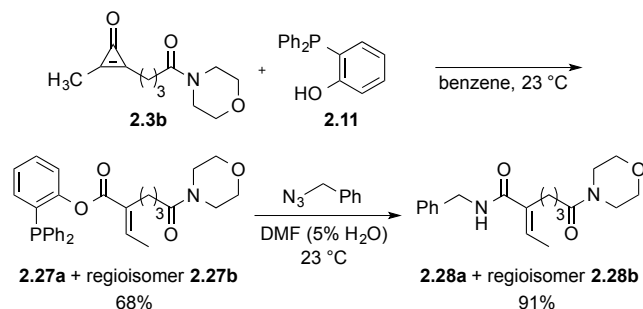


**Figure 2-14.** GFP-Cpo can be labeled with phosphine-biotin **2.25** in a time and dose dependent manner. GFP-Cpo (2 μg/mL) was reacted with **2.25** (0–200 μM) in PBS (pH 7.0) at 37 °C for 0–60 min. Reaction progress was assessed by Western blot.

carbamate cleavage (Figure 2-12) or reduced synthetase fidelity (i.e., canonical lysine was incorporated in response to the amber codon). Lysine incorporation was also observed when G1-RS was used to install PPK or PPO into GFP-150-TAG, (Figure 2-13D).

We further identified conditions to ligate cyclopropenone-modified proteins with phosphine probes. GFP-Cpo was incubated with various concentrations of phosphine-biotin **2.25** in PBS (pH 7) at 37 °C. Dose- and time-dependent labeling was observed via Western blot (Figure 2-14), and reactions appeared complete within 1 h (using 50 μM phosphine-biotin). The identity of the ligated product was confirmed using mass spectrometry (expected 28763.4 Da; observed 28762.3 ± 1 Da, Figure 2-10D). Successful ligation of GFP-Cpo was also achieved using triaryl phosphine probe **2.26** (Figure 2-13).

**Scheme 2-3.** Sequential Cyclopropenone-Phosphine and Traceless Staudinger Ligations



As a testament to the exquisite selectivity of the cyclopropenone–phosphine reaction, **GFP-Cpo** was successfully ligated in complex mixtures. Micromolar concentrations of phosphine-biotin **2.25** and short labeling times (1 h) were sufficient to detect **GFP-Cpo** in cell lysate, with no background labeling observed (Figure 2-10E). Overall, these data suggest that cyclopropenone noncanonical amino acids will be suitable for genetic code expansion and other applications in the most complex biological settings.

As noted earlier, the unique mechanism of the cyclopropenone–phosphine ligation makes it a good candidate for labeling applications in conjunction with other bioorthogonal chemistries, including inverse electron-demand Diels–Alder cycloadditions [17, 38, 39], dipolar cycloadditions, and several azide–alkyne reactions [1, 2, 14]. The latter class of transformations is particularly noteworthy, as the reagents – like the cyclopropenones reported here – are robust enough for intracellular work. It also did not escape our attention that the products of the cyclopropenone–phosphine ligation are analogous to classic traceless Staudinger reagents [40, 41], making them potential bioorthogonal probes for azides. To demonstrate this reactivity, we treated

regioisomers **2.27a,b** with a model azide (benzyl azide) in acetonitrile (Scheme 2-3). Only trace amounts of the desired amides were observed, although the starting materials were fully consumed. Mass spectrometry and NMR analyses indicated the formation of the stabilized aza-ylide (data not shown) [42-44]. More polar solvents (5% H<sub>2</sub>O/DMF) facilitated clean conversion to the expected amides **2.28a,b** [44]. Collectively, these data demonstrate that the cyclopropenone ligation will be useful for sequential labeling applications with azides and other bioorthogonal reagents. Future studies will examine the sequential ligations in cellular environments.

### **2.3 Conclusions**

In conclusion, improved dialkyl cyclopropenones for bioorthogonal labeling were generated. These motifs are highly stable in aqueous environments and in the presence of biological nucleophiles. Through kinetic analyses, we further identified phosphines that react with dialkyl cyclopropenones at rates suitable for biological application. Interestingly, our data suggest that hydrogen bonding can accelerate the reactions.

We also synthesized a noncanonical amino acid comprising a cyclopropenone motif, and identified compatible mutant synthetases for genetic incorporation. These tools can be employed for recombinant protein production and site-specific tagging experiments. Downstream cellular applications will benefit from improved incorporation efficiencies with the PyIRS/tRNA pairs, and work along these lines is underway.

More broadly, the stabilized cyclopropenones identified here will provide new opportunities for biological application. The cyclopropenones are suitable for use in intracellular and other stringent environments, and by virtue of their unique reactivities,



these scaffolds are likely compatible with a variety of other bioorthogonal groups. The products of the cyclopropanone–phosphine ligation are also reactive with azides, suggesting utility for in-tandem labeling experiments.

## **2.4 Materials and methods**

### **2.4a General information**

All reagents and solvents were used as received, unless specified otherwise. Anhydrous organic solvents were prepared by degassing with argon and passing through two 4 x 36 in. columns of anhydrous neutral A2 (8 x 12 mesh; LaRoche Chemicals; activated at 350 °C for 12 h under a flow of argon). Column chromatography was carried out using Silicycle 60 Å (32–64 mesh) silica gel. Thin layer chromatography (TLC) was carried out with Merck Millipore 250 mm silica gel F-254 plates, and plates were visualized using UV light or KMnO<sub>4</sub> stain. Organic solutions were concentrated under reduced pressure using a Büchi rotary evaporator. HPLC purifications were performed on a Varian ProStar equipped with 325 Dual Wavelength UV-Vis Detector, using an Agilent Prep-C18 Scalar column (9.4 x 150 mm, 5 µm) with a 4 mL/min flow rate.

<sup>1</sup>H, <sup>13</sup>C, <sup>19</sup>F, and <sup>31</sup>P NMR spectra were obtained using either a Bruker DRX400 or a Bruker DRX500 instrument equipped with a cryo probe. <sup>1</sup>H NMR spectra were acquired at 400 MHz or 500 MHz, <sup>13</sup>C NMR spectra were acquired at 126 MHz, <sup>19</sup>F NMR spectra were obtained at 376 MHz, and <sup>31</sup>P NMR spectra were acquired at 162 MHz. Spectra are internally referenced to residual solvent signals (CDCl<sub>3</sub> is referenced to 7.27 ppm for <sup>1</sup>H and 77.16 ppm for <sup>13</sup>C, CD<sub>3</sub>OD is referenced to 3.31 ppm for <sup>1</sup>H and

49.0 for  $^{13}\text{C}$ ,  $\text{CD}_3\text{CN}$  is referenced to 1.94 ppm for  $^1\text{H}$  and 118.26 ppm for  $^{13}\text{C}$ ,  $\text{D}_2\text{O}$  is referenced to 4.79 ppm for  $^1\text{H}$ ,  $\text{C}_6\text{D}_6$  is referenced to 7.16 ppm for  $^1\text{H}$  and 128.06 for  $^{13}\text{C}$ ).  $^{19}\text{F}$  and  $^{31}\text{P}$  NMR spectra were referenced by indirect absolute chemical shift to residual protio solvent signals. All spectra were acquired at 298 K. Chemical shifts are reported in ppm, and coupling constants ( $J$ ) are reported in Hz. Mass spectra were acquired at the University of California, Irvine Mass Spectrometry Facility.

### **2.4b Stability experiments**

Cyclopropenone aqueous stabilities were assessed by dissolving compounds **2.3b**, **2.5**, **2.7–2.10** and **2.24a** in 20%  $\text{CD}_3\text{CN}/d\text{-PBS}$  or 100%  $d\text{-PBS}$  (final concentration 10 mM). The solutions were incubated in NMR tubes at room temperature or in an incubator at 37 °C.  $^1\text{H}$ -NMR spectra were acquired periodically for 0–7 d.

Cyclopropenone stability to L-cysteine was assessed by dissolving compounds **2.3b**, **2.5**, **2.7–2.10**, and **2.24a** in a 1:1 ratio with L-cysteine in 20%  $\text{CD}_3\text{CN}/d\text{-PBS}$  or 100%  $d\text{-PBS}$  (final concentration 5 mM). The solutions were incubated in NMR tubes at room temperature or in an incubator at 37 °C.  $^1\text{H}$ -NMR spectra were acquired periodically for 0–24 h.

### **2.4c Kinetic experiments**

All kinetic experiments were carried out at room temperature in benzene- $d_6$ . Reaction progress was monitored via  $^1\text{H}$  NMR spectroscopy, using trimethylsilylacetylene as an internal standard. In all cases, phosphines (**2.11–2.18**) and cyclopropenones (**2.3b** or **2.8**) were combined in a 1:1 ratio (final concentration = 10

mM, 20 mM, or 50 mM). Second order rate constants were calculated using the method of initial rates. The reported errors for second order rate constants are the standard deviation of the mean for  $n \geq 3$  independent experiments.

#### **2.4d Permissivity screening and protein characterization**

*Pyl* aminoacyl-tRNA synthetases that had been previously selected to have efficiency and fidelity for ncAAs were assessed for their ability to charge *Pyl Mb* tRNA<sub>CUA</sub> with **2.24b**. A *pALS* plasmid containing TAG 150 interrupted superfolder GFP (sfGFP) under an AraBAD promoter, and an orthogonalized copy of the *Pyl Mb* tRNA<sub>CUA</sub> under an *lpp* promoter, had been transformed into DH10b cells with a *pBK-RS* plasmid containing *Pyl* aminoacyl-tRNA synthetases. These cell stocks containing the *pALS* reporter and *pBK-RS* plasmids were used to inoculate a 96-well 3 mL deep block containing 500  $\mu$ L of non-Inducing media (NIM) per well. NIM was made with tetracycline (25  $\mu$ g/mL) and ampicillin (100  $\mu$ g/mL).

After 24 h of growth at 37 °C with shaking (250 rpm), 50  $\mu$ L NIM from each of the 48 starter block wells was used to inoculate a 96-well 3 mL deep block containing 500  $\mu$ L auto-inducing media (AIM) with 1 mM **2.24b** or no ncAA. Fluorescence measurements of the cultures were collected 30 and 48 h after inoculation using a Synergy 2 Multi-Mode Reader (BioTEK). The excitation and emission wavelengths were set to 485 nm and 528 nm, respectively. Samples were prepared by placing 200  $\mu$ L of cell suspension directly in Nunc MicroWell 96 well polypropylene plates (Sigma Aldrich).

Cell stocks of *pULTRA-PylRS-Y306T/pALS-GFP-150-TAG E. coli* TOP10 cells were used to inoculate 3 mL of LB containing ampicillin (100  $\mu$ g/mL) and spectinomycin

(50 µg/mL). After ~10 h, starter cultures were used to inoculate expression cultures. AIM expression media (25 mL) containing 1 mM **2.24b**, ampicillin (100 µg/mL), and spectinomycin (50 µg/mL) were inoculated with 250 µL of *pULTRA-PyIRS-Y306T/pALS-GFP-150* starter culture. Cultures were then incubated at 37 °C with shaking (225 rpm) for 48 h.

Cells were collected via centrifugation at 4500 rpm for 20 min at 4 °C. The supernatant was decanted and pellets were resuspended in 5 mL phosphate buffered saline (PBS, pH 7.0). Halt™ Protease Inhibitor Cocktail (Thermo Scientific) and phenylmethylsulfonyl fluoride (PMSF, 500 µM final concentration) were added. The cells were then sonicated and the lysate was centrifuged at 14,500 rpm for 30 min at 4 °C. Profinity™ IMAC resin (BioRad, 100 µL bed volume) was added to the clarified lysate and gently rocked at 4 °C for 2 h. The resin was then washed with wash buffer (20 mM imidazole in PBS, pH 7.0, 3 x 5 mL), and **GFP-Cpo** was eluted using 0.5 mL of elution buffer (250 mM imidazole in PBS, pH 7.0). The protein was then concentrated in a centrifuge spin concentration column (3 kDa MW cutoff) to 100 µL. PBS (pH 7.0) was added to bring the volume to 500 µL, and the sample was again concentrated to 100 µL. This was repeated four times to remove excess imidazole. Protein concentration was measured with a BioSpec-mini UV-vis spectrophotometer (Shimadzu), measuring absorbance at 488 nm and using an extinction coefficient of 88,300 M<sup>-1</sup> cm<sup>-1</sup> [45]. Purified samples were analyzed by SDS-PAGE (12%, 150 V, 70 min).

To assess incorporation of **2.24b** into site 150 of GFP, pure protein was analyzed using an FT LTQ mass spectrometer and Millipore C<sub>4</sub> zip tips at the Oregon State University mass spectrometry facility. Pure **GFP-Cpo** (200 nM) was reacted with

phosphine-biotin **2.26** (~20 mM) for 20 hrs. **GFP-WT** was also incubated with **2.26** as a negative control. The reactions were analyzed using an FT LTQ mass spectrometer and Millipore C<sub>4</sub> zip tips at the Oregon State University mass spectrometry facility. Reactions with phosphine-biotin **2.25** were analyzed by mass spectrometry at the University of California, Irvine Mass Spectrometry Facility. **GFP-Cpo** (30 μM) was reacted with phosphine-biotin **2.25** (500 μM) for 4 h at 37 °C, then analyzed using a Waters Xevo G2-XS QToF mass spectrometer.

#### ***2.4e Western blot analysis of GFP-Cpo conjugates***

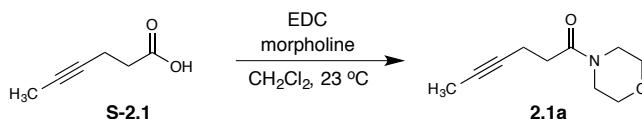
**GFP-Cpo** (4 μL, 1 mg/mL in PBS, 2 μg/mL final concentration) and phosphine-biotin **2.25** (0.75 μL, 1–10 mM in DMSO; final concentration of **2.25** was 5–200 μM) were mixed in a total volume of 30 μL (PBS, pH 7.0), and incubated at 37 °C for 0–60 min. For time and dose experiments, reactions were quenched by the addition of 1 μL of a solution of **2.8** (100 mM in DMSO). For cell lysate experiments, overnight cultures of *E. coli* XL1 cells were grown in LB containing tetracyclin (10 μg/mL) at 37 °C with shaking (225 rpm). Cells were collected via centrifugation, resuspended in PBS (pH 7.0), sonicated, and then centrifuged (14,500 rpm, 20 min 4 °C). The total protein concentration of the clarified lysate was determined using a BCA protein assay kit (Pierce). Lysate was then used directly in labeling experiments at a final concentration of 30 μg/mL.

At the conclusion of each reaction, 10 μL of SDS-PAGE loading dye (containing 8% BME) were added, and samples were heated at 95 °C for 5 min. The samples were split evenly into 2 portions and separated by gel electrophoresis using 12%

polyacrylamide gels. For each experiment, one gel was stained with Coomassie Blue to assess protein loading, while the second gel was electroblotted to a nitrocellulose membrane (0.2  $\mu\text{m}$ , BioRad). Membranes were stained with Ponceau S to assess transfer efficiency, then rinsed with  $\text{H}_2\text{O}$  and incubated with blocking buffer (7% BSA in PBS containing 1% Tween-20<sup>®</sup>, PBST) for 1 h at room temperature or overnight at 4  $^\circ\text{C}$ . The membranes were then treated with IRDye<sup>®</sup> 800CW streptavidin (LI-COR Biosciences; 1:10,000 dilution in blocking buffer) for 2 h at room temperature. Membranes were then washed with PBST (6 x 10 min) and PBS (3 x 5 min). Blots were imaged using an Odyssey infrared imaging system (LI-COR, Odyssey version 3.0).

#### 2.4f Synthetic procedures

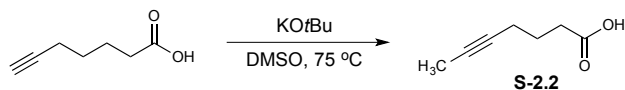
**S-2.1** [46], **S-2.5** [31], **S-2.8** [47], **S-2.10** [48], **2.11–2.13** [23], and **2.14** [49] were prepared according to literature procedures.



#### 1-Morpholinohex-4-yn-1-one (2.1a)

This compound was prepared following the general procedure of King-Underwood *et al.* [50], with some modifications. To a flame-dried 100 mL round-bottom flask containing a stir bar was added anhydrous  $\text{CH}_2\text{Cl}_2$  (20 mL), followed by **S-2.1** (620 mg, 5.54 mmol), under an atmosphere of  $\text{N}_2$ . 1-Ethyl-3-(3-dimethylaminopropyl) carbodiimide (EDC, 1.17 g, 7.55 mmol) was then added with rapid stirring. Morpholine

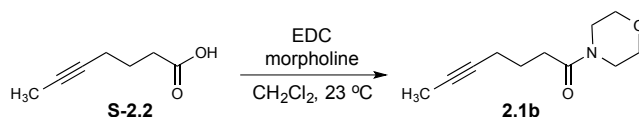
(0.60 mL, 6.9 mmol) was added dropwise, and the reaction was stirred at room temperature overnight. The reaction was then diluted with CH<sub>2</sub>Cl<sub>2</sub> (50 mL) and washed with H<sub>2</sub>O (2 x 25 mL), brine (1 x 25 mL), and 1 M HCl (2 x 25 mL). The organic layer was then dried over MgSO<sub>4</sub> and filtered. The filtrate was concentrated *in vacuo*, and the residue was purified by flash column chromatography (eluting with 50% EtOAc/hexanes) to provide **2.1a** (610 mg, 3.37 mmol, 61%) as a yellow oil. <sup>1</sup>H NMR (400 MHz, CDCl<sub>3</sub>) δ 3.69–3.67 (m, 4H), 3.64–3.62 (m, 2H), 3.50–3.48 (m, 2H), 2.52–2.49 (m, 4H), 1.78 (app t, 3H). <sup>13</sup>C (126 MHz, CDCl<sub>3</sub>) δ 170.3, 78.1, 76.3, 67.0, 66.8, 46.0, 42.1, 32.7, 15.0, 3.7. HRMS (ESI+) calculated for C<sub>10</sub>H<sub>15</sub>NO<sub>2</sub>Na [M+Na]<sup>+</sup> *m/z* 204.1001, found 204.1005.



### Hept-5-ynoic acid (S-2.2)

Compound **S-2.2** was prepared following the general procedure of Schulz *et al.* [46] To a flame-dried round-bottom flask equipped with a stir bar was added 6-heptynoic acid (1.10 g, 8.73 mmol), followed by anhydrous DMSO (18 mL). While stirring vigorously, potassium *tert*-butoxide (2.05 g, 18.3 mmol) was added. The reaction was then immersed in an oil bath at 75 °C and stirred rapidly with venting for 10 min. The flask was allowed to cool to room temperature before quenching with 1 M HCl (50 mL). The organic layer was separated and the aqueous layer was extracted with diethyl ether (3 x 20 mL). The combined organic layers were then dried over MgSO<sub>4</sub> and filtered. The filtrate was concentrated *in vacuo*, and the residue was purified by flash column

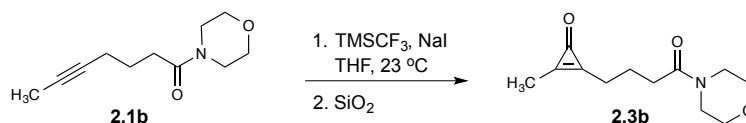
chromatography (eluting with 25% EtOAc/hexanes) to provide **S-2.2** (885 mg, 7.02 mmol, 80%) as a white solid. NMR spectra matched those previously reported [47].



### 1-Morpholinohept-5-yn-1-one (**2.1b**)

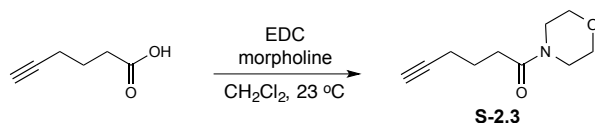
This compound was prepared following the general procedure of King-Underwood *et al.* [50], with some modifications. To a flame-dried 100 mL round-bottom flask containing a stir bar was added anhydrous  $\text{CH}_2\text{Cl}_2$  (20 mL), followed by **S-2.2** (0.708 g, 5.62 mmol), under an atmosphere of  $\text{N}_2$ . EDC (1.22 g, 7.86 mmol) was then added with rapid stirring. Morpholine (0.59 mL, 6.8 mmol) was added dropwise, and the solution was stirred at room temperature overnight. The reaction was then diluted into  $\text{CH}_2\text{Cl}_2$  (50 mL) and washed with  $\text{H}_2\text{O}$  (2 x 25 mL), brine (1 x 25 mL), and 1 M HCl (2 x 25 mL). The organic layer was dried over  $\text{MgSO}_4$  and filtered. The filtrate was concentrated *in vacuo*, and the residue was purified by flash column chromatography (eluting with 50% EtOAc/hexanes) to provide **2.1b** (730 mg, 3.74 mmol, 66%) as a yellow oil.  $^1\text{H}$  NMR (400 MHz,  $\text{CDCl}_3$ )  $\delta$  3.70–3.67 (m, 2H), 3.64–3.61 (m, 2H), 3.52–3.49 (m, 2H), 2.44 (t,  $J = 7.5$  Hz, 2H), 2.23 (tq,  $J = 6.8, 2.5$  Hz, 2H) 1.82 (quin,  $J = 7.2$  Hz, 2H), 1.78 (t,  $J = 2.6$  Hz, 3H).  $^{13}\text{C}$  (126 MHz,  $\text{CDCl}_3$ )  $\delta$  171.4, 78.5, 76.5, 67.1, 66.8, 46.1, 42.0, 31.8, 24.5, 18.5, 3.6. HRMS (ESI+) calculated for  $\text{C}_{11}\text{H}_{17}\text{NO}_2\text{Na}$   $[\text{M}+\text{Na}]^+$   $m/z$  218.1157, found 218.1158.





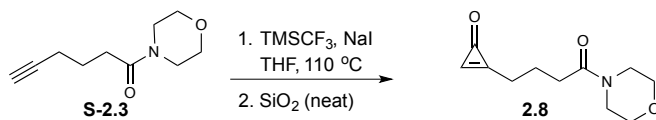
### 2-Methyl-3-(4-morpholino-4-oxobutyl)cycloprop-2-en-1-one (2.3b)

To an oven-dried Schlenk tube containing a stir bar was added NaI (0.330 g, 2.20 mmol). The NaI was then gently flame-dried under vacuum. Compound **2.1b** (0.195 g, 1.00 mmol) and anhydrous THF (3.0 mL) were then added against positive N<sub>2</sub> flow. Trifluoromethyltrimethylsilane (0.30 mL, 2.0 mmol) was added, and the Schlenk tube was sealed. The reaction was stirred vigorously at room temperature for 24 h, and then diluted with H<sub>2</sub>O (20 mL) and extracted into CH<sub>2</sub>Cl<sub>2</sub> (3 x 10 mL). The combined organic layers were dried over MgSO<sub>4</sub> and filtered. The filtrate was concentrated *in vacuo*, and the residue was purified by flash column chromatography (eluting with 5% MeOH/CH<sub>2</sub>Cl<sub>2</sub>) to give **2.3b** as a yellow oil (79 mg, 0.35 mmol, 35%). <sup>1</sup>H NMR (500 MHz, CDCl<sub>3</sub>) δ 3.70–3.67 (m, 4H), 3.63–3.61 (m, 2H), 3.52–3.50 (m, 2H), 2.71 (app t, *J* = 7.1 Hz, 2H), 2.50 (t, *J* = 7.1 Hz, 2H), 2.28 (t, *J* = 0.9 Hz, 3H), 2.06 (quin, *J* = 7.1 Hz, 2H). <sup>13</sup>C NMR (126 MHz, CDCl<sub>3</sub>) δ 170.4, 161.0, 159.7, 157.4, 67.0, 66.7, 46.0, 42.1, 31.7, 26.0, 21.6, 11.5. HRMS (ESI+) calculated for C<sub>12</sub>H<sub>17</sub>NO<sub>3</sub>Na [M+Na]<sup>+</sup> *m/z* 246.1106, found 246.1117.



### 1-Morpholinohex-5-yn-1-one (S-2.3)

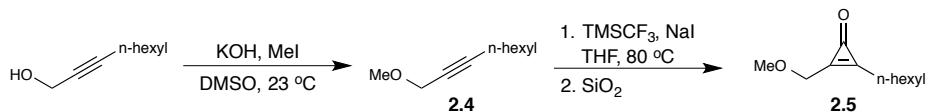
This compound was prepared following the general procedure of King-Underwood *et al.* [50] with some modifications. To a flame-dried 100 mL round-bottom flask containing a stir bar was added anhydrous  $\text{CH}_2\text{Cl}_2$  (20 mL), followed by 5-heptynoic acid (1.00 g, 8.93 mmol), under an atmosphere of  $\text{N}_2$ . EDC (1.93 g, 12.5 mmol) was added with rapid stirring. Morpholine (0.93 mL, 11 mmol) was added dropwise, and the solution was stirred at room temperature overnight. The reaction was then diluted into  $\text{CH}_2\text{Cl}_2$  (50 mL) and washed with  $\text{H}_2\text{O}$  (2 x 20 mL), brine (1 x 20 mL), and 1 M HCl (2 x 20 mL). The organic layer was dried over  $\text{MgSO}_4$  and filtered. The filtrate was concentrated *in vacuo*, and the residue was purified by flash column chromatography (eluting with 50% EtOAc/hexanes) to provide **S-2.3** (1.00 g, 5.52 mmol, 62%) as a yellow oil. Spectra matched those previously reported [50].



### 2-(4-Morpholino-4-oxobutyl)cycloprop-2-en-1-one (2.8)

This compound was made following our previously reported procedure [23] with some modifications. To an oven-dried Schlenk tube containing a stir bar was added NaI (0.330 g, 2.20 mmol). The NaI was then gently flame-dried under vacuum. Compound **S-2.3** (0.181 g, 1.00 mmol) and anhydrous THF (3.0 mL) were added against positive

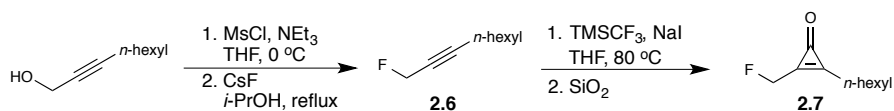
N<sub>2</sub> flow. Trifluoromethyltrimethylsilane (0.30 mL, 2.0 mmol) was added, and the Schlenk tube was sealed. The reaction was stirred vigorously in an oil bath at 110 °C for 3 h, then removed and allowed to cool to room temperature. The reaction was diluted with H<sub>2</sub>O (20 mL) and extracted into Et<sub>2</sub>O (3 x 10 mL). The combined organic layers were then dried over MgSO<sub>4</sub> and filtered. The filtrate was concentrated *in vacuo*, and the residue was dry-loaded onto silica (1 g) and left at room temperature for 24 h. The silica was then loaded directly onto a column and purified by flash column chromatography (eluting with 5% MeOH/CH<sub>2</sub>Cl<sub>2</sub>) to give **2.8** as a yellow solid (22 mg, 0.11 mmol, 11%). NMR spectra matched those previously reported [23].



### 2-Hexyl-3-(methoxymethyl)cycloprop-2-en-1-one (2.5)

To a flame-dried 100 mL round-bottom flask was added 2-nonyn-1-ol (280 mg, 2.00 mmol), anhydrous DMSO (40 mL), and KOH (450 mg, 8.04 mmol). The solution was stirred under N<sub>2</sub> at room temperature for 20 min. Methyl iodide (0.13 mL, 4.0 mmol) was then added dropwise and the reaction was stirred for 2 h. The reaction was then quenched with saturated NH<sub>4</sub>Cl and diluted with H<sub>2</sub>O (50 mL). The aqueous layer was extracted into Et<sub>2</sub>O (3 x 20 mL), and the combined organic layers were washed with brine (50 mL), dried over MgSO<sub>4</sub>, and filtered. The filtrate was then concentrated *in vacuo* to give **2.4** as a colorless oil, which was used directly without additional purification.

To an oven-dried Schlenk tube containing a stir bar was added NaI (146 mg, 0.973 mmol). The NaI was then gently flame-dried under vacuum. Compound **2.4** and anhydrous THF (1.3 mL) were added against positive N<sub>2</sub> flow. Trifluoromethyltrimethylsilane (0.13 mL, 0.88 mmol) was added, and the Schlenk tube was sealed. The reaction was stirred vigorously in an oil bath at 80 °C for 2 h, then removed and allowed to cool to room temperature. The solution was diluted with H<sub>2</sub>O (20 mL) and extracted into CH<sub>2</sub>Cl<sub>2</sub> (3 x 10 mL). The combined organic layers were dried over MgSO<sub>4</sub> and filtered. The filtrate was then concentrated *in vacuo*, and the residue was dry-loaded onto silica (1 g) and left at room temperature for 24 h. The silica residue was then loaded directly onto a column and purified by flash column chromatography (eluting with 10% acetone/EtOAc) to give **2.5** as a colorless oil (25 mg, 0.14 mmol, 7% over 2 steps). <sup>1</sup>H NMR (500 MHz, CDCl<sub>3</sub>) δ 4.50 (t, *J* = 1.2 Hz, 2H), 3.46 (s, 3H), 2.65 (tt, *J* = 7.4, 1.1 Hz, 2H), 1.72 (quin, *J* = 7.5 Hz, 2H), 1.43–1.37 (m, 2H), 1.33–1.30 (m, 4H), 0.90 (app t, *J* = 7.0 Hz, 3H). <sup>13</sup>C NMR (126 MHz, CDCl<sub>3</sub>) δ 160.8, 158.4, 157.9, 67.6, 59.2, 31.5, 29.0, 26.6, 26.3, 22.6, 14.2. HRMS (ESI+) calculated for C<sub>11</sub>H<sub>18</sub>O<sub>2</sub>Na [M+Na]<sup>+</sup> 205.1205 *m/z*, found 205.1205.



### 2-(Fluoromethyl)-3-hexylcycloprop-2-en-1-one (2.7)

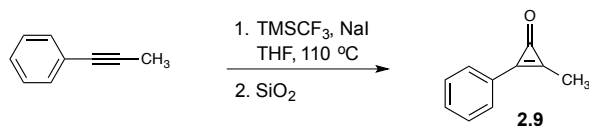
To a flame-dried 100 mL round-bottom flask containing a stir bar was added 2-nonyn-1-ol (500 mg, 3.57 mmol), anhydrous THF (20 mL), and triethylamine (1.4 mL, 7.2 mmol). The solution was then cooled to 0 °C with stirring under an atmosphere of

N<sub>2</sub>. Methanesulfonyl chloride (0.70 mL, 6.5 mmol) was added dropwise, and the reaction was stirred for an additional 5 min. The solution was then diluted with Et<sub>2</sub>O (20 mL) and washed with 1 M HCl (1 x 20 mL), H<sub>2</sub>O (1 x 20 mL), saturated NaHCO<sub>3</sub> (1 x 20 mL), and brine (1 x 20 mL). The organic layer was then dried over MgSO<sub>4</sub> and filtered. The filtrate was concentrated *in vacuo* to provide the mesylate as a yellow oil which was used directly without further purification.

To a flame-dried two-necked round bottom flask containing a stir bar was added CsF (790 mg, 5.20 mmol), followed by *i*-PrOH (5 mL, dried over 4 Å molecular sieves). The solution was heated to reflux and stirred rapidly until the CsF dissolved completely. The crude mesylate was then added dropwise as a solution in *i*-PrOH (2.0 mL), and the reaction was stirred at reflux overnight. The mixture was filtered, the filtrate was washed with H<sub>2</sub>O (3 x 15 mL), dried over MgSO<sub>4</sub>, and filtered. The filtrate was concentrated *in vacuo* at 4 °C to give **2.6**, which was found to be volatile and was used directly without purification.

To an oven-dried Schlenk tube containing a stir bar was added NaI (251 mg, 1.67 mmol). The NaI was then gently flame-dried under vacuum. Compound **2.6** and anhydrous THF (2.3 mL) were then added against positive N<sub>2</sub> flow. Trifluoromethyltrimethylsilane (0.23 mL, 1.5 mmol) was added, and the Schlenk tube was sealed. The reaction was stirred vigorously in an oil bath at 80 °C for 2.5 h, then removed and allowed to cool to room temperature. The solution was then diluted with H<sub>2</sub>O (20 mL) and extracted into CH<sub>2</sub>Cl<sub>2</sub> (3 x 10 mL). The combined organic layers were then dried over MgSO<sub>4</sub> and filtered. The filtrate was concentrated *in vacuo*, and the residue was dry-loaded onto silica (1 g) and left at room temperature for 24 h. The silica

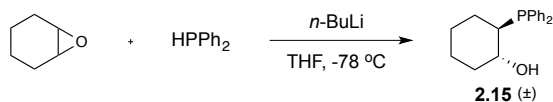
was then loaded directly onto a column and purified by flash column chromatography (eluting with 50% EtOAc/hexanes) to give **2.7** as a yellow oil (62 mg, 0.36 mmol, 10% over 3 steps).  $^1\text{H}$  NMR (500 MHz,  $\text{CDCl}_3$ )  $\delta$  5.46 (dt,  $J = 47.9, 1.4$  Hz, 2H), 2.70 (tt,  $J = 7.4, 1.2$  Hz, 2H), 1.73 (quin,  $J = 7.3$  Hz, 2H), 1.44–1.30 (m, 6H), 0.90 (app t,  $J = 7.0$  Hz, 3H).  $^{13}\text{C}$  NMR (126 MHz,  $\text{CDCl}_3$ )  $\delta$  160.8 (d,  $J = 14.6$  Hz), 156.5 (d,  $J = 20.9$  Hz), 156.0 (d,  $J = 12.5$  Hz), 78.9 (d,  $J = 181.8$  Hz), 31.4, 29.0, 26.4 (d,  $J = 1.6$  Hz), 26.2 (d,  $J = 1.1$  Hz), 22.6, 14.1.  $^{19}\text{F}$  NMR (376 MHz,  $\text{CDCl}_3$ )  $\delta$  -225.8. HRMS (ESI+) calculated for  $\text{C}_{10}\text{H}_{15}\text{FONa}$   $[\text{M}+\text{Na}]^+$  193.1005  $m/z$ , found 193.0997.



## 2-Methyl-3-phenylcycloprop-2-en-1-one (**2.9**)

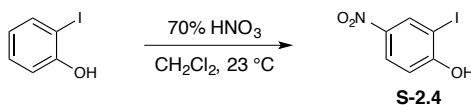
To an oven-dried Schlenk tube containing a stir bar was added NaI (0.330 g, 2.20 mmol). The NaI was then gently flame-dried under vacuum. 1-Phenyl-1-propyne (0.116 g, 1.00 mmol) and anhydrous THF (3.0 mL) were added against positive  $\text{N}_2$  flow. Trifluoromethyltrimethylsilane (0.30 mL, 2.0 mmol) was added, and the Schlenk tube was sealed. The reaction was stirred vigorously in an oil bath at 110 °C for 2 h. The pressure tube was then allowed to cool to room temperature before the solution was diluted with  $\text{H}_2\text{O}$  (20 mL) and extracted into  $\text{CH}_2\text{Cl}_2$  (3 x 10 mL). The organic layers were combined, dried over  $\text{MgSO}_4$ , and filtered. The filtrate was concentrated *in vacuo*, and the residue was dry loaded on silica and purified by flash chromatography (eluting with 75% EtOAc/hexanes) to give **2.9** as a yellow solid (100 mg, 0.694 mmol, 69%).  $^1\text{H}$  NMR (500 MHz,  $\text{CDCl}_3$ )  $\delta$  7.81–7.79 (m, 2H), 7.58–7.52 (m, 2H), 2.51 (s, 3H).  $^{13}\text{C}$  NMR

(126 MHz, CDCl<sub>3</sub>)  $\delta$  156.9, 155.0, 151.8, 132.7, 131.2, 129.4, 124.0, 11.8. HRMS (ESI+) calculated for C<sub>10</sub>H<sub>8</sub>ONa [M+Na]<sup>+</sup> 167.0473 *m/z*, found 167.0474.



### ***trans*-2-(Diphenylphosphanyl)cyclohexan-1-ol (2.15)**

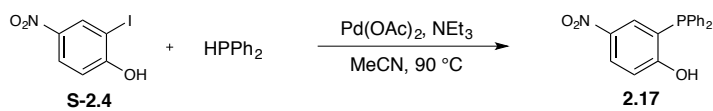
This compound was prepared following the procedure of Muller *et al.* [51], with some modifications. To a flame-dried 25 mL round-bottom flask containing a stir bar were added anhydrous THF (3 mL), cyclohexene oxide (0.10 mL, 1.0 mmol) and diphenylphosphine (0.17 mL, 1.0 mmol) under an atmosphere of argon. After cooling to  $-78$  °C, *n*-BuLi (1.2 M, 0.83 mL, 1 mmol) was added dropwise. The solution was then allowed to warm to room temperature over the course of 2 h. The reaction was quenched with brine (15 mL) and extracted into Et<sub>2</sub>O (3 x 5 mL). The organic layers were combined, dried over MgSO<sub>4</sub>, and filtered. The filtrate was concentrated *in vacuo*, and the residue was purified by flash column chromatography (eluting with 20% EtOAc/hexanes) to give **2.15** (94 mg, 0.33 mmol, 33%) as a white solid. NMR spectra matched those previously reported [51].



### **2-Iodo-4-nitrophenol (S-2.4)**

This compound was prepared following the procedure of Wynne *et al.* [52]. To a 25 mL round-bottom flask was added 2-iodophenol (280 mg, 1.3 mmol), followed by

anhydrous  $\text{CH}_2\text{Cl}_2$  (3.0 mL). Aqueous 70% nitric acid (100  $\mu\text{L}$ ) was added dropwise under  $\text{N}_2$ , at which point the solution became dark red. The solution was stirred for 3.5 h, and then diluted with  $\text{H}_2\text{O}$  (30 mL). The organic layer was removed and the aqueous layer was extracted into  $\text{CH}_2\text{Cl}_2$  (3 x 15 mL). The organic layers were combined, dried over  $\text{MgSO}_4$ , and filtered. The filtrate was concentrated *in vacuo*, and the residue was purified by flash chromatography (eluting with 25% EtOAc/hexanes) to give **S-2.4** (89 mg, 0.34 mmol, 26%) as a yellow solid. NMR spectra matched those previously reported [52].

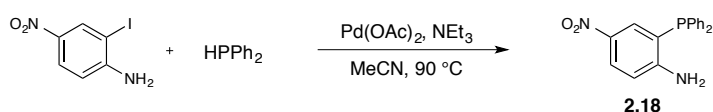


### 2-(Diphenylphosphanyl)-4-nitrophenol (2.17)

To an oven-dried Schlenk tube containing a stir bar was added **S-2.4** (68 mg, 0.26 mmol), followed by palladium acetate (2 mg, 0.01 mmol) and anhydrous acetonitrile (1 mL). The Schlenk tube was then flushed with argon before adding triethylamine (72  $\mu\text{L}$ , 0.52 mmol) and diphenylphosphine (45  $\mu\text{L}$ , 0.26 mmol). The Schlenk tube was then subjected to three freeze-pump-thaw cycles (10 min each) and sealed. The reaction was heated in an oil bath at 90  $^\circ\text{C}$  for 24 h with rapid stirring. After cooling to room temperature, the reaction was diluted with  $\text{H}_2\text{O}$  (30 mL), acidified with 1 M HCl (5 mL) and extracted into EtOAc (3 x 15 mL). The organic layers were combined, dried over  $\text{MgSO}_4$ , and filtered. The filtrate was concentrated *in vacuo*, and the residue was purified by flash chromatography (eluting with 25% EtOAc/hexanes) to give **2.17** (33 mg, 0.10 mmol, 39%) as an air-sensitive yellow solid (trace amounts of the



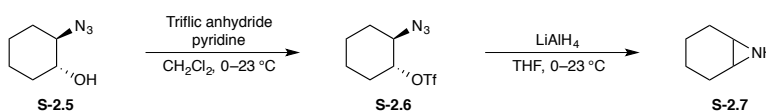
phosphine oxide present in spectra).  $^1\text{H}$  NMR (400 MHz,  $\text{C}_6\text{D}_6$ )  $\delta$  8.03 (dd,  $J = 4.3, 2.8$  Hz, 1H), 7.76 (dd,  $J = 8.9, 2.7$  Hz, 1H), 7.24–7.20 (m, 4H), 7.02–6.99 (m, 6H), 6.21 (dd,  $J = 8.9, 4.9$  Hz, 1H).  $^{31}\text{P}$  NMR (162 MHz,  $\text{C}_6\text{D}_6$ )  $\delta$  -24.8.  $^{13}\text{C}$  NMR (126 MHz,  $\text{CDCl}_3$ )  $\delta$  164.2 (d,  $J = 18.6$  Hz), 142.1, 133.6 (d,  $J = 19.3$  Hz), 133.1 (d,  $J = 4.2$  Hz), 130.8 (d,  $J = 4.0$  Hz), 130.0, 129.3 (d,  $J = 7.4$  Hz), 127.5, 123.6 (d,  $J = 11.6$  Hz), 116.3. HRMS (ESI-) calculated for  $\text{C}_{18}\text{H}_{13}\text{NO}_3\text{P}$   $[\text{M}-\text{H}]^-$  322.0633  $m/z$ , found 322.0637.



## 2-(Diphenylphosphanyl)-4-nitroaniline (2.18)

To an oven-dried Schlenk tube (with a stir bar) was added 2-iodo-4-nitroaniline (264 mg, 1.00 mmol), followed by palladium acetate (1.0 mg, 0.0040 mmol) and anhydrous acetonitrile (2.5 mL). The pressure tube was then flushed with argon before adding triethylamine (278  $\mu\text{L}$ , 2.00 mmol) and diphenylphosphine (174  $\mu\text{L}$ , 1.00 mmol). The Schlenk tube was then subjected to three freeze-pump-thaw cycles (10 min each) and sealed. The reaction was then heated in an oil bath at 90  $^\circ\text{C}$  for 24 h with rapid stirring. After cooling to room temperature, the reaction was diluted with  $\text{H}_2\text{O}$  (30 mL) and extracted into EtOAc (3 x 15 mL). The organic layers were combined, dried over  $\text{MgSO}_4$ , and filtered. The filtrate was concentrated *in vacuo*, and the residue was purified by flash chromatography (eluting with 25% EtOAc/hexanes) to give **2.18** (274 mg, 0.85 mmol, 85%) as an air-sensitive yellow solid (trace amounts of the phosphine oxide present in spectra).  $^1\text{H}$  NMR (400 MHz,  $\text{CDCl}_3$ )  $\delta$  8.07 (dd,  $J = 8.9, 2.6$  Hz, 1H), 7.74 (dd,  $J = 4.8, 2.6$  Hz, 1H), 7.44–7.38 (m, 6H), 7.35–7.32 (m, 4H), 6.66 (dd,  $J = 8.9,$

5.0 Hz, 1H), 4.87 (bs, 2H).  $^{31}\text{P}$  NMR (162 MHz,  $\text{C}_6\text{D}_6$ )  $\delta$  -19.7.  $^{13}\text{C}$  NMR (126 MHz,  $\text{CDCl}_3$ )  $\delta$  155.1 (d,  $J$  = 19.5 Hz), 139.5, 133.8 (d,  $J$  = 19.8 Hz), 133.6 (d,  $J$  = 6.9 Hz), 131.0 (d,  $J$  = 2.8 Hz), 129.8, 129.2 (d,  $J$  = 7.4 Hz), 126.9, 119.7 (d,  $J$  = 14.1 Hz), 114.1 (d,  $J$  = 2.3 Hz). HRMS (ESI+) calculated for  $\text{C}_{18}\text{H}_{15}\text{N}_2\text{O}_2\text{PNa}$   $[\text{M}+\text{Na}]^+$  345.0769  $m/z$ , found 345.0762.

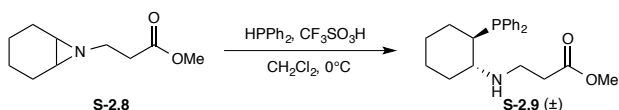


### ***cis*-7-Azabicyclo[4.1.0]heptane (S-2.7)**

To a flame-dried 50 mL round bottom flask, containing a stir bar, was added **S-2.5** (525 mg, 3.72 mmol), anhydrous  $\text{CH}_2\text{Cl}_2$  (15 mL), and pyridine (2.3 mL, 24 mmol) under an atmosphere of  $\text{N}_2$ . After cooling in an ice bath, trifluoromethanesulfonic anhydride (2.0 mL, 12 mmol) was added dropwise. The solution became dark red upon addition. The reaction was then allowed to warm to room temperature with stirring. After 30 min, the reaction was diluted with  $\text{H}_2\text{O}$  (60 mL) and extracted into  $\text{CH}_2\text{Cl}_2$  (3 x 20 mL). The organic layers were combined, dried over  $\text{MgSO}_4$ , and filtered. The filtrate was concentrated *in vacuo* to give the crude product **S-2.6** as a red oil, which was used without further purification.

To a flame-dried 50 mL round bottom flask, containing a stir bar, was added crude **S-2.6**. Anhydrous THF (20 mL) was added under an atmosphere of  $\text{N}_2$ , and the solution was cooled in an ice bath.  $\text{LiAlH}_4$  (2.0 M in THF, 3.0 mL, 6.0 mmol) was added dropwise, and the reaction was allowed to warm to room temperature. After 1 h, the reaction was cooled in an ice bath and quenched by slow addition of MeOH (0.5 mL),

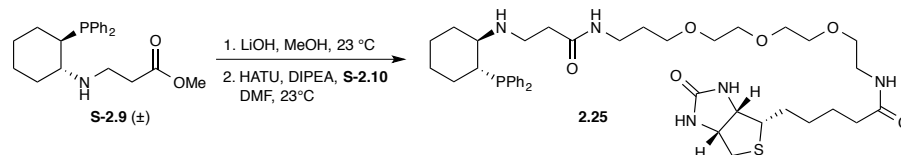
followed by H<sub>2</sub>O (1.0 mL). The reaction was allowed to warm to room temperature, and then filtered to remove lithium salts. The filtrate was diluted with H<sub>2</sub>O (50 mL) and extracted into CH<sub>2</sub>Cl<sub>2</sub> (3 x 20 mL). The organic layers were combined, dried over MgSO<sub>4</sub>, and filtered. The filtrate was concentrated *in vacuo*, and the residue was purified by flash column chromatography (eluting with 5% MeOH/CH<sub>2</sub>Cl<sub>2</sub>) to give **S-2.7** (120 mg, 1.24 mmol, 33% over 2 steps) as a light yellow oil. Spectra matched those previously reported [31].



### ***trans*-Methyl-3-((2-(diphenylphosphanyl)cyclohexyl)amino)propanoate (S-2.9)**

This compound was synthesized using the general procedure of Caiazza *et al* [31], with some modifications. To a flame-dried 25 mL round bottom flask containing a stir bar was added **S-2.8** (90 mg, 0.49 mmol). Dry, degassed CH<sub>2</sub>Cl<sub>2</sub> (5.0 mL) and diphenylphosphine (130 μL, 0.74 mmol) were added under an atmosphere of argon, and the solution was cooled to 0 °C in an ice bath. Triflic acid (44 μL, 0.49 mmol) was then added, and the reaction was allowed to warm to room temperature. After 2.5 h, degassed 1 M KOH (1 mL) was added. The reaction then was diluted with H<sub>2</sub>O (20 mL) and extracted into CH<sub>2</sub>Cl<sub>2</sub> (3 x 10 mL). The organic layers were combined, dried over MgSO<sub>4</sub>, and filtered. The filtrate was concentrated *in vacuo*, and the residue was purified by flash column chromatography (eluting with 25% EtOAc/hexanes) to give **S-2.9** (76 mg, 0.21 mmol, 42%) as an air-sensitive white solid (trace amounts of the phosphine oxide present in spectra). <sup>1</sup>H NMR (400 MHz, CDCl<sub>3</sub>) δ 7.50–7.45 (m, 4H),

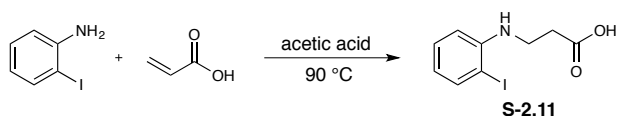
7.36–7.29 (m, 6H), 2.94 (dt,  $J = 12.0, 6.7$  Hz, 1H), 2.80 (dt,  $J = 11.8, 6.7$  Hz, 1H), 2.41 (t,  $J = 6.7$  Hz, 2H), 2.39–2.34 (m, 1H), 2.29 (td,  $J = 10.0, 3.3$  Hz, 1H), 2.17–2.12 (m, 1H), 1.75–1.66 (m, 4H), 1.26–1.19 (m, 4H), 1.03–0.95 (m, 1H).  $^{31}\text{P}$  NMR (162 MHz,  $\text{CDCl}_3$ )  $\delta$  –7.51.  $^{13}\text{C}$  NMR (126 MHz,  $\text{CDCl}_3$ )  $\delta$  173.3, 137.4 (d,  $J = 11.6$  Hz), 135.8 (d,  $J = 15.5$  Hz), 134.9 (d,  $J = 20.6$  Hz), 132.6 (d,  $J = 17.2$  Hz), 129.1, 128.5 (d,  $J = 5.9$  Hz), 128.3 (d,  $J = 7.6$  Hz), 128.1, 58.2 (d,  $J = 13.6$  Hz), 51.8, 42.3, 40.5 (d,  $J = 14.1$  Hz), 35.0, 32.6 (d,  $J = 6.4$  Hz), 27.1 (d,  $J = 2.6$  Hz), 26.1 (d,  $J = 4.7$  Hz), 24.4. HRMS (ESI+) calculated for  $\text{C}_{22}\text{H}_{28}\text{NO}_2\text{PNa}$   $[\text{M}+\text{Na}]^+$  392.1755  $m/z$ , found 392.1761.



### Biotinylated phosphine (2.25)

To a 25 mL round bottom flask containing a stir bar was added **S-2.9** (38 mg, 0.14 mmol) and degassed  $\text{MeOH}$  (2 mL) under an atmosphere of argon. Degassed 1 M  $\text{LiOH}$  (2 mL) was added dropwise and the reaction was stirred at room temperature for 4.5 h. The reaction was then neutralized with addition of 1 M  $\text{HCl}$ , and the solvent was removed *in vacuo*. The crude carboxylic acid was transferred to a flame-dried 25 mL round bottom flask and dissolved in anhydrous, degassed  $\text{DMF}$  (5 mL) under an atmosphere of argon. Diisopropylethylamine (145  $\mu\text{L}$ , 0.84 mmol) and  $\text{HATU}$  (65 mg, 0.17 mmol) were then added. After 1 min, **S-2.10** (125 mg, 0.28 mmol) was added as a solution in anhydrous, degassed  $\text{DMF}$  (3 mL), and the reaction was stirred at room temperature. After 6 h, the solvent was removed *in vacuo* and the residue was purified via HPLC (eluting with 10–90%  $\text{MeCN}$  in  $\text{H}_2\text{O}$  over 25 min) and lyophilized to provide

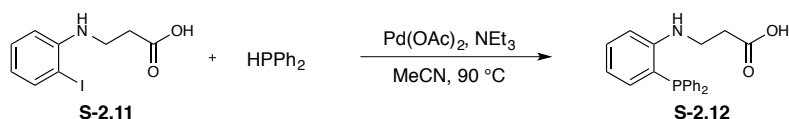
the product **2.25** (20 mg, 0.025 mmol, 18% over 2 steps) as a mixture of diastereomers. Product is a white, air sensitive solid (note phosphine oxide peaks are present in spectra).  $^1\text{H}$  NMR (400 MHz,  $\text{CD}_3\text{OD}$ )  $\delta$  7.55–7.50 (m, 4H), 7.44–7.38 (m, 6H), 4.48 (dd,  $J = 8.0, 4.9$  Hz, 1H), 4.31–4.27 (m, 1H), 3.64–3.49 (m, 12H), 3.28–3.17 (m, 5H), 2.92 (dd,  $J = 12.8, 4.8$  Hz, 1H), 2.86 (bs, 1H), 2.69 (d,  $J = 12.8$  Hz, 1H), 2.61–2.55 (m, 2H), 2.30 (bs, 1H), 2.19 (t,  $J = 7.1$  Hz, 2H), 1.90 (bs, 1H), 1.83–1.71 (m, 7H), 1.68–1.54 (m, 4H), 1.46–1.35 (m, 4H), 1.08 (bs, 1H).  $^{31}\text{P}$  NMR (162 MHz,  $\text{CD}_3\text{OD}$ )  $\delta$  -13.4.  $^{13}\text{C}$  NMR (126 MHz,  $\text{CD}_3\text{OD}$ )  $\delta$  175.9, 173.0, 166.1, 135.9 (d,  $J = 21.2$  Hz), 135.6 (d,  $J = 9.8$  Hz), 134.7 (d,  $J = 14.2$  Hz), 134.1 (d,  $J = 11.0$  Hz), 133.6 (d,  $J = 18.1$  Hz), 132.3 (d,  $J = 9.5$  Hz), 131.1, 130.5 (d,  $J = 12.9$  Hz), 130.2, 130.1 (d,  $J = 6.5$  Hz), 129.8 (d,  $J = 8.1$  Hz), 71.54, 71.50, 71.2, 69.91, 69.86, 63.4, 61.6, 59.0 (d,  $J = 17.7$  Hz), 58.1 (d,  $J = 3.8$  Hz), 57.0, 43.0, 42.5, 41.0, 38.2 (d,  $J = 17.1$  Hz), 37.9 (d,  $J = 22.4$  Hz), 36.9, 30.6, 30.3 (d,  $J = 13.9$  Hz), 29.8, 29.5, 28.4 (d,  $J = 6.7$  Hz), 27.8, 26.9, 26.8, 24.9, 24.4, 23.8. HRMS (ESI+) calculated for  $\text{C}_{41}\text{H}_{62}\text{N}_5\text{O}_6\text{PSNa}$   $[\text{M}+\text{Na}]^+$  806.4056  $m/z$ , found 806.4056.



### 3-((2-Iodophenyl)amino)propanoic acid (**S-2.11**)

To a 15 mL Schlenk tube was added 2-iodoaniline (219 mg, 1.0 mmol), followed by acetic acid (2.0 mL) and acrylic acid (0.14 mL, 2.0 mmol). The Schlenk tube was then sealed and stirred at 90 °C for 16 h. After cooling to room temperature, the reaction was diluted with  $\text{H}_2\text{O}$  (20 mL) and extracted into EtOAc (3 x 10 mL). The organic layers were combined, dried over  $\text{MgSO}_4$ , and filtered. The filtrate was concentrated *in vacuo*,

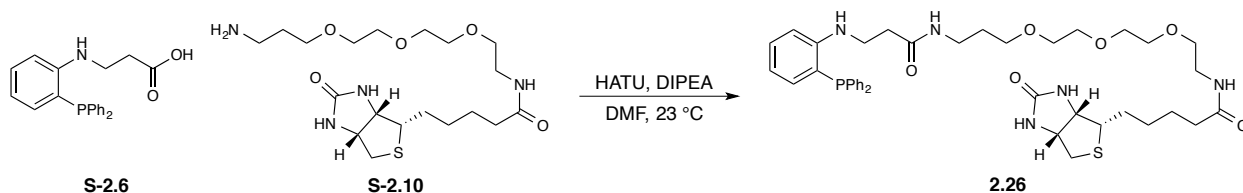
and the residue was purified by flash chromatography (eluting with 0–25% EtOAc/hexanes) to give **S-2.11** (166 mg, 0.57 mmol, 57%) as a white solid.  $^1\text{H}$  NMR (400 MHz,  $\text{CD}_3\text{CN}$ )  $\delta$  9.10 (br, 1H), 7.67, (dd,  $J = 7.8, 1.5$  Hz, 1H), 7.23 (ddd,  $J = 8.2, 7.2, 1.5$  Hz, 1H), 6.66 (dd,  $J = 8.2, 1.5$  Hz, 1H), 6.45 (ddd,  $J = 7.8, 7.3, 1.5$  Hz, 1H), 4.56 (bs, 1H), 3.44 (t,  $J = 6.4$  Hz, 2H), 2.60 (t,  $J = 6.6$  Hz, 2H).  $^{13}\text{C}$  NMR (126 MHz,  $\text{CD}_3\text{CN}$ )  $\delta$  173.8, 148.1, 140.1, 130.5, 119.6, 111.7, 85.5, 40.2, 33.7. HRMS (ESI+) calculated for  $\text{C}_9\text{H}_{10}\text{INO}_2\text{Na}$   $[\text{M}+\text{Na}]^+$  313.9654  $m/z$ , found 313.9656.



### 3-((2-(Diphenylphosphanyl)phenyl)amino)propanoic acid (**S-2.12**)

To a flame-dried 15 mL Schlenk tube was added **S-2.11** (100 mg, 0.34 mmol), followed by palladium acetate (3.0 mg, 0.014 mmol) and anhydrous acetonitrile (1.4 mL). The pressure tube was then flushed with argon before adding triethylamine (95  $\mu\text{L}$ , 0.68 mmol) and diphenylphosphine (59  $\mu\text{L}$ , 0.34 mmol). The Schlenk tube was then subjected to three freeze-pump-thaw cycles (10 min each) and sealed. The reaction was then heated in an oil bath at 90 °C for 24 h with rapid stirring. After cooling to room temperature, the reaction was diluted with  $\text{H}_2\text{O}$  (20 mL) and extracted into EtOAc (3 x 10 mL). The organic layers were combined, dried over  $\text{MgSO}_4$ , and filtered. The filtrate was concentrated *in vacuo*, and the residue was purified by flash chromatography (eluting with 0–50% EtOAc/hexanes) to give **S-2.12** (64 mg, 0.18 mmol, 54%) as a white solid.  $^1\text{H}$  NMR (400 MHz,  $\text{CD}_3\text{CN}$ )  $\delta$  7.38–7.35 (m, 6H), 7.29–7.23 (m, 5H), 6.77–6.71 (m, 2H), 6.61 (app t,  $J = 7.5$  Hz, 1H), 3.38 (t,  $J = 6.5$  Hz, 2H), 2.46 (t,  $J = 6.6$  Hz,

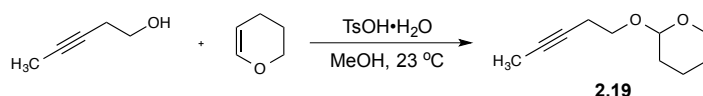
2H).  $^{31}\text{P}$  NMR (162 MHz,  $\text{CD}_3\text{CN}$ )  $\delta$  -21.7.  $^{13}\text{C}$  NMR (126 MHz,  $\text{CD}_3\text{CN}$ )  $\delta$  173.6, 151.8 (d,  $J$  = 18.6 Hz), 136.7 (d,  $J$  = 7.9 Hz), 135.3 (d,  $J$  = 2.3 Hz), 134.3 (d,  $J$  = 19.3 Hz), 131.8, 129.8, 129.6 (d,  $J$  = 7.0 Hz), 120.2 (d,  $J$  = 8.3 Hz), 111.4 (d,  $J$  = 2.7 Hz), 40.0, 33.9. HRMS (ESI+) calculated for  $\text{C}_{21}\text{H}_{19}\text{NO}_2\text{P}$   $[\text{M}+\text{H}]^+$  348.1154  $m/z$ , found 348.1158.



### Biotinylated triaryl phosphine (2.26)

To a flame-dried 25 mL round bottom flask containing a stir bar was added **S-2.12** (30 mg, 0.086 mmol), followed by HATU (36 mg, 0.095 mmol), anhydrous DMF (4.0 mL), and diisopropylethylamine (16  $\mu\text{L}$ , 0.095 mmol). A solution of **S-2.10** (36 mg, 0.086 mmol) in DMF (2.0 mL) was added dropwise under  $\text{N}_2$ , and the reaction was stirred overnight. Excess solvent was then removed *in vacuo*, and the residue was purified by HPLC (eluting with 50–90% MeCN in  $\text{H}_2\text{O}$  over 15 min) and then lyophilized to give **2.26** (25 mg, 0.032 mmol, 37%) as a white solid.  $^1\text{H}$  NMR (400 MHz,  $\text{CD}_3\text{CN}$ )  $\delta$  7.38–7.35 (m, 6H), 7.28–7.22 (m, 5H), 6.75–6.71 (m, 2H), 6.61 (bs, 1H), 6.60 (td,  $J$  = 7.4, 1.0 Hz, 1H), 6.52 (bs, 1H), 5.29 (bs, 1H), 5.18 (q,  $J$  = 7.0 Hz, 1H), 5.00 (bs, 1H), 4.40–4.36 (m, 1H), 4.21 (ddd,  $J$  = 7.7, 4.4, 2.0 Hz, 1H), 3.55–3.52 (m, 4H), 3.51–3.48 (m, 4H), 3.44 (q,  $J$  = 6.0 Hz, 4H), 3.36 (q,  $J$  = 6.2 Hz, 2H), 3.18 (q,  $J$  = 6.4 Hz, 2H), 3.16–3.11 (m, 2H), 2.86 (dd,  $J$  = 12.7, 5.0 Hz, 1H), 2.62 (d,  $J$  = 12.6 Hz, 1H), 2.32 (t,  $J$  = 6.4 Hz, 2H), 2.10 (t,  $J$  = 7.4 Hz, 2H), 1.69–1.54 (m, 8H), 1.39–1.35 (m, 2H).  $^{31}\text{P}$  NMR

(162 MHz, CD<sub>3</sub>CN)  $\delta$  -22.1. <sup>13</sup>C NMR (126 MHz, CD<sub>3</sub>CN)  $\delta$  173.5, 171.9, 163.7, 152.1 (d,  $J$  = 19.0 Hz), 136.8 (d,  $J$  = 7.8 Hz), 135.2, 134.3 (d,  $J$  = 19.3 Hz), 131.8, 129.8, 129.6 (d,  $J$  = 6.9 Hz), 120.0 (d,  $J$  = 8.0 Hz), 118.0, 111.3 (d,  $J$  = 2.8 Hz), 71.0, 70.78, 70.75, 69.7, 69.6, 62.3, 60.7, 56.3, 41.1, 40.9, 37.52, 37.49, 36.4, 36.0, 30.3, 30.2, 28.92, 28.89, 26.4. HRMS (ESI+) calculated for C<sub>41</sub>H<sub>56</sub>N<sub>5</sub>O<sub>6</sub>PSNa [M+Na]<sup>+</sup> 800.3586  $m/z$ , found 800.3573.



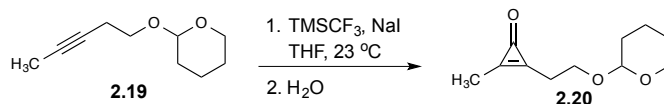
## 2-(Pent-3-yn-1-yloxy)tetrahydro-2H-pyran (2.19)

This compound was made following the general procedure of Allegretti *et al* [53]. To a flame-dried 100 mL round bottom flask containing a stir bar was added 3-pentyn-1-ol (1.26 g, 15.0 mmol), followed by anhydrous CH<sub>2</sub>Cl<sub>2</sub> (30 mL) and *para*-toluenesulfonic acid (29 mg, 0.15 mmol), under an atmosphere of N<sub>2</sub>. The solution was then cooled to 0 °C, and 3,4-dihydro-2H-pyran (1.4 mL, 17 mmol) was added dropwise. The reaction was allowed to warm to room temperature and stirred overnight. The reaction was then diluted with saturated NaHCO<sub>3</sub> (50 mL) and extracted into CH<sub>2</sub>Cl<sub>2</sub> (3 x 20 mL). The combined organic layers were dried over MgSO<sub>4</sub> and filtered. The filtrate was concentrated *in vacuo*, and the residue was purified by flash chromatography (eluting with 5% Et<sub>2</sub>O/hexanes) to give **2.19** (2.02 g, 12.0 mmol, 80%) as a colorless liquid. <sup>1</sup>H NMR (500 MHz, CDCl<sub>3</sub>)  $\delta$  4.64 (app t,  $J$  = 3.6 Hz, 1H), 3.89 (ddd,  $J$  = 11.3, 8.1, 3.3 Hz, 1H), 3.80 (td,  $J$  = 9.6, 7.2 Hz, 1H), 3.55–3.49 (m, 2H), 2.44 (tq,  $J$  = 7.2, 2.5 Hz, 2H), 1.87–1.80 (m, 1H), 1.78 (t,  $J$  = 2.6 Hz, 3H), 1.75–1.69 (m, 1H), 1.63–1.51 (m, 4H). <sup>13</sup>C



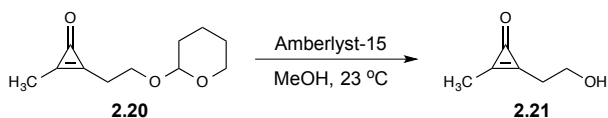
NMR (126 MHz, CDCl<sub>3</sub>)  $\delta$  98.8, 76.6, 75.9, 66.1, 62.3, 30.6, 25.4, 20.2, 19.5, 3.5.

HRMS (ESI+) calculated for C<sub>10</sub>H<sub>16</sub>O<sub>2</sub> [M+H]<sup>+</sup> 169.1228 *m/z*, found 169.1230.



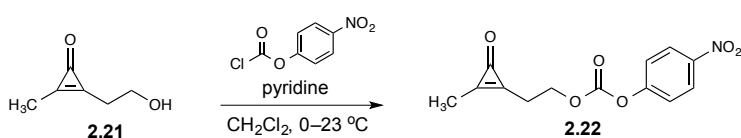
### 2-Methyl-3-(2-((tetrahydro-2H-pyran-2-yl)oxy)ethyl)cycloprop-2-en-1-one (**2.20**)

To an oven-dried Schlenk tube containing a stir bar was added NaI (0.330 g, 2.20 mmol). The NaI was then gently flame-dried under vacuum. Compound **2.19** (0.168 g, 1.00 mmol) and anhydrous THF (3.0 mL) were then added against positive N<sub>2</sub> flow. Trifluoromethyltrimethylsilane (0.30 mL, 2.0 mmol) was added, and the Schlenk tube was sealed. The reaction was stirred vigorously at room temperature for 24 h, then diluted with H<sub>2</sub>O (20 mL) and extracted into CH<sub>2</sub>Cl<sub>2</sub> (3 x 10 mL). The combined organic layers were then dried over MgSO<sub>4</sub> and filtered. The filtrate was concentrated *in vacuo*, and the residue was purified by flash column chromatography (eluting with 25% acetone/EtOAc) to give **2.20** (133 mg, 0.679 mmol, 68%) as a yellow oil. <sup>1</sup>H NMR (400 MHz, CDCl<sub>3</sub>)  $\delta$  4.66–4.64 (m, 1H), 4.05 (dt, *J* = 9.9, 6.0 Hz, 1H), 3.85 (ddd, *J* = 11.2, 7.6, 3.7 Hz, 1H), 3.71 (dt, *J* = 10.0, 6.3 Hz, 1H), 3.56–3.50 (m, 1H), 2.88 (td, *J* = 6.1, 0.9 Hz, 2H), 2.28 (t, *J* = 0.9 Hz, 3H), 1.82–1.71 (m, 2H), 1.63–1.51 (m, 4H). <sup>13</sup>C NMR (126 MHz, CDCl<sub>3</sub>)  $\delta$  159.4, 159.3, 158.5, 99.3, 63.5, 62.8, 30.8, 27.5, 25.4, 19.7, 11.7. HRMS (ESI+) calculated for C<sub>11</sub>H<sub>16</sub>O<sub>3</sub>Na [M+Na]<sup>+</sup> 219.0997 *m/z*, found 219.1002.



### 2-(2-Hydroxyethyl)-3-methylcycloprop-2-en-1-one (2.21)

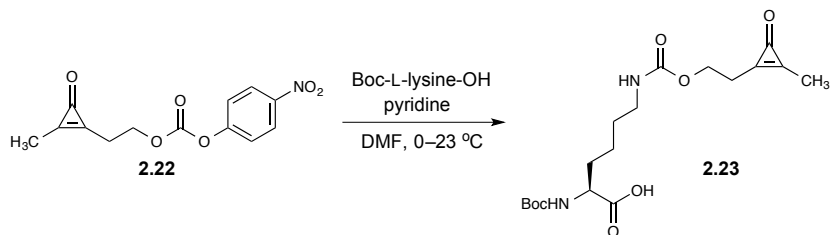
This compound was prepared following the general procedure of Murayama *et al* [54]. To a glass vial containing **2.20** (419 mg, 2.14 mmol) was added anhydrous methanol (2 mL), followed by Amberlyst-15 (158 mg). The reaction was then stirred at room temperature under N<sub>2</sub> and monitored by TLC until completion (~2 h). The solution was filtered, and the filtrate was concentrated *in vacuo*. The residue was purified by flash column chromatography (eluting with 50% acetone/EtOAc) to give **2.21** (231 mg, 2.06 mmol, 96%) as a yellow oil. <sup>1</sup>H NMR (500 MHz, CDCl<sub>3</sub>) δ 3.97 (t, *J* = 5.9 Hz, 2H), 2.85 (tq, *J* = 5.9, 0.9 Hz, 2H), 2.79 (bs, 1H), 2.31 (t, *J* = 0.9 Hz, 3H). <sup>13</sup>C NMR (126 MHz, CDCl<sub>3</sub>) δ 160.2, 159.4, 158.3, 58.8, 29.9, 11.7. HRMS (ESI+) calculated for C<sub>6</sub>H<sub>8</sub>O<sub>2</sub> [M+H]<sup>+</sup> 113.0603 *m/z*, found 113.0607.



### 2-(2-Methyl-3-oxocycloprop-1-en-1-yl)ethyl (4-nitrophenyl) carbonate (2.22)

To a flame-dried 50 mL round-bottom flask containing a stir bar was added **2.21** (125 mg, 1.12 mmol), followed by anhydrous CH<sub>2</sub>Cl<sub>2</sub> (10 mL) and anhydrous pyridine (0.54 mL, 6.7 mmol), under an atmosphere of N<sub>2</sub>. The solution was cooled to 0 °C in an ice bath and 4-nitrophenylchloroformate (494 mg, 2.46 mmol) was added while stirring rapidly. The reaction was then allowed to warm to room temperature and stirred for 3 h.

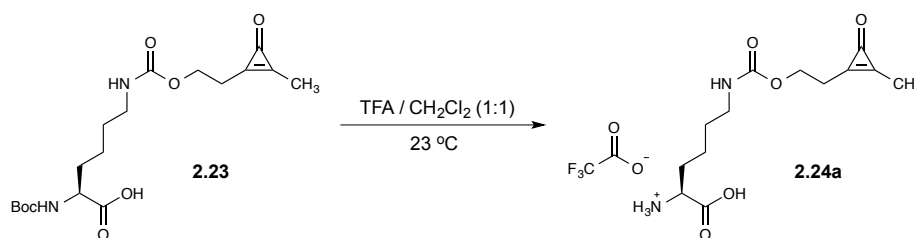
The solution was diluted with H<sub>2</sub>O (30 mL) and the organic layer was separated. The aqueous layer was then extracted into CH<sub>2</sub>Cl<sub>2</sub> (3 x 20 mL). The organic layers were combined, dried over MgSO<sub>4</sub>, and filtered. The filtrate was concentrated *in vacuo*, and the residue was purified by flash column chromatography (eluting with 25% acetone/EtOAc) to give **2.22** (240 mg, 0.866 mmol, 77%) as a white solid. <sup>1</sup>H NMR (500 MHz, CDCl<sub>3</sub>) δ 8.32–8.29 (m, 2H), 7.43–7.39 (m, 2H), 4.61 (t, *J* = 6.1 Hz, 2H), 3.08 (tq, *J* = 6.1, 0.9 Hz, 2H), 2.35 (t, *J* = 0.9 Hz, 3H). <sup>13</sup>C NMR (126 MHz, CDCl<sub>3</sub>) δ 159.5, 158.3, 157.1, 155.2, 152.2, 145.6, 125.4, 121.7, 64.7, 26.2, 11.7. HRMS (ESI+) calculated for C<sub>13</sub>H<sub>11</sub>NO<sub>6</sub>Na [M+Na]<sup>+</sup> 300.0484 *m/z*, found 300.0488.



### Boc-Lys-cyclopropenone (2.23)

To a flame-dried 50 mL round bottom flask containing a stir bar was added anhydrous DMF (8 mL), followed by anhydrous pyridine (0.22 mL, 2.8 mmol) and Boc-L-lysine-OH (458 mg, 1.86 mmol). The mixture was stirred and cooled to 0 °C in an ice bath. Compound **2.22** (258 mg, 0.931 mmol) was then added dropwise as a solution in anhydrous DMF (8.0 mL). The reaction was allowed to warm to room temperature and stirred overnight. The solution was then diluted with H<sub>2</sub>O (50 mL) and acidified with 1 M HCl. The organic layer was separated and the aqueous layer was extracted into CH<sub>2</sub>Cl<sub>2</sub> (2 x 10 mL). The organic layers were then combined, dried over MgSO<sub>4</sub>, and filtered.

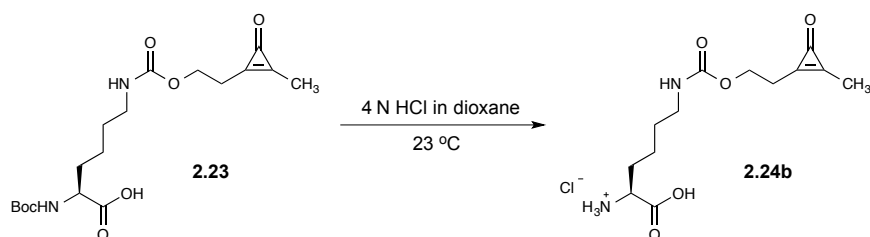
The filtrate was concentrated *in vacuo*, and the residue was purified by flash column chromatography (eluting with 10% MeOH/CH<sub>2</sub>Cl<sub>2</sub>) to give **2.23** as a white solid (126 mg, 0.328 mmol, 35%). <sup>1</sup>H NMR (400 MHz, CD<sub>3</sub>OD) δ 4.34 (t, *J* = 6.0 Hz, 2H), 4.06–4.03 (m, 1H), 3.12 (t, *J* = 6.6 Hz, 2H), 2.97 (t, *J* = 6.0 Hz, 2H), 2.31 (s, 3H), 1.80–1.76 (m, 1H), 1.69–1.60 (m, 1H), 1.53–1.47 (m, 4H) 1.44 (s, 9H). <sup>13</sup>C NMR (126 MHz, CDCl<sub>3</sub>) δ 175.3, 160.5, 158.7, 158.4, 156.2, 155.7, 80.0, 60.5, 56.1, 53.4, 40.5, 29.8, 29.0, 28.5, 26.8, 22.0, 11.6. HRMS (ESI+) calculated for C<sub>18</sub>H<sub>28</sub>N<sub>2</sub>O<sub>7</sub>Na [M+Na]<sup>+</sup> 407.1794 *m/z*, found 407.1799.



### Lys-cyclopropenone trifluoroacetate salt (**2.24a**)

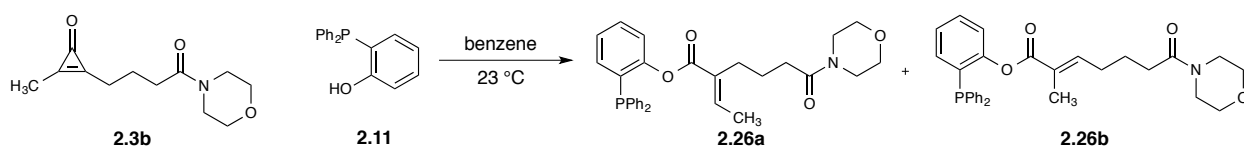
To a 20 mL glass vial containing **2.23** (86 mg, 0.22 mmol) was added anhydrous CH<sub>2</sub>Cl<sub>2</sub> (1 mL) and trifluoroacetic acid (TFA, 1 mL). The vial was then capped, and the solution was stirred at room temperature. The reaction was monitored by TLC until completion. The solvent was then removed *in vacuo* and the residue was precipitated in cold Et<sub>2</sub>O to give **2.24a** as a white solid (80 mg, 0.20 mmol, 91%). <sup>1</sup>H NMR (500 MHz, D<sub>2</sub>O) δ 4.33 (t, *J* = 5.8 Hz, 2H), 4.04 (t, *J* = 6.3 Hz, 1H), 3.11 (t, *J* = 6.8 Hz, 2H), 2.99 (t, *J* = 5.8 Hz, 2H), 2.28 (s, 3H), 2.01–1.85 (m, 2H), 1.56–1.35 (m, 4H). <sup>13</sup>C NMR (126 MHz, D<sub>2</sub>O) δ 172.2, 162.7, 158.68, 158.27, 157.8, 61.1, 52.8, 39.9, 29.4, 28.4, 25.6,

21.4, 10.0. HRMS (ESI+) calculated for  $C_{13}H_{20}O_5N_2Na$   $[M+Na]^+$  307.1270  $m/z$ , found 307.1277.



### Lys-cyclopropenone hydrochloride salt (**2.24b**)

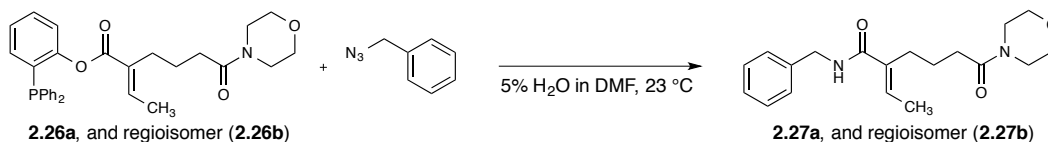
To a glass vial containing **2.23** (106 mg, 0.276 mmol) and a stir bar was added cold anhydrous 4 N HCl in dioxane (2.8 mL) under an atmosphere of  $N_2$ . The reaction was stirred at room temperature until TLC indicated that **2.23** had been consumed (~1 h). The solvent was then removed *in vacuo*. The residue was then dissolved in  $H_2O$  (5 mL) and lyophilized to give the product **2.24b** (83 mg, 0.26 mmol, 93%) as a white solid. Spectra matched those given for **2.24a**.



### 2-(Diphenylphosphanyl)phenyl(*E*)-2-ethylidene-6-morpholino-6-oxohexanoate (**2.26a**) and regioisomer (**2.26b**)

To a 4 dram glass vial containing a stir bar was added **2.3b** (45 mg, 0.20 mmol), followed by anhydrous benzene (4.0 mL) and **2.11** (83 mg, 0.30 mmol). The vial was capped and stirred at room temperature overnight. Approximately half of the solvent was then removed *in vacuo*, and the remainder was purified directly using flash column

chromatography (eluting with 50% EtOAc/hexanes) to give the products **2.26a:2.26b** as a 4:1 mixture of regioisomers (69 mg, 0.14 mmol, 69%).  $^1\text{H}$  NMR (400 MHz,  $\text{C}_6\text{D}_6$ )  $\delta$  (**2.26a**) 7.40–7.36 (m, 4H), 7.25 (ddd,  $J = 8.2, 4.1, 1.0$  Hz, 1H), 7.07–7.03 (m, 6H), 6.97 (ddd,  $J = 7.7, 4.1, 1.6$  Hz, 1H), 6.92 (q,  $J = 7.1$  Hz, 1H), 6.83–6.79 (m, 1H), 3.44 (app t,  $J = 4.2$  Hz, 2H), 3.25 (app t,  $J = 5.2$  Hz, 2H), 3.15 (app t,  $J = 4.6$  Hz, 2H), 2.73 (app t,  $J = 4.4$  Hz, 2H), 2.44 (app t,  $J = 7.7$  Hz, 2H), 1.92–1.88 (m, 4H), 1.52 (d,  $J = 7.2$  Hz, 3H). (**2.26b**) 7.40–7.36 (m, 4H), 7.29 (ddd,  $J = 7.8, 3.9, 1.0$ , 1H), 7.07–7.03 (m, 6H), 6.97 (ddd,  $J = 7.7, 4.1, 1.6$  Hz, 1H), 6.91–6.86 (m, 1H), 6.83–6.79 (m, 1H), 3.44 (app t,  $J = 4.2$  Hz, 2H), 3.25 (app t,  $J = 5.2$  Hz, 2H), 3.15 (app t,  $J = 4.6$  Hz, 2H), 2.67 (app t,  $J = 4.4$  Hz, 2H), 1.98 (q,  $J = 7.1$  Hz, 2H), 1.82 (m, 3H), 1.76 (m, 2H), 1.67 (q,  $J = 7.0$  Hz, 2H).  $^{31}\text{P}$  NMR (162 MHz,  $\text{C}_6\text{D}_6$ )  $\delta$  (**2.26a**)  $-14.5$ , (**2.26b**)  $-14.2$ .  $^{13}\text{C}$  NMR (126 MHz,  $\text{C}_6\text{D}_6$ )  $\delta$  (**2.26a** and **2.26b**) 170.4, 170.0, 165.4, 154.2 (d,  $J = 17.9$  Hz), 144.0, 140.7, 136.7 (d,  $J = 11.3$  Hz), 136.5 (d,  $J = 11.3$  Hz), 134.4 (d,  $J = 20.5$  Hz), 134.0, 133.9, 132.5, 131.2 (d,  $J = 15.1$  Hz), 131.1 (d,  $J = 14.4$  Hz), 130.1, 129.04 (d,  $J = 23.4$  Hz), 128.98 (d,  $J = 25.1$  Hz), 128.8, 128.4, 123.3 (d,  $J = 1.6$  Hz), 126.1, 66.9, 66.5, 45.6, 45.5, 42.0, 32.3, 31.8, 30.2, 28.3, 26.3, 24.6, 24.0, 14.3, 12.6. HRMS (ESI+) calculated for  $\text{C}_{30}\text{H}_{32}\text{NO}_4\text{PH}$   $[\text{M}+\text{H}]^+$  502.2147  $m/z$ , found 502.2141.



**(*E*)-*N*-Benzyl-2-ethylidene-6-morpholino-6-oxohexanamide (2.27a) and regioisomer (2.27b)**

To a 4-dram glass vial containing a stir bar was added a mixture of **26a** and **26b** (4:1) (53 mg, 0.10 mmol), followed by DMF (1.9 mL), and H<sub>2</sub>O (100 μL). Benzyl azide (29 μL, 0.15 mmol) was then added, and the solution was stirred at room temperature for two days. The reaction was then diluted with H<sub>2</sub>O (15 mL) and extracted into EtOAc (3 x 5 mL). The organic layers were combined, dried over MgSO<sub>4</sub>, and filtered. The filtrate was concentrated *in vacuo*, and the residue was purified by flash chromatography (eluting with 50–100% EtOAc/hexanes) to give **2.27a-b** as a 4:1 mixture of regioisomers (30 mg, 0.090 mmol, 91%) as a clear oil. <sup>1</sup>H NMR (500 MHz, CDCl<sub>3</sub>) δ (**2.27a**) 7.69 (s, 1H), 7.37–7.28 (m, 5H), 6.68 (q, *J* = 7.1 Hz, 1H), 4.55 (d, *J* = 5.6 Hz, 2H), 3.67–3.65 (m, 4H), 3.59–3.57 (m, 2H), 3.45–3.43 (m, 2H), 2.37–2.31 (m, 4H), 1.78 (d, *J* = 7.1 Hz, 3H), 1.76–1.72 (m, 2H). (**2.27b**) 7.37–7.28 (m, 5H), 6.39–6.35 (m, 1H), 6.05 (s, 1H), 4.51 (d, *J* = 5.7 Hz, 2H), 3.67–3.65 (m, 4H), 3.59–3.57 (m, 2H), 3.45–3.43 (m, 2H), 2.34–2.31 (m, 2H), 2.23, (q, *J* = 7.5 Hz, 2H), 1.83–1.77 (m, 2H), 1.77 (s, 3H). <sup>13</sup>C NMR (126 MHz, CDCl<sub>3</sub>) δ (**2.27a** and **2.27b**) 171.6, 171.3, 169.3, 168.3, 139.3, 138.6, 135.5, 135.2, 132.5, 131.6, 128.9, 128.6, 128.1, 127.7, 127.1, 67.1, 67.0, 66.8, 66.7, 46.0, 45.8, 44.0, 43.9, 42.1, 42.0, 32.4, 28.0, 26.2, 24.2, 23.8, 13.9, 13.0. HRMS (ESI+) calculated for C<sub>19</sub>H<sub>26</sub>N<sub>2</sub>O<sub>3</sub>Na [M+Na]<sup>+</sup> 353.1841 *m/z*, found 353.1840.

## 2.5 References

1. D. M. Patterson, L. A. Nazarova, J. A. Prescher. Finding the right (bioorthogonal) chemistry. *ACS Chem. Biol.* **2014**, *9*, 592–605.
2. J. A. Prescher, C. R. Bertozzi. Chemistry in living systems. *Nat. Chem. Biol.* **2005**, *1*, 13–21.

3. P. V. Chang, J. A. Prescher, M. J. Hangauer, C. R. Bertozzi. Imaging cell surface glycans with bioorthogonal chemical reporters. *J. Am. Chem. Soc.* **2007**, *129*, 8400–8401.
4. J. A. Prescher, D. H. Dube, C. R. Bertozzi. Chemical remodelling of cell surfaces in living animals. *Nature* **2004**, *430*, 873–877.
5. Y. Kho, S. C. Kim, C. Jiang, D. Barma, S. W. Kwon, J. Cheng, J. Jaunbergs, C. Weinbaum, F. Tamanoi, J. Falck, Y. Zhao. A tagging-via-substrate technology for detection and proteomics of farnesylated proteins. *Proc. Natl. Acad. Sci. USA* **2004**, *101*, 12479–12484.
6. G. Charron, M. M. Zhang, J. S. Yount, J. Wilson, A. S. Raghavan, E. Shamir, H. C. Hang. Robust fluorescent detection of protein fatty-acylation with chemical reporters. *J. Am. Chem. Soc.* **2009**, *131*, 4967–4975.
7. K. Lang, J. W. Chin. Cellular incorporation of unnatural amino acids and bioorthogonal labeling of proteins. *Chem. Rev.* **2014**, *114*, 4764–4806.
8. G. Charron, M. M. H. Li, M. R. MacDonald, H. C. Hang. Prenylome profiling reveals S-farnesylation is crucial for membrane targeting and antiviral activity of ZAP long-isoform. *Proc. Natl. Acad. Sci. USA* **2013**, *110*, 11085–11090.
9. B. W. Zaro, Y. Y. Yang, H. C. Hang, M. R. Pratt. Chemical reporters for fluorescent detection and identification of O-GlcNAc-modified proteins reveal glycosylation of the ubiquitin ligase NEDD4-1. *Proc. Natl. Acad. Sci. USA* **2011**, *108*, 8146–8151.



10. M. S. Siegrist, S. Whiteside, J. C. Jewett, A. Aditham, F. Cava, C. R. Bertozzi. D-Amino acid chemical reporters reveal peptidoglycan dynamics of an intracellular pathogen. *ACS Chem. Biol.* **2013**, *8*, 500–505.
11. G. W. Liechti, E. Kuru, E. Hall, A. Kalinda, Y. V. Brun, M. VanNieuwenhze, A. T. Maurelli. A new metabolic cell-wall labelling method reveals peptidoglycan in *Chlamydia trachomatis*. *Nature* **2014**, *5065*, 507–510.
12. T. S. Elliott, F. M. Townsley, A. Bianco, R. J. Ernst, A. Sachdeva, S. J. Elsässer, L. Davis, K. Lang, R. Pisa, S. Greiss, K. S. Lilley, J. W. Chin. Proteome labeling and protein identification in specific tissues and at specific developmental stages in an animal. *Nat. Biotechnol.* **2014**, *32*, 465–472.
13. K. P. Yuet, M. K. Doma, J. T. Ngo, M. J. Sweredoski, R. L. J. Graham, A. Moradian, S. Hess, E. M. Schuman, P. W. Sternberg, D. A. Tirrell. Cell-specific proteomic analysis in *Caenorhabditis elegans*. *Proc. Natl. Acad. Sci. USA* **2015**, *112*, 2705–2710.
14. D. M. Patterson, J. A. Prescher. Orthogonal bioorthogonal chemistries. *Curr. Opin. Chem. Biol.* **2015**, *28*, 141–149.
15. M. R. Karver, R. Weissleder, S. A. Hilderbrand. Bioorthogonal reaction pairs enable simultaneous, selective, multi-target imaging. *Angew. Chem. Int. Ed.* **2012**, *51*, 920–922.
16. K. Lang, L. Davis, S. Wallace, M. Mahesh, D. J. Cox, M. L. Blackman, J. M. Fox, J. W. Chin. Genetic encoding of bicyclononynes and *trans*-cyclooctenes for site-specific protein labeling in vitro and in live mammalian cells via rapid fluorogenic Diels–Alder reactions. *J. Am. Chem. Soc.* **2012**, *134*, 10317–10320.

17. D. M. Patterson, L. A. Nazarova, B. Xie, D. N. Kamber, J. A. Prescher. Functionalized cyclopropenes as bioorthogonal chemical reporters. *J. Am. Chem. Soc.* **2012**, *134*, 18638–18643.
18. D. N. Kamber, L. A. Nazarova, Y. Liang, S. A. Lopez, D. M. Patterson, H.-W. Shih, K. N. Houk, J. A. Prescher. Isomeric cyclopropenes exhibit unique bioorthogonal reactivities. *J. Am. Chem. Soc.* **2013**, *135*, 13680–13683.
19. D. N. Kamber, Y. Liang, R. J. Blizzard, F. Liu, R. A. Mehl, K. N. Houk, J. A. Prescher. 1,2,4-Triazines are versatile bioorthogonal reagents. *J. Am. Chem. Soc.* **2015**, *137*, 8388–8391.
20. H. Kogen, T. Kiho, K. Tago, S. Miyamoto, T. Fujioka, N. Otsuka, K. Suzuki-Konagai, T. Ogita. Alutacenoic acids A and B, rare naturally occurring cyclopropenone derivatives isolated from fungi: Potent non-peptide Factor XIIIa inhibitors. *J. Am. Chem. Soc.* **2000**, *122*, 1842–1843.
21. T. Okuda, K. Yokose, T. Furumai, H. B. Maruyama. Penitricin, a new class of antibiotic produced by *Penicillium aculearum* I. Isolation and characterization. *J. Antibiot.* **1984**, *37*, 718–722.
22. F. Bohlmann, J. Jakupovic, L. Müller, A. Schusser. Naturally occurring cyclopropenone derivatives. *Angew. Chem. Int. Ed.* **1981**, *3*, 292–293.
23. H.-W. Shih, J. A. Prescher. A bioorthogonal ligation of cyclopropenones mediated by triarylphosphines. *J. Am. Chem. Soc.* **2015**, *137*, 10036–10039.
24. A. Hamada, T. Takizawa. Synthesis of phosphorane having ketene group at alpha-position. *Tetrahedron Lett.* **1972**, *13*, 1849–1850.

25. E. Saxon, C. R. Bertozzi. Cell surface engineering by a modified Staudinger reaction. *Science* **2000**, *287*, 2007–2010.
26. R. Breslow, L. J. Altman, A. Krebs, E. Mohacsi, I. Murata, R. A. Peterson, J. Posner. Substituted cyclopropenones. *J. Am. Chem. Soc.* **1965**, *87*, 1326–1331.
27. K. T. Potts, J. S. Baum. The chemistry of cyclopropenones. *Chem. Rev.* **1974**, *74*, 189–213.
28. F. Wang, T. Luo, J. Hu, Y. Wang, H. S. Krishnan, P. V. Jog, S. K. Ganesh, G. K. S. Prakash, G. A. Olah. Synthesis of *gem*-difluorinated cyclopropanes and cyclopropenes: Trifluoromethyltrimethylsilane as a difluorocarbene source. *Angew. Chem. Int. Ed.* **2011**, *50*, 7153–7157.
29. Z. L. Cheng, Q. Y. Chen. Difluorocarbene chemistry: A simple transformation of 3,3-*gem* difluorocyclopropenes to cyclopropenones. *Chin. J. Chem.* **2006**, *24*, 1219–1224.
30. M. G. Wilkerson, J. Henkin, J. K. Wilkin. Diphenylcyclopropenone: Examination for potential contaminants, mechanisms of sensitization, and photochemical stability. *J. Am. Acad. Dermatol.* **2015**, *11*, 802–807.
31. A. Caiazzo, S. Dalili, A. K. Yudin. Design and development of cyclohexane-based P,N-ligands for transition metal catalysis. *Org. Lett.* **2002**, *4*, 2597–2600.
32. T. E. Barder, S. L. Buchwald. Rationale behind the resistance of dialkylbiaryl phosphines toward oxidation by molecular oxygen. *J. Am. Chem. Soc.* **2007**, *129*, 5096–5101.

33. D. Bostwick, H. F. Henneike, H. P. Hopkins. Relative basicities of cyclic polyenones from hydrogen-bonding studies. *J. Am. Chem. Soc.* **1975**, *97*, 1505–1509.
34. F. G. Bordwell, R. J. McCallum, W. N. Olmstead. Acidities and hydrogen bonding of phenols in dimethyl sulfoxide. *J. Org. Chem.* **1984**, *49*, 1424–1427.
35. F. G. Bordwell, D. J. Algrim. Acidities of anilines in dimethyl sulfoxide solution. *J. Am. Chem. Soc.* **1988**, *110*, 2964–2968.
36. A. Pini, L. Lozzi, A. Bernini, J. Brunetti, C. Falciani, S. Scali, S. Bindi, T. D. Maggio, G. M. Rossolini, N. Niccolai, L. Bracci. Efficacy and toxicity of the antimicrobial peptide M33 produced with different counter-ions. *Amino Acids* **2012**, *43*, 467-473.
37. R. B. Cooley, P. A. Karplus, R. A. Mehl. Gleaning unexpected fruits from hard-won synthetases: Probing principles of permissivity in non-canonical amino acid-tRNA synthetases. *ChemBioChem* **2014**, *15*, 1810–1819.
38. R. J. Blizzard, D. R. Backus, W. Brown, C. G. Bazewicz, Y. Li, R. A. Mehl. Ideal bioorthogonal reactions using a site-specifically encoded tetrazine amino acid. *J. Am. Chem. Soc.* **2015**, *137*, 10044–10047.
39. M. L. Blackman, M. Royzen, J. M. Fox. Tetrazine ligation: Fast bioconjugation based on inverse-electron-demand Diels–Alder reactivity. *J. Am. Chem. Soc.* **2008**, *130*, 13518–13519.
40. E. Saxon, J. I. Armstrong, C. R. Bertozzi. A “Traceless” Staudinger ligation for the chemoselective synthesis of amide bonds. *Org. Lett.* **2000**, *2*, 2141–2143.

41. M. B. Soellner, B. L. Nilsson, R. T. Raines. Reaction mechanism and kinetics of the traceless Staudinger ligation. *J. Am. Chem. Soc.* **2006**, *128*, 8820–8828.
42. A. Bianchi, A. Russo, A. Bernardi. Neo-glycoconjugates: stereoselective synthesis of  $\alpha$ -glycosyl amides via Staudinger ligation reactions. *Tetrahedron: Asymmetry* **2005**, *16*, 381–386.
43. A. Bianchi, A. Bernardi. Traceless Staudinger ligation of glycosyl azides with triaryl phosphines: Stereoselective synthesis of glycosyl amides. *J. Org. Chem.* **2006**, *71*, 4565–4577.
44. G. J. L. Bernardes, L. Linderoth, K. J. Doores, O. Boutureira, B. G. Davis. Site-selective traceless Staudinger ligation for glycoprotein synthesis reveals scope and limitations. *ChemBioChem* **2011**, *12*, 1383–1386.
45. P. Metzner, in *Organosulfur Chemistry I*, P. C. B. Page, Ed. (Springer Berlin Heidelberg, Berlin, Heidelberg, 1999), pp. 127–181.
46. S. Schulz, S. Yildizhan, K. Stritzke, C. Estrada, L. E. Gilbert. Macrolides from the scent glands of the tropical butterflies *Heliconius cydno* and *Heliconius pachinus* *Org. Biomol. Chem.* **2007**, *5*, 3434–3441.
47. I. D. G. Watson, A. K. Yudin. Ring-opening reactions of nonactivated aziridines catalyzed by tris(pentafluorophenyl)borane. *J. Org. Chem.* **2003**, *68*, 5160–5167.
48. D. S. Wilbur, P. M. Pathcare, D. K. Hamlin, F. Wan. (University of Washington, United States of America, 2006).
49. G. D. Figuly, C. K. Loop, J. C. Martin. Directed ortho-lithiation of lithium thiophenolate. New methodology for the preparation of ortho-substituted thiophenols and related compounds. *J. Am. Chem. Soc.* **1989**, *111*, 654–658.

50. J. King-Underwood, K. Ito, P. J. Murray, G. Hardy, F. A. Brookfield, C. J. Brown. Compounds. US Patent US2012/0208799 A1.
51. G. Muller, D. Sainz. Synthesis of monohydroxy -methyl- and -ethyl-phosphines  $\text{PPh}_2\text{CHROH}$ . *J. Organomet. Chem.* **1995**, *495*, 103–111.
52. D. R. Chancellor, K. E. Davies, O. De Moor, C. R. Dorgan, P. D. Johnson, A. G. Lambert, D. Lawrence, C. Lecci, C. Maillol, P. J. Middleton, G. Nugent, S. D. Poignant, A. C. Potter, P. D. Price, R. J. Pye, R. Storer, J. M. Tinsely, R. van Well, R. Vickers, J. Vile, F. J. Wilkes, F. X. Wilson, S. P. Wren, G. M. J. Wynne. Discovery of 2-arylbenzoxazoles as upregulators of utrophin production for the treatment of Duchenne muscular dystrophy. *J. Med. Chem.* **2011**, *54*, 3241–3250.
53. P. A. Allegretti, E. M. Ferreira. Generation of  $\alpha,\beta$ -unsaturated platinum carbenes from homopropargylic alcohols: Rearrangements to polysubstituted furans. *Org. Lett.* **2011**, *13*, 5924–5927.
54. T. Murayama, T. Sugiyama, Y. Kyohei. Synthesis of natural (–)-osmundalactone and its epimer. *Agric. Biol. Chem.* **1986**, *50*, 2347–2351.

## Chapter 3: A cyclopropenethione-phosphine ligation for rapid bioorthogonal labeling

### 3.1 Introduction

Bioorthogonal chemistries have enabled a broad range of applications in living organisms [1, 2], including biomolecule imaging [3], metabolic profiling [4-6], and targeted drug delivery [7, 8]. Despite their ubiquity in numerous fields, these reactions are not without limitation. Only a handful of bioorthogonal reagents are reliable in the most demanding environments, including inside cells. Additionally, many bioorthogonal probes cross-react with one another, precluding dual imaging and other multi-component studies [9]. These and other applications demand new reagents and new reactions.

Our lab has focused on expanding the scope of bioorthogonal chemistries by developing probes that are small, stable, and tunable [10]. We recently reported one class of such reagents—cyclopropenones [11, 12]. These motifs are stable in biological solutions and react robustly with *ortho*-substituted phosphines. The ligation involves initial formation of a reactive ketene-ylide, followed by intramolecular trapping (Figure 3-1A). The resulting products are stable in cellular environments. The unique mechanism of the cyclopropenone-phosphine ligation renders this reaction compatible with many classic bioorthogonal reagents [12]. Cyclopropenones are also small and compatible with cellular enzymes and metabolic pathways [12]. Dialkyl-substituted probes, in particular, are well suited for time intensive studies. We used these probes in long-term bacterial cultures for site-specific protein modification [12]. The most stable cyclopropenones, though, required long reaction times with bioorthogonal phosphines. Faster rates

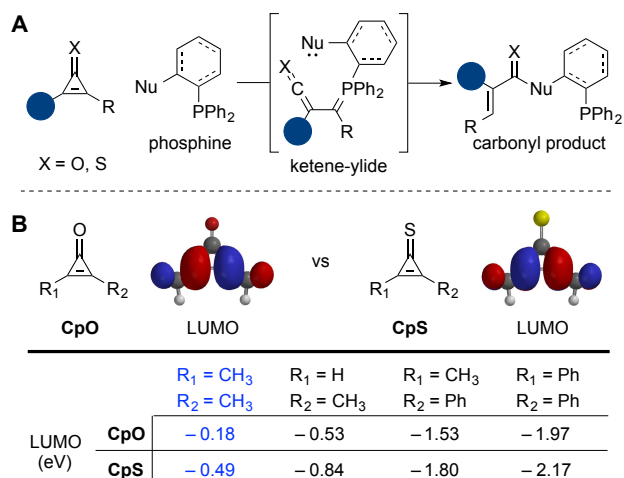


**Figure 3-1.** Bioorthogonal ligations of cyclopropenones and cyclopropenethiones. A) Cyclopropenones (**CpO**, X=O) react with phosphines to form ketene-ylides. These intermediates can be trapped with pendant nucleophiles to afford stable adducts. Cyclopropenethiones (**CpS**, X=S) were hypothesized to react similarly with phosphine probes. B) CpS scaffolds harbor lower LUMO energies than analogous CpO probes. Density functional theory (DFT) calculations were performed with Spartan, using the B3LYP level of theory and basis set 6-31G\*.

could be achieved with mono-substituted scaffolds, but these probes were more susceptible to side reactions with biological nucleophiles.

We hypothesized that cyclopropenone heteroanalogs could strike the right balance between kinetic stability and rapid reactivity. We were particularly drawn to cyclopropenethione (CpS) scaffolds. CpS differs from CpO by only a single atom, and would thus likely be small enough to minimally impact target biomolecules or pathways. While a less widely used synthon, CpS is known to participate in a variety of transformations, including photocleavage reactions [13, 14] and ring-opening cycloadditions [15, 16]. Previous work by Yoneda and Matsumura further revealed that triarylphosphines can react with diphenyl CpS via nucleophilic addition to the alkene

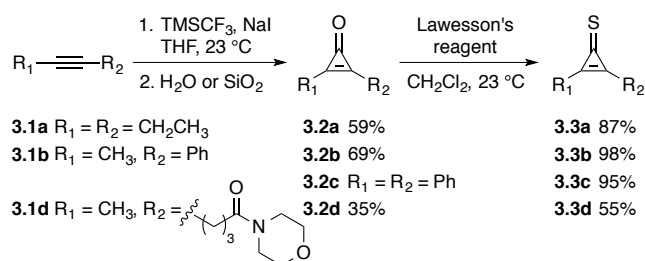


[17, 18]. Thus, we surmised that CpS derivatives could react with substituted phosphines similarly to CpO probes, ultimately providing thiocarbonyl products (Figure 3-1A). Thiocarbonyls are widely used in fluorescence quenching and other biophysical experiments with proteins [19, 20]. Thioamides, in particular, are known to exhibit improved proteolytic stability and can increase peptide half-lives in biological media [21].

### 3.2 Results and discussion

To evaluate the proposed phosphine ligation, we first examined the frontier molecular orbitals of CpS derivatives. Density functional theory (DFT) calculations revealed that the LUMO values for CpS scaffolds were consistently lower than those for analogous CpO molecules (Figure 3-1B). The reduced LUMO values suggested the potential for increased reactivity with phosphines. Whether or not CpS molecules would also be susceptible to increased reactivity with thiols or other biological nucleophiles remained to be determined.

**Scheme 3-1.** Synthesis of model cyclopropenethiones.



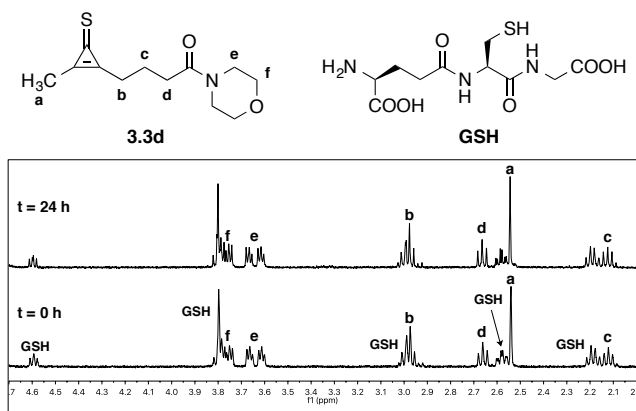
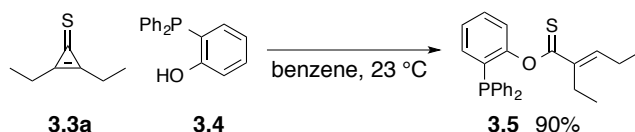


**Figure 3-2.** Cyclopropenethiones are stable to L-glutathione (GSH) at physiological pH. Cyclopropenethione **3.3d** (5 mM) was incubated with GSH (5 mM) in *d*-PBS (pH 7.4) and monitored by  $^1\text{H}$ -NMR spectroscopy.

We synthesized a panel of CpS compounds to examine their suitability as bioorthogonal reagents. A symmetric dialkyl CpS (**3.3a**) was included for ease of product characterization. We also prepared scaffolds bearing aryl substituents (**3.3b–c**) and water-solubilizing groups (**3.3d**). All of the desired cyclopropenethiones were prepared via the corresponding cyclopropenones (**3.2a–d**, Scheme 3-1). Alkynes **3.1a–d** were first treated with difluorocarbene to generate 3,3-difluorocyclopropenes [22]. These intermediates were then hydrolyzed to provide **3.2a–d**. The desired cyclopropenethiones were ultimately obtained by treating **3.2a–d** with Lawesson's reagent. We also attempted to prepare mono-substituted CpS probes. However, these less substituted scaffolds were not stable to concentration (data not shown), and were likely subject to intermolecular attack.

With the CpS scaffolds in hand, we first evaluated their stabilities in aqueous solution. Compounds **3.3b–d** were incubated in *d*-PBS (pH 7.4) and monitored by <sup>1</sup>H-NMR spectroscopy (see Appendix B). Probes **3.3b** and **3.3d** were stable for >1 week at 37 °C. The diaryl scaffold **3.3c** degraded, resulting in an insoluble and unidentified precipitate. CpS **3.3c** may be susceptible to dimerization or intermolecular reactivity over prolonged time periods [13, 23]. The stabilities of **3.3b** and **3.3d** toward biological nucleophiles were further examined. The molecules were incubated with L-glutathione (GSH) in *d*-PBS (pH 7.4) and monitored via <sup>1</sup>H-NMR spectroscopy (Figures 3-2 and Appendix B). No reactivity was observed over 24 h at 37 °C, indicating that both scaffolds were stable to thiols.

**Scheme 3-2.** Thionoester product formation.



Encouraged by the biocompatibility of di-alkylated CpS scaffolds, we investigated their reactivities with a panel of phosphines. Symmetric analog **3.3a** was initially used to determine the structure of the ligated adduct. When **3.3a** was incubated with phosphine **3.4**, the thionoester **3.5** was formed (Scheme 3-2). The expected thiocarbonyl was also observed upon treating **3.3d** with phosphine **3.4**. Importantly, this latter reaction proceeded ~300-fold faster than the analogous CpO-phosphine ligation

**Scheme 3-3.** Cyclopropenethiones exhibit faster ligation rates than analogous cyclopropenones.

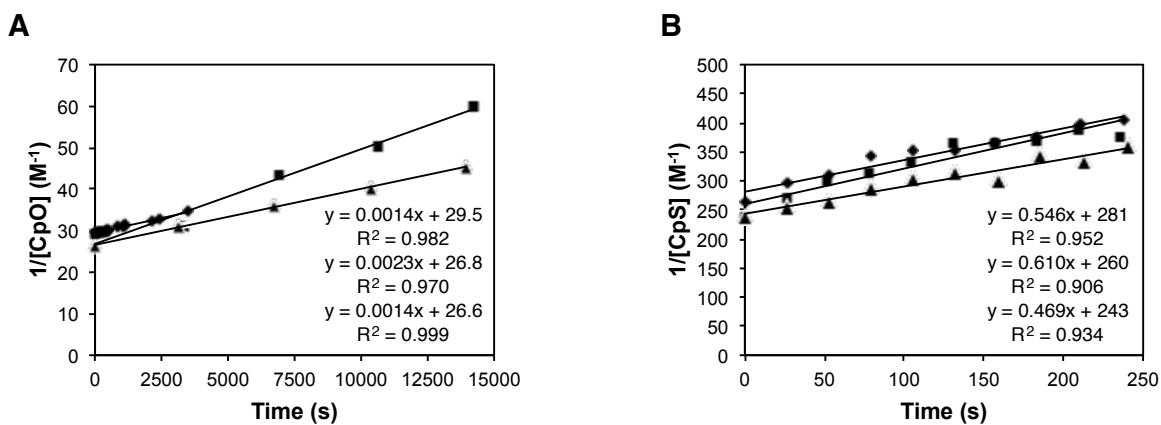
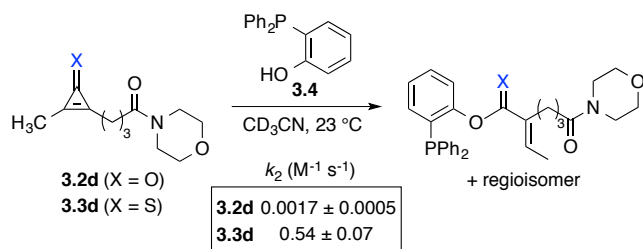
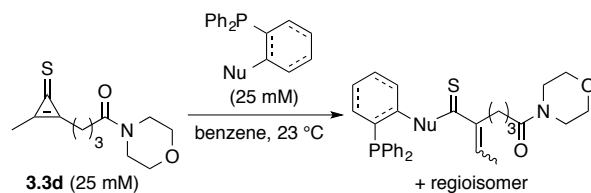


**Figure 3-3.** Rate comparison of compounds **3.2d** and **3.3d**. Second order rate constants were measured for reactions of phosphine **3.4** (5 or 25 mM) with A) cyclopropenone **3.2d** (25 mM) and B) cyclopropenethione **3.3d** (5 mM).

(Scheme 3-3 and Figure 3-3). Such rapid reactions are often desirable for live cell and tissues studies, where only small amounts of reagents are tolerated. By contrast, CpS **3.3d** reacted sluggishly with thiol-substituted phosphine **3.6** (Table 3-1). The reduced rate may be attributed to increased steric congestion near the reactive site or decreased phosphine nucleophilicity [24]. Dithioester products were also initially detected via NMR spectroscopy, but complex mixtures were ultimately formed. It is likely that the initial dithioesters reacted with leftover CpS.

To form more stable thioamides, we evaluated CpS reactivity with amine-substituted triarylphosphine **3.7**. This probe did not react with **3.3d** even at elevated (50 mM) concentrations. This sluggish reactivity is consistent with our previous observations with CpO probes [12]. Rapid CpO ligations in organic solvent required hydrogen-bond activation (Figure 3-4). We hypothesized that phosphines bearing stronger hydrogen-bond donors could similarly boost reactivity with CpS probes. Indeed, when phosphine **3.8** (bearing a nitro group *para* to the amine) was incubated with **3.3d**, ligation products were observed within a few hours. The lowered  $pK_a$  of the pendant amine promotes reactivity, despite deactivating the phosphine via inductive effects. More nucleophilic phosphines also reacted rapidly in aqueous solution (Table 3-1 and Figure 3-5). Surprisingly, phosphine **3.9** reacted significantly more slowly with **3.3d** than did phosphine **3.4**. The opposite trend was observed with CpO analogs [12], suggesting that CpS reactivity may be more dependent on initial hydrogen bond activation. These data further imply that, despite their structural similarity, CpO and CpS probes could be used in orthogonal labeling applications.

**Table 3-1.** Cyclopropenethione reactivity with phosphine probes.

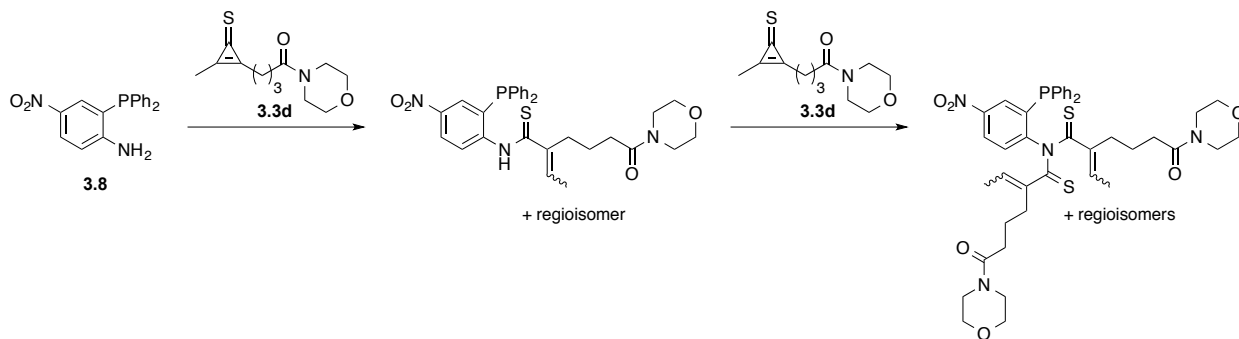


Entry	Phosphine	Time
1	 3.4	< 5 min
2	 3.6	2 h <sup>a</sup>
3	 3.7	N.R.
4	 3.8	4 h <sup>a,b</sup>
5	 3.9	1 h

<sup>a</sup> Products were not stable to isolation conditions.

<sup>b</sup> Multiple addition products were observed (see Scheme 3-4).

**Scheme 3-4.** Phosphine **3.8** can react with more than one equivalent of **3.3d** to form multiple products.



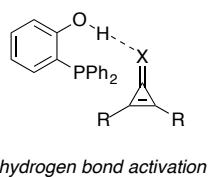


**Figure 3-4.** Hydrogen bond activation. Previously, we showed that cyclopropenones may be activated for attack via intermolecular hydrogen bonding in organic solvents [12]. Cyclopropenethiones may undergo similar activation.

The reactivity and stability data suggested that CpS probes would be viable for biomolecule labeling. To assess the efficiency of the CpS-phosphine ligation in this context, we performed reactions on a model protein. Hen egg-white lysozyme was non-specifically functionalized with CpS motifs. Mass spectrometry analysis revealed 1–5 CpS units were appended to the protein surface (Figures 3-6 and 3-7B). The functionalized protein (**Lys-CpS**) was then treated with a phosphine-biotin probe (**3.13**). This phosphine was selected for labeling due to its rapid reactivity and the stability of the resulting thioamide products. Mass spectrometry revealed quantitative conversion to the expected ligation adducts (Figures 3-7B). Importantly, the resulting conjugates were stable for >1 week at 37 °C (Figure 3-8). The reactions were also faster than those carried out with analogous cyclopropenones. Lysozyme samples functionalized with CpO or CpS (**Lys-CpO** or **Lys-CpS**, respectively) were prepared as above. Mass spectrometry confirmed that both conjugates were modified to a similar extent (Figure 3-6). The proteins were then treated with phosphine **3.13** and analyzed via Western blot. As shown in Figure 3-7C, shorter reaction times and lower phosphine concentrations were required to achieve robust labeling with **Lys-CpS**. Adducts were observed within

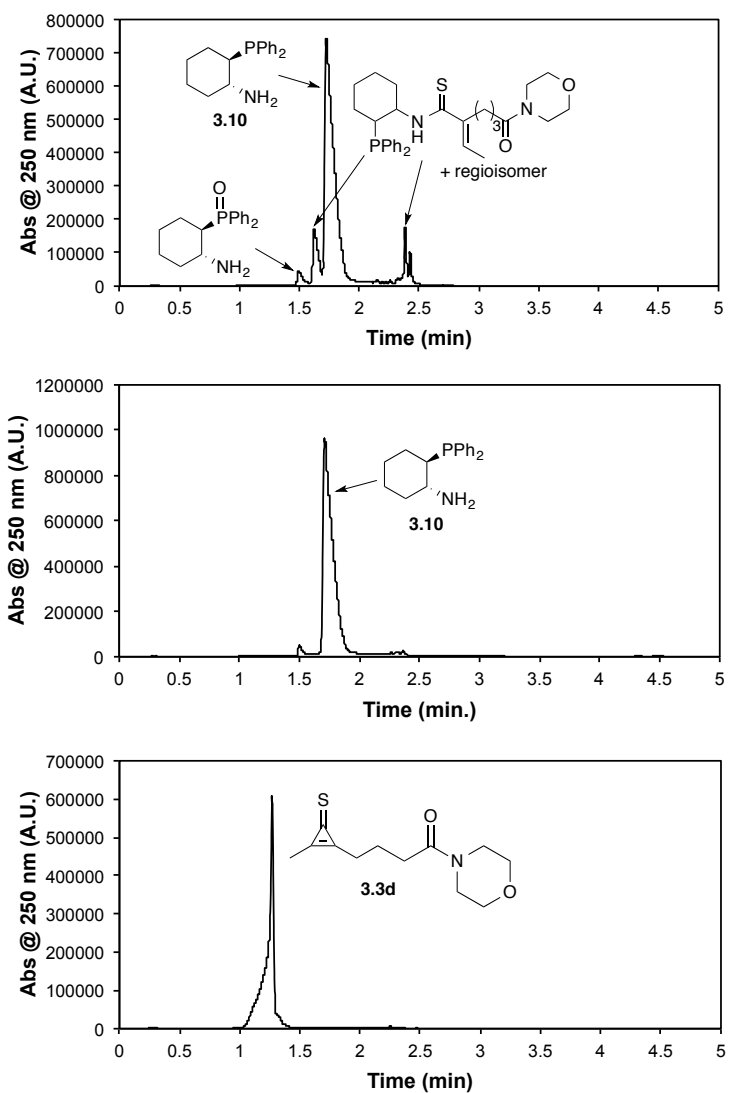


**Figure 3-5.** LC-MS plots of CpS-phosphine ligations. Compound **3.3d** (250  $\mu\text{M}$  final concentration) and phosphine **3.10** (500  $\mu\text{M}$  final concentration) were combined in PBS containing 50% MeCN and incubated at room temperature for 2 h.



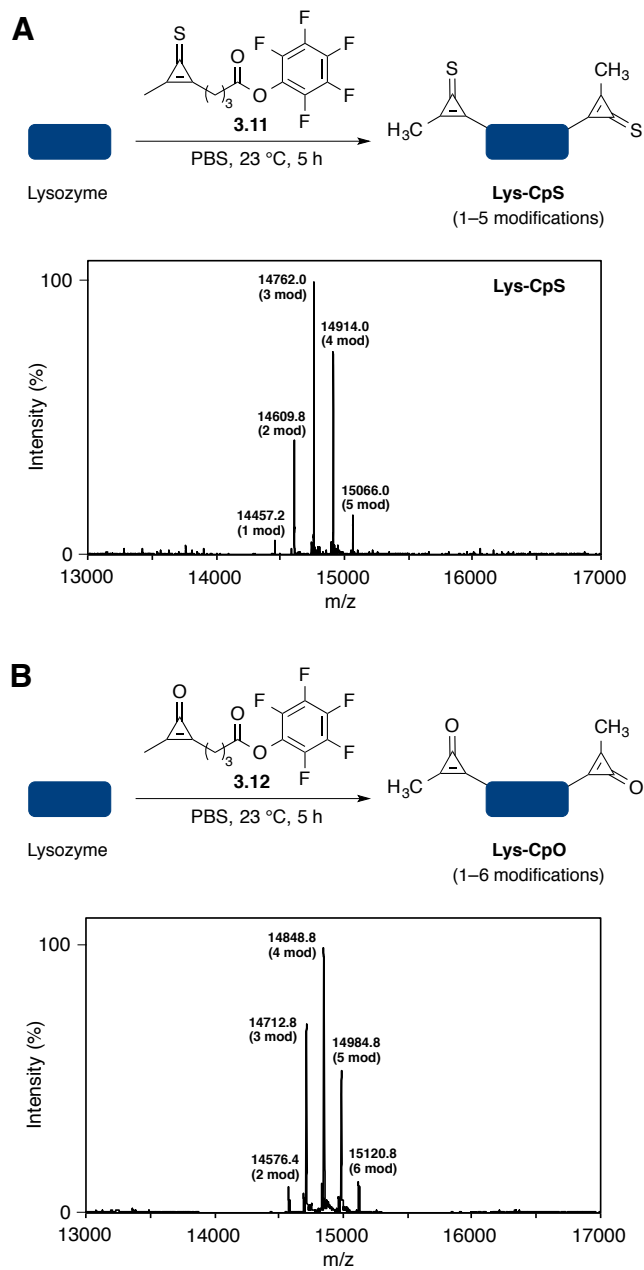


**Figure 3-6.** Mass spectrometry analysis of functionalized lysozyme. Lysozyme functionalized with A) cyclopropenethione **3.11** and B) cyclopropenone **3.12** was confirmed via mass spectrometry (ESI). The functionalized proteins comprised 1–6 modifications.

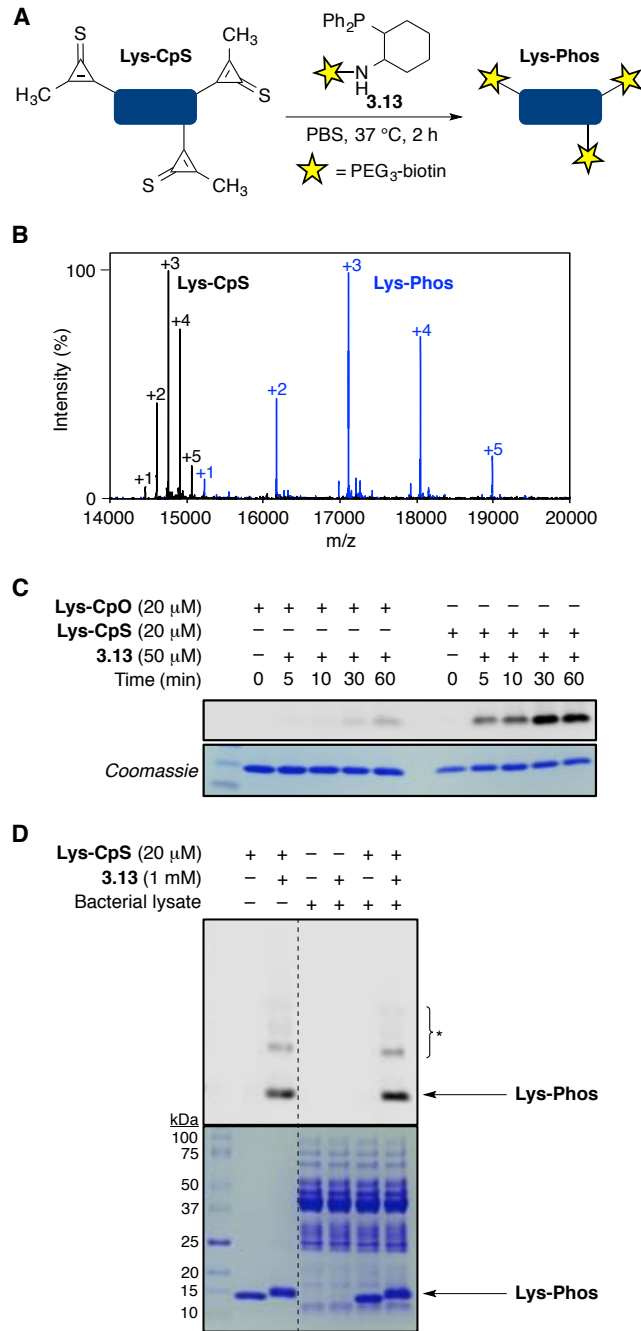


**Figure 3-7.** Cyclopropenethione conjugates are readily ligated *in vitro* and in cell lysate. A) **Lys-CpS** samples were treated with a phosphine-biotin probe. B) **Lys-CpS** (20  $\mu$ M, 1–5 modifications) was incubated with phosphine-biotin probe **3.13** (500  $\mu$ M), and the reaction was monitored by mass spectrometry. Full conversion to the expected product (**Lys-Phos**, 1–5 modifications) was observed. C) **Lys-CpS** and **Lys-CpO** (20  $\mu$ M) were reacted with phosphine **3.13** (50  $\mu$ M) for 0–60 min at 37 °C. Covalent adducts were detected via Western blot (top). Coomassie staining was used to assess protein loading (bottom). D) **Lys-CpS** (20  $\mu$ M) was incubated with **3.13** (1 mM) in bacterial lysate for 1 h at 37 °C. Covalent adducts were detected via Western blot (top). Coomassie staining was used to assess protein loading (bottom). \*Protein impurities present in commercial lysozyme stock.

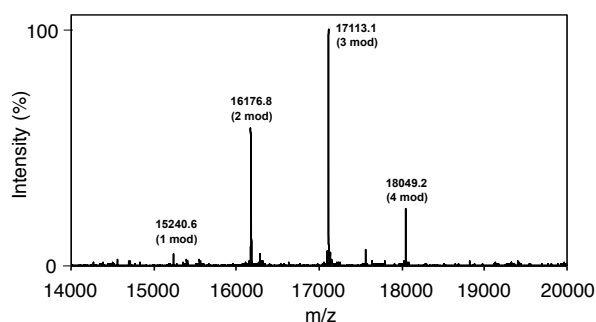


**Figure 3-8.** **Lys-Phos** is stable for up to 7 days. **Lys-Phos** (20  $\mu$ M) was incubated in PBS (pH 7.4) at 37  $^{\circ}$ C for 1 week. The presence of **Lys-Phos** was confirmed via mass spectrometry.

minutes and reactions were complete by 30 min. By contrast, reactions with **Lys-CpO** required  $\sim$ 1 h to observe covalent adducts and remained incomplete at this timepoint.

The rapid reactivity and compatibility of the CpS-phosphine ligation suggested that it could be performed in more complex setting. Probes compatible with intracellular environments are often in high demand [1, 25]. To investigate cyclopropenethione in this setting, **Lys-CpS** was incubated with freshly prepared cell lysate (Figure 3-7D). The samples were then treated with phosphine **3.13** and analyzed via Western blot as described above. Rapid and selective labeling was observed after just 1 h. Larger concentrations of **3.13** were required to achieve robust ligation, though, likely due to competing phosphine oxidation pathways. The lack of background reactivity observed demonstrates that CpS-phosphine ligations proceed with high selectivity even in complex lysate.

### **3.3 Conclusion**

In summary, we found that substituted cyclopropenethiones are viable bioorthogonal reagents. These scaffolds are stable in aqueous buffers in the presence of biological nucleophiles. Cyclopropenethiones differ from cyclopropenones by a single atom, but can react ~300-fold faster with some phosphines. Biocompatible probes that exhibit improved reaction rates can broaden the scope of this ligation reaction. Cyclopropenethiones also exhibit distinct reactivity profiles compared to other bioorthogonal reagents – including cyclopropenones – suggesting further opportunities for multi-component labeling. As the bioorthogonal toolkit continues to expand, so too will the number of new applications and cellular pursuits.

### **3.4 Materials and methods**

#### ***3.4a General information***

All reagents and solvents were used as received, unless specified otherwise. Anhydrous organic solvents were prepared by degassing with argon and passing through two 4 x 36 in. columns of anhydrous neutral A2 (8 x 12 mesh; LaRoche Chemicals; activated at 350 °C for 12 h under a flow of argon). Column chromatography was carried out using Silicycle 60 Å (32–64 mesh) silica gel. Thin layer chromatography (TLC) was carried out with Merck Millipore 250 mm silica gel F-254 plates. Plates were visualized using UV light or KMnO<sub>4</sub> stain. Organic solutions were concentrated under reduced pressure using a Büchi rotary evaporator. HPLC purifications were performed on a Varian ProStar equipped with 325 Dual Wavelength UV-Vis Detector, using an Agilent Prep-C18 Scalar column (9.4 x 150 mm, 5 µm) with a 4 mL/min flow rate.

$^1\text{H}$ ,  $^{13}\text{C}$ ,  $^{19}\text{F}$ , and  $^{31}\text{P}$  NMR spectra were obtained using either a Bruker DRX400 or a Bruker DRX500 instrument equipped with a cryo probe.  $^1\text{H}$  NMR spectra were acquired at 400 MHz or 500 MHz,  $^{13}\text{C}$  NMR spectra were acquired at 126 MHz,  $^{19}\text{F}$  NMR spectra were obtained at 376 MHz, and  $^{31}\text{P}$  NMR spectra were acquired at 162 MHz. Spectra were internally referenced to residual solvent signals ( $\text{CDCl}_3$  was referenced to 7.27 ppm for  $^1\text{H}$  and 77.16 ppm for  $^{13}\text{C}$ ,  $\text{CD}_3\text{CN}$  was referenced to 1.94 ppm for  $^1\text{H}$  and 118.26 ppm for  $^{13}\text{C}$ ,  $\text{D}_2\text{O}$  was referenced to 4.79 ppm for  $^1\text{H}$ ,  $\text{C}_6\text{D}_6$  was referenced to 7.16 ppm for  $^1\text{H}$  and 128.06 for  $^{13}\text{C}$ ).  $^{19}\text{F}$  and  $^{31}\text{P}$  NMR spectra were referenced by indirect absolute chemical shift to residual protio solvent signals. All spectra were acquired at 298 K. Chemical shifts are reported in ppm, and coupling constants ( $J$ ) are reported in Hz. Mass spectra were acquired at the University of California, Irvine Mass Spectrometry Facility. Protein mass spectra were acquired using a Waters Xevo G2-XS QToF mass spectrometer.

### **3.4b Stability experiments**

Cyclopropenethione aqueous stabilities were assessed by dissolving compounds **3.3b–d** (final concentration 10 mM) in *d*-PBS (50 mM, pH 7.4). The solutions were incubated in an NMR tube at 37 °C. NMR spectra were acquired periodically over 0–7 d. For compound **3.3c**, a precipitate formed during the course of the experiment.

Cyclopropenethione stabilities to thiols were assessed by dissolving compounds **3.3b** or **3.3d** with L-glutathione (final concentration of 5 mM for each reagent) in *d*-PBS (50 mM, pH 7.4). The solutions were then incubated in an NMR tube at 37 °C. NMR spectra were acquired periodically over 0–24 h.

### **3.4c Kinetics experiments**

All kinetics experiments were performed at room temperature. Reaction progress was monitored via  $^1\text{H}$  NMR spectroscopy, using trimethylsilylacetylene as an internal standard. Phosphines and cyclopropenethiones or cyclopropenones were combined in equimolar ratios (final concentrations of 5 mM or 25 mM). Second order rate constants were calculated using the method of initial rates. Error values are the standard deviation of the mean for  $n = 3$  independent experiments.

### **3.4d CpS reactivity with model phosphines**

#### NMR spectroscopy reaction analysis

Compound **3.3d** (25 mM final concentration) was treated with phosphines **3.4**, **3.6**, **3.7**, **3.8**, or **3.9** (25 mM final concentrations) in 650  $\mu\text{L}$  of benzene- $d_6$ . Reactions were incubated at room temperature and product formation was monitored over time via  $^1\text{H}$  and  $^{31}\text{P}$  NMR spectroscopy.

#### LC-MS reaction analysis

Reactions between **3.3d** and **3.10** were analyzed via LC-MS. Compound **3.3d** (250  $\mu\text{M}$  final concentration) and **3.10** (500  $\mu\text{M}$  final concentration) were mixed in PBS containing 50% MeCN and incubated at room temperature for 2 h. Reactions were analyzed on a Waters ACQUITY UPLC with an ACQUITY QDa Mass Detector, using a C18 column and eluting with a gradient of 10-90% MeCN/ $\text{H}_2\text{O}$  (containing 0.1% formic acid) over 3.5 min.

### **3.4e Protein functionalization and mass spectrometry**

**Lys-CpS** and **Lys-CpO** were prepared by treating lysozyme with cyclopropenethione **3.11** or cyclopropenone **3.12** using previously reported conditions [26]. Hen egg-white lysozyme (Sigma Aldrich, 1 mL of a 10 mg/mL solution in 1:1 DMSO/PBS) was treated with 100  $\mu\text{L}$  of either **3.11** or **3.12** (100 mM stock in DMSO). The solution was allowed to stand at room temperature for 3–5 h. The functionalized proteins were isolated using P-10 Biogel (BioRad), eluting with PBS (12 mM, pH 7.4). Protein-containing fractions were combined and concentrated to a volume of  $\sim 100$   $\mu\text{L}$  using a spin filter (3 kDa molecular weight cutoff). PBS (12 mM, pH 7.4) was then added to bring the volume to 400  $\mu\text{L}$ , and the sample was concentrated again. This process was repeated 3 times to remove excess small molecules. Protein concentrations were measured with a Nanodrop® ND- 1000 (Thermo Scientific), using absorbance readings at 280 nm and an extinction coefficient of  $36 \text{ mM}^{-1} \text{ cm}^{-1}$  [27].

### **3.4f Western blot analysis of protein conjugates**

**Lys-CpS** (2.7  $\mu\text{L}$  of a 150  $\mu\text{M}$  solution in PBS, 20  $\mu\text{M}$  final concentration) and phosphine **3.13** (2  $\mu\text{L}$  of a 1 or 10 mM stock in DMSO, 250  $\mu\text{M}$  or 1 mM final concentration, respectively) were mixed with PBS (12 mM, pH 7.4) to total 20  $\mu\text{L}$ . The reactions were incubated at 37 °C for 0–60 min. For time course experiments, reactions were quenched with 2-(4-morpholino-4-oxobutyl)cycloprop-2-en-1-one [11] (1  $\mu\text{L}$ , 100 mM in DMSO) and stored at  $-20$  °C until SDS-PAGE analysis. For cell lysate experiments, overnight cultures of *E. coli* XL1 cells were grown in Luria-Bertani broth containing tetracycline (10  $\mu\text{g}/\text{mL}$ ). Cultures were incubated at 37 °C with shaking (225

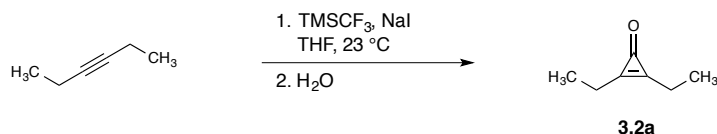
rpm). Cells were collected by centrifugation, resuspended in PBS (pH 7.4), sonicated, and centrifuged (14,500 rpm, 30 min). Total protein concentration was determined using UV-vis spectroscopy.

To prepare samples for SDS-PAGE and Western blot, 6.7  $\mu$ L of 4X SDS-PAGE loading buffer (containing 8%  $\beta$ ME) was added to each reaction mixture. For lysate labeling experiments, 5  $\mu$ L of 8 M urea and 8.3  $\mu$ L of 4X SDS-PAGE loading buffer (containing 8%  $\beta$ ME) were added. Samples were then split evenly into 2 portions and subjected to SDS-PAGE using 4–20% polyacrylamide gels (BioRad). For each experiment, one gel was stained with Coomassie Blue, and the second was electroblotted to a nitrocellulose membrane (0.2  $\mu$ m, BioRad). Membranes were stained with Ponceau C to assess transfer efficiency, then rinsed with H<sub>2</sub>O and incubated with blocking buffer (7% BSA in PBS containing 1% Tween-20<sup>®</sup>, PBST) overnight at 4 °C. The membranes were then treated with IRDye<sup>®</sup> 800CW streptavidin (LI-COR Biosciences; 1:10,000 dilution in blocking buffer) for 2 h at room temperature. Membranes were then washed with PBST (6 x 10 min) and PBS (3 x 5 min). Blots were imaged using an Odyssey infrared imaging system (LI-COR, Odyssey<sup>®</sup> CLx).

### ***3.4g Synthetic procedures***

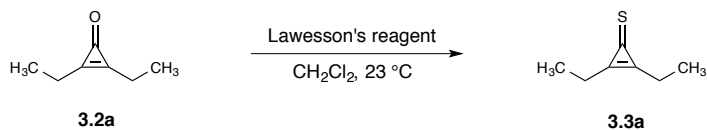
Compounds **S-3.1** [12], **3.3b–c** [28], **3.4** and **3.7** [11], **3.6** [29], and **3.8–3.9** [12] were prepared as previously reported.





### 2,3-Diethylcycloprop-2-en-1-one (3.2a)

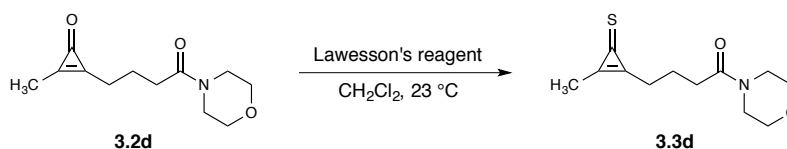
This compound was synthesized following the general procedure of Wang, *et al.* [22] with some modifications. To an oven-dried Schlenk tube containing a stir bar was added NaI (330 mg, 2.2 mmol). The NaI was gently flame-dried under vacuum. A solution of 3-hexyne (0.11 mL, 1.0 mmol) in anhydrous THF (3.0 mL) was then added against positive N<sub>2</sub> flow. Trifluoromethyltrimethylsilane (0.30 mL, 2.0 mmol) was added, and the Schlenk tube was sealed. The reaction was stirred vigorously at room temperature for ~14 h, then diluted with H<sub>2</sub>O (20 mL) and extracted with CH<sub>2</sub>Cl<sub>2</sub> (3 x 10 mL). The combined organic layers were dried over MgSO<sub>4</sub> and filtered. The filtrate was concentrated *in vacuo*, and the residue was purified by flash column chromatography (eluting with 0–10% acetone/CH<sub>2</sub>Cl<sub>2</sub>) to give **3.2a** as a yellow oil (65 mg, 0.59 mmol, 59%). <sup>1</sup>H NMR (400 MHz, CDCl<sub>3</sub>) δ 2.64 (qt, *J* = 7.6, 0.9 Hz, 4H), 1.31 (t<sub>app</sub>, *J* = 7.6 Hz, 6H). <sup>13</sup>C NMR (126 MHz, CDCl<sub>3</sub>) δ 161.5, 159.8, 20.0, 11.3. HRMS (ESI+) calculated for C<sub>7</sub>H<sub>10</sub>ONa [M+Na]<sup>+</sup> 133.0629 *m/z*, found 133.0629.



### 2,3-Diethylcycloprop-2-ene-1-thione (3.3a)

This compound was synthesized following the general procedure of Zhao, *et al.* [28]. To a flame-dried 50 mL round-bottom flask was added **3.2a** (110 mg, 1.0 mmol).

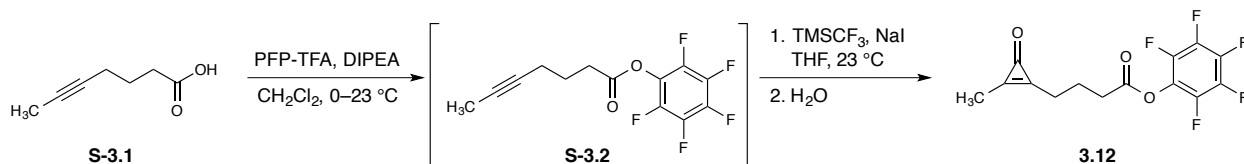
Anhydrous  $\text{CH}_2\text{Cl}_2$  (10 mL) was added under an atmosphere of  $\text{N}_2$ . Lawesson's reagent (200 mg, 0.50 mmol) was then added, and the reaction was stirred at room temperature for 1 h. Approximately half of the solvent was removed *in vacuo*, and the crude reaction mixture was purified by flash column chromatography (eluting with 0–10% acetone/ $\text{CH}_2\text{Cl}_2$ ) to give **3.3a** as a pale yellow oil (110 mg, 0.87 mmol, 87%).  $^1\text{H}$  NMR (400 MHz,  $\text{CDCl}_3$ )  $\delta$  2.85 (qt,  $J = 7.6, 0.9$  Hz, 4H), 1.39 (t<sub>app</sub>,  $J = 7.5$  Hz, 6H).  $^{13}\text{C}$  NMR (126 MHz,  $\text{CDCl}_3$ )  $\delta$  186.2, 169.1, 19.9, 10.1. HRMS (ESI+) calculated for  $\text{C}_7\text{H}_{10}\text{SNa}$   $[\text{M}+\text{Na}]^+$  149.0401  $m/z$ , found 149.0403.



#### 4-(2-Methyl-3-thioxocycloprop-1-en-1-yl)-1-morpholinobutan-1-one (**3.3d**)

This compound was synthesized following the general procedure of Zhao, *et al* [28]. To a flame-dried 25 mL round-bottom flask was added **3.2d** (185 mg, 0.830 mmol). Anhydrous  $\text{CH}_2\text{Cl}_2$  (10 mL) was added under an atmosphere of  $\text{N}_2$ . Lawesson's reagent (170 mg, 0.420 mmol) was then added, and the reaction was stirred at room temperature for 2 h. Approximately half of the solvent was removed *in vacuo*, and the crude reaction mixture was purified by flash column chromatography (eluting with 0–2% MeOH/ $\text{CH}_2\text{Cl}_2$ ) to give **3.3d** as a pale yellow oil (132 mg, 0.552 mmol, 66.5%).  $^1\text{H}$  NMR (400 MHz,  $\text{CDCl}_3$ )  $\delta$  3.76–3.72 (m, 4H), 3.63–3.61 (m, 2H), 3.60–3.57 (m, 2H), 2.95 (tq,  $J = 6.7, 0.8$  Hz, 2H), 2.72 (t,  $J = 7.1$  Hz, 2H), 2.49 (t,  $J = 0.8$  Hz, 3H), 2.13 (quin,  $J = 6.9$  Hz, 2H).  $^{13}\text{C}$  NMR (126 MHz,  $\text{CDCl}_3$ )  $\delta$  186.4, 170.5, 168.6, 164.9, 67.0, 66.8, 46.1,

42.1, 31.9, 26.0, 21.2, 11.3. HRMS (ESI+) calculated for  $C_{12}H_{17}NO_2SNa$   $[M+Na]^+$  262.0878  $m/z$ , found 262.0868.

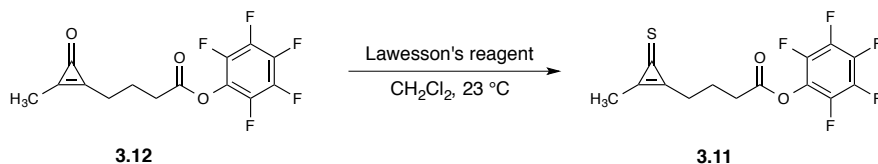


### Perfluorophenyl 4-(2-methyl-3-oxocycloprop-1-en-1-yl)butanoate (**3.12**)

To a flame-dried 50 mL round-bottom flask was added **S-3.1** (2.00 g, 15.9 mmol), anhydrous  $CH_2Cl_2$  (50 mL), and diisopropylethylamine (5.50 mL, 31.7 mmol). The solution was stirred under an atmosphere of  $N_2$  and cooled in an ice bath. Pentafluorophenyl trifluoroacetate (4.10 mL, 23.8 mmol) was added dropwise over ~5 min. The reaction was warmed to room temperature and stirred for 45 min. Excess solvent was then removed *in vacuo*, and the crude reaction mixture was purified by flash column chromatography (eluting with 0–5%  $Et_2O$ /hexanes) to give **S-3.2** as a pale yellow oil. This material was used directly in the next step.

Compound **3.12** was synthesized following the general procedure of Wang *et al.* [22] with some modifications. To an oven-dried Schlenk tube containing a stir bar was added NaI (4.15 g, 27.7 mmol). The NaI was gently flame-dried under vacuum. Compound **S-3.2** was dissolved in anhydrous THF (38.0 mL) and added against positive  $N_2$  flow. Trifluoromethyltrimethylsilane (3.70 mL, 25.1 mmol) was added, and the Schlenk tube was sealed. The reaction was stirred vigorously at room temperature for ~36 h, and then diluted with  $H_2O$  (100 mL) and extracted with  $CH_2Cl_2$  (3 x 30 mL). The combined organic layers were dried over  $MgSO_4$ , then filtered. The filtrate was

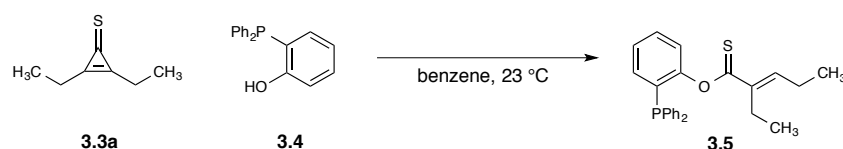
concentrated *in vacuo*, and the residue was purified by flash column chromatography (eluting with 50–100% EtOAc/hexanes) to give **3.12** as a dark yellow solid (2.75 g, 8.59 mmol, 54.0% over 2 steps).  $^1\text{H}$  NMR (400 MHz,  $\text{CDCl}_3$ )  $\delta$  2.85 (t,  $J = 7.3$  Hz, 2H), 2.77 (tq,  $J = 7.4, 0.9$  Hz, 2H), 2.31 (t,  $J = 0.9$  Hz, 3H), 2.20 (quin,  $J = 7.3$  Hz, 2H).  $^{19}\text{F}$  NMR (376 MHz,  $\text{CDCl}_3$ )  $\delta$  - 153.0 (d,  $J = 16.9$  Hz, 2F), -157.9 (t,  $J = 21.8$  Hz, 1F), -162.3 (dd,  $J = 21.7, 17.2$  Hz, 2F).  $^{13}\text{C}$  NMR (126 MHz,  $\text{CDCl}_3$ )  $\delta$  168.6, 159.9, 159.2, 158.1, 141.1 (ddq,  $J = 251.4, 12.3, 4.1$  Hz), 139.6 (dtt<sub>app</sub>,  $J = 253.8, 13.8, 3.9$  Hz), 137.9 (m), 124.9 (m), 32.4, 25.4, 21.3, 11.4. HRMS (ESI+) calculated for  $\text{C}_{14}\text{H}_9\text{F}_5\text{O}_3\text{Na}$   $[\text{M}+\text{Na}]^+$  343.0370  $m/z$ , found 343.0378.



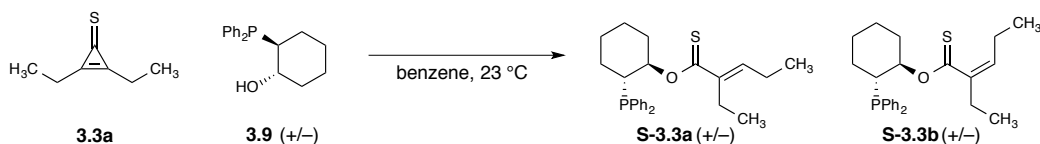
### Perfluorophenyl 4-(2-methyl-3-thioxocycloprop-1-en-1-yl)butanoate (**3.11**)

This compound was synthesized following the general procedure of Zhao, *et al.* [28]. To a flame-dried 50 mL round-bottom flask was added **3.12** (143 mg, 0.450 mmol). Anhydrous  $\text{CH}_2\text{Cl}_2$  (6.0 mL) was added under an atmosphere of  $\text{N}_2$ . Lawesson's reagent (100 mg, 0.247 mmol) was then added, and the reaction was stirred at room temperature for 2 h. Approximately half of the solvent was removed *in vacuo*, and the crude reaction mixture was purified by flash column chromatography (eluting with 50–100% EtOAc/hexanes) to give **3.11** as a pale yellow solid (121 mg, 0.360 mmol, 80.0%).  $^1\text{H}$  NMR (400 MHz,  $\text{CDCl}_3$ )  $\delta$  2.99 (t,  $J = 7.2$  Hz, 2H), 2.98 (tq,  $J = 7.2, 0.9$  Hz, 2H), 2.52 (t,  $J = 0.9$  Hz, 3H), 2.29 (quin,  $J = 7.2$  Hz, 2H).  $^{19}\text{F}$  NMR (376 MHz,  $\text{CDCl}_3$ )  $\delta$  -

153.0 (d,  $J = 17.1$  Hz, 2F), -157.8 (t,  $J = 21.7$  Hz, 1F), -162.3 (dd,  $J = 21.8, 17.2$  Hz, 2F).  $^{13}\text{C}$  NMR (126 MHz,  $\text{CDCl}_3$ )  $\delta$  186.1, 168.6, 167.2, 165.3, 141.1 (ddq,  $J = 251.2, 12.5, 4.0$  Hz), 139.6 (dt<sub>app</sub>,  $J = 253.8, 13.9, 4.5$  Hz), 137.9 (dt<sub>app</sub>,  $J = 252.5, 14.0, 4.3$  Hz), 124.8 (m), 32.4, 25.3, 20.8, 11.3. HRMS (ESI+) calculated for  $\text{C}_{14}\text{H}_9\text{F}_5\text{O}_2\text{SNa}$   $[\text{M}+\text{Na}]^+$  359.0141  $m/z$ , found 359.0145.



**O-(2-(Diphenylphosphanyl)phenyl) (E)-2-ethylpent-2-enethioate (3.5)** To a glass vial was added **3.3a** (6.3 mg, 0.050 mmol) and benzene (0.65 mL). Phosphine **3.4** (14 mg, 0.050 mmol) was added, and the reaction was stirred at room temperature for 10 min. The crude material was then passed through a small plug of neutral alumina, eluting with hexanes. The yellow fractions were collected, and the solvent was removed *in vacuo* to give **3.5** (18 mg, 0.045 mmol, 90%) as a yellow solid.  $^1\text{H}$  NMR (400 MHz,  $\text{C}_6\text{D}_6$ )  $\delta$  7.40–7.33 (m, 4H), 7.04–7.02 (m, 9H), 6.88 (t,  $J = 7.6$  Hz, 1H), 6.85–6.82 (m, 1H), 2.64 (q,  $J = 7.5$  Hz, 2H), 1.83 (quin,  $J = 7.5$  Hz, 2H), 1.11 (t,  $J = 7.5$  Hz, 3H), 0.75 (t,  $J = 7.5$  Hz, 3H).  $^{31}\text{P}$  NMR (162 MHz,  $\text{C}_6\text{D}_6$ )  $\delta$  -15.31.  $^{13}\text{C}$  NMR (126 MHz,  $\text{C}_6\text{D}_6$ )  $\delta$  211.0, 157.8 (d,  $J = 18.6$  Hz), 141.98, 141.96, 136.8 (d,  $J = 12.1$  Hz), 134.5, 134.4 (d,  $J = 20.5$  Hz), 131.7 (d,  $J = 16.1$  Hz), 130.1, 129.0, 128.8 (d,  $J = 7.0$  Hz), 126.5, 123.9 (d,  $J = 2.2$  Hz), 22.9, 22.7, 14.3, 13.2. HRMS (ESI+) calculated for  $\text{C}_{25}\text{H}_{25}\text{OPSH}$   $[\text{M}+\text{H}]^+$  405.1442  $m/z$ , found 405.1451.



**O-((1R,2R)-2-(Diphenylphosphanyl)cyclohexyl) (E)-2-ethylpent-2-enethioate (S-3.3a) and O-((1R,2R)-2-(diphenylphosphanyl)cyclohexyl) (Z)-2-ethylpent-2-enethioate (S-3.3b).**

To a glass vial was added **3.3a** (6.3 mg, 0.050 mmol) and benzene (1.3 mL). Phosphine **3.9** (16 mg, 0.050 mmol) was added, and the reaction was stirred at room temperature for 2 h. The crude material was then passed through a small plug of neutral alumina, eluting with hexanes. The yellow fractions were collected, and the solvent was removed *in vacuo* to give **S-3.3a** and **S-3.3b** in a 2.1:1.0 ratio (12 mg, 0.029 mmol, 58%) as a yellow oil.  $^1\text{H}$  NMR (400 MHz,  $\text{C}_6\text{D}_6$ )  $\delta$  7.59–7.51 (m, 4H), 7.12–7.01 (m, 6H), 6.85 (t,  $J = 7.5, 1.0$  Hz, 1H), 5.93–5.88 (m, 1H), 5.87–5.83 (m, 1H), 2.87 (td,  $J = 8.4, 3.7$  Hz, 1H), 2.80 (td,  $J = 8.7, 3.9$  Hz, 1H), 2.62–2.54 (m, 2H), 2.48–2.26 (m, 2H), 1.92–1.78 (m, 2H), 1.78–1.72 (m, 2H), 1.62–1.40 (m, 3H), 1.24–1.11 (m, 2H), 1.09 (td,  $J = 7.5, 1.0$  Hz, 3H), 1.04 (td,  $J = 7.5, 1.0$  Hz, 3H), 0.96 (td,  $J = 7.5, 0.8$  Hz, 3H), 0.81 (t,  $J = 7.6$  Hz, 3H).  $^{31}\text{P}$  NMR (162 MHz,  $\text{C}_6\text{D}_6$ )  $\delta$  -7.75, -8.30.  $^{13}\text{C}$  NMR (126 MHz,  $\text{C}_6\text{D}_6$ )  $\delta$  216.1, 212.3, 144.1, 143.0, 141.1, 137.4 (d,  $J = 14.4$  Hz), 136.77 (d,  $J = 17.3$  Hz), 136.71 (d,  $J = 17.3$  Hz), 135.1, 135.0, 134.9, 133.6 (d,  $J = 19.3$  Hz), 133.4 (d,  $J = 18.7$ ), 132.4, 129.3, 129.2, 128.7, 128.63, 128.58, 128.5, 128.4, 81.0 (d,  $J = 17.4$  Hz), 80.9 (d,  $J = 16.7$  Hz), 39.6 (d,  $J = 16.7$  Hz), 39.3 (d,  $J = 17.3$  Hz), 30.56, 30.51, 30.4, 30.3, 30.2, 27.0, 26.91, 26.87, 24.8 (d,  $J = 5.3$  Hz), 23.7, 23.6, 23.3, 22.5 (d,  $J = 7.0$  Hz), 14.4,

14.3, 13.4, 13.4. HRMS calculated for C<sub>25</sub>H<sub>31</sub>O<sub>3</sub>S [M+H]<sup>+</sup> 411.1912 *m/z*, found 411.1916.

### 3.5 References

1. D. M. Patterson, L. A. Nazarova, J. A. Prescher. Finding the right (bioorthogonal) chemistry. *ACS Chem. Biol.* **2014**, *9*, 592–605.
2. K. Lang, J. W. Chin. Cellular incorporation of unnatural amino acids and bioorthogonal labeling of proteins. *Chem. Rev.* **2014**, *114*, 4764–4806.
3. T. Peng, H. C. Hang. Site-specific bioorthogonal labeling for fluorescence imaging of intracellular proteins in living cells. *J. Am. Chem. Soc.* **2016**, *138*, 14423–14433.
4. J. A. Prescher, D. H. Dube, C. R. Bertozzi. Chemical remodelling of cell surfaces in living animals. *Nature* **2004**, *430*, 873–877.
5. B. Alvarez-Castelao, C. T. Schanzenbächer, C. Hanus, C. Glock, S. T. Dieck, A. R. Dörrbaum, I. Bartnik, B. Nassim-Assir, E. Ciirdaeva, A. Mueller, D. C. Dieterich, D. A. Tirrell, J. D. Langer, E. M. Schuman. Cell-type-specific metabolic labeling of nascent proteomes *in vivo*. *Nat. Biotechnol.* **2017**, *35*, 1196–1201.
6. T. S. Elliott, F. M. Townsley, A. Bianco, R. J. Ernst, A. Sachdeva, S. J. E. A. Elsässer, L. Davis, K. Lang, R. Pisa, S. Greiss, K. S. Lilley, J. W. Chin. Proteome labeling and protein identification in specific tissues and at specific developmental stages in an animal. *Nat. Biotechnol.* **2014**, *32*, 465–472.

7. R. M. Versteegen, R. Rossin, W. ten Hoeve, H. M. Janssen, M. S. Robillard. Click to release: Instantaneous doxorubicin elimination upon tetrazine ligation. *Angew. Chem. Int. Ed.* **2013**, *52*, 14112–14116.
8. J. M. Mejia Oneto, I. Khan, L. Seebald, M. Royzen. *In vivo* bioorthogonal chemistry enables local hydrogel and systemic pro-drug to treat soft tissue sarcoma. *ACS Cent. Sci.* **2016**, *2*, 476–482.
9. D. M. Patterson, J. A. Prescher. Orthogonal bioorthogonal chemistries. *Curr. Opin. Chem. Biol.* **2015**, *28*, 141–149.
10. R. D. Row, J. A. Prescher. Constructing new bioorthogonal reagents and reactions. *Acc. Chem. Res.* **2018**, *51*, 1073–1081.
11. H.-W. Shih, J. A. Prescher. A bioorthogonal ligation of cyclopropenones mediated by triarylphosphines. *J. Am. Chem. Soc.* **2015**, *137*, 10036–10039.
12. R. D. Row, H.-W. Shih, A. T. Alexander, R. A. Mehl, J. A. Prescher. Cyclopropenones for metabolic targeting and sequential bioorthogonal labeling. *J. Am. Chem. Soc.* **2017**, *139*, 7370–7375.
13. S. Shingh, M. M. Bhadbhade, K. Venkatesan, V. Ramamurthy. Strain-assisted  $\alpha$ -cleavage reactions of thioketones: Diphenylcyclopropenethione. *J. Org. Chem.* **1982**, *47*, 3550–3553.
14. S. Shingh, V. Ramamurthy. Regioselectivity in  $\alpha$ -cleavage reactions: arylalkylcyclopropenethiones. *J. Org. Chem.* **1985**, *50*, 3732–3738.
15. B. Niu, B. Jiang, L.-Z. Yu, M. Shi. Base-promoted [3 + 3] cyclization of cyclopropenones and cyclopropenethiones with amides for the synthesis of 6H-



- 1,3-oxazin-6-ones and 6H-1,3-thiazin-6-ones. *Org. Chem. Front.* **2018**, *5*, 1267–1271.
16. K. T. Potts, J. Baum. Ring expansion of heteroaromatic betaines with cyclopropene derivatives. *Chem. Commun.* **1973**, *0*, 833–834.
17. S. Yoneda, K. Ozaki, T. Inoue, A. Sugimoto. Novel dimerization reaction of bis(alkylthio)cyclopropenethiones affording tetrakis(alkylthio)thieno[3,4-c]thiophene. *J. Am. Chem. Soc.* **1985**, *107*, 5801–5802.
18. N. Matsumura, H. Tanaka, Y. Yagyu, K. Mizuno, H. Inoue, K. Takada, M. Yasui, F. Iwasaki. Synthesis and reactivity of new 1,4-bis(alkylthio)-3,6-diarylthieno[3,4-c]thiophene derivatives. *J. Org. Chem.* **1998**, *63*, 163–168.
19. C. R. Walters, D. M. Szantai-Kis, Y. Zhang, Z. E. Reinert, W. S. Horne, D. M. Chenoweth, E. J. Petersson. The effects of thioamide backbone substitution on protein stability: A study in  $\alpha$ -helical,  $\beta$ -sheet, and polyproline II helical contexts. *Chem. Sci.* **2017**, *8*, 2868–2877.
20. A. Choudhary, R. T. Raines. An evaluation of peptide-bond isosteres. *ChemBioChem* **2011**, *12*, 1801–1807.
21. X. Chen, E. G. Mietlicki-Baase, T. M. Barrett, L. E. McGrath, K. Koch-Laskowski, J. J. Ferrie, M. R. Hayes, E. J. Petersson. Thioamide substitution selectively modulates proteolysis and receptor activity of therapeutic peptide hormones. *J. Am. Chem. Soc.* **2017**, *139*, 16688–16695.
22. F. Wang, T. Luo, J. Hu, Y. Wang, H. S. Krishnan, P. V. Jog, S. K. Ganesh, G. K. S. Prakash, G. A. Olah. Synthesis of *gem*-difluorinated cyclopropanes and

- cyclopropenes: Trifluoromethyltrimethylsilane as a difluorocarbene source. *Angew. Chem. Int. Ed.* **2011**, *50*, 7153–7157.
23. A. Schönberg, M. Mamluk. Photo-dimerisierung des diphenylcyclopropenthions zu einem thiophenderivat. *Tetrahedron Lett.* **1971**, *52*, 4993–4994.
  24. M. B. Soellner, B. L. Nilsson, R. T. Raines. Reaction mechanism and kinetics of the traceless Staudinger ligation. *J. Am. Chem. Soc.* **2006**, *128*, 8820–8828.
  25. H.-W. Shih, D. N. Kamber, J. A. Prescher. Building better bioorthogonal reactions. *Curr. Opin. Chem. Biol.* **2014**, *21*, 103–111.
  26. G. T. Hermanson, *Bioconjugate Techniques*. (Academic Press, San Diego, 1996).
  27. R. C. Davies, A. Neuberger, B. M. Wilson. The dependence of lysozyme activity on pH and ionic strength. *Biochim. Biophys. Acta.* **1969**, *178*, 294–305.
  28. W.-T. Zhao, M. Shi. Reactions of cyclopropenethiones and acetylenedicarboxylates: Synthesis of substituted thioethers and thiocyclobutanones. *Tetrahedron Lett.* **2015**, *56*, 5086–5089.
  29. G. D. Figuly, C. K. Loop, J. C. Martin. Directed *ortho*-lithiation of lithium thiophenolate. New methodology for the preparation of *ortho*-substituted thiophenols and related compounds. *J. Am. Chem. Soc.* **1989**, *111*, 654–658.

## **Chapter 4: Chemically triggered crosslinking with bioorthogonal cyclopropenones**

### **4.1 Introduction**

Biomolecular interactions play many vital roles in cell biology. Proteins, nucleic acids, lipids, and small metabolites often contact numerous other biomolecules, and these interactions impact cell function, communication, and disease states [1, 2]. Identifying and understanding these interactions would provide a more complete picture of cell biology. Assays to interrogate binding events are also highly valuable for confirming drug target engagement and investigating mechanisms of action [3]. Identifying biomolecule interactions should also improve our understanding of diseases and reveal new therapeutic targets [4, 5].

Several platforms exist for monitoring biomolecule interactions. Genetic reporters are commonly used to probe binding partners through Förster resonance energy transfer (FRET) assays [6]. These assays involve spectrally matched fluorescent proteins that provide different wavelengths of light depending on their relative proximity. When fused to proteins of interest, FRET reporters can provide a readout on protein-protein interactions [7]. Such protein fusion reporters have been extensively applied to map signal transduction networks and other features [8-10], but limitations remain. For example, genetically encoded reporters can only be routinely employed to protein targets. Other biomolecules can be tagged with small fluorophores, but such probes cannot be easily delivered in the context of living cells. Additionally, the fusion of fluorescent proteins to a target of interest can impact the target's expression levels, fold and stability, and interactions with other biomolecules.

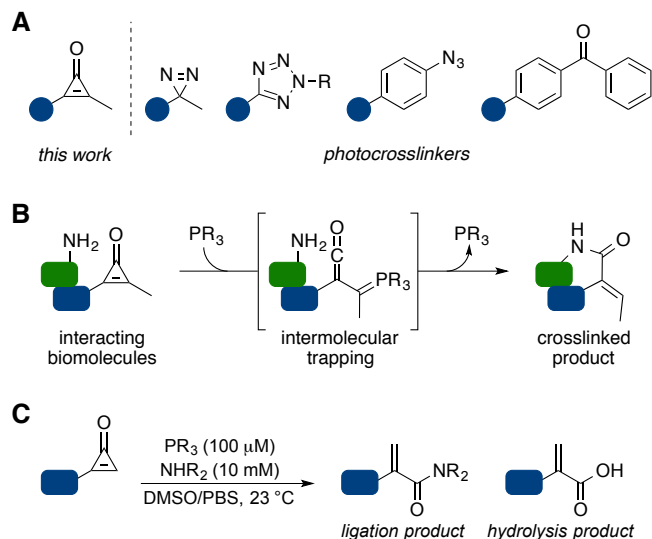


**Figure 4-1.** Chemically activated crosslinking with cyclopropanones. A) A variety of photoactivatable crosslinkers are commonly in use. The unique mechanism of cyclopropanone-phosphine reactions may complement these reagents. B) Cyclopropanones react with phosphines to form ketene-ylides. These reactive intermediates can be trapped intramolecularly for biomolecule labeling, or intermolecularly to trap biomolecular interactions. C) Trapping with exogenous nucleophiles requires high concentrations. Previous work in the Prescher lab [11] showed that, even with high concentrations of amine present, significant hydrolysis of the ketene intermediate occurred.

Another common strategy to profile biomolecule interactions is covalent photocrosslinking [12]. Diazirines [13], aryl azides [12], benzophenones [14], and nitrile imines [15, 16] are among the most popular photocrosslinkers. All of these motifs have been used *in vitro* and in cells to monitor interactions between proteins [17-19], nucleic acids [20, 21], and other molecules [22, 23]. Once installed, photocrosslinkers can be activated to high energy species upon irradiation with UV light. Subsequent trapping (typically via endogenous nucleophiles) affords the covalent crosslink. Photocrosslinkers have the advantage of being both spatially and temporally controlled,

as UV light can be selectively delivered to cultured cells. The small size of most crosslinkers also minimizes their impact on target biomolecules. Many of these scaffolds can be installed via cellular enzymes and metabolic incorporation, including genetic code expansion [17, 19, 20, 24].

While widely employed, photocrosslinkers also have limitations. Many suffer from high background levels via off-target crosslinking [25]. This is partially due to the non-specific nature of their reactivity, which also makes the site of crosslinking random for many photocrosslinkers. Perhaps a greater liability is the need for irradiation with UV light. This limits the compatibility of photocrosslinkers for many experiments in live cells and organisms – environments that are refractory to illumination or not tolerant of long exposures. These limitations have prompted others to use electrophilic warheads to trap interactions [26-28]. However, these electrophiles are also notoriously non-specific and generally not responsive to external stimuli. Thus, there is a continuing need for complementary crosslinking methods.

To develop a complementary method to crosslink biomolecules, we investigated cyclopropenones as *chemically* activatable motifs. We previously demonstrated that these scaffolds could undergo bioorthogonal ligations with substituted phosphines [11, 29]. In the ligations, phosphines react with cyclopropenones to form reactive ketene-ylides (Figure 4-1). These intermediates can then be trapped intramolecularly to provide covalent adducts. We hypothesized that the ketene-ylide could also be trapped by *intermolecular* interactions. If positioned near a nucleophile on a nearby biomolecule, phosphine activation of a cyclopropenone should result in a covalent crosslink (Figure 4-1B). Using a model protein-peptide interaction, we showed that these ligations

proceed readily to form covalent adducts. We also demonstrated that cyclopropenones can be site-specifically installed in proteins of interest for future studies. This approach was enabled by genetic code expansion, setting the stage for applications with site-specifically installed cyclopropenone crosslinkers.

## **4.2 Results and discussion**

A previous member of the Prescher laboratory (Dr. Hui-Wen Shih) showed that cyclopropenones could be activated with phosphines and subsequently trapped with exogenous amines [11]. The intermolecular reactions could be performed both in aqueous solution and on protein surfaces. The trapping step required large (>10 mM) concentrations of amine nucleophiles. Even at these concentrations, though, significant hydrolysis was observed due to competitive trapping by water (Figure 4-1C). These data indicated that high concentrations of exogenous nucleophiles are required to trap the ketene-ylide in aqueous solutions. We hypothesized that this feature would be ideal for protein crosslinking. A high local concentration of nucleophilic residues (necessary for efficient trapping) would be achieved only with interacting biomolecules. In the absence of an effective nucleophile, hydrolysis would be dominant, minimizing non-specific crosslinking.

We proceeded to test cyclopropenone crosslinking on a model protein interaction. We selected a previously reported split luciferase reporter, Nanoluciferase (Nluc), for these studies (Figure 4-2A) [30]. In split Nluc, an 11-13 residue peptide (“smallbit”) is removed from the N-terminus of a larger engineered Nluc fragment (“largebit”). These peptides bind readily to form an active, light-emitting enzyme. Based

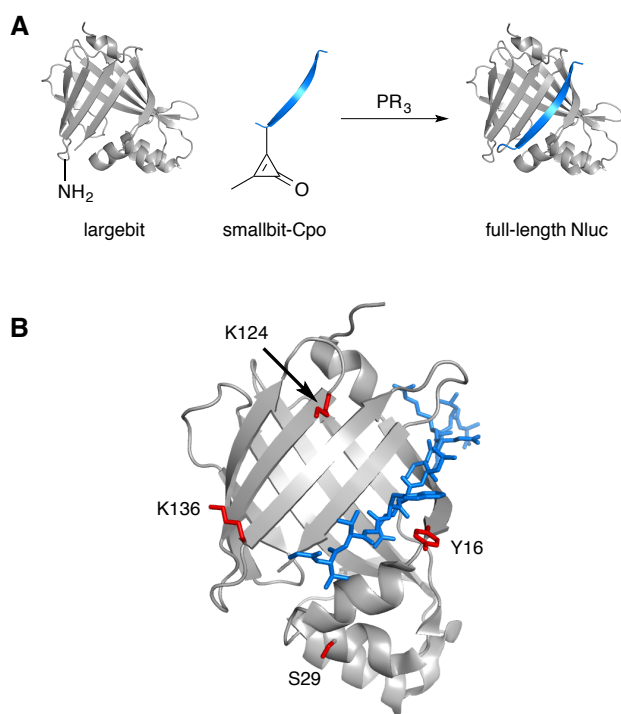


**Figure 4-2.** Split luciferase model system. A) Strategy for analyzing bioorthogonal crosslinking of largebit and smallbit. B) The crystal structure of Nluc (PDB 5B0U), showing the smallbit peptide in blue. Potential trapping residues are highlighted in red.

on the available crystallography data for Nluc [31], we hypothesized that a cyclopropanone appended to the N-terminus of the smallbit peptide would be within reach of several potential nucleophilic side chains when bound to largebit (Figure 4-2B). Incubation with phosphine would enable covalent trapping of the two pieces. Additionally, there are several variants of smallbit that span a range of largebit-binding affinities [30]. Testing these peptide fragments in tandem would allow us to examine trapping efficiency as a function of binding affinity.





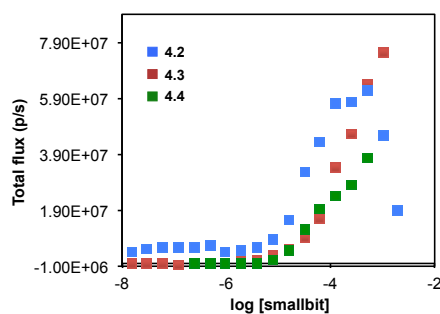


**Figure 4-4.** Smallbit dissociation constants. Peptides **4.2–4.4** (0.5 nM – 2 mM) were combined with largebit (40 pM) and incubated at room temperature for 30 min. Furimazine (Promega, 100  $\mu$ L of a 50X dilution of the commercial stock) was added, and bioluminescence output was measured. Largebit luminescence decreased at high concentrations of **4.2** (> 1 mM), indicating possible inhibition. The limited solubility of **4.4** prevented measurements at concentrations above 500  $\mu$ M.

**Table 4-1.** Apparent  $K_D$  values for largebit and peptides **4.2–4.4**.

smallbit peptide	dissociation constant ( $K_D$ )
H <sub>2</sub> N-K(Cpo)VSGWRLFKKISN-NH <sub>2</sub> <b>4.2</b>	20 $\mu$ M
H <sub>2</sub> N-K(Cpo)VTGWRLSERILA-NH <sub>2</sub> <b>4.3</b>	250 $\mu$ M
H <sub>2</sub> N-K(Cpo)VTGWRLFEEIL-NH <sub>2</sub> <b>4.4</b>	> 500 $\mu$ M

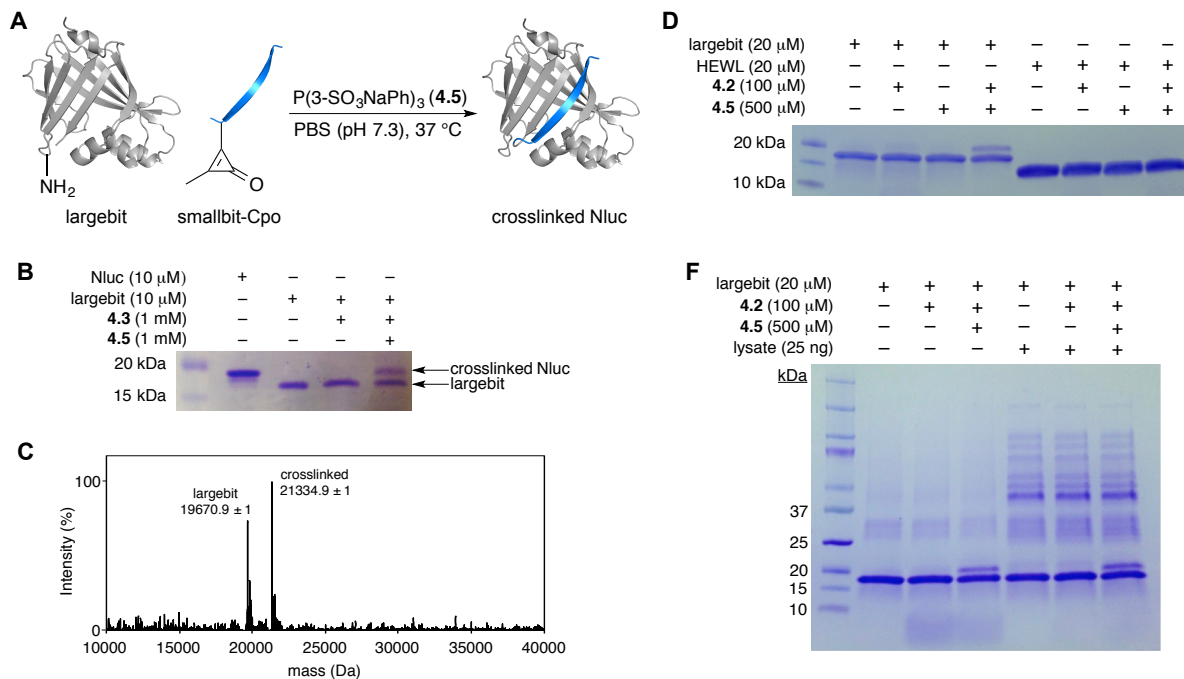


**Figure 4-5.** Covalent crosslinking is possible through activation and subsequent trapping of cyclopropenones. A) Largebit and peptides **4.2–4.4** were combined in PBS (pH 7.4), treated with phosphine **4.5** and analyzed via mass spectrometry and SDS-PAGE. B) Largebit (10  $\mu\text{M}$ ) and peptide **4.3** (1 mM) were combined and treated with phosphine **4.5** (1 mM) for 16 h at 37  $^\circ\text{C}$ . The reactions were analyzed via SDS-PAGE, and C) mass spectrometry. D) Smallbit **4.2** does not form covalent adducts with hen egg-white lysozyme (HEWL). Largebit (20  $\mu\text{M}$ ) or HEWL (20  $\mu\text{M}$ ) and **4.2** (100  $\mu\text{M}$ ) were incubated in PBS (pH 7.4) in the presence of phosphine **4.5** (500  $\mu\text{M}$ ) at 37  $^\circ\text{C}$  for 10 h. Samples were analyzed via SDS-PAGE. No crosslinking to HEWL was observed. E) Crosslinking in bacterial lysate. Largebit (20  $\mu\text{M}$ ) and peptide **4.2** (100  $\mu\text{M}$ ) were incubated in PBS (pH 7.4) containing bacterial lysate (25  $\mu\text{g}$ ) and phosphine **4.5** (500  $\mu\text{M}$ ) at 37  $^\circ\text{C}$  for 4 h.

We synthesized a panel of smallbit peptides (**4.2–4.4**) (Scheme 4-1 and Figure 4-3) bearing appended cyclopropanones. The sequences of **4.2–4.4** were based on previously reported peptides [30] that we anticipated would have significantly different binding affinities for largebit. To install cyclopropanones, an Fmoc-protected lysine analog bearing an appended cyclopropanone (**4.1**) was attached at the N-terminal positions. The peptides were prepared by solid phase peptide synthesis (Scheme 4-1). The peptides were purified via HPLC and subsequently analyzed for binding to largebit. Peptide affinities were measured using light emission upon complementation with largebit [30]. The apparent  $K_D$  values for **4.2–4.4** were decreased relative to the parent peptides [30], but the values matched the expected trends (Figure 4-4). Smallbit **4.2** exhibited the highest affinity ( $K_D = 20 \mu\text{M}$ ), **4.3** had weaker binding ( $K_D = 250 \mu\text{M}$ ), and peptide **4.4** had the lowest affinity ( $K_D > 500 \mu\text{M}$ , Figure 4-4 and Table 4-1).

With peptides **4.2–4.4** in hand, we proceeded to test their ability to form covalent adducts with largebit (Figure 4-5A). Largebit and **4.2** were first incubated with phosphine **4.5**. SDS-PAGE analysis revealed a higher molecular weight band (Figure 4-5B), indicating a crosslinked product. Mass spectrometry analysis confirmed that the expected product (Figure 4-5C) was formed. Notably, the crosslinked adduct was observed by SDS-PAGE after just 1 h with phosphine **4.5** (Figure 4-6A). This result shows that crosslinking occurs on a timescale that will be useful for biological assays. Using more nucleophilic phosphines, it is likely that these reaction times can be further reduced.

As an additional confirmation that the crosslinking observed with largebit was not due to non-specific trapping, we attempted the same crosslinking in the presence of a

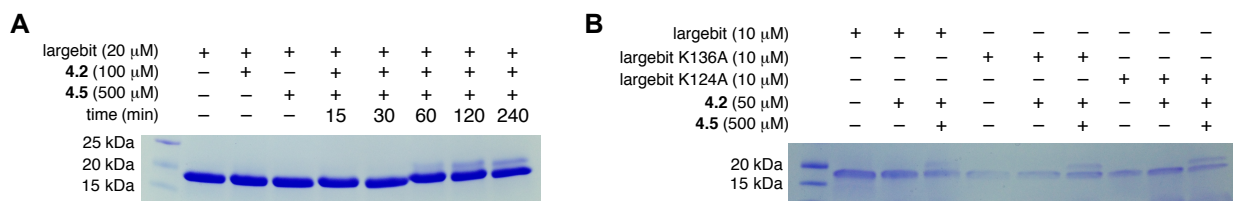


**Figure 4-6.** A) Lysine K124 and K136 are not necessary for crosslinking. Largebit fragments comprising mutations K124A or K136A (10  $\mu$ M) were combined with **4.2** (50  $\mu$ M) and phosphine **4.5** (500  $\mu$ M) and incubated at 37 °C for 4 h. Samples were analyzed via SDS-PAGE. B) Cyclopropanone crosslinking time course. Largebit (20  $\mu$ M) and peptide **4.2** (100  $\mu$ M) were combined in PBS (pH 7.4). Phosphine **4.5** (500  $\mu$ M) was added, and the reactions were incubated at 37 °C for 15–240 min. Samples were analyzed via SDS-PAGE.

non-target protein, hen egg-white lysozyme (HEWL). HEWL is similar in size to largebit, and both have 6-7 surface exposed lysines that could potentially trap the activated cyclopropanone. When the reactions were analyzed by gel electrophoresis, no higher molecular weight adducts were observed with HEWL, indicating no significant background due to non-specific trapping events (Figure 4-5D). We also attempted reactions in cellular lysate. Smallbit **4.2** (100  $\mu$ M) and largebit (20  $\mu$ M) were incubated in freshly prepared bacterial lysate at 37 °C for 4 h (Figure 4-5F). In the presence of phosphine **4.5**, the expected crosslinking band was observed. There was no apparent decrease in the amount of crosslinked Nluc in the presence of cell lysate, confirming that this methodology can be extended to complex biological environments.

From our analysis of the crystal structure of Nluc (Figure 4-2), we initially suspected that largebit lysine residues K124 and K136 were involved in forging the crosslink via nucleophilic trapping. However, when these residues were mutated to K124A and K136A, the resulting fragments were still able to crosslink peptide **4.2**

(Figure 4-6B). This result implicated Y16, Ser29, or Thr172 as the most likely trapping residues, based on the predicted binding site of the peptide (Figure 4-2). In-gel trypsin digestion and mass spectrometry identified a fragment comprising largebit residues 16–64 that was involved in the crosslink (Figure 4-7). Further attempts at digestion were inconclusive, possibly due to non-specific cleavage of the crosslink, and additional experiments are currently ongoing.

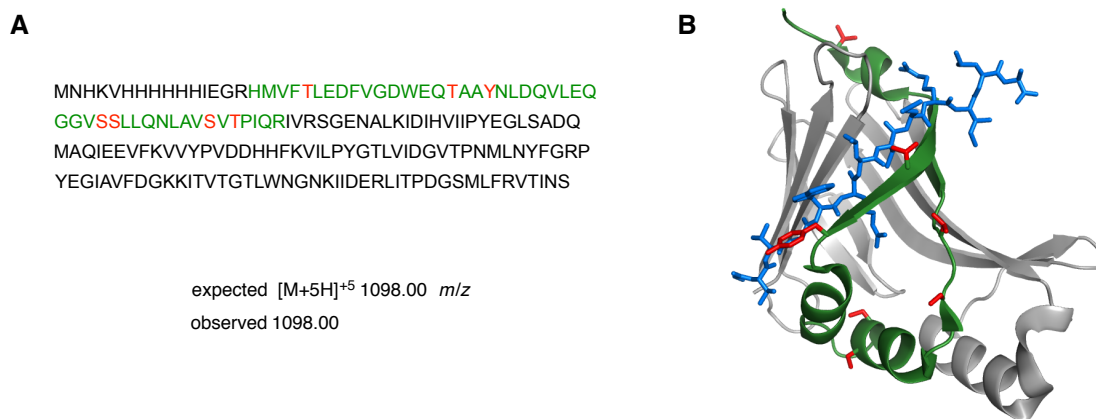


**Figure 4-7.** Trypsin digest of crosslinked Nluc to identify site of ligation. A) Largebit (20  $\mu$ M) was incubated with smallbit **4.2** (100  $\mu$ M) and phosphine **4.5** (500  $\mu$ M) for 4 h. Samples were then analyzed via SDS-PAGE. Bands corresponding to the crosslinked product were excised and subjected to trypsin digestion at 37 °C overnight. Peptides were eluted in 0.1% formic acid and analyzed via LC-MS. A peptide matching residues 1–43 (blue) showed a mass shift corresponding to the addition of the first 6 residues of peptide **4.2**. Residues bearing potential trapping sidechains are highlighted in red. B) Possible sites of crosslinking. The residues 16-64 are highlighted in green. Potential nucleophilic side chains within the sequence are highlighted in red.

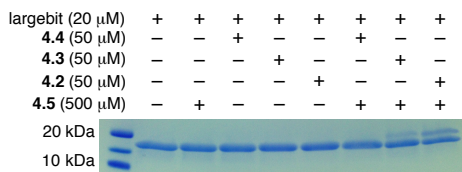


**Figure 4-8.** Crosslinking is affinity-dependent. Largebit (20  $\mu$ M) was incubated with smallbit peptides **4.2–4.4** (50  $\mu$ M) in PBS (pH 7.4) in the presence of phosphine **4.5** (500  $\mu$ M) at 37 °C for 4 h. Samples were analyzed via SDS-PAGE.

Having confirmed the overall specificity of the crosslinking approach, we further evaluated the panel of smallbit peptides **4.2–4.4**. We hypothesized that the differential binding affinities of these probes would manifest in different degrees of crosslinking to largebit (Figure 4-8). When largebit was combined with equimolar **4.2–4.4**, a clear trend in crosslinking efficiency was observed. The highest affinity peptide (**4.2**) showed the most crosslinking, while the lower affinity peptide (**4.3**) had a weaker signal. No crosslinking was observed with the weakest binder (**4.4**). These results indicate that the crosslink is driven by association of the split fragments.

With the goal of using chemically triggered crosslinking in a broader context, we sought to move beyond cyclopropanone-modified peptides to larger protein scaffolds. Genetic code expansion offered a potentially modular and general route to label numerous protein targets. Moreover, we previously had succeeded in incorporating a Cpo-modified amino acid into model proteins via this platform [29]. As noted in Chapter 2, though, this amino acid was prone to degradation over prolonged culture periods, resulting from base-promoted cleavage of the linker (Chapter 2, Figure 2-12). Amino acid **4.6** – featuring a more stable linker – would likely be a better candidate for future

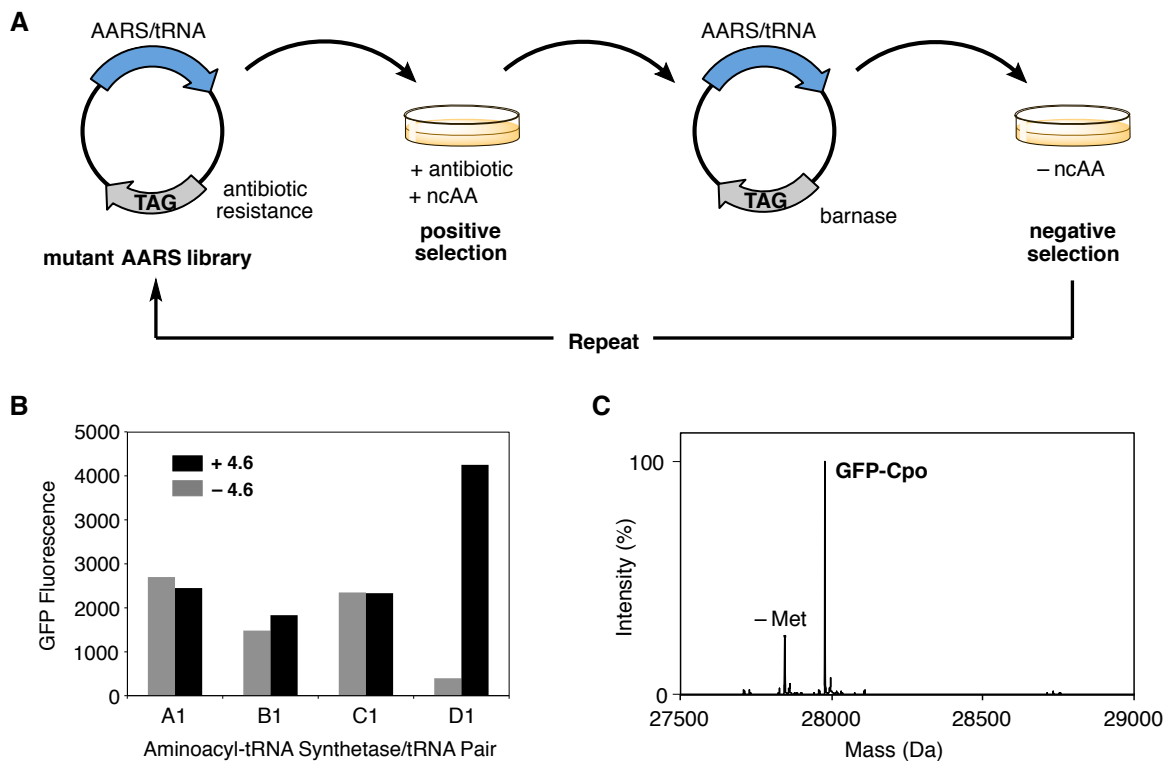


**Figure 4-9.** Cyclopropenone-bearing lysine analog **4.6** can be genetically encoded into proteins. A) Selections were performed, using positive and negative selections, to identify a PylRS mutant (D1) that could process **4.6**. B) Bacterial cultures expressing mutant PylRS variants were grown in the presence of **4.6** (1 mM). Successful processing of **4.6** resulted in GFP production. B) GFP comprising genetically encoded **4.6** (**GFP-Cpo**) was purified and analyzed by mass spectrometry (expected 27976.5 Da, observed 27977.0 Da).

studies. With these considerations, we sought to select an aminoacyl-tRNA synthetase (AARS)/tRNA pair that would incorporate the cyclopropenone-bearing lysine analog **4.6** into proteins of interest. In collaboration with Prof. Ryan Mehl (Oregon State University), we used established screening methods to identify a mutant PylRS that could process

**4.6** (Figure 4-9). In these selections, cells containing the AARS library were put through a series of positive and negative selections. Positive selections required successful amber codon suppression in an antibiotic resistance gene (chloramphenicol) for cell survival. The remaining members were collected and put through a negative selection. In this step, cells were grown in the absence of the amino acid of interest, and amber suppression of a lethal gene (barnase) resulted in cell death. The negative selection ensured that the remaining AARS had specificity towards the amino acid of interest (in this case, **4.6**). After multiple rounds of selection, the incorporation of the target amino acid was assessed via GFP fluorescence. In this assay, a GFP reporter construct with an amber codon at position 150 was expressed in the presence and absence of amino acid **4.6** (Figure 4-9B). We identified a single mutant (D1) that showed significantly increased fluorescence in the presence of **4.6**. To confirm that the increased fluorescence was due to incorporation of the cyclopropenone amino acid, we isolated the protein (**GFP-Cpo**) and analyzed it by mass spectrometry (Figure 4-9C). Importantly, we found that the side chain linker of **4.6** remained stable in these experiments, resolving previous liabilities with cleavable linkers (Chapter 2, Figure 2-12). The ability to genetically encode the cyclopropenone will facilitate its use as a small and stable crosslinker for trapping a wide variety of interactions.

### **4.3 Conclusion**

In conclusion, we demonstrated that cyclopropenones are viable, chemically triggered, crosslinkers for detecting biomolecule interactions. Using a model split protein system, we found that crosslinking proceeds readily in physiological buffers and in the



presence of cell lysate. We also found that the efficiency of crosslinking tracks with binding affinity, and that no significant non-specific crosslinking is observed in the presence of non-binding proteins. The low background reactivity in this methodology will make it a valuable addition to the available photocrosslinking methods. Importantly, the cyclopropanone-phosphine crosslinking strategy has the added advantage of being chemically activatable and specific to nucleophilic trapping. The ability to genetically encode these tools provides direct opportunities for interrogating protein-binding events. Additional work in our lab is under way to employ these reagents in intracellular investigations of biomolecule interactions. We anticipate that this methodology will be useful for trapping protein-protein interactions, identifying drug targets, and other applications.

## **4.4 Materials and methods**

### ***4.4a General Information***

All reagents and solvents were used as received, unless specified otherwise. Anhydrous organic solvents were prepared by degassing with argon and passing through two 4 x 36 in. columns of anhydrous neutral A2 (8 x 12 mesh; LaRoche Chemicals; activated at 350 °C for 12 h under a flow of argon). Column chromatography was carried out using Silicycle 60 Å (32–64 mesh) silica gel. Thin layer chromatography (TLC) was carried out with Merck Millipore 250 mm silica gel F-254 plates, and plates were visualized using UV light or KMnO<sub>4</sub> stain. Organic solutions were concentrated under reduced pressure using a Büchi rotary evaporator. HPLC purifications were performed on a Varian ProStar equipped with 325 Dual Wavelength UV-Vis Detector,

using an Agilent Prep-C18 Scalar column (9.4 x 150 mm, 5  $\mu$ m) with a 4 mL/min flow rate.

$^1\text{H}$  and  $^{13}\text{C}$  NMR spectra were obtained using either a Bruker DRX400 or a Bruker DRX500 instrument equipped with a cryo probe.  $^1\text{H}$  NMR spectra were acquired at 400 MHz or 500 MHz,  $^{13}\text{C}$  NMR spectra were acquired at 126 MHz. Spectra are internally referenced to residual solvent signals ( $\text{CDCl}_3$  is referenced to 7.27 ppm for  $^1\text{H}$  and 77.16 ppm for  $^{13}\text{C}$ ,  $\text{D}_2\text{O}$  is referenced to 4.79 ppm for  $^1\text{H}$ ). All spectra were acquired at 298 K. Chemical shifts are reported in ppm, and coupling constants ( $J$ ) are reported in Hz. Mass spectra were acquired at the University of California, Irvine Mass Spectrometry Facility.

#### ***4.4b Peptide synthesis and characterization***

Synthesis of smallbit peptides:  $\text{H}_2\text{N-K(CpO)VSGWRLFKKISN-NH}_2$  (**4.2**),  $\text{H}_2\text{N-K(CpO)VTGWRLSERILA-NH}_2$  (**4.3**), and  $\text{H}_2\text{N-K(CpO)VTGWRLFEEIL-NH}_2$  (**4.4**).

To a fritted glass reservoir was added NovaPEG Rink Amide Resin (0.46 mmol/g, 108-217 mg, 0.05-0.10 mmol respectively). The resin was continuously mixed by bubbling  $\text{N}_2$  through the reservoir. The resin was initially swelled and washed with DMF (2 x 15 mL, 15 min per cycle), then treated with 20% 4-methylpiperidine/DMF (10 mL, 20 min) for Fmoc removal. After the initial deprotection step, the resin was washed with DMF (3 x 10 mL, 5 min). Protected amino acids were then coupled in the following manner: Fmoc-protected amino acid (0.30 mmol), HCTU (124 mg, 0.3 mmol), and diisopropylethylamine (155  $\mu$ L, 0.89 mmol) were dissolved in 3.0 mL of DMF. The solution was mixed thoroughly, incubated at room temperature for ~3 min, and then

added to the deprotected resin. Each coupling step was performed at room temperature for > 45 min. The resin was then washed with DMF (3 x 10 mL, 5 min). Subsequent Fmoc deprotection was achieved by incubating the resin with 10 mL of 20% 4-methylpiperidine/DMF (20 min). The resin was then washed with DMF (3 x 10 mL, 5 min) prior to the next coupling step. Repeated cycles of amino acid coupling and deprotection were used to achieve the desired peptides. After the final cycle, the resin was washed with CH<sub>2</sub>Cl<sub>2</sub> (3 x 10 mL, 5 min). Peptides were isolated by incubating the resin with 95:2.5:2.5 trifluoroacetic acid/triisopropylsilane/H<sub>2</sub>O (2 x 5 mL, 30 min). The cleavage solutions were combined, concentrated *in vacuo*, and treated with 40 mL cold diethyl ether. The precipitate was then collected via centrifugation (3000 x *g*, 5 min) and dried under vacuum. The peptides were purified by HPLC (eluting with 40-90% MeCN (0.1%TFA) over 15 min), and the purified products were lyophilized. Product identity and purity were assessed via LC-MS. Peptide stocks were prepared in PBS (pH 7.4), and concentrations were determined by absorbance at 280 nm using an extinction coefficient of 5500 M<sup>-1</sup> cm<sup>-1</sup> (calculated using ExPASy ProtParam).

#### **4.4c Protein expression and purification**

*E. coli* TOP10 cells expressing pZER09 (pCOLD-WT\_largebit), pDR15 (pCOLD largebit K136A), or pDR16 (pCOLD largebit K124A) plasmids were used to inoculate 50 mL of LB containing ampicillin (100 µg/mL). After overnight incubation at 37 °C with shaking (225 rpm), 15 mL of the starter cultures were used to inoculate 1 L of Luria-Bertani broth. The cultures were incubated at 37 °C with shaking until an O.D.<sub>600</sub> of ~0.6 was achieved. The cultures were then chilled in an ice bath for 20 min. IPTG was added

(1 mM final concentration) to induce protein expression, and cultures were incubated at 16 °C with shaking (225 rpm) for 20 h.

Cells were collected via centrifugation at 4000 rpm for 20 min at 4 °C. The supernatant was decanted and the pellets were suspended in 25 mL of 50 mM phosphate buffer (pH 7.8). Protease inhibitor cocktail (Sigma-Aldrich) and phenylmethylsulfonyl fluoride (PMSF, 500 µM final concentration) were added. The cells were sonicated and the lysate was centrifuged at 10,000 rpm for 40 min at 4 °C. The clarified lysate was filtered using a 0.45 µm filter. Profinity<sup>TM</sup> IMAC resin (BioRad, 5 mL bed volume) was added to the clarified lysate, and the mixture was rocked at 4 °C for 30 min. The resin was then rinsed with wash buffer (50 mM phosphate, 20 mM imidazole, pH 7.8, 50 mL), and proteins were isolated with elution buffer (50 mM phosphate, 250 mM imidazole, pH 7.8, 3 x 5 mL). The fractions were analyzed by SDS-PAGE, and those containing the desired protein were combined and concentrated via spin filter centrifugation (3 kDa MW cutoff). Protein concentration was determined using a JASCO V730 UV-vis spectrophotometer and an extinction coefficient of 19,940 M<sup>-1</sup> cm<sup>-1</sup> (calculated using Expasy ProtParam).

#### ***4.4d. Crosslinking reactions with split Nluc***

All crosslinking experiments were carried out in PBS (pH 7.4) at 37 °C. Largebit (10-20 µM final concentration) was combined with peptides **4.2–4.4** (50 µM-1 mM) and incubated at room temperature for 10 min. Phosphine **4.5** (500 µM-1 mM) was then added, and the reactions were incubated at 37 °C for 4–16 h. Reactions were then analyzed by SDS-PAGE (4–20% gradient, BioRad, 110 V, 70–80 min). For time course

analyses, reactions were quenched with H<sub>2</sub>O<sub>2</sub> (1% final concentration). For cellular lysate crosslinking experiments, samples were denatured with urea (1.6 M final concentration) prior to SDS-PAGE analysis.

#### **4.4e Synthetase selection and protein expression.**

##### Synthetase selections

Synthetase screening was performed in collaboration with Richard Cooley and Prof. Ryan Mehl at the Unnatural Protein Facility at Oregon State University.

A library of *M. barkeri* pyrrolysine aminoacyl-tRNA synthetase mutants was generously provided by Prof. Ryan Mehl. The library encoded synthetases with random mutations at positions L305, Y306, L309, N346, and C348. Library DNA was encoded on a kanamycin-resistant plasmid (pBK). The pBK plasmid was alternately transformed into cells containing positive (pREP) or negative (pYOBB2) selection plasmids. The positive selection plasmid (pREP) contained *M. barkeri* (Mb) pyrrolyl-tRNA and chloramphenicol acetyltransferase containing an amber codon. The negative selection plasmid (pYOBB2) contained *M. barkeri* (Mb) pyrrolyl-tRNA and a barnase gene containing an amber codon.

For the first round of positive selection, the pBK library DNA was transformed 12 times via electroporation into DH10B electrocompetent *E. coli* cells containing the positive selection plasmid (pREP). The transformed cells were then combined in a total of 500 mL Luria-Bertani broth (containing 25 µg/mL tetracycline and 50 µg/mL kanamycin, but lacking chloramphenicol) and incubated overnight at 37 °C with shaking. The overnight culture was then used to inoculate 500 mL of fresh Luria-Bertani broth.

The culture was incubated at 37 °C with shaking until reaching an O.D.<sub>600</sub> of ~1.0. Following incubation, the culture was plated on 12 15-cm agar plates (250 µL on each plate) containing amino acid **4.6** (1 mM final concentration), tetracycline (25 µg/mL), kanamycin (50 µg/mL), and chloramphenicol (60 µg/mL). The plates were then incubated at 37 °C overnight. The surviving colonies were collected by adding 5 mL of Luria-Bertani broth to each plate and gently scrapping the surface of the agar with a glass spreader. Resuspended colonies from all twelve plates were combined and incubated at 37 °C with shaking for 1 h. The cells were then pelleted via centrifugation, and plasmid DNA was extracted using a Quigen miniprep kit. The library DNA plasmid (pBK) was then separated from the positive selection plasmid (pREP) using gel electrophoresis followed by gel extraction (Quigen gel extraction kit).

For the negative selection, the library DNA obtained from the positive selection was transformed via electroporation into DH10B electrocompetent cells containing the negative selection plasmid (pYOBB2). The transformed cells were plated on 4 15-cm agar plates containing kanamycin (50 µg/mL), chloramphenicol (60 µg/mL), and L-arabinose (0.04%). The plates were then incubated overnight at 37 °C. Surviving colonies were collected and combined as outlined above. Library plasmid DNA was collected and isolated as outlined above.

For the second positive selection, library DNA obtained from the first negative selection was transformed via electroporation into cells containing the positive selection plasmid (pREP). The transformants were plated on 2 15 cm agar plates prepared as in the first positive selection (see above). Library DNA was then isolated as described above.

For the second negative selection, library DNA obtained from the second positive selection was transformed via electroporation into cells containing the positive selection plasmid (pREP). The transformants were plated on 2 15 cm agar plates prepared as in the first negative selection (see above). Library DNA was then isolated as described above.

To identify functional synthetases resulting from the selection process, library DNA obtained after the second negative selection was transformed into TOP10 *E. coli* electrocompetent cells containing the pALS-GFP-150 plasmid. pALS-GFP-150 encodes GFP with an amber codon (TAG) at position 150. The transformed cells were then plated on agar plates containing amino acid **4.6** (1 mM), kanamycin (50 µg/mL), tetracycline (25 µg/mL), and L-arabinose (0.05%). Plates were incubated overnight at 37 °C, then at room temperature for 24 h. A total of 95 colonies were selected and grown overnight in a 96-well plate containing 500 µL of Luria-Bertani broth per well. These cultures were then used to inoculate 2 freshly prepared 96-well plates. One plate was prepared with auto-induction media (500 µL per well) [32] containing amino acid **4.6** (1 mM), kanamycin (50 µg/mL), tetracycline (25 µg/mL), and L-arabinose (0.05%). The second plate was prepared similarly, but did not contain the amino acid **4.6**. The plates were then incubated at 37 °C with shaking for 48 h. To measure GFP fluorescence, 50 µL of each culture was mixed with 150 µL of PBS (pH 7.4) in clear-bottom, black 96-well plates (Grenier-Bio). GFP fluorescence was measured using a fluorescence plate reader (Molecular Devices SpectrMax Gemini XPS, ex. 488 nm, em. 519 nm).

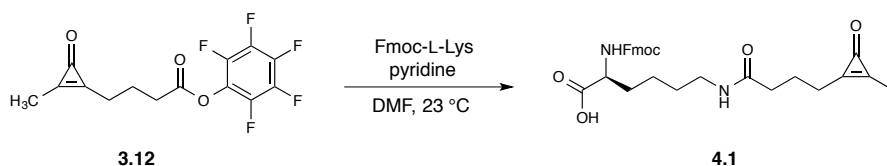
## GFP expression and purification

*E. coli* TOP10 cells transformed with pBK-PylRS mutant (Y306C, C346V, M382V) and pALS-GFP-150 were used to inoculate 3 mL of Luria-Bertani broth containing tetracycline (25 µg/mL) and kanamycin (50 µg/mL). After ~16 h, starter cultures were used to inoculate expression cultures. AIM expression media (25 mL) containing 1 mM **4.6**, tetracycline (25 µg/mL), and kanamycin (50 µg/mL) were inoculated with 250 µL of the overnight starter culture. The culture was then incubated at 37 °C with shaking (225 rpm) for 48 h.

Cells were pelleted via centrifugation (4000 rpm, 30 min, 4 °C). The pellets were then resuspended in 5 mL PBS (pH 7.4). Protease inhibitor cocktail (Sigma-Aldrich) and phenylmethylsulfonyl fluoride (PMSF, 500 µM final concentration) were added. The resuspended cells were sonicated and then centrifuged (14,500 rpm, 30 min, 4 °C). The supernatant was then syringe filtered with a 0.4 µm syringe filter. Profinity<sup>TM</sup> IMAC resin (BioRad, 200 µL bed volume) was added to the clarified lysate and it was rocked at 4 °C for 2 h. The resin was washed with wash buffer (20 mM imidazole in PBS, pH 7.4, 3 x 5 mL), and **GFP-Cpo** was eluted using 0.5 mL of elution buffer (250 mM imidazole in PBS, pH 7.4). Fractions containing the desired protein were concentrated using a centrifuge spin concentration column (3 kDa MW cutoff) to a volume of ~100 µL. PBS (pH 7.4) was added to bring the volume to 400 µL, and the sample was again concentrated to ~100 µL. This was repeated three times to remove excess imidazole. Protein concentration was measured with a Nanodrop<sup>®</sup> ND-1000 (Thermo Scientific), measuring absorbance at 488 nm and using an extinction coefficient of 88,300 M<sup>-1</sup> cm<sup>-1</sup> [33]. Purified samples were analyzed by mass spectrometry.

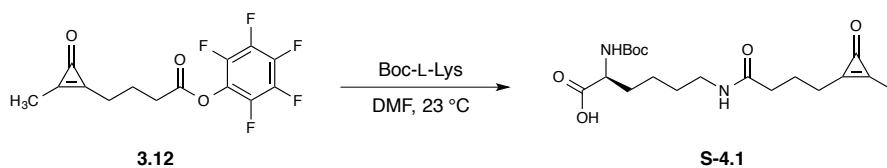


#### 4.4f. Synthetic Procedures



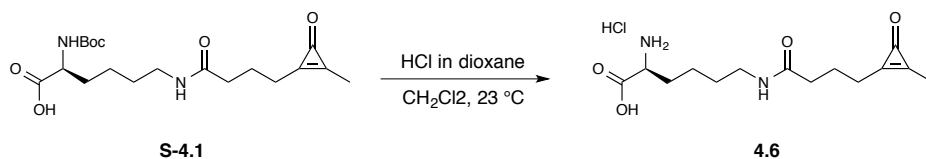
#### Fmoc-protected amino acid **4.1**

To a flame-dried 50 mL round bottom flask containing a stir bar was added **3.12** (298 mg, 0.930 mmol). After purging the flask with N<sub>2</sub>, a solution of Fmoc-L-Lys (450 mg, 1.22 mmol) in anhydrous DMF (4 mL) was delivered. Anhydrous pyridine (0.22 mL, 2.8 mmol) was then added, and the reaction was stirred at room temperature overnight. The crude reaction was diluted with toluene (~100 mL) and concentrated *in vacuo* to remove excess DMF. This dilution-concentration sequence was repeated two additional times. The residue was then diluted with 1 M HCl (100 mL) and extracted into CH<sub>2</sub>Cl<sub>2</sub> (3 x 30 mL). The combined organic layers were dried over MgSO<sub>4</sub> and filtered. The filtrate was concentrated *in vacuo*, and the residue was purified by flash column chromatography (eluting with a gradient of 2-10% MeOH/CH<sub>2</sub>Cl<sub>2</sub>) to give **4.1** as a white solid (97 mg, 0.19 mmol, 21%). <sup>1</sup>H NMR (400 MHz, CDCl<sub>3</sub>) δ 7.76 (d, *J* = 7.4 Hz, 2H), 7.63–7.60 (m, 2H), 7.40 (t, *J* = 7.5 Hz, 2H), 7.31 (t, *J* = 7.5 Hz, 2H), 6.34 (bs, 1H), 5.72 (d, *J* = 6.9 Hz, 1H), 4.45–4.37 (m, 3H), 4.22 (t, *J* = 7.0 Hz, 1H), 3.36–3.24 (m, 3H), 2.66 (t, *J* = 7.0 Hz, 2H), 2.32 (t, *J* = 6.7 Hz, 2H), 2.29 (s, 3H), 2.07–2.00 (m, 2H), 1.90–1.83 (m, 2H), 1.59–1.45 (m, 4H). HRMS (ESI+) calculated for C<sub>29</sub>H<sub>32</sub>N<sub>2</sub>O<sub>6</sub>Na [M+Na]<sup>+</sup> 527.2158 *m/z*, found 527.2162.



### Boc-protected amino acid **S-4.1**

To a 100 mL flame-dried round bottom flask was added **3.12** (1.00 g, 3.13 mmol) and anhydrous DMF (20 mL) under an atmosphere of N<sub>2</sub>. Boc-L-Lys-OH (2.31 g, 9.39 mmol) was added, and the mixture was stirred at room temperature overnight. The crude reaction was diluted with toluene (~100 mL) and concentrated *in vacuo* to remove excess DMF. This dilution-concentration sequence was repeated two additional times. The residue was then diluted with HCl (100 mL) and extracted into CH<sub>2</sub>Cl<sub>2</sub> (3 x 30 mL). The combined organic layers were dried over MgSO<sub>4</sub> and filtered. The filtrate was concentrated *in vacuo*, and the residue was purified by flash column chromatography (eluting with a gradient of 0-10% MeOH/CH<sub>2</sub>Cl<sub>2</sub>) to give **S-4.1** as a white solid (524 mg, 1.37 mmol, 43.8%). <sup>1</sup>H NMR (400 MHz, CDCl<sub>3</sub>) δ 6.37 (bs, 1H), 5.29 (bs, 1H), 4.43 (bs, 1H), 3.32–3.36 (m, 3H), 2.68 (t, *J* = 7.0 Hz, 2H), 2.33 (t, *J* = 7.1 Hz, 2H), 2.32 (s, 3H), 2.10–2.02 (m, 2H), 1.85–1.75 (m, 2H), 1.61–1.52 (m, 3H), 1.45 (s, 9H), 1.37–1.30 (m, 1H). HRMS (ESI+) calculated for C<sub>19</sub>H<sub>30</sub>N<sub>2</sub>O<sub>6</sub>Na [M+Na]<sup>+</sup> 405.2002 *m/z*, found 405.2003.



## Amino acid 4.6

Compound **S-4.1** (0.20 g, 0.52 mmole) was dissolved in anhydrous  $\text{CH}_2\text{Cl}_2$  (5 mL) under an atmosphere of  $\text{N}_2$ . A solution of 4 M HCl in dioxane (0.8 mL) was added dropwise, and the reaction was stirred at room temperature for 2 h. The solvent was then removed *in vacuo*, and the residue was dissolved in  $\text{H}_2\text{O}$  and lyophilized to give amino acid **4.6** as a brown solid (0.17 g, 0.52 mmol, 100%).  $^1\text{H}$  NMR (400 MHz,  $\text{D}_2\text{O}$ )  $\delta$  4.07 (t,  $J = 6.2$  Hz, 1H), 3.20 (t,  $J = 6.9$  Hz, 2H), 2.71 (t,  $J = 7.0$  Hz, 2H), 2.35 (t,  $J = 7.3$  Hz, 2H), 2.31 (s, 3H), 2.03 (quint,  $J = 7.3$  Hz, 2H), 1.99–1.90 (m, 2H), 1.57 (sext,  $J = 7.1$  Hz, 2H), 1.51–1.41 (m, 2H). HRMS (ESI+) calculated for  $\text{C}_{14}\text{H}_{22}\text{N}_2\text{O}_4\text{Na}$   $[\text{M}+\text{Na}]^+$  305.1477  $m/z$ , found 305.1489.

## 4.5 References

1. D. Cox, C. Raeburn, X. Sui, D. M. Hatters. Protein aggregation in cell biology: An aggregomics perspective of health and disease. *Semin. Cell Dev. Biol.* **2018**, <https://doi.org/10.1016/j.semcdb.2018.05.003>.
2. M. Vidal, M. E. Cusick, A.-L. Barabási. Interactome networks and human disease. *Cell* **2011**, *144*, 986–998.
3. M. Schürmann, P. Janning, S. Ziegler, H. Waldmann. Small-molecule target engagement in cells. *Cell Chem. Biol.* **2016**, *23*, 435–441.

4. E. Smith, I. Collins. Photoaffinity labeling in target- and binding-site identification. *Future Med. Chem.* **2015**, *7*, 159–183.
5. M. H. Wright, S. A. Sieber. Chemical proteomics approaches for identifying the cellular targets of natural products. *Nat. Prod. Rep.* **2016**, *33*, 681–708.
6. L. Saford, A. Palmer. Recent advances in development of genetically encoded fluorescent sensors. *Methods Enzymol.* **2017**, *589*, 15737–15741.
7. A. Miyawaki. Development of probes for cellular functions using fluorescent proteins and fluorescence resonance energy transfer. *Annu. Rev. Biochem.* **2011**, *80*, 357–373.
8. X. Zhou, K. J. Herbst-Robinson, J. Zhang. Visualizing dynamic activities of signaling enzymes using genetically encodable FRET-based biosensors: From designs to applications. *Methods Enzymol.* **2012**, *504*, 317–340.
9. C. D. Harvey, A. G. Ehrhardt, C. Cellurale, H. Zhong, R. Yasuda, R. J. Davis, K. Svoboda. A genetically encoded fluorescent sensor of ERK activity. *Proc. Natl. Acad. Sci. USA* **2008**, *105*, 19264–19269.
10. A. Miyawaki. Visualization of the spatial and temporal dynamics of intracellular signaling. *Dev. Cell* **2003**, *4*, 295–305.
11. H.-W. Shih, J. A. Prescher. A bioorthogonal ligation of cyclopropenones mediated by triarylphosphines. *J. Am. Chem. Soc.* **2015**, *137*, 10036–10039.
12. G. W. Preston, A. J. Wilson. Photo-induced covalent cross-linking for the analysis of biomolecular interactions. *Chem. Soc. Rev.* **2013**, *42*, 3289–3301.
13. J. Das. Aliphatic diazirines as photoaffinity probes for proteins: Recent developments. *Chem. Rev.* **2011**, *111*, 4405–4417.

14. G. Dormán, H. Nakamura, A. Pulsipher, G. D. Prestwich. The life of pi star: Exploring the exciting and forbidden worlds of the benzophenone photophore. *Chem. Rev.* **2016**, *116*, 15284–15398.
15. A. Herner, J. Marjanovic, T. M. Lewandowski, V. Marin, M. Patterson, L. Miesbauer, D. Ready, J. Williams, A. Vasudevan, Q. Lin. 2-Aryl-5-carboxytetrazole as a new photoaffinity label for drug target identification. *J. Am. Chem. Soc.* **2016**, *138*, 14609–14615.
16. Y. Tian, Q. Lin. Genetic encoding of 2-aryl-5-carboxytetrazole-based protein photo-cross-linkers. *Chem. Commun.* **2018**, *54*, 4449–4452.
17. J. W. Chin, S. W. Santoro, A. B. Martin, D. S. King, L. Wang, P. G. Schultz. Addition of p-azido-L-phenylalanine to the genetic code of *Escherichia coli*. *J. Am. Chem. Soc.* **2002**, *124*, 9026–9027.
18. E. M. Tippmann, W. Liu, D. Summerer, A. V. Mack, P. G. Schultz. A Genetically encoded diazirine photocrosslinker in *Escherichia coli*. *ChemBioChem* **2007**, *8*, 2210–2214.
19. J. W. Chin, A. B. Martin, D. S. King, L. Wang, P. G. Schultz. Addition of a photocrosslinking amino acid to the genetic code of *Escherichia coli*. *Proc. Natl. Acad. Sci. USA* **2002**, *99*, 11020–11024.
20. Z. Qiu, L. Lu, X. Jian, C. He. A Diazirine-based nucleoside analogue for efficient DNA interstrand photocross-linking. *J. Am. Chem. Soc.* **2008**, *130*, 14398–14399.

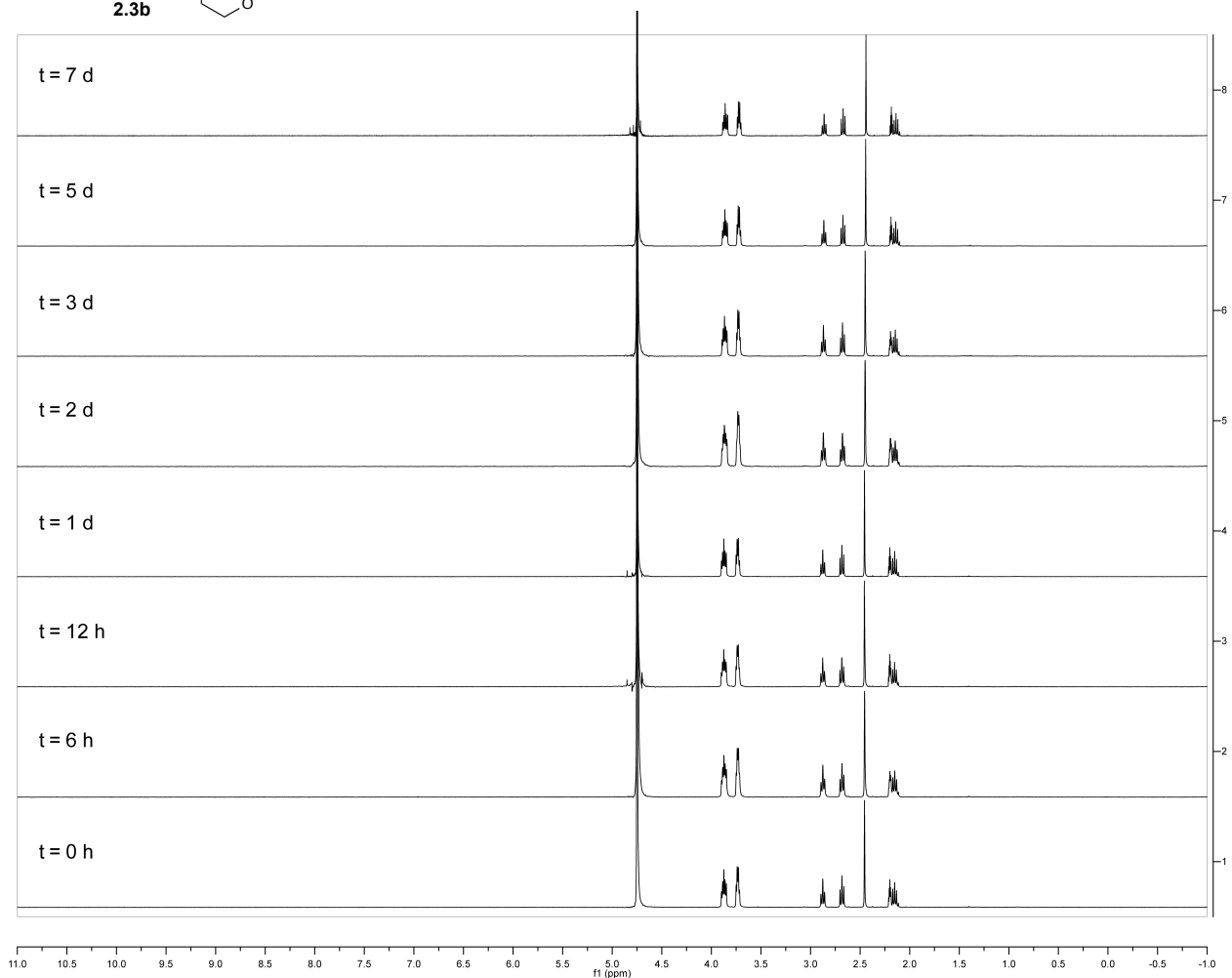
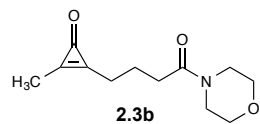
21. K. L. Buchmueller, B. T. Hill, M. S. Platz, K. M. Weeks. RNA-tethered phenyl azide photocrosslinking via a short-lived indiscriminant electrophile. *J. Am. Chem. Soc.* **2003**, *125*, 10850–10861.
22. C. G. Parker, A. Galmozzi, Y. Wang, B. E. Correia, K. Sasaki, C. M. Joslyn, A. S. Kim, C. L. Cavallaro, R. M. Lawrence, S. R. Johnson, I. Narvaiza, E. Saez, B. F. Cravatt. Ligand and target discovery by fragment-based screening in human cells. *Cell* **2017**, *168*, 527–541.
23. M. J. Niphakis, K. M. Lum, A. B. C. III, B. E. Correia, T.-A. Ichu, J. Olucha, S. J. Brown, S. Kundu, F. Piscitelli, H. Rosen, B. F. Cravatt. A global map of lipid-binding proteins and their ligandability in cells. *Cell* **2015**, 1668–1680.
24. S.-H. Yu, M. Boyce, A. M. Wands, M. R. Bond, C. R. Bertozzi, J. J. Kohler. Metabolic labeling enables selective photocrosslinking of O-GlcNAc-modified proteins to their binding partners. *Proc. Natl. Acad. Sci. USA* **2012**, *109*, 4834–4839.
25. P. Kleiner, W. Heydenreuter, M. Stahl, V. S. Korotkov, S. A. Sieber. A Whole proteome inventory of background photocrosslinker binding. *Angew. Chem. Int. Ed.* **2017**, *56*, 1396–1401.
26. M. Cigler, T. G. Müller, D. Horn-Ghetko, M.-K. v. Wrisberg, M. Fottner, R. S. Goody, A. Itzen, M. P. Müller, K. Lang. Proximity-triggered covalent stabilization of low-affinity protein complexes *in vitro* and *in vivo*. *Angew. Chem. Int. Ed.* **2017**, *56*, 15737–15741.

27. W. Xuan, J. Li, X. Luo, P. G. Schultz. Genetic incorporation of a reactive isothiocyanate group into proteins. *Angew. Chem. Int. Ed.* **2016**, *55*, 10065–10068.
28. W. Xuan, S. Shao, P. G. Schultz. Protein crosslinking by genetically encoded noncanonical amino acids with reactive aryl carbamate side chains. *Angew. Chem. Int. Ed.* **2017**, *56*, 5096–5100.
29. R. D. Row, H.-W. Shih, A. T. Alexander, R. A. Mehl, J. A. Prescher. Cyclopropenones for metabolic targeting and sequential bioorthogonal labeling. *J. Am. Chem. Soc.* **2017**, *139*, 7370–7375.
30. A. S. Dixon, M. K. Schwinn, M. P. Hall, K. Zimmerman, P. Otto, T. H. Lubben, B. L. Butler, B. F. Binkowski, T. Machleidt, T. A. Kirkland, M. G. Wood, C. T. Eggers, L. P. Encell, K. V. Wood. NanoLuc complementation reporter optimized for accurate measurement of protein interactions in cells. *ACS Chem. Biol.* **2016**, *11*, 400–408.
31. Y. Tomabechi, T. Hosoya, H. Ehara, S.-i. Sekine, M. Shirouzu, S. Inouye. Crystal structure of nanoKAZ: The mutated 19 kDa component of *Oplophorus* luciferase catalyzing the bioluminescent reaction with coelenterazine. *Biochem. Biophys. Res. Commun.* **2016**, *470*, 88–93.
32. J. C. Jackson, J. T. Hammill, R. A. Mehl. Site-specific incorporation of a <sup>19</sup>F-amino acid into proteins as an NMR probe for characterizing protein structure and reactivity. *J. Am. Chem. Soc.* **2007**, *129*, 1160–1166.

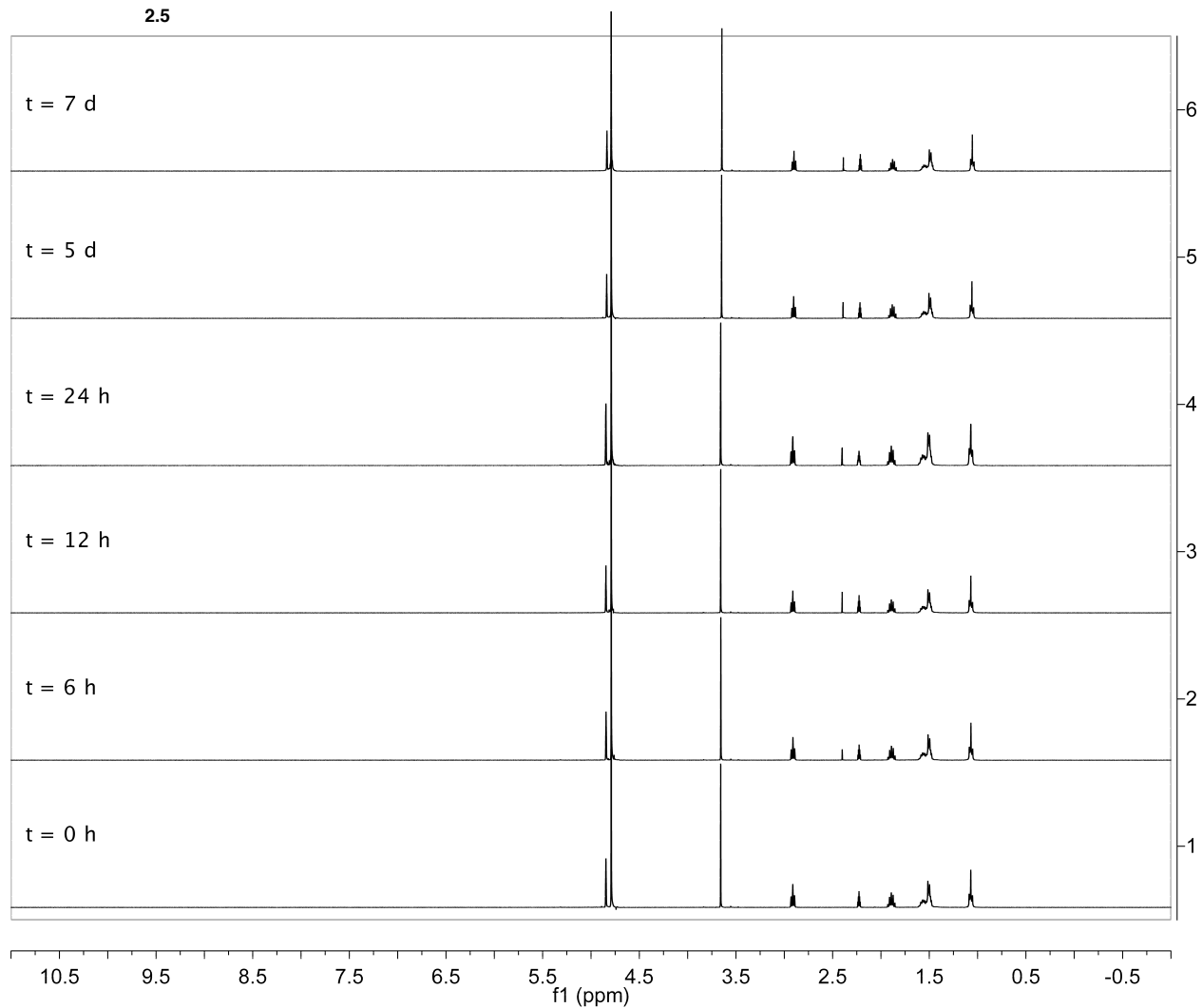
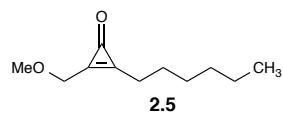
33. J.-D. Pédelacq, S. Cabantous, T. Tran, T. C. Terwilliger, G. S. Waldo. Engineering and characterization of a superfolder green fluorescent protein. *Nat. Biotechnol.* **2006**, 24, 79–88.



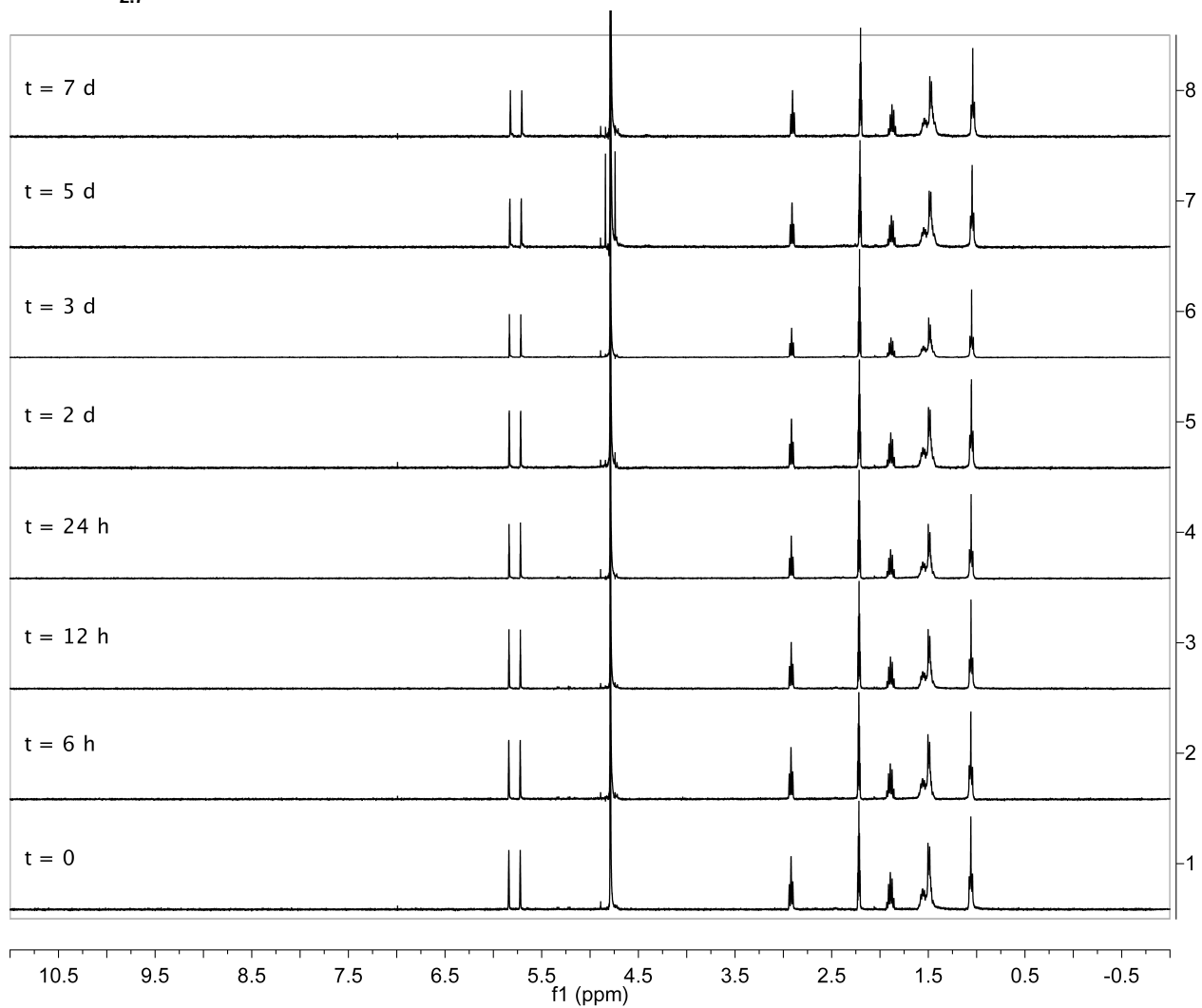
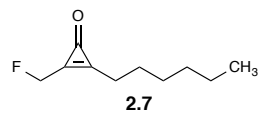
## **APPENDIX A: NMR Spectra for Chapter 2**



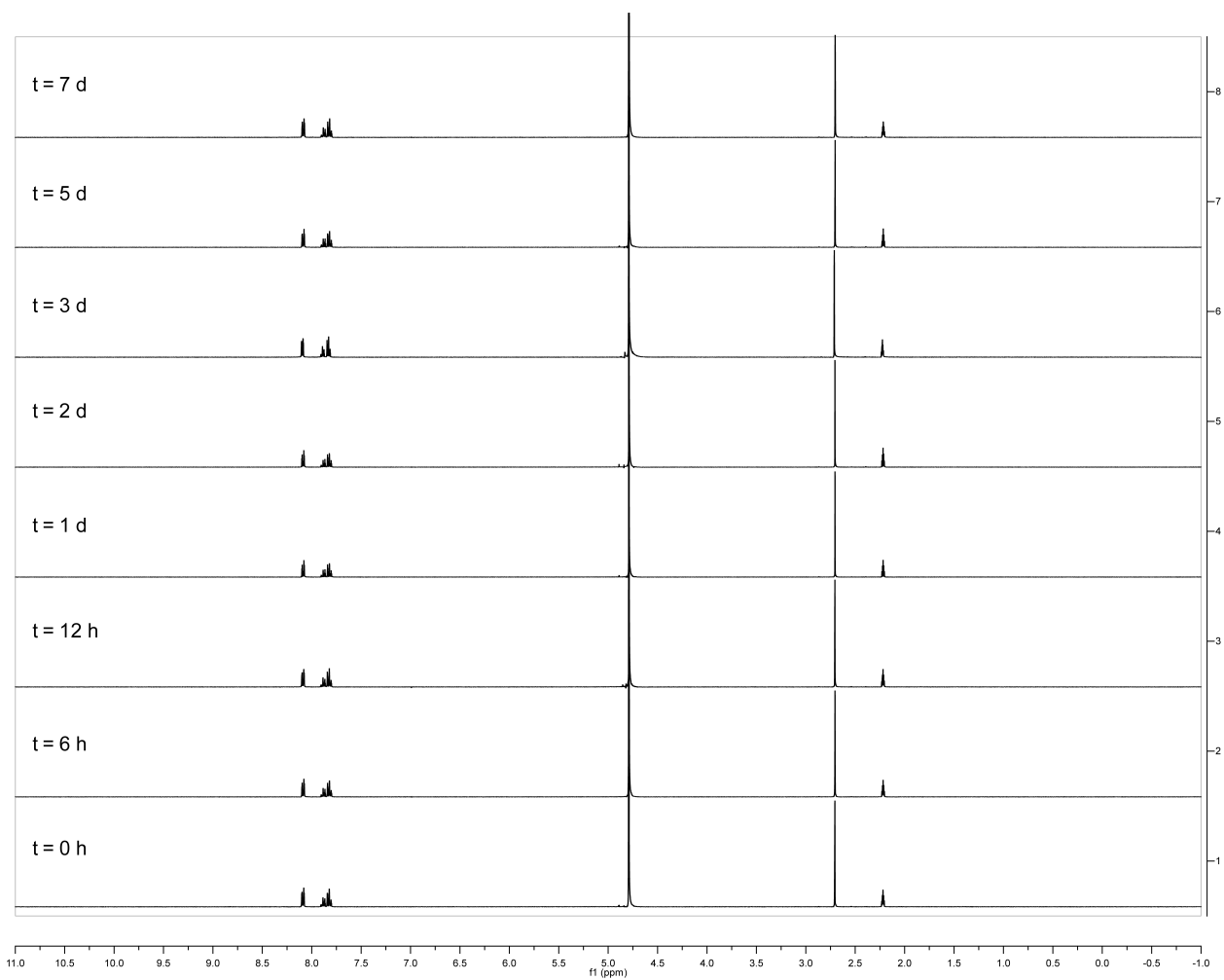
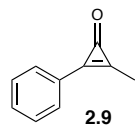
**Figure S2-1.** Dialkyl cyclopropanone **2.3b** is stable in aqueous solution for 1 week. Compound **2.3b** (10 mM) was incubated in *d*-PBS (pH = 7.4) at 37 °C and monitored via  $^1\text{H}$  NMR spectroscopy.



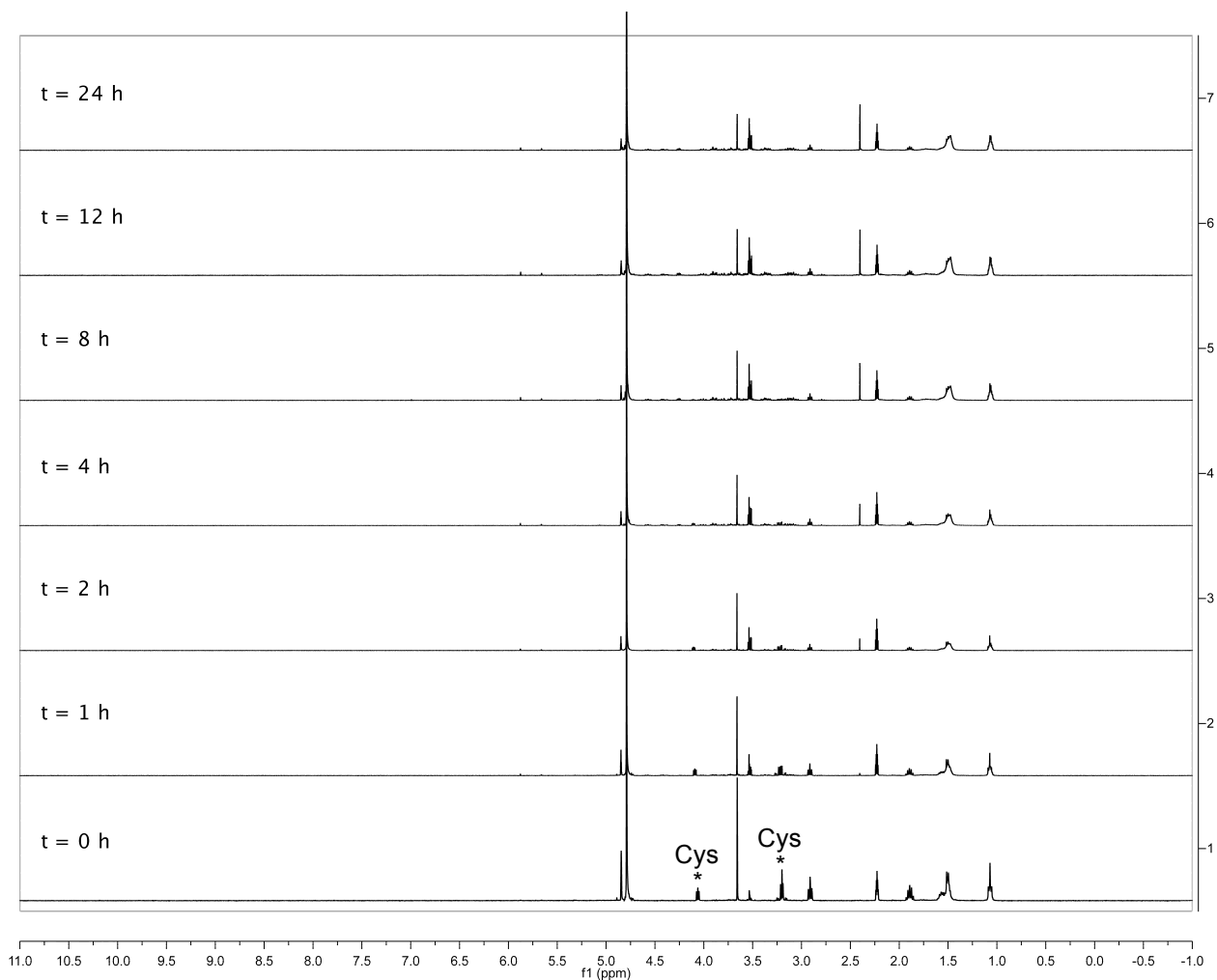
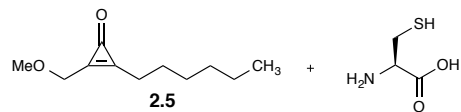
**Figure S2-2.** Cyclopropenone **2.5** is stable in aqueous solution for 1 week. Compound **2.5** (10 mM) was incubated in 20% CD<sub>3</sub>CN/*d*-PBS (pH = 7.4) at 37 °C and monitored via <sup>1</sup>H NMR spectroscopy.



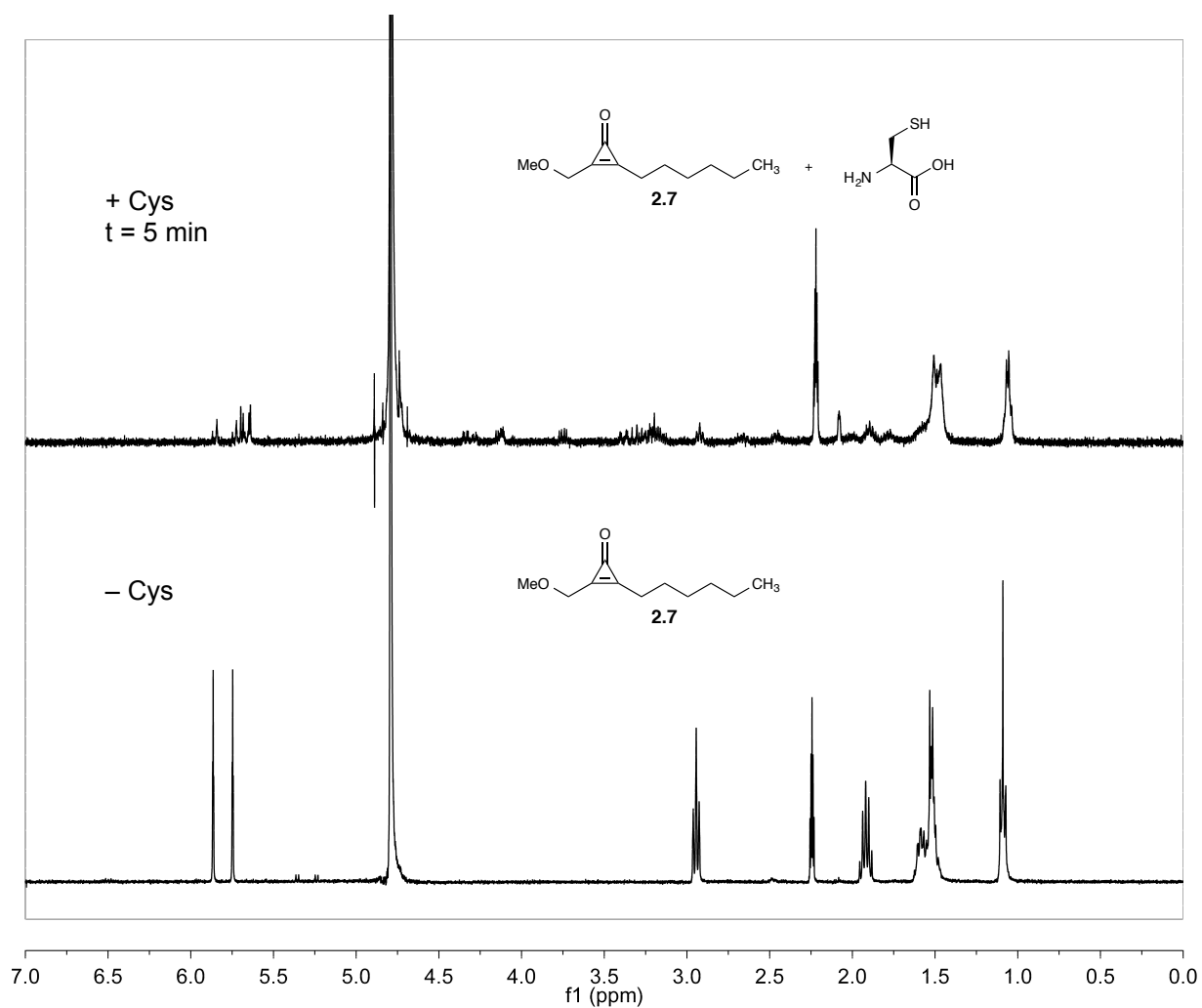
**Figure S2-3.** Cyclopropanone **2.7** is stable in aqueous solution for 1 week. Compound **2.7** (10 mM) was incubated in 20% CD<sub>3</sub>CN/*d*-PBS (pH = 7.4) at 37 °C and monitored via <sup>1</sup>H NMR spectroscopy.



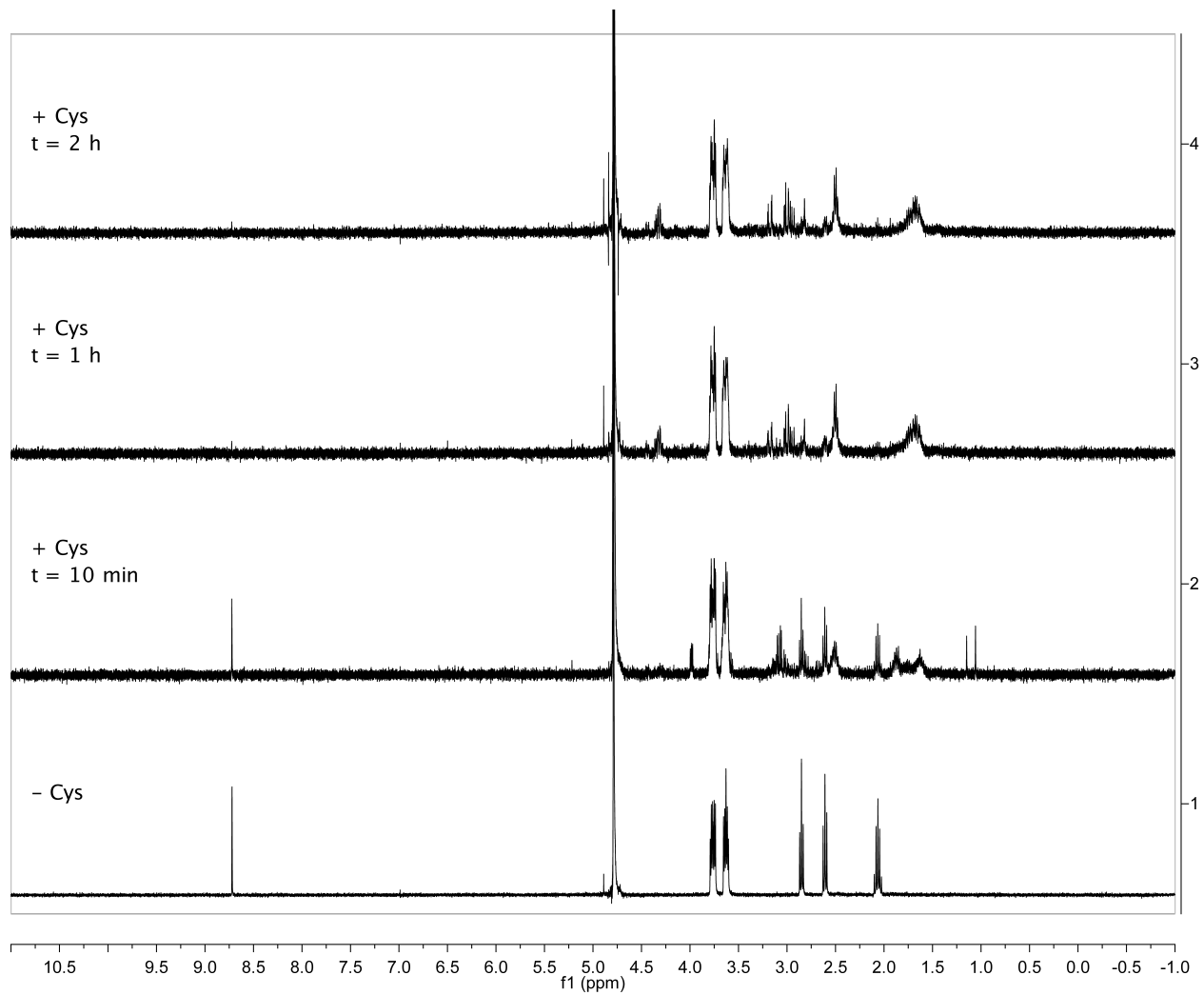
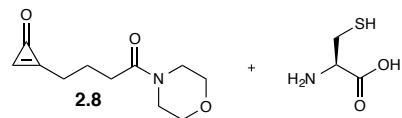
**Figure S2-4.** Cyclopropanone **2.9** is stable in aqueous solution for 1 week. Compound **2.9** (10 mM) was incubated in 20% CD<sub>3</sub>CN/*d*-PBS (pH = 7.4) at 23 °C and monitored via <sup>1</sup>H NMR spectroscopy.



**Figure S2-5.** Cyclopropanone **2.5** is not stable to L-cysteine. Compound **2.5** (5 mM) and L-cysteine (5 mM) were incubated in 20% CD<sub>3</sub>CN/*d*-PBS (pH = 7.4) at 37 °C and monitored via <sup>1</sup>H NMR spectroscopy.

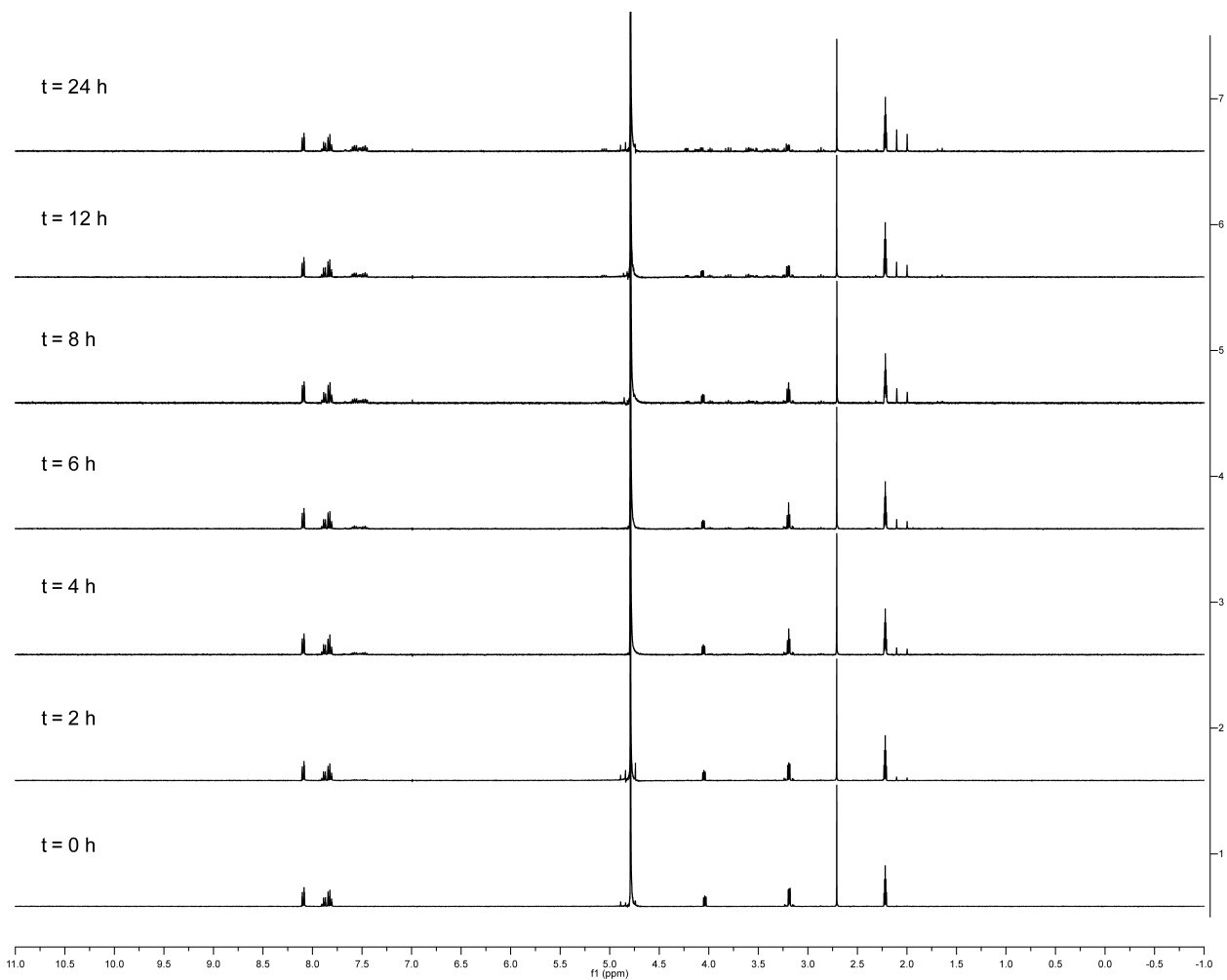
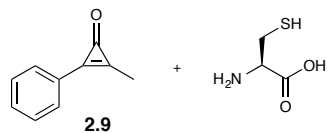


**Figure S2-6.** Cyclopropenone **2.7** is not stable to L-cysteine. Compound **2.7** (5 mM) and L-cysteine (5 mM) were incubated in 20% CD<sub>3</sub>CN/*d*-PBS (pH = 7.4) at room temperature and monitored via <sup>1</sup>H NMR spectroscopy. The lower spectra shows **7** in 20% CD<sub>3</sub>CN/*d*-PBS without L-cysteine.

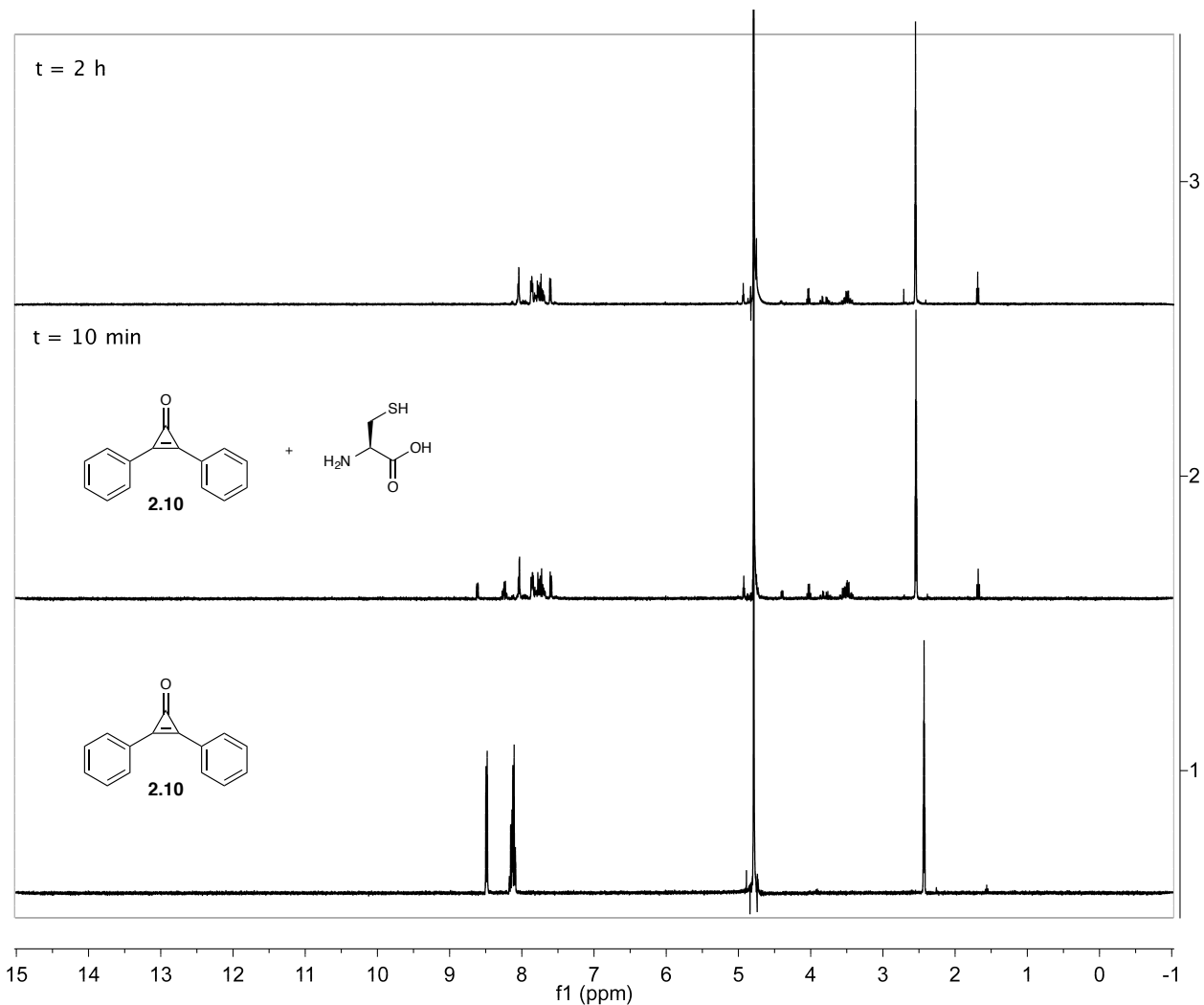


**Figure S2-7.** Cyclopropenone **2.8** is not stable to L-cysteine. Compound **2.8** (5 mM) and L-cysteine (5 mM) were incubated in *d*-PBS (pH = 7.4) at 37 °C and monitored via  $^1\text{H}$  NMR spectroscopy.

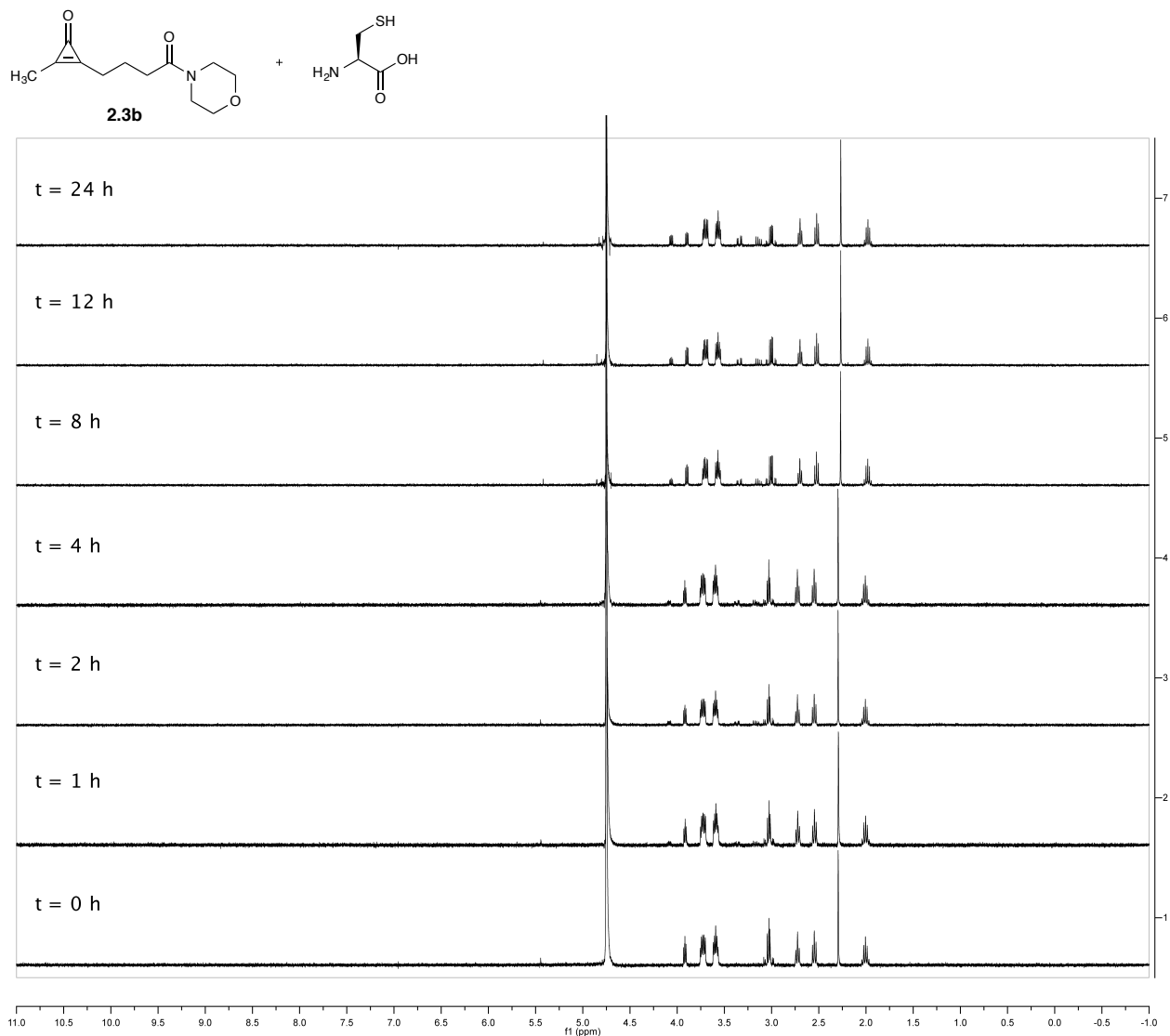




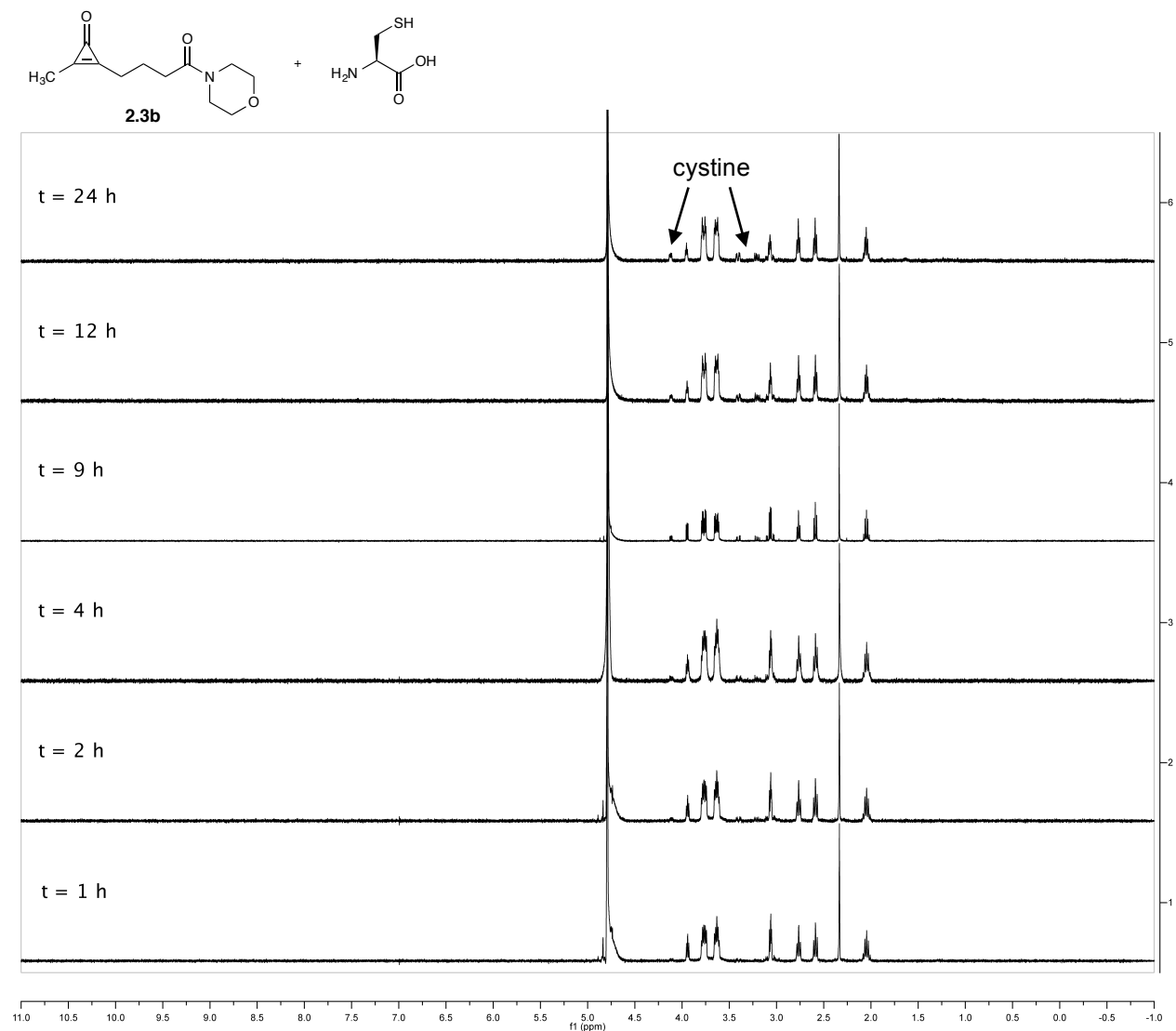
**Figure S2-9.** Cyclopropenone **2.9** is not stable to L-cysteine. Compound **2.9** (5 mM) and L-cysteine (5 mM) were incubated in 20% CD<sub>3</sub>CN/*d*-PBS (pH = 7.4) at 23 °C and monitored via <sup>1</sup>H NMR spectroscopy.



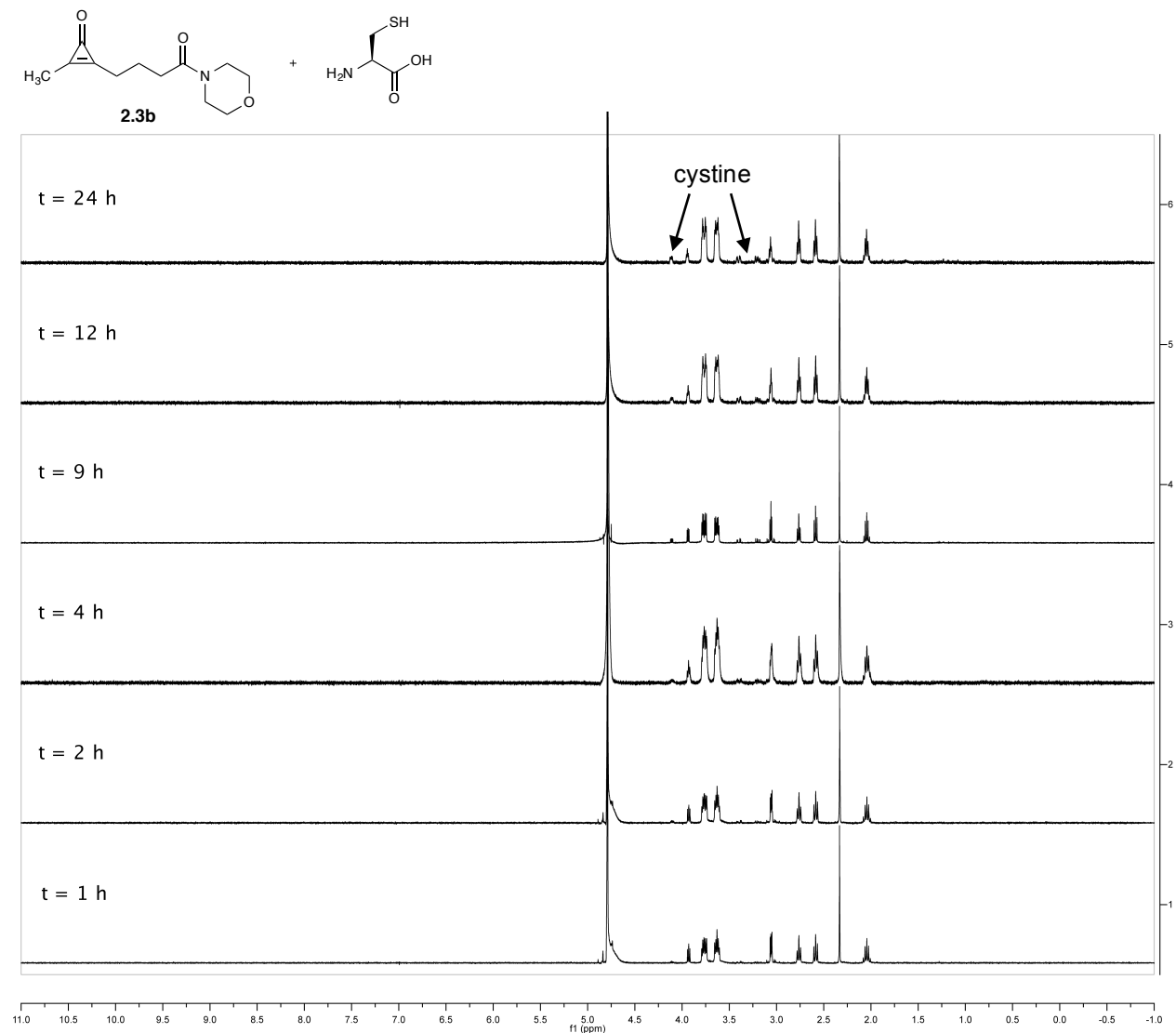
**Figure S2-10.** Cyclopropanone **2.10** is not stable to L-cysteine. Compound **2.10** (5 mM) and L-cysteine (5 mM) were incubated in 20%  $\text{CD}_3\text{CN}/d\text{-PBS}$  (pH = 7.4) at room temperature and monitored via  $^1\text{H}$  NMR spectroscopy. The lower spectra shows **2.10** in 20%  $\text{CD}_3\text{CN}/d\text{-PBS}$  without L-cysteine.



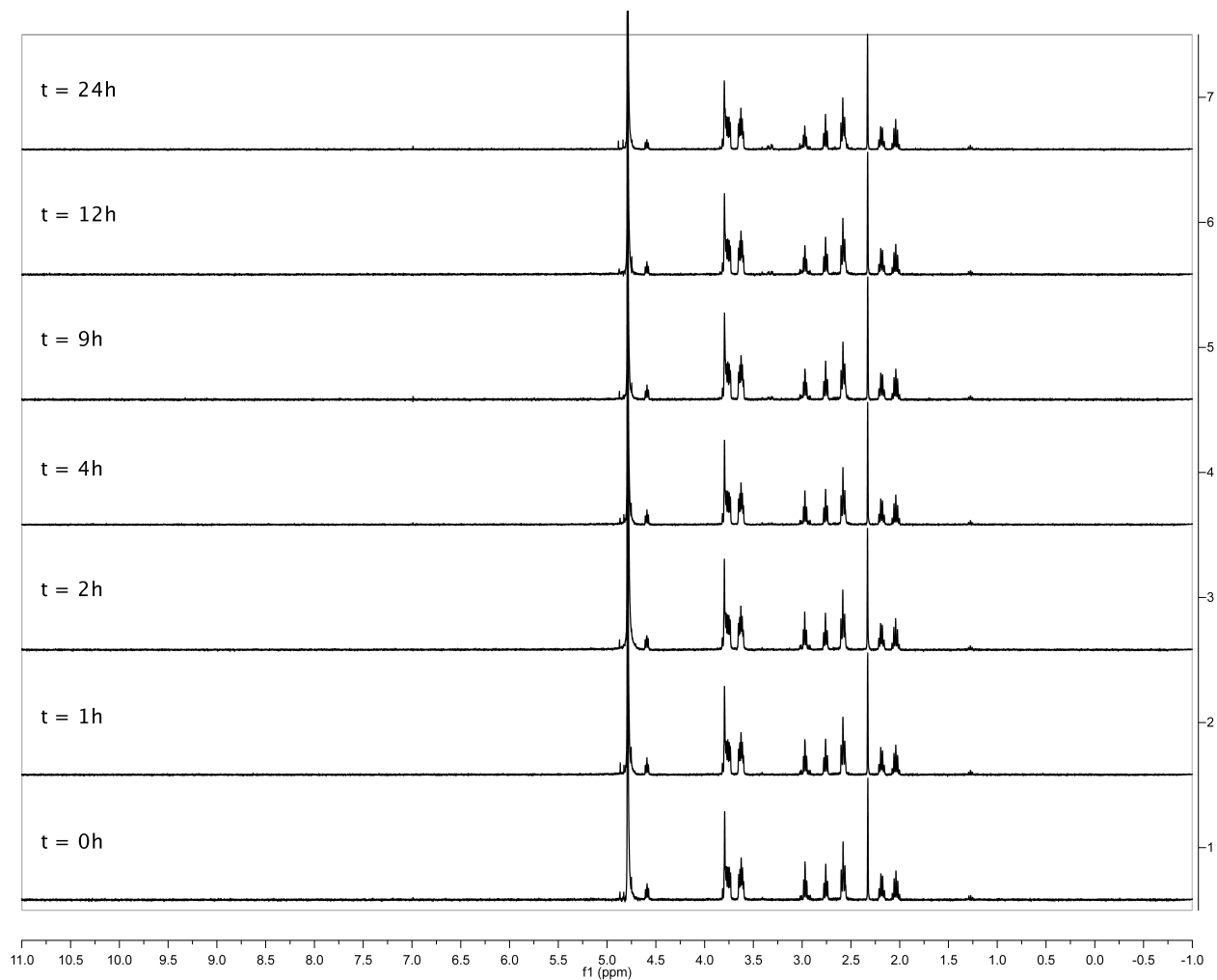
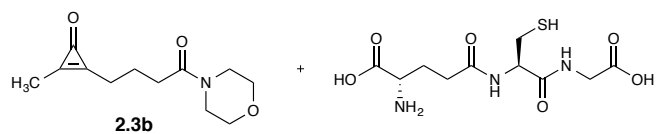
**Figure S2-11.** Cyclopropanone **2.3b** is stable to L-cysteine at pH = 7.4. Compound **2.3b** (5 mM) and L-cysteine (5 mM) were incubated in *d*-PBS (pH = 7.4) at 37 °C and monitored via <sup>1</sup>H NMR spectroscopy. Some L-cysteine oxidation was observed, as shown in inset, after 24 h.



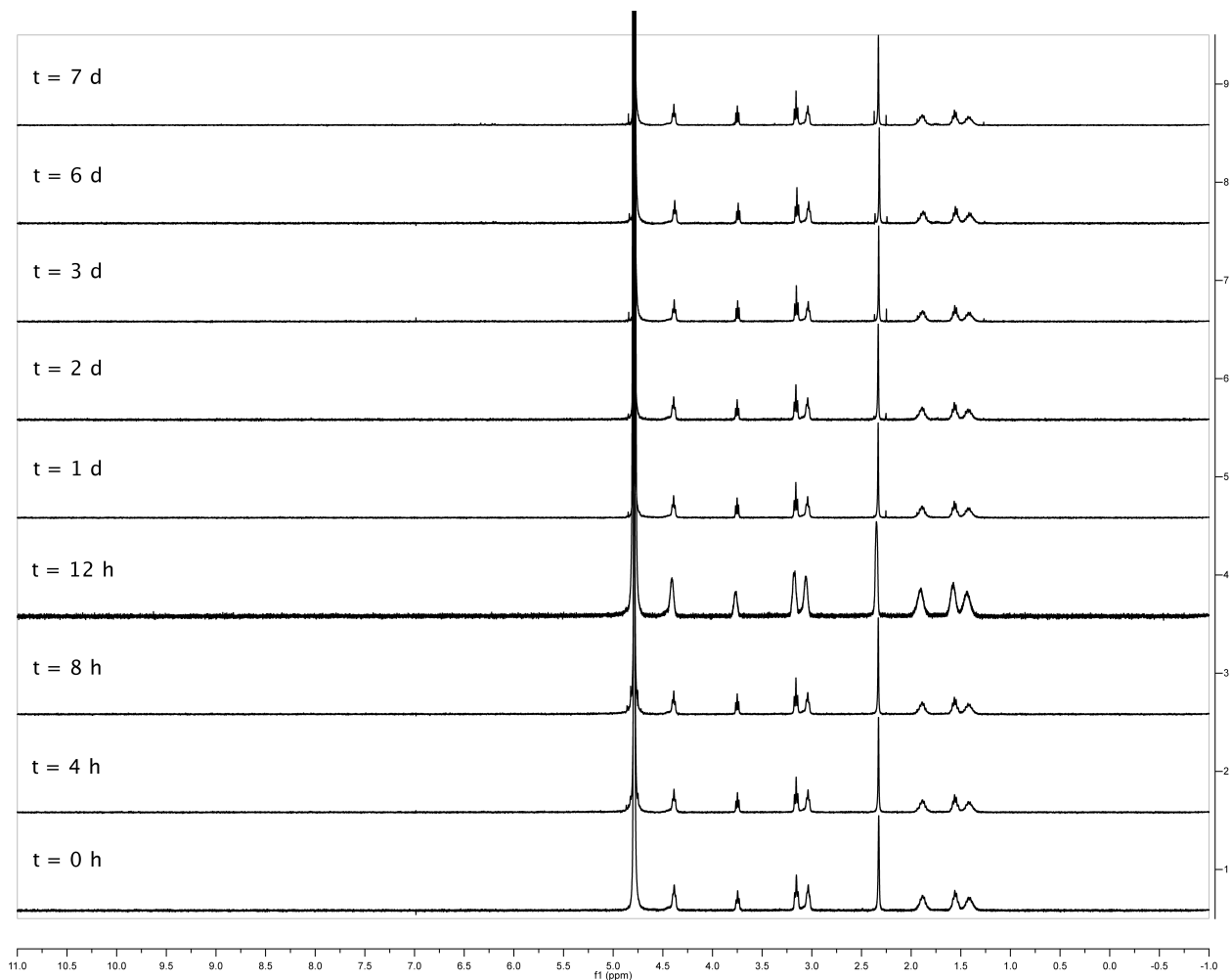
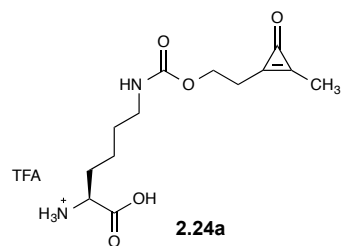
**Figure S2-12.** Cyclopropenone **2.3b** is stable to L-cysteine at pH = 8.0. Compound **2.3b** (5 mM) and L-cysteine (5 mM) were incubated in *d*-PBS (pH = 8.0) at 37 °C and monitored via  $^1\text{H}$  NMR spectroscopy. Some L-cysteine oxidation was observed, as indicated by the presence of cystine.



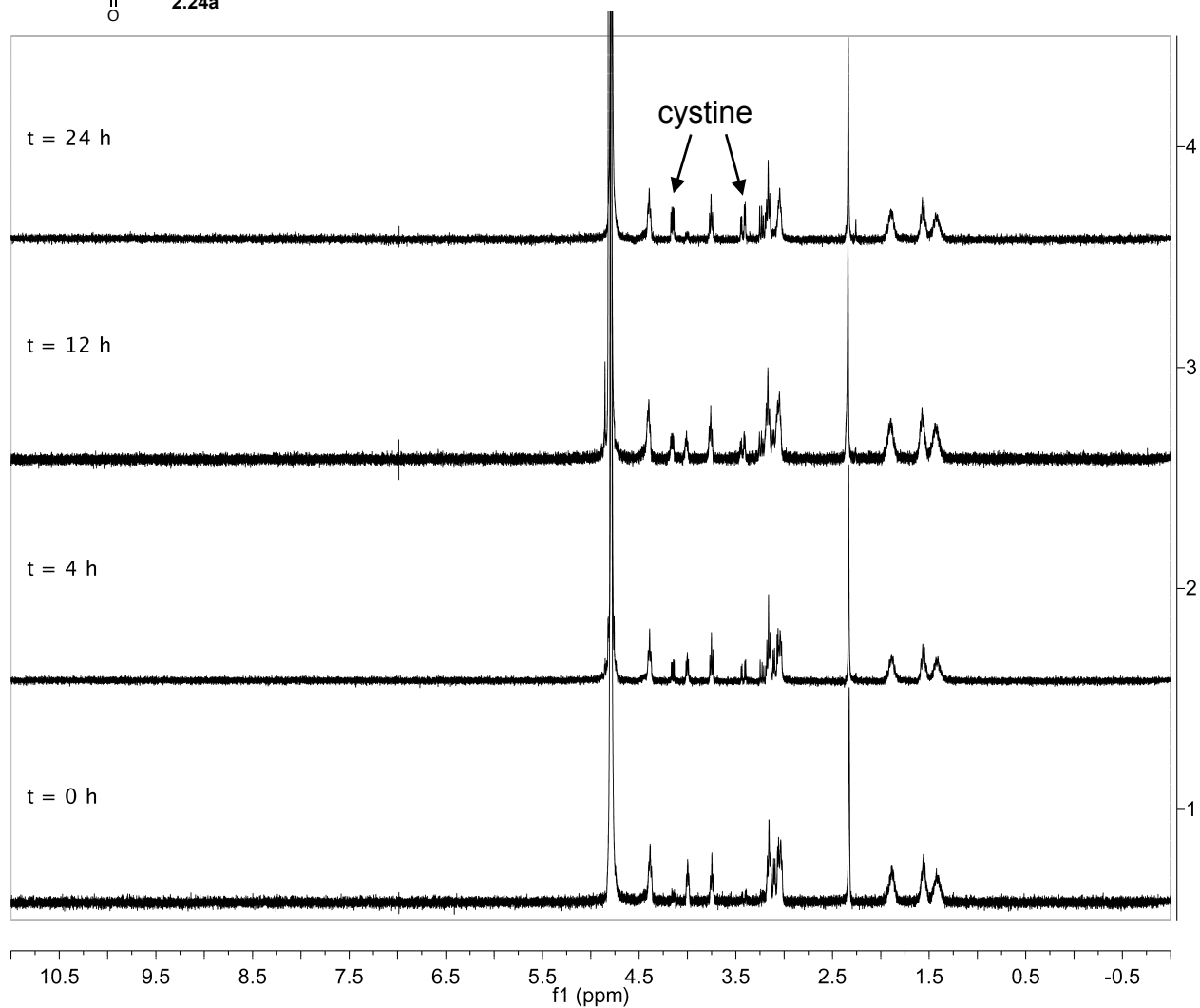
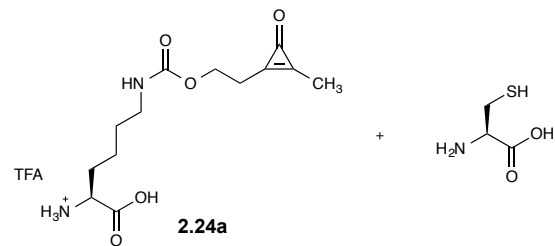
**Figure S2-13.** Cyclopropenone **2.3b** is stable to L-cysteine at pH = 8.4. Compound **2.3b** (5 mM) and L-cysteine (5 mM) were incubated in *d*-PBS (pH = 8.4) at 37 °C and monitored via  $^1\text{H}$  NMR spectroscopy. Some L-cysteine oxidation was observed, as indicated by the presence of cystine.



**Figure S2-14.** Cyclopropenone **2.3b** is stable to L-glutathione. Compound **2.3b** (5 mM) and L-glutathione (5 mM) were incubated in *d*-PBS (pH = 7.4) at 37 °C and monitored via  $^1\text{H}$  NMR spectroscopy.

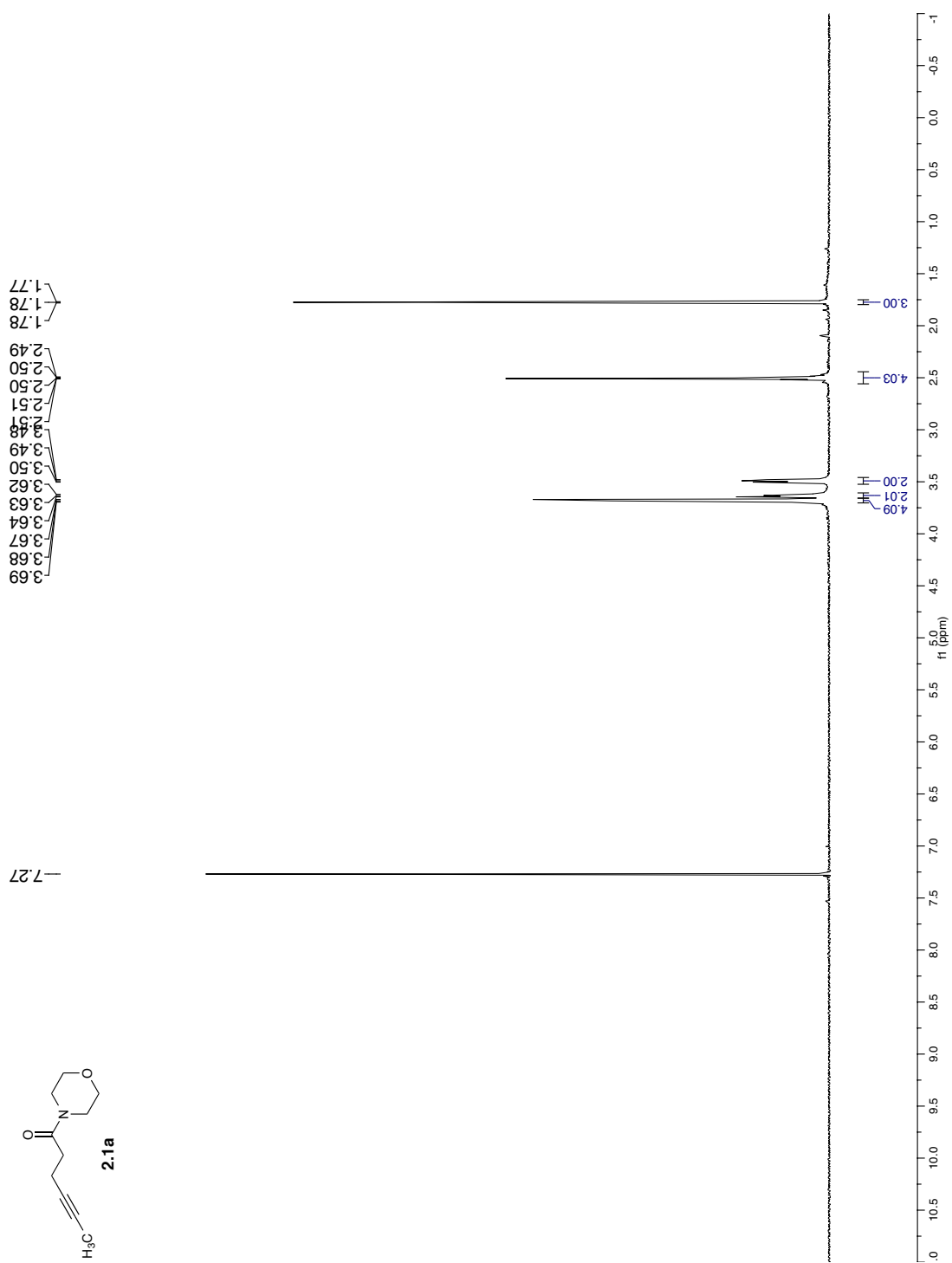


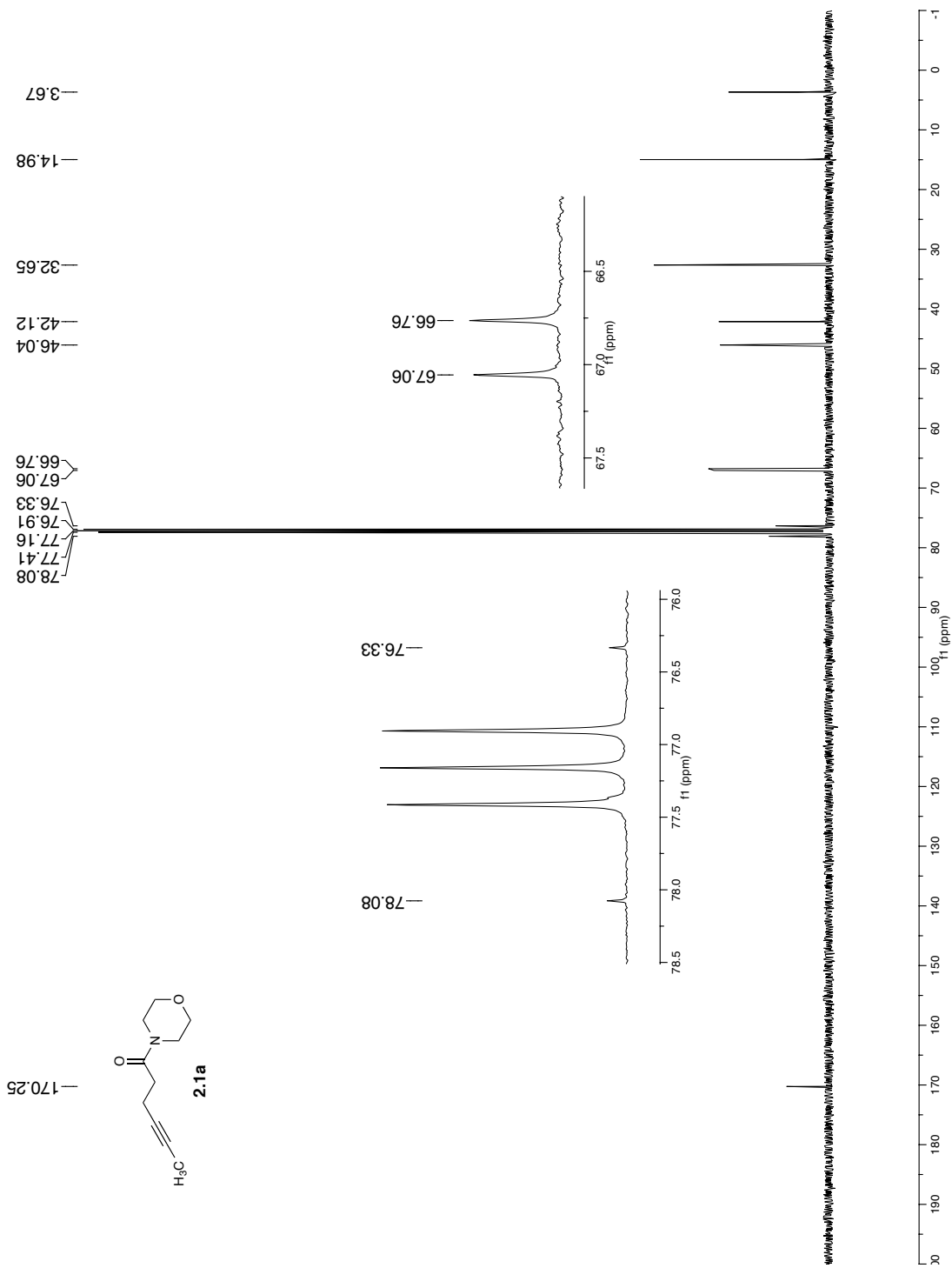
**Figure S2-15.** The non-canonical amino acid **2.24a** is stable in aqueous solution for 1 week. Compound **2.24a** (10 mM) was incubated in *d*-PBS (pH = 7.4) at 37 °C and monitored via <sup>1</sup>H NMR spectroscopy.

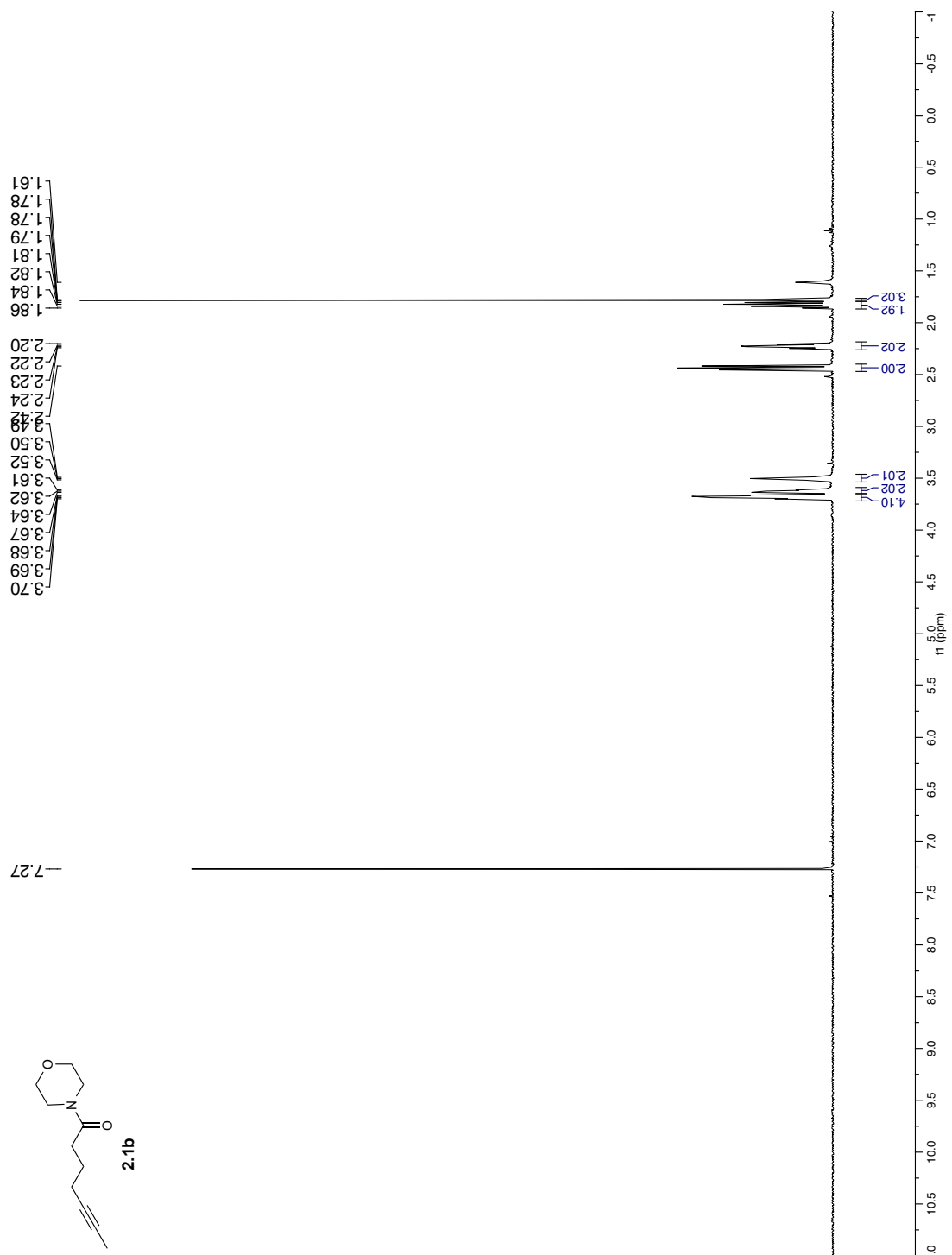


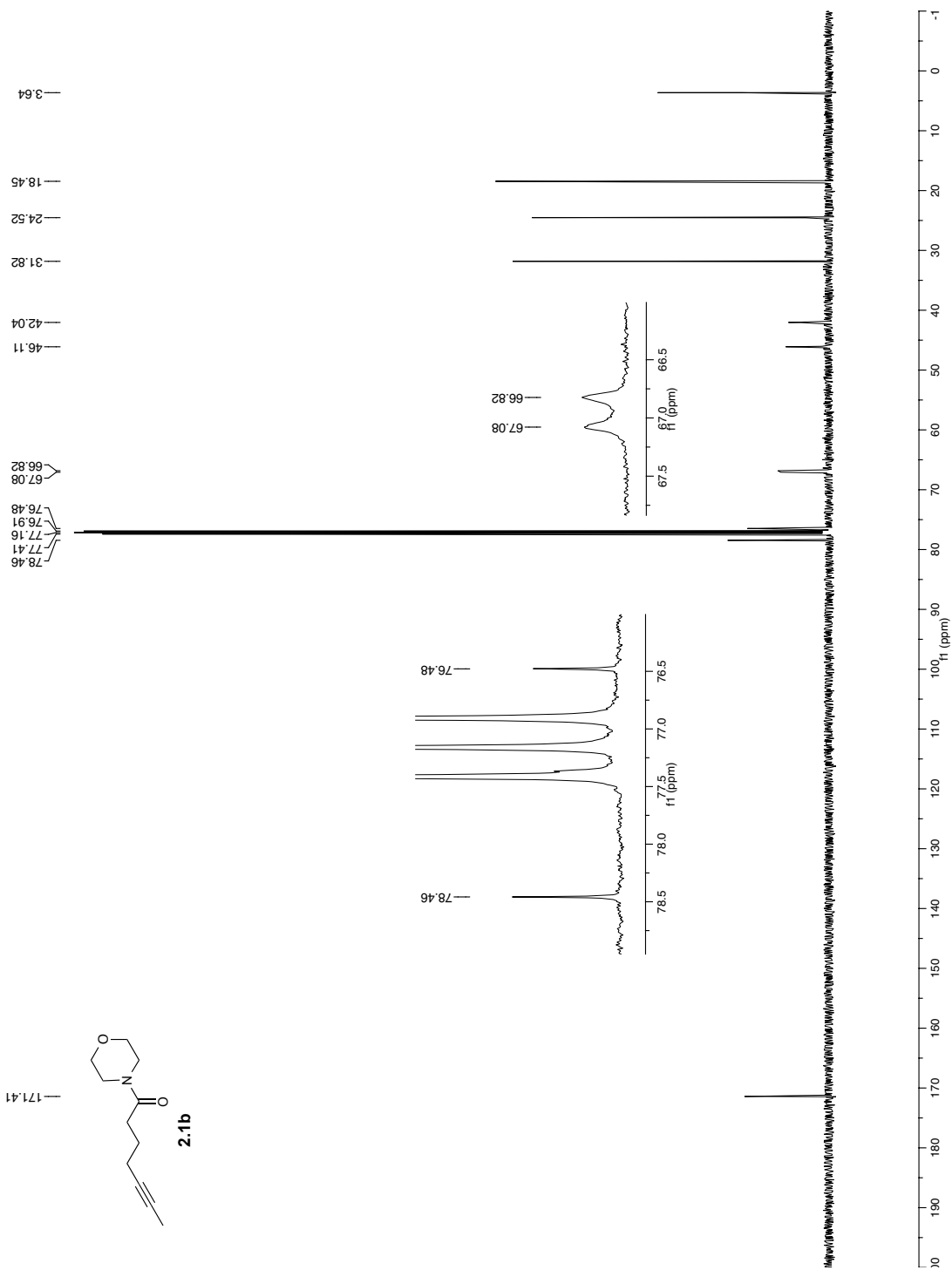
**Figure S2-16.** Cyclopropanone **2.24a** is stable to L-cysteine. Compound **2.24a** (5 mM) and L-cysteine (5 mM) were incubated in *d*-PBS (pH = 7.4) at 37 °C and monitored via  $^1\text{H}$  NMR spectroscopy. Some L-cysteine oxidation was observed, as indicated by the presence of cystine.

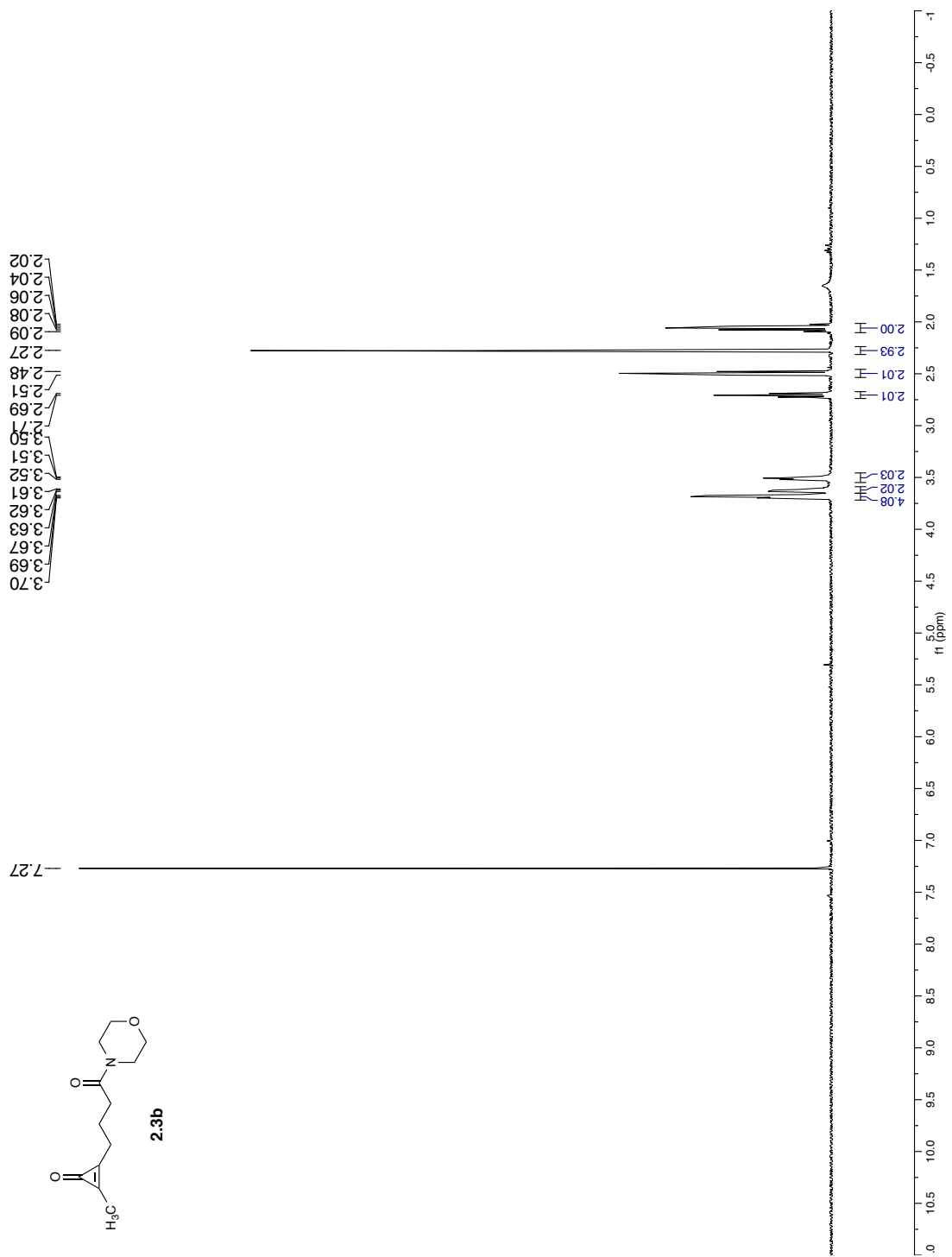


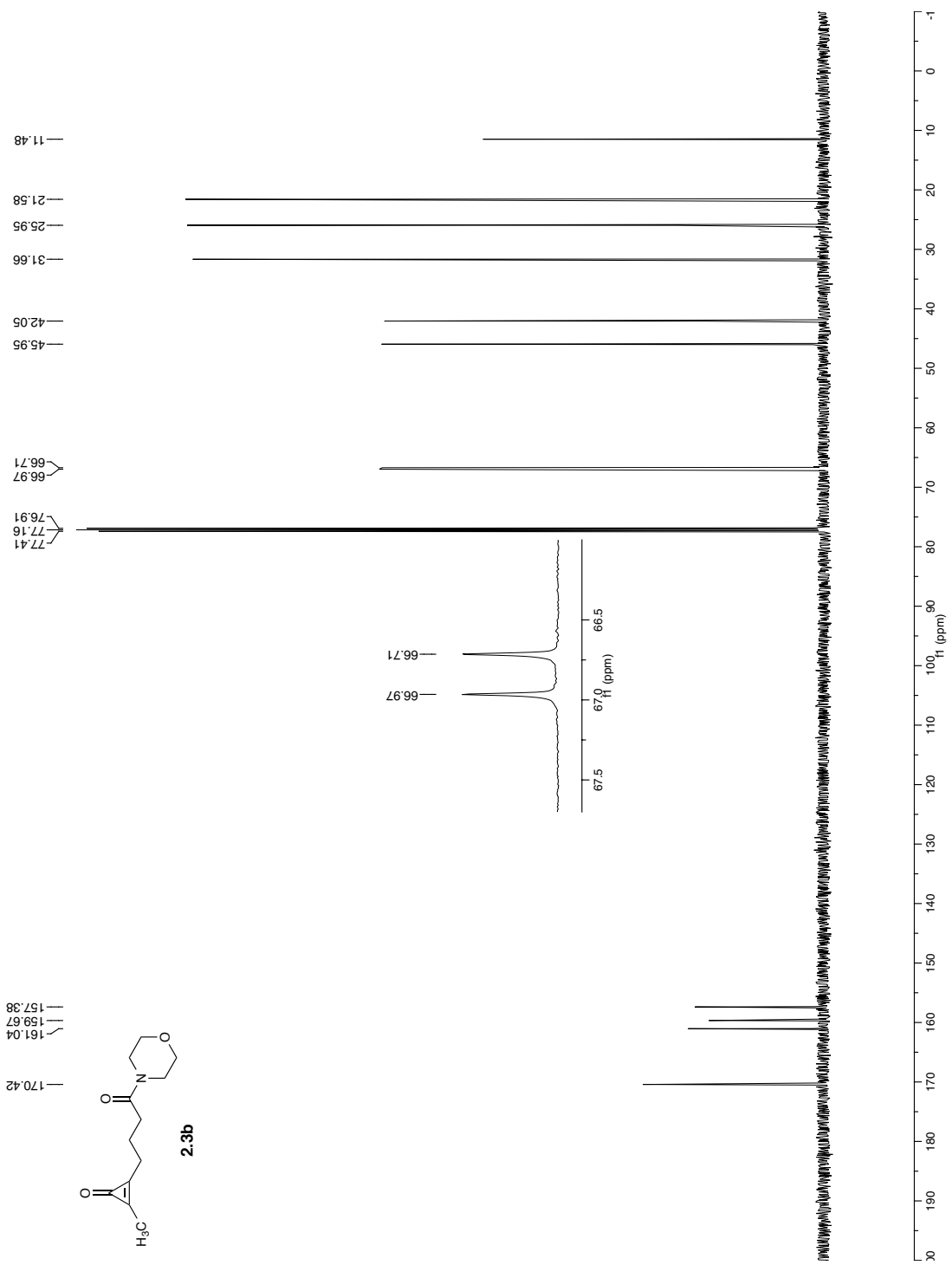


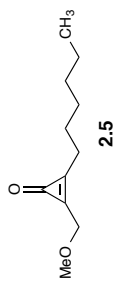
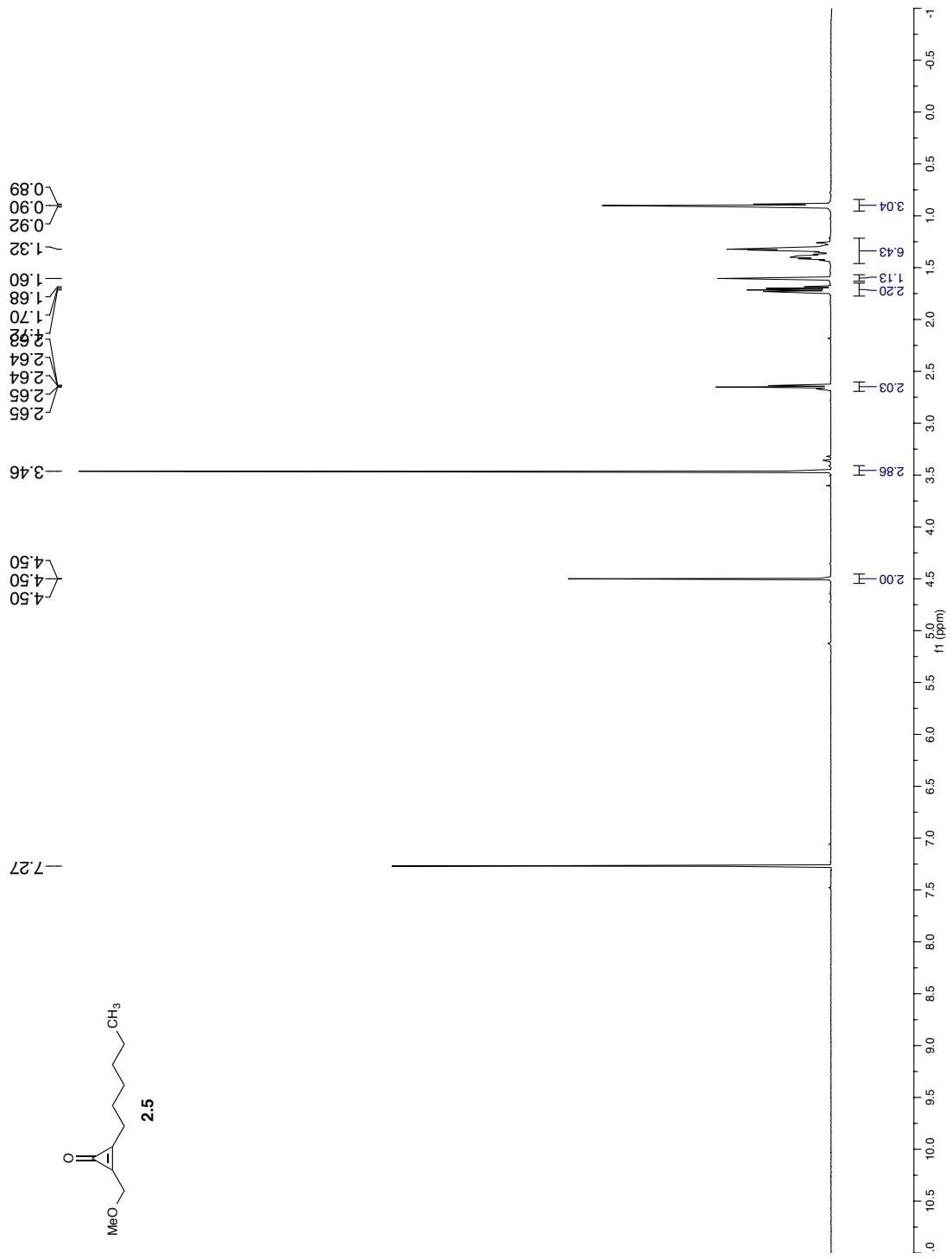


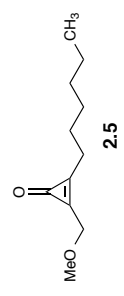
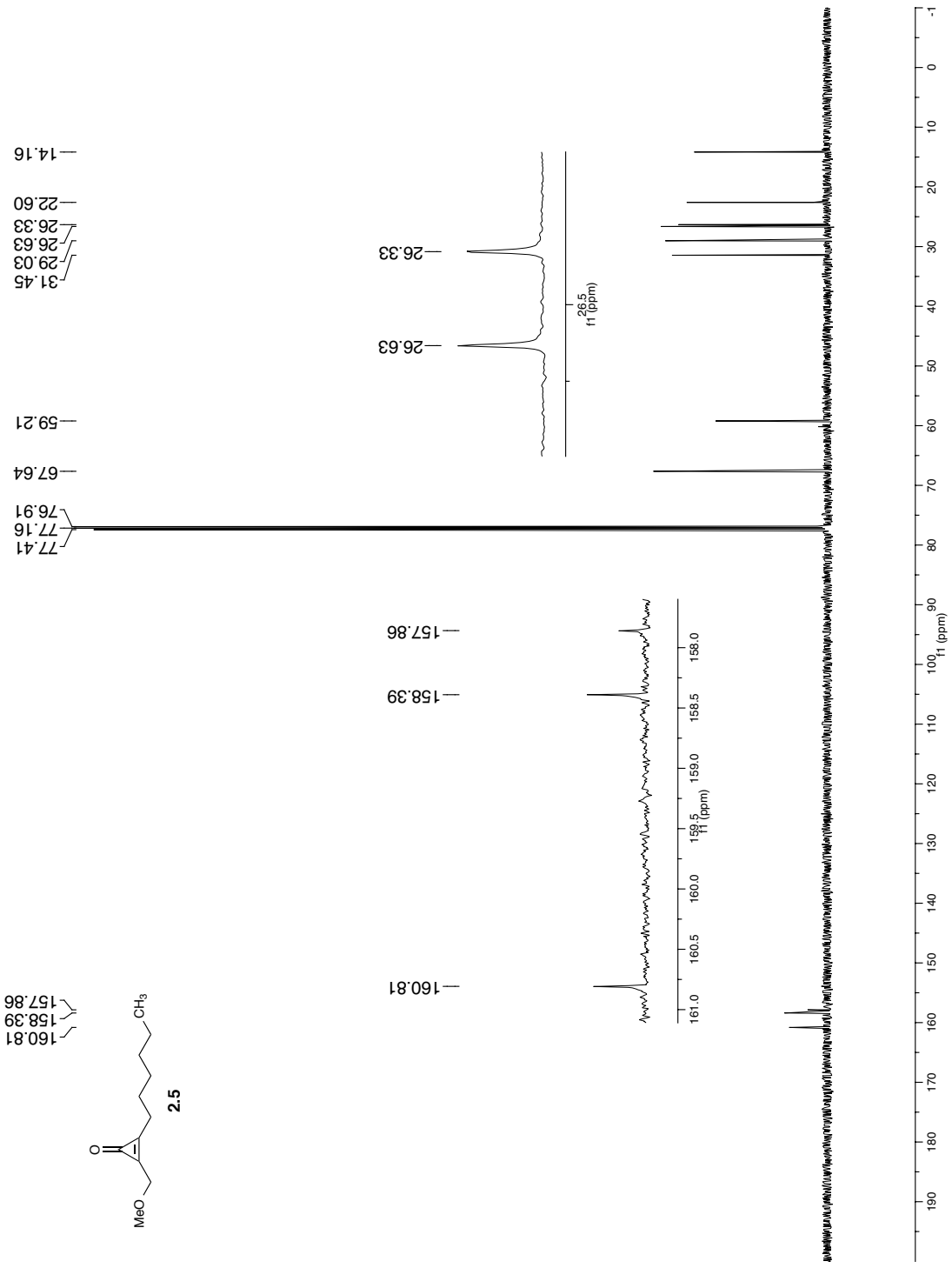






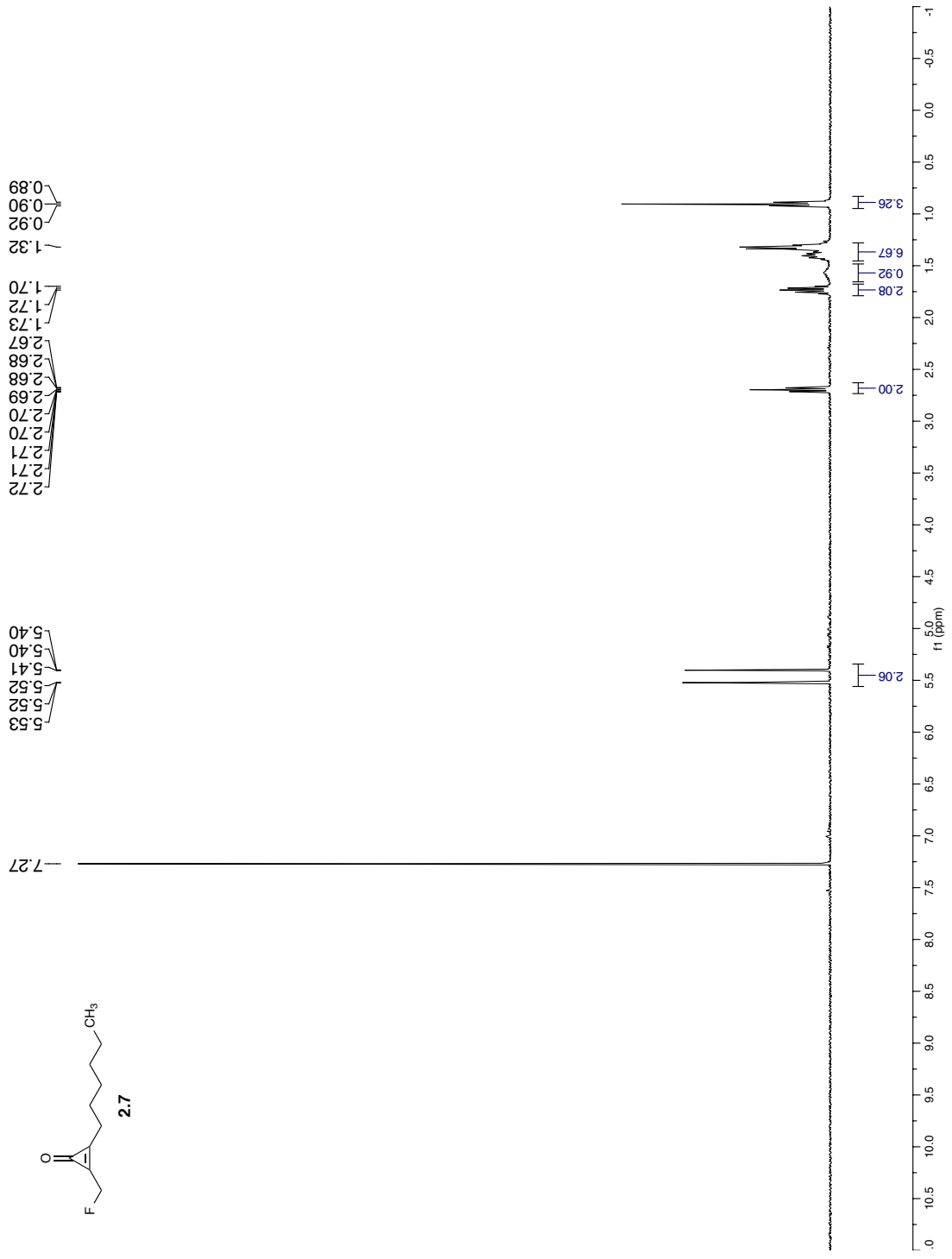


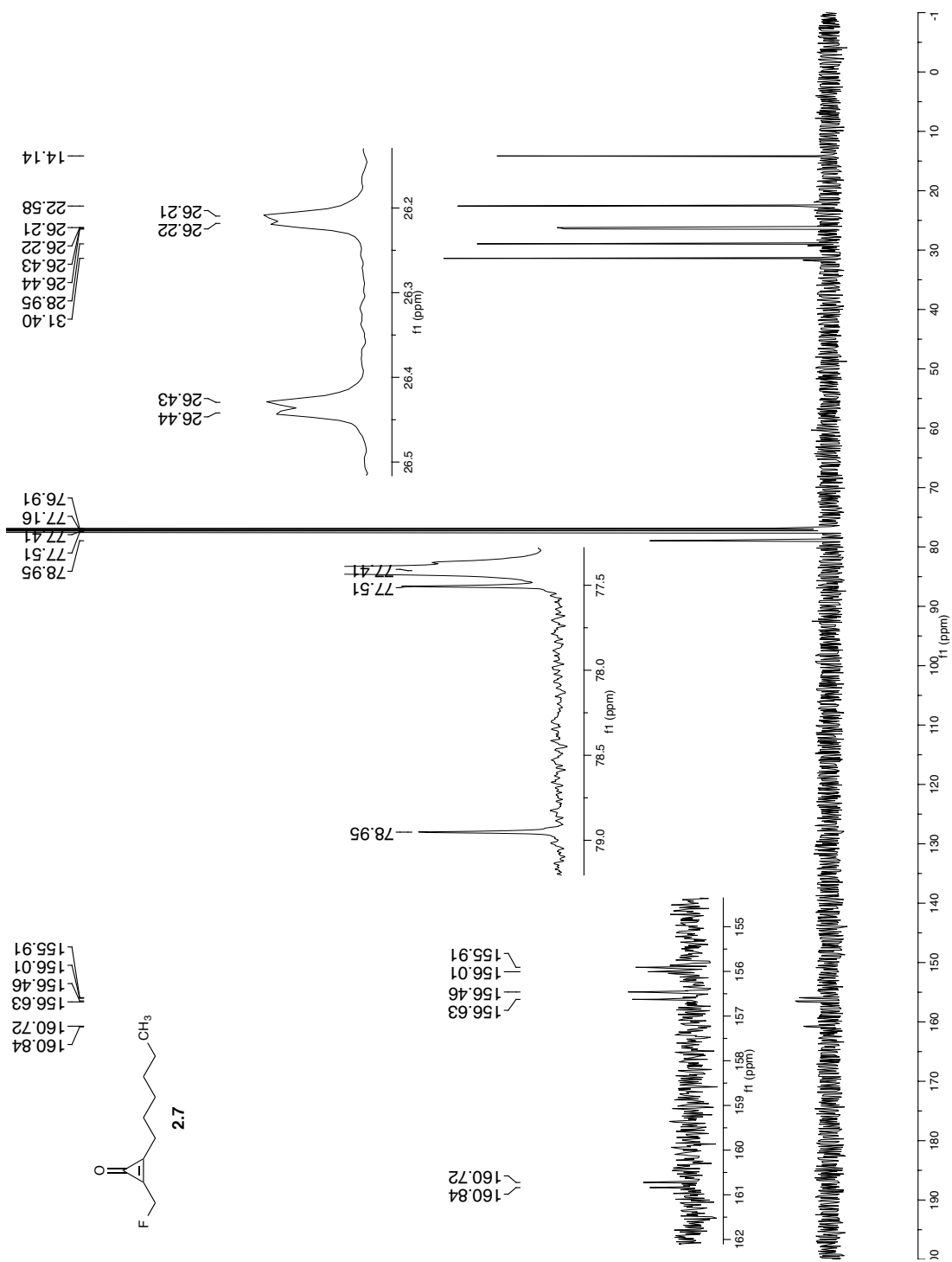


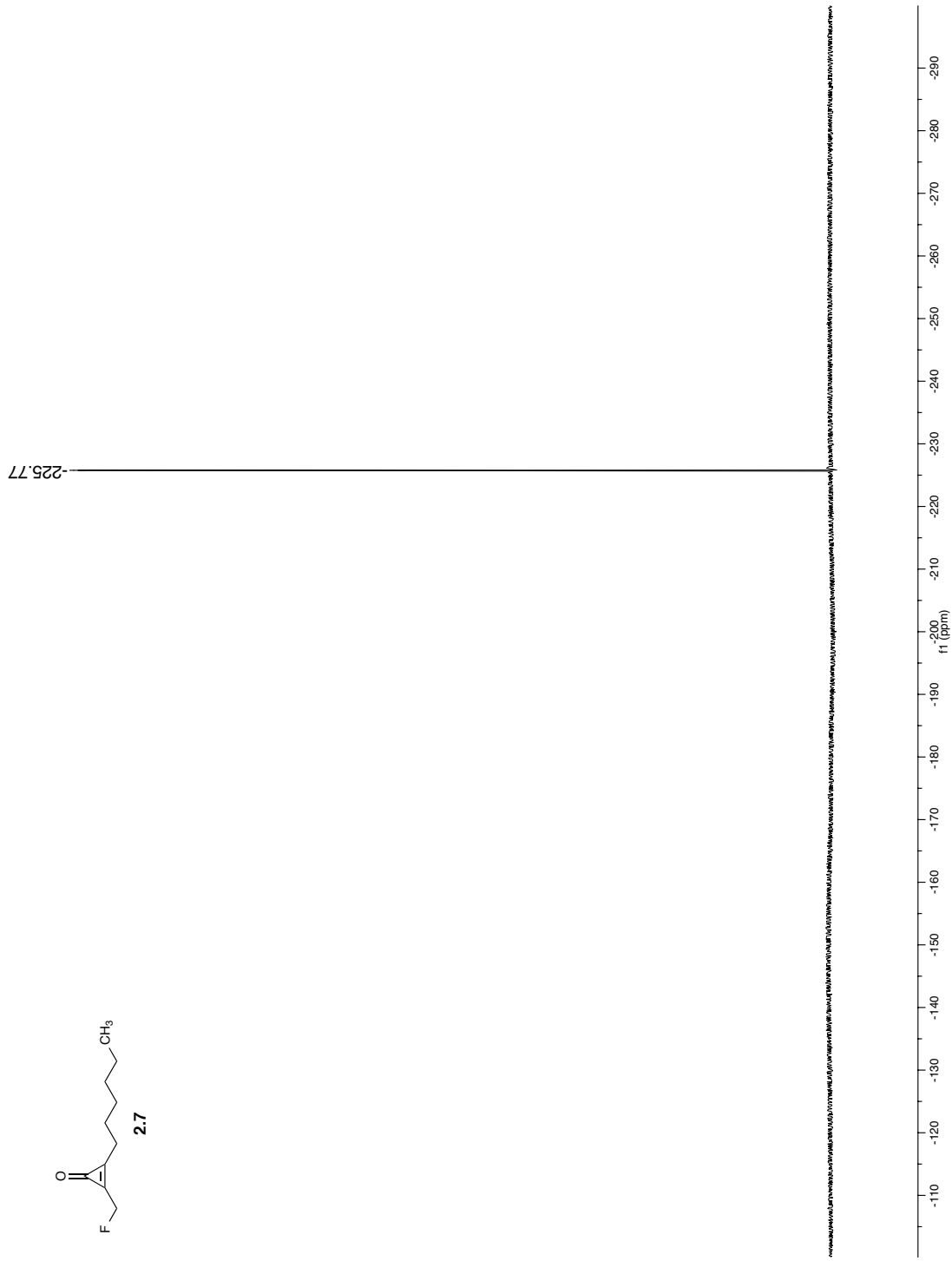
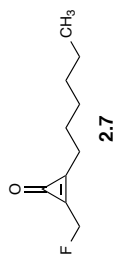


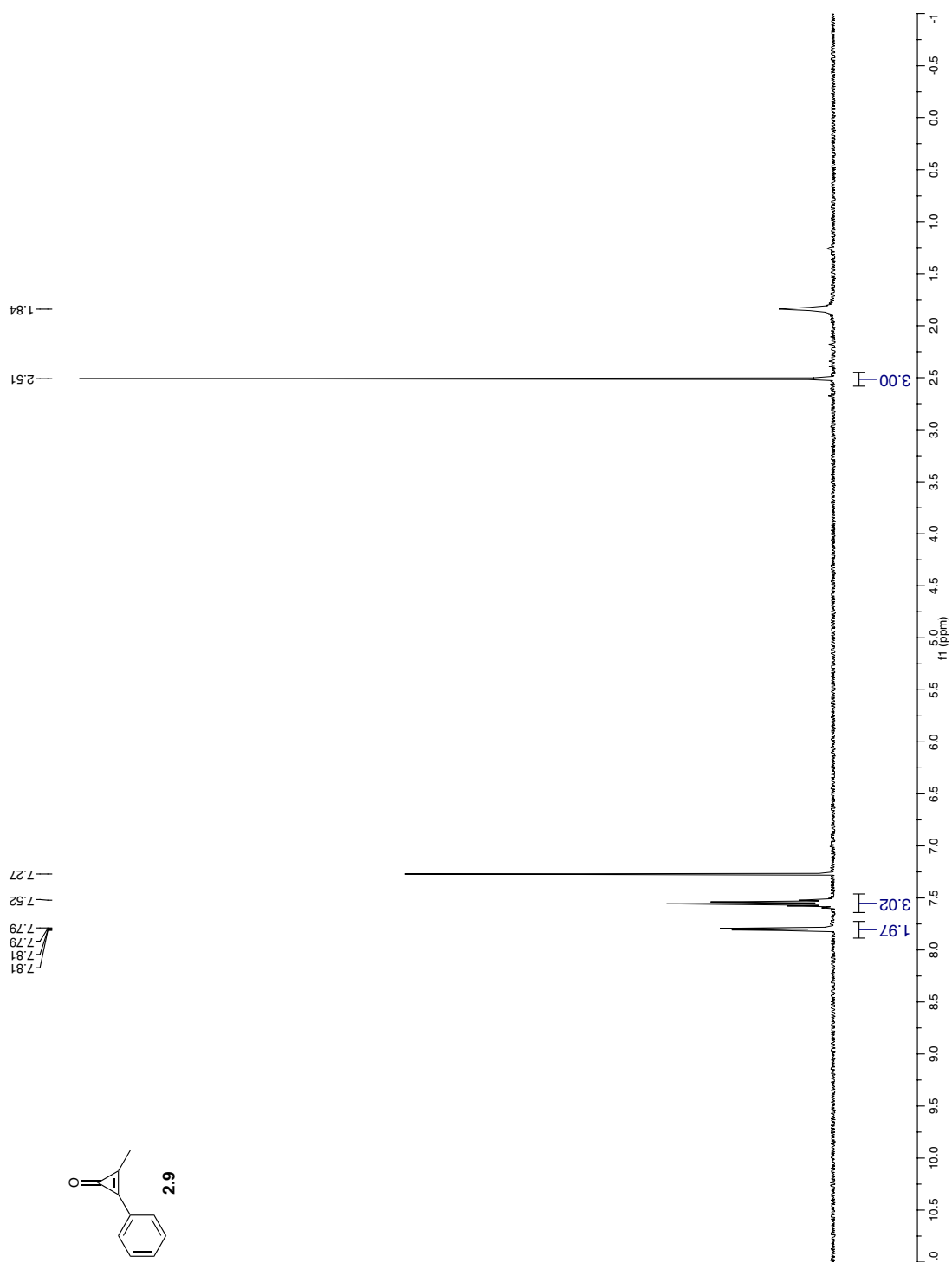
- 157.86
- 158.39
- 160.81

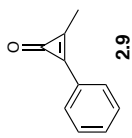
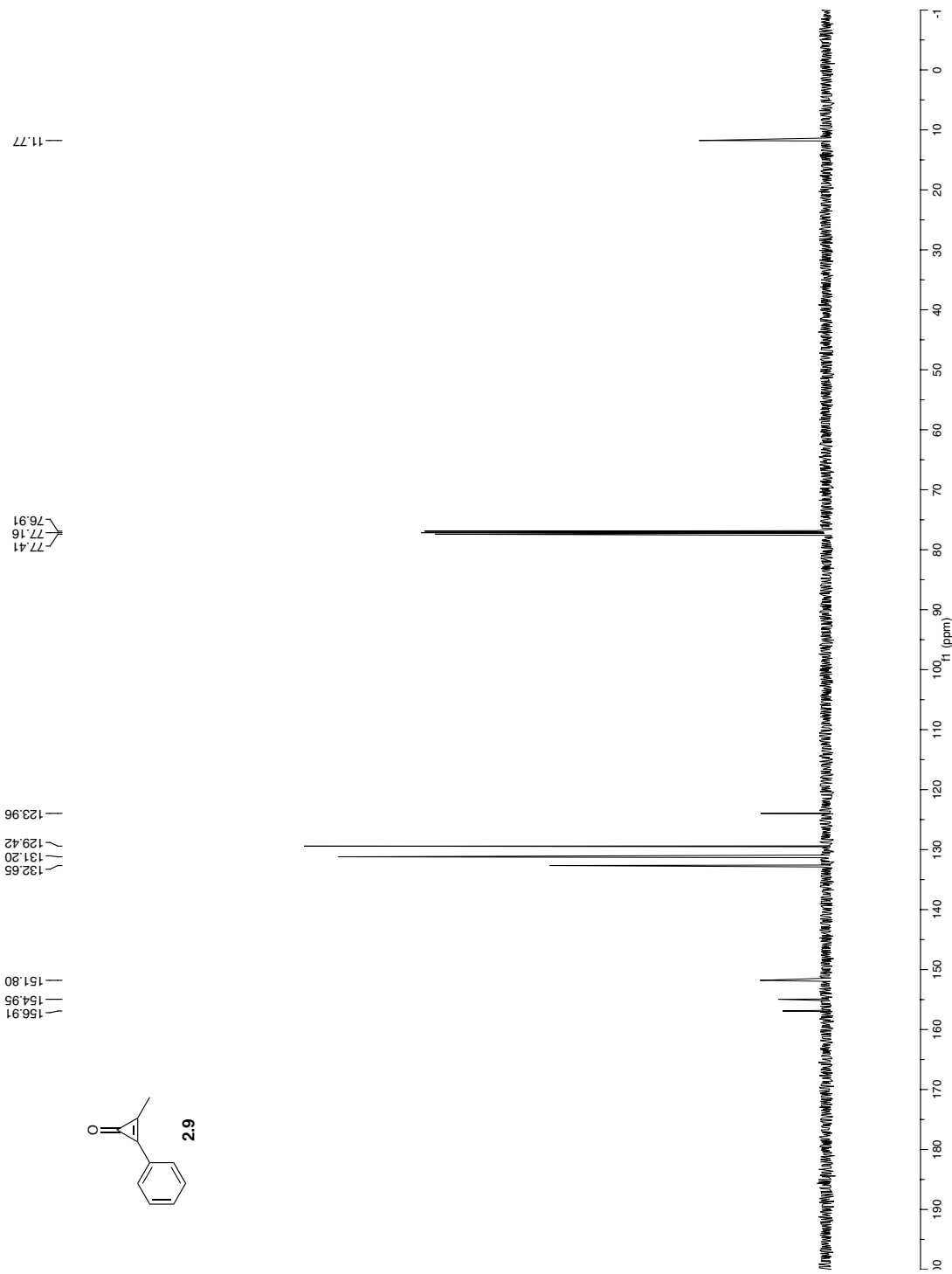


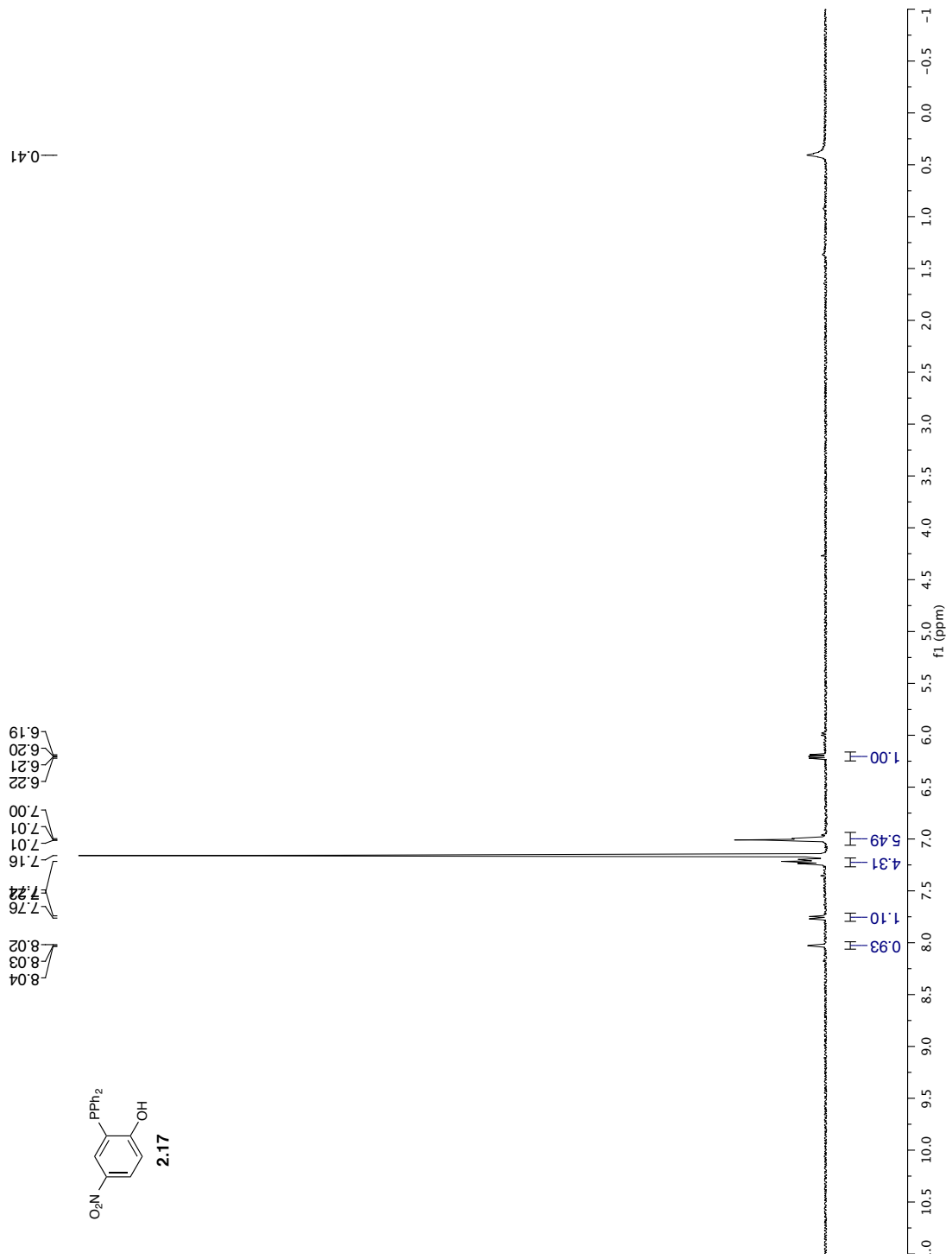


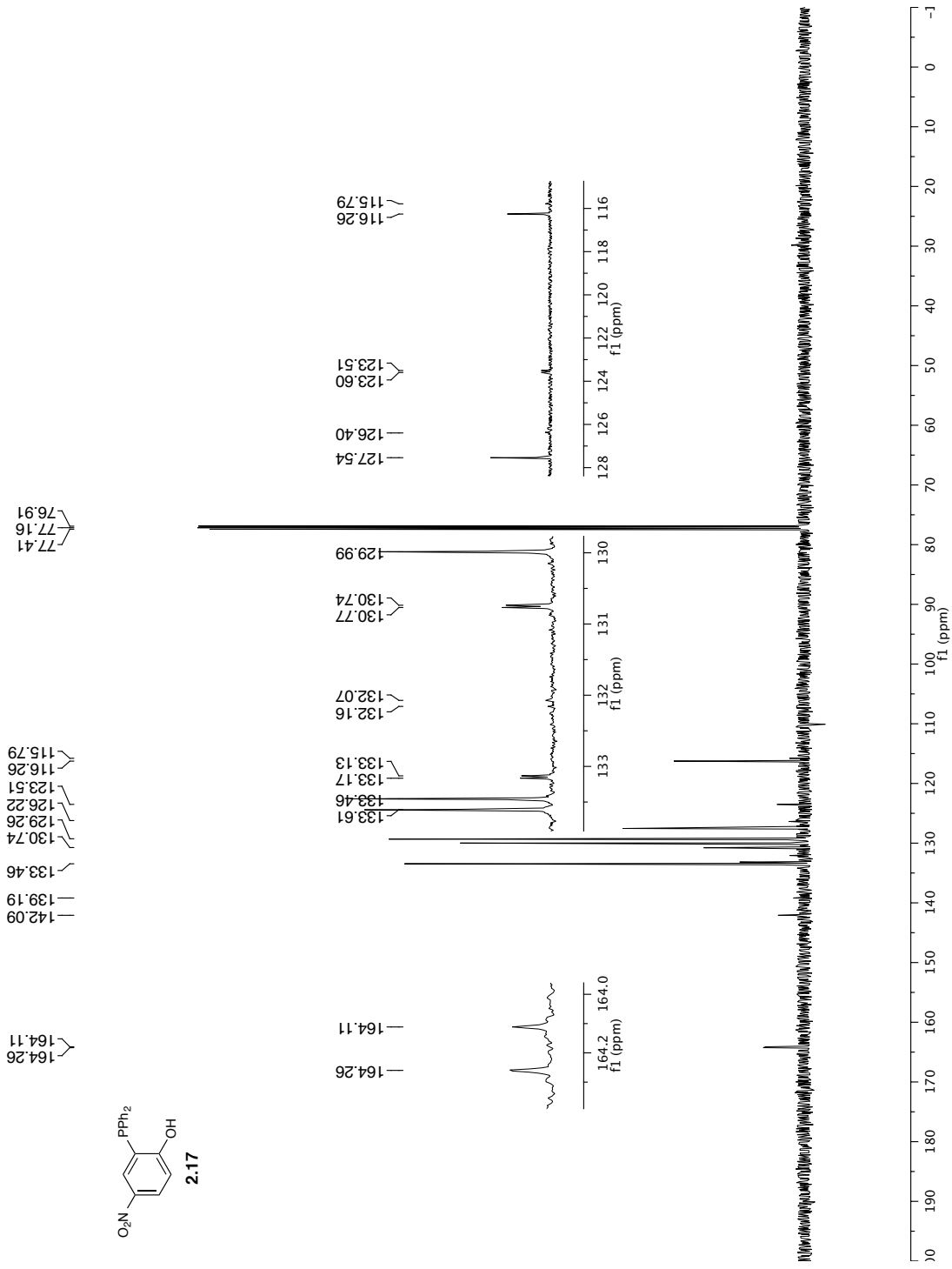
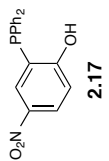


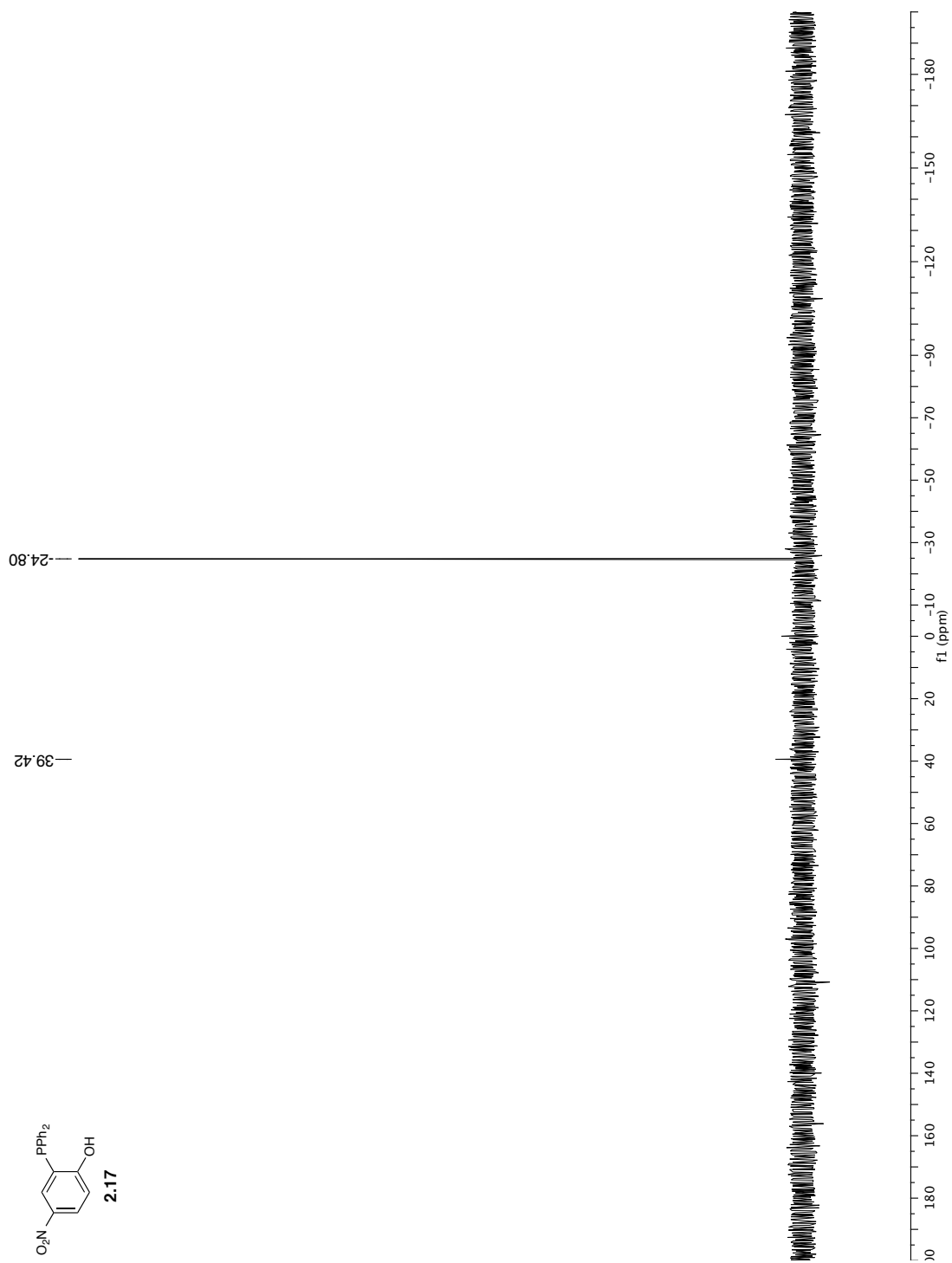




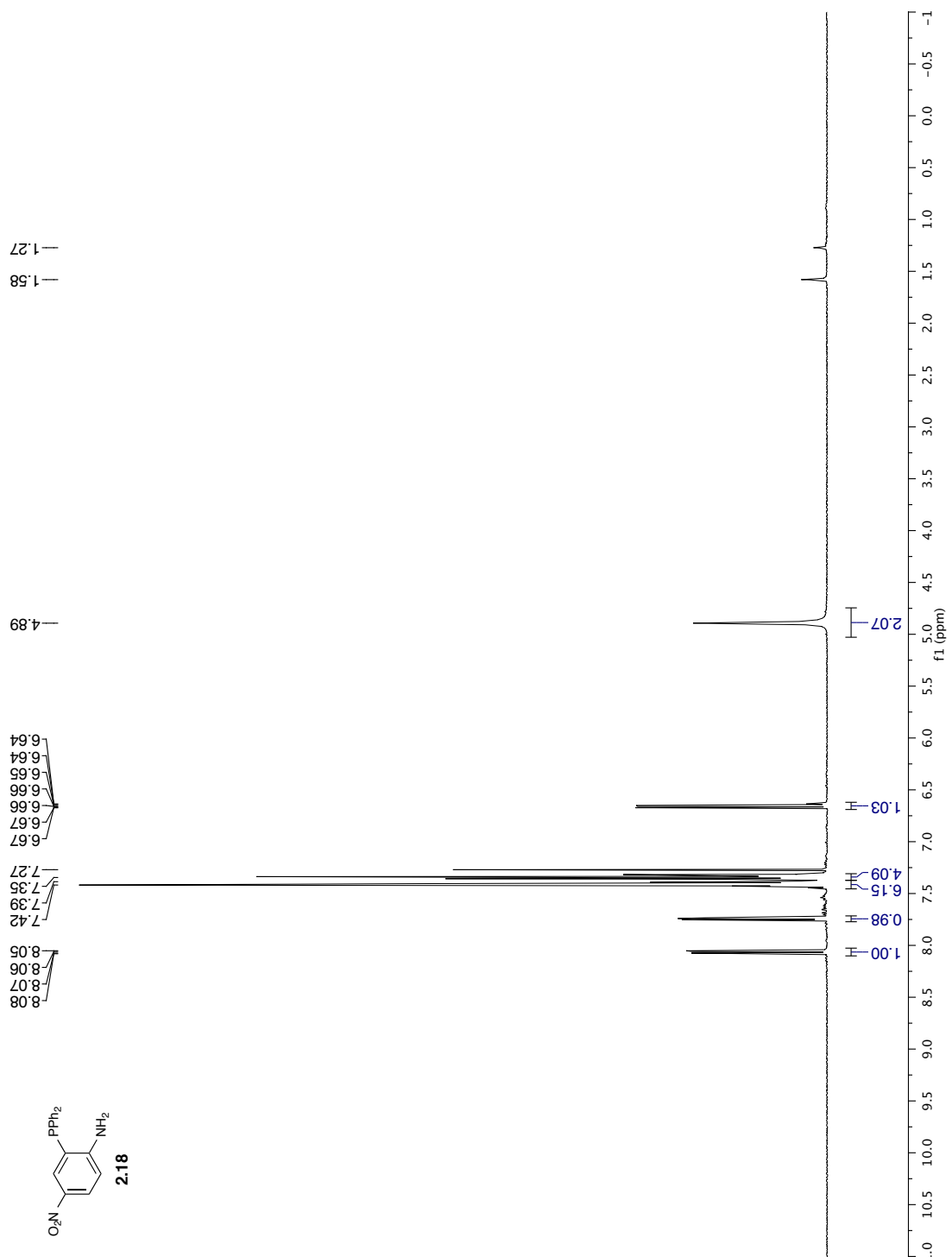


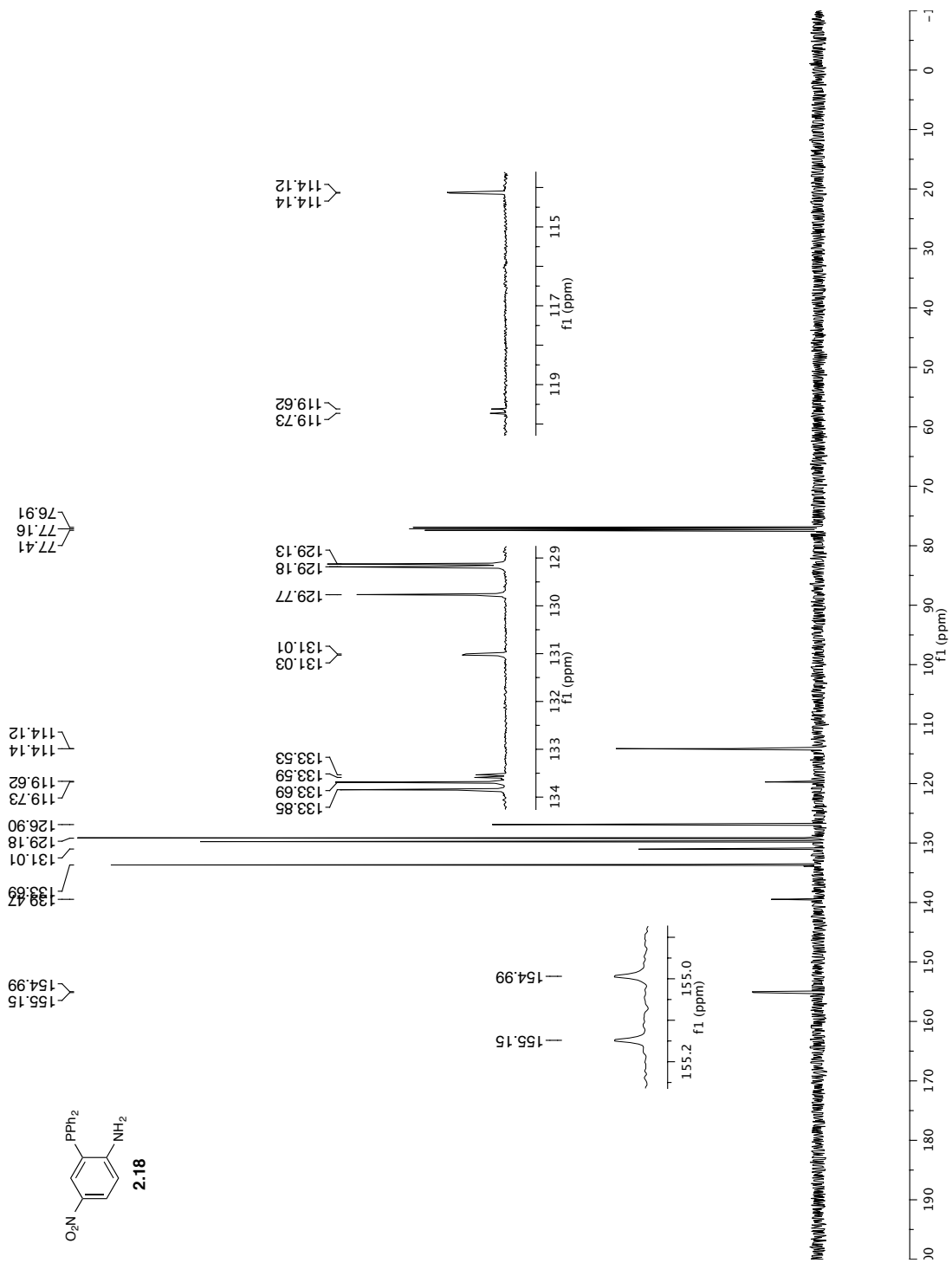


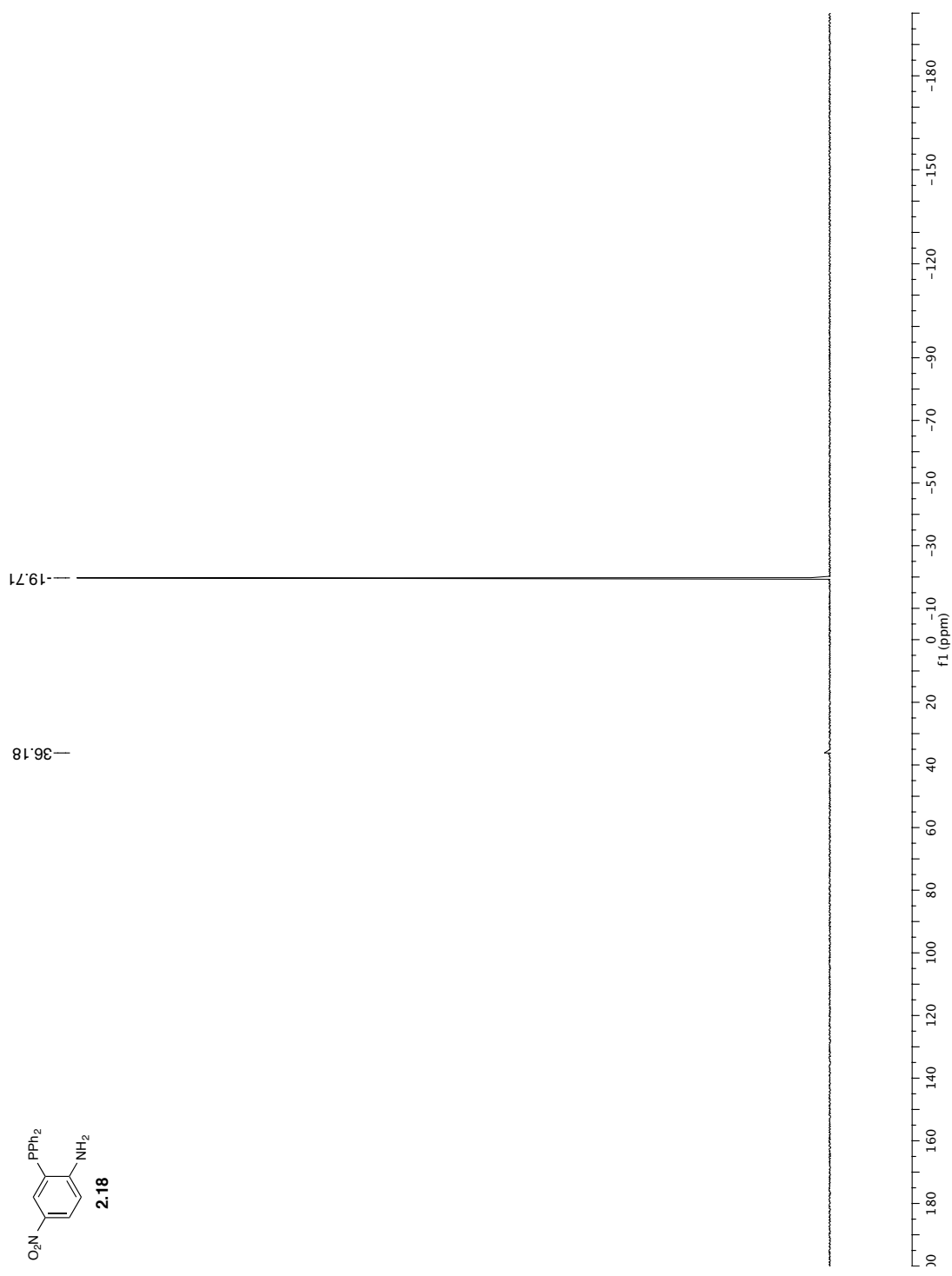


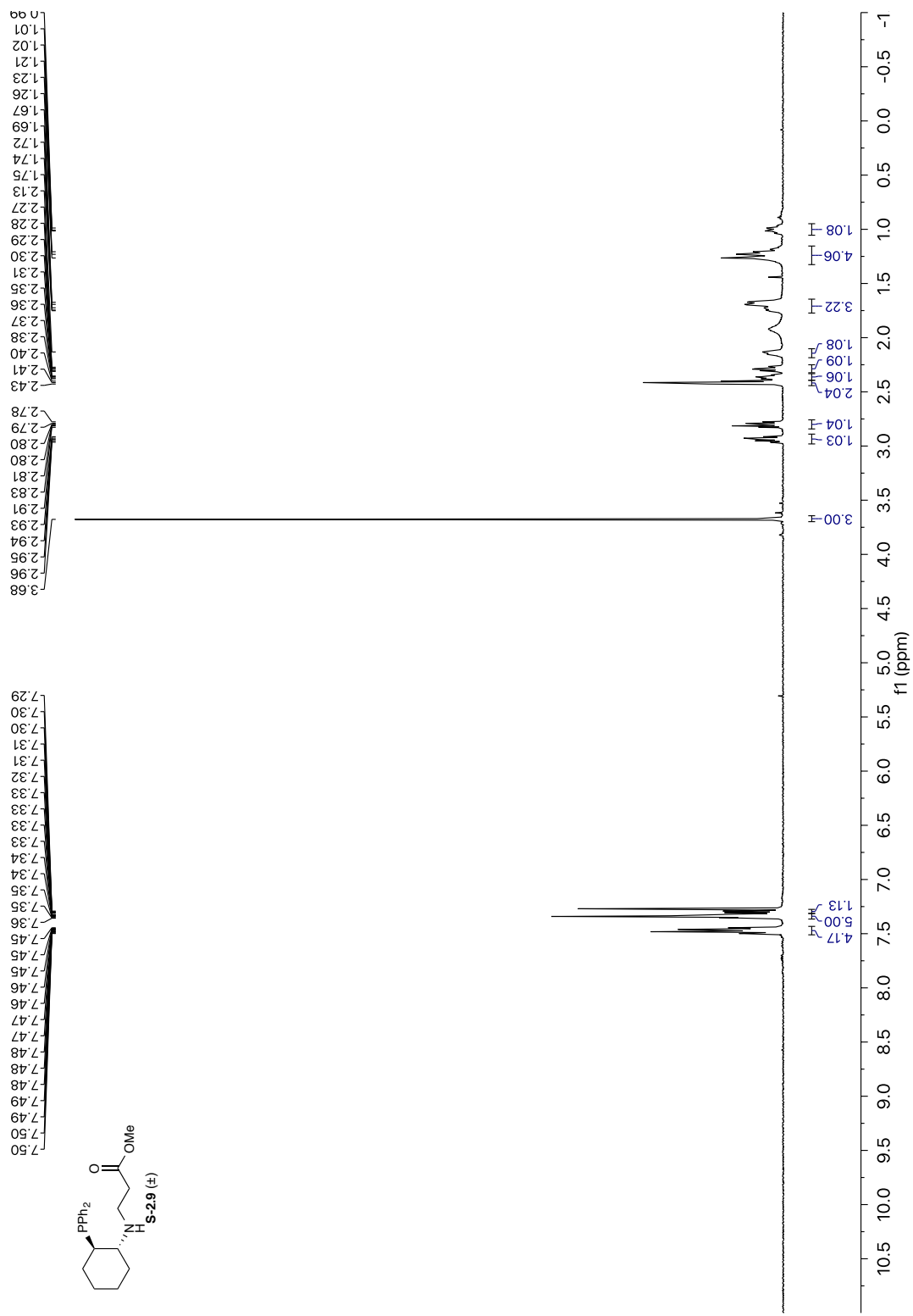


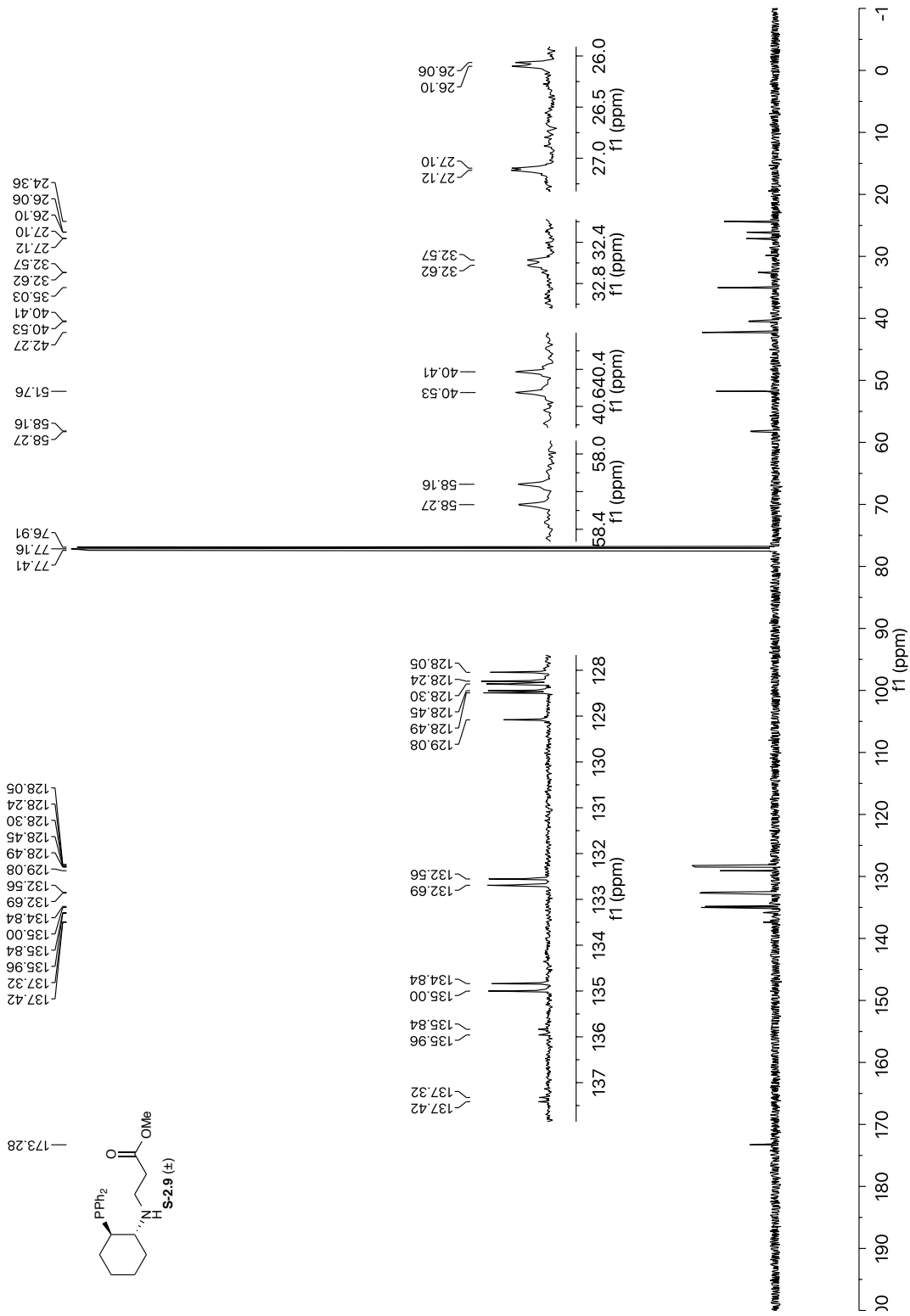


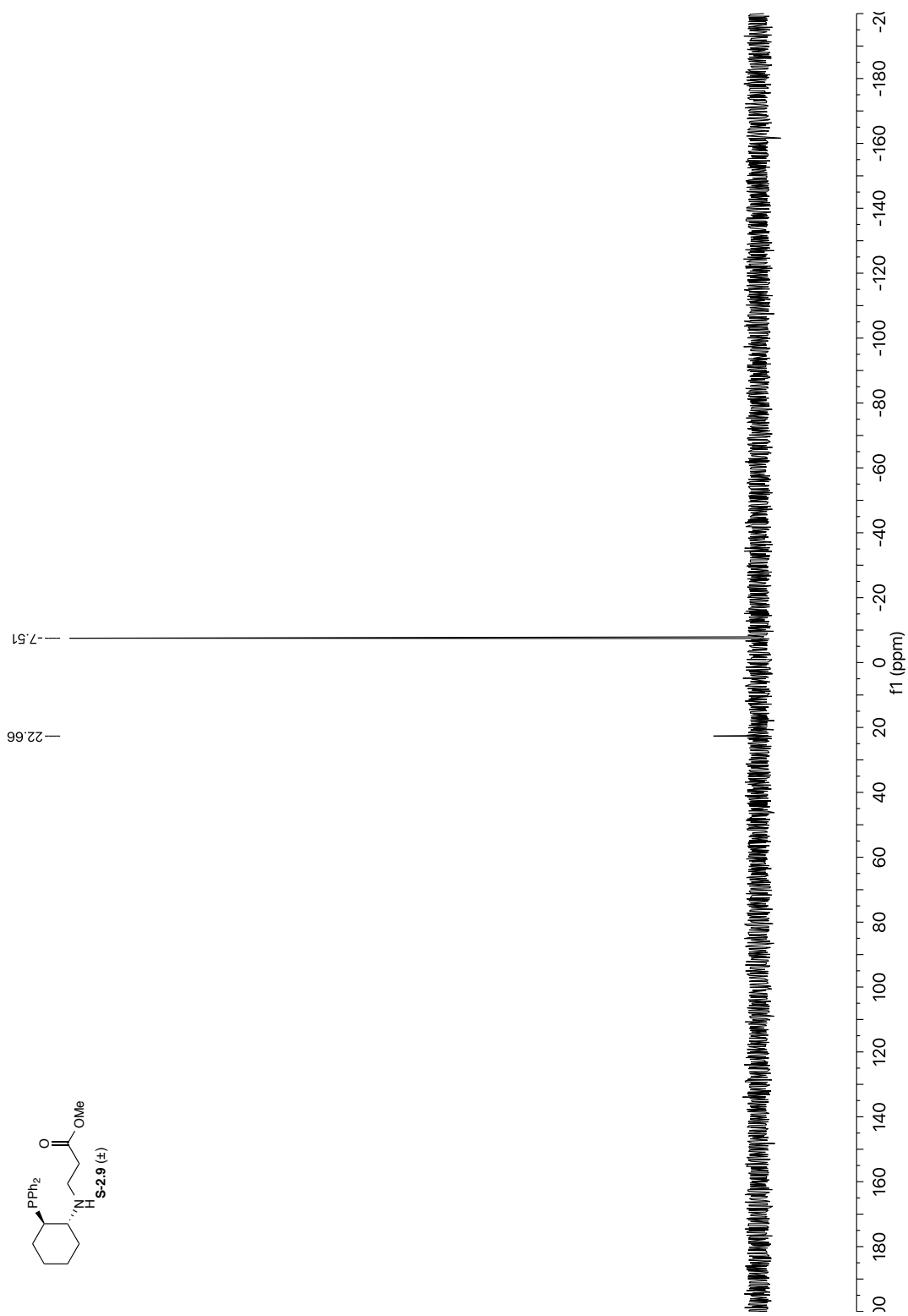




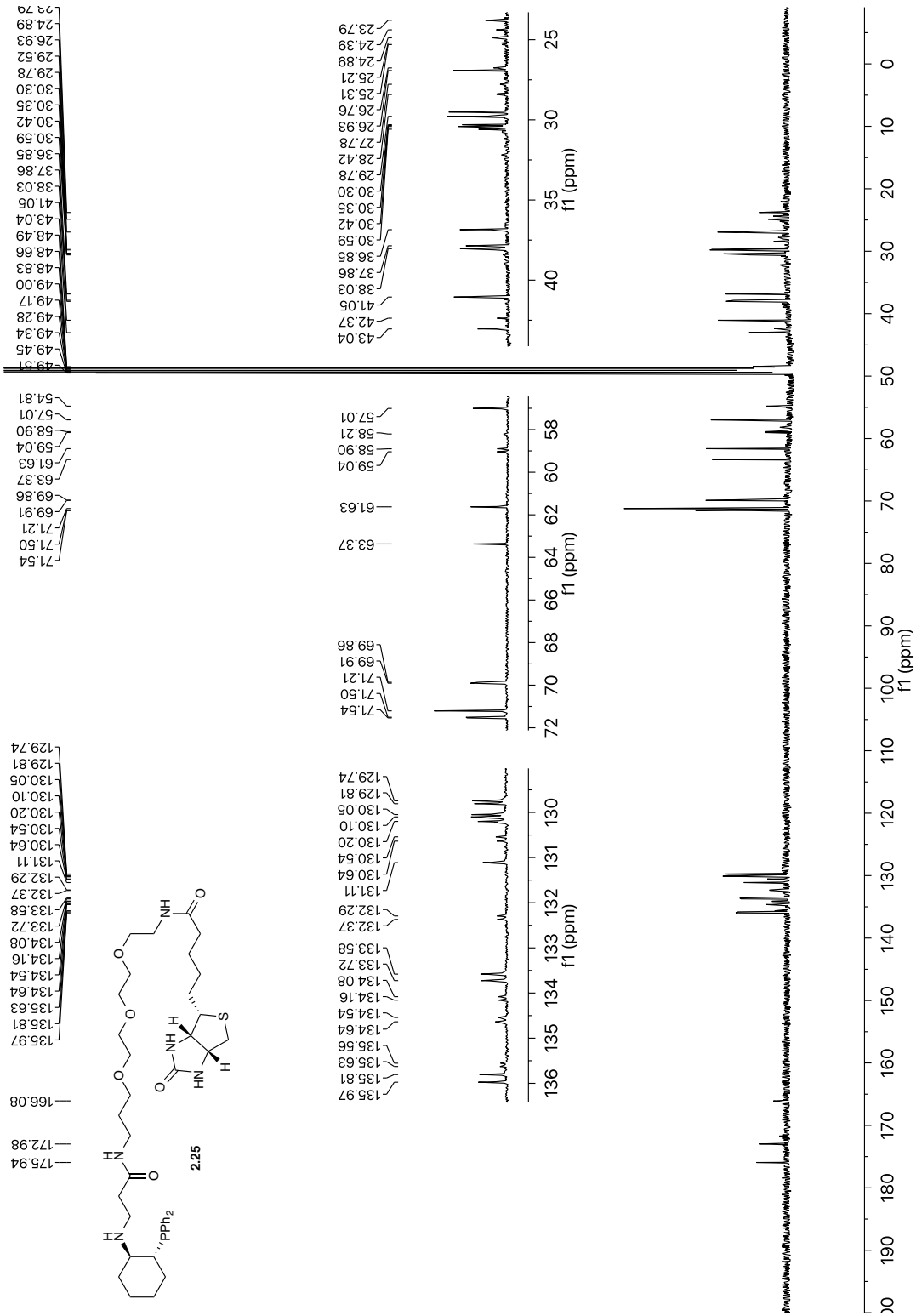




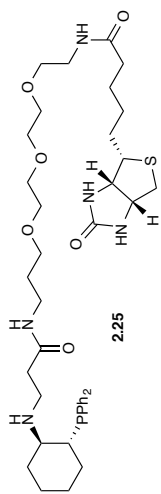




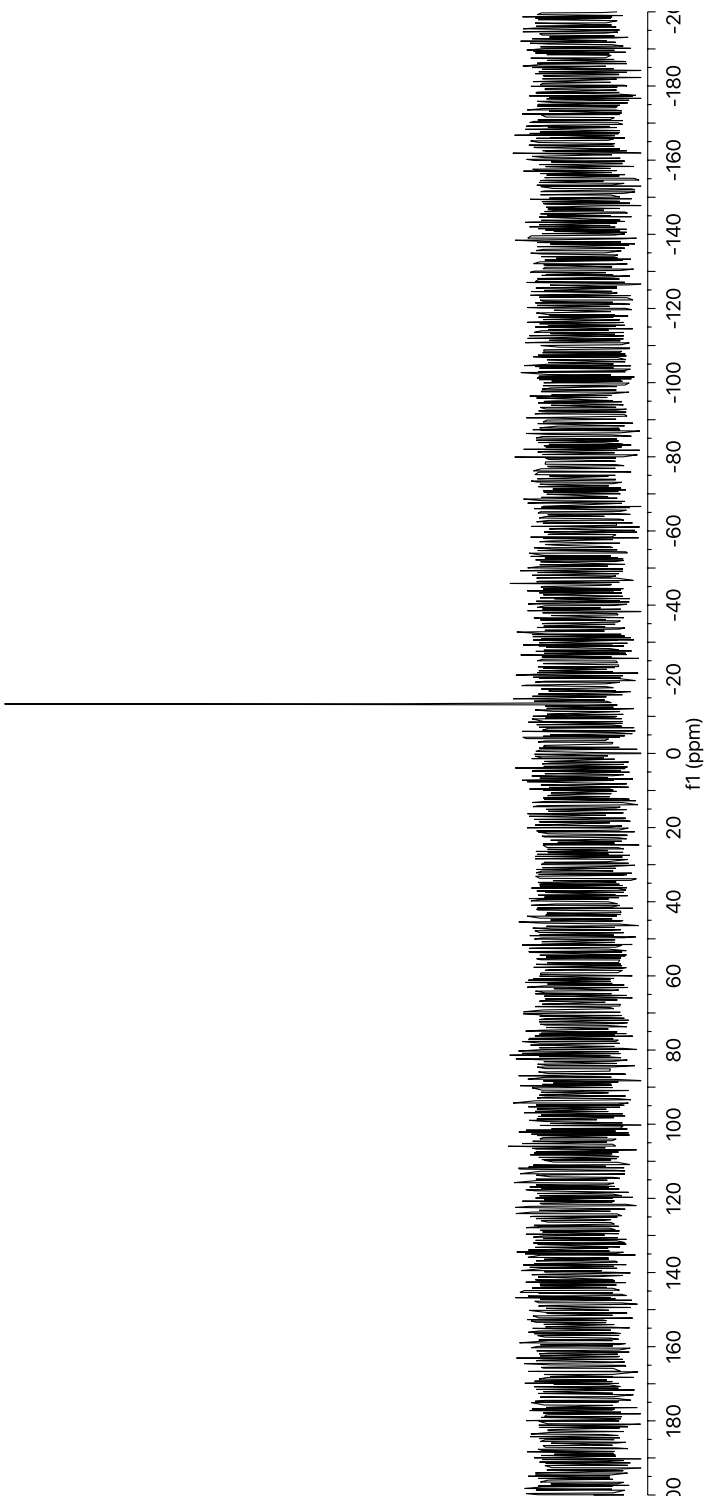


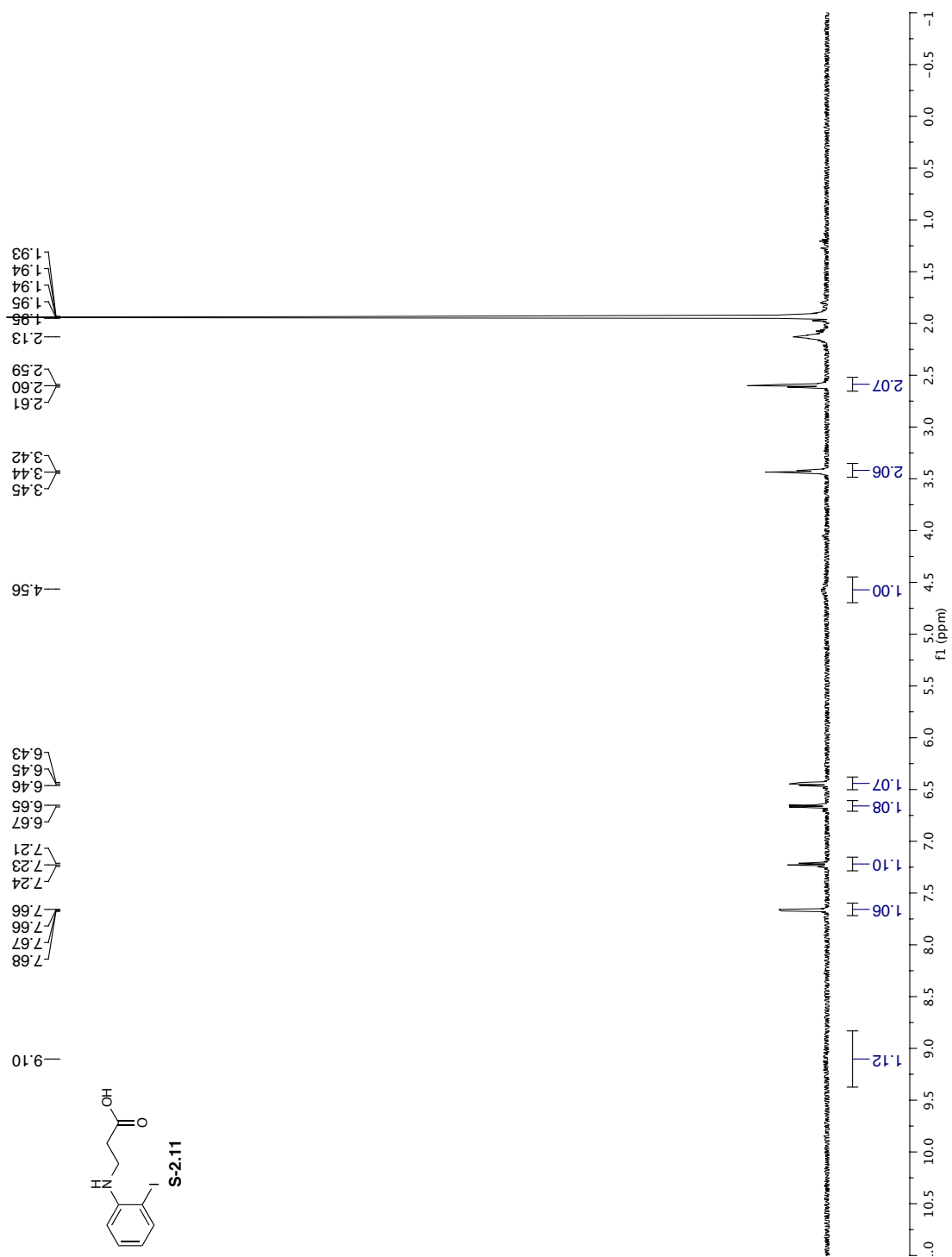


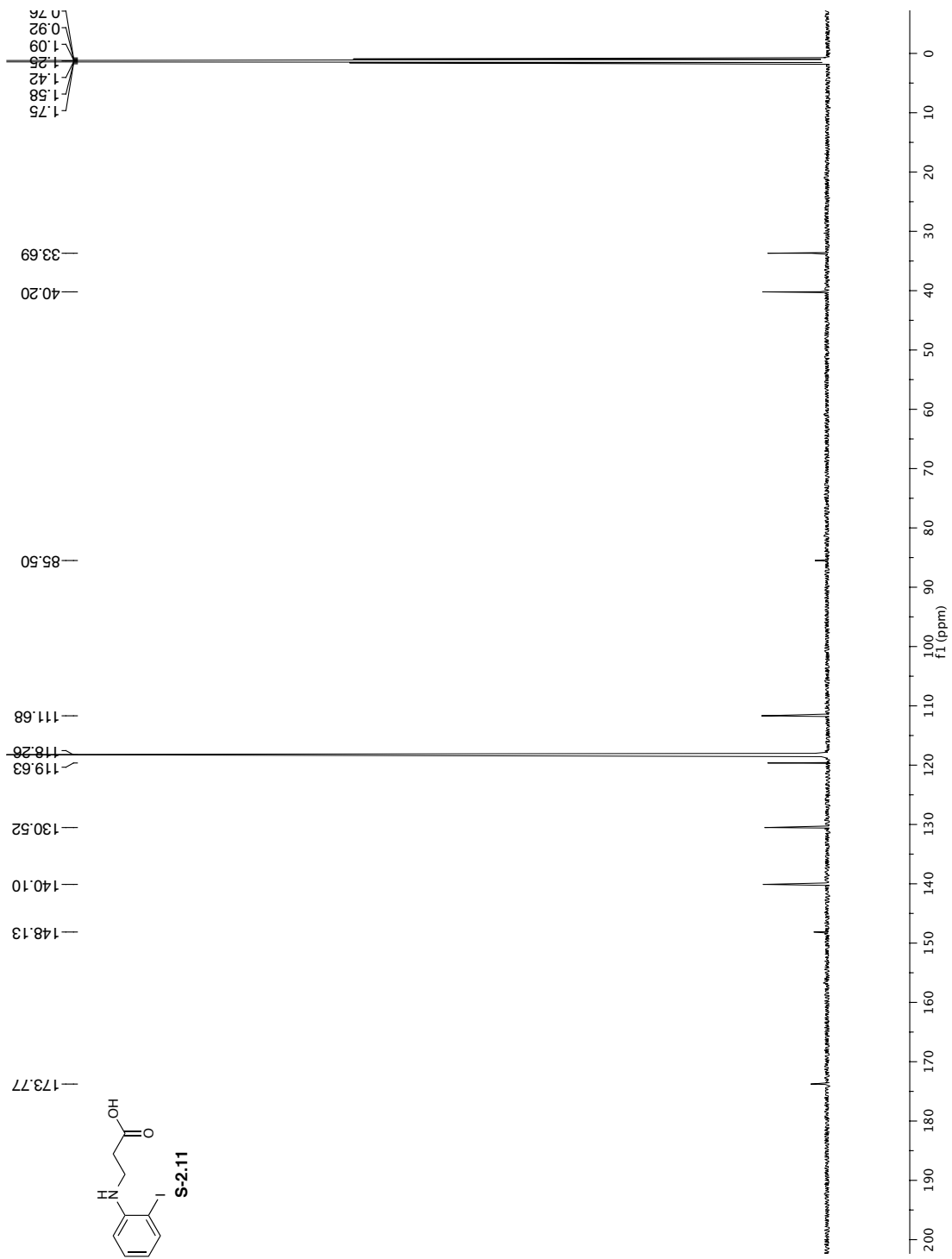


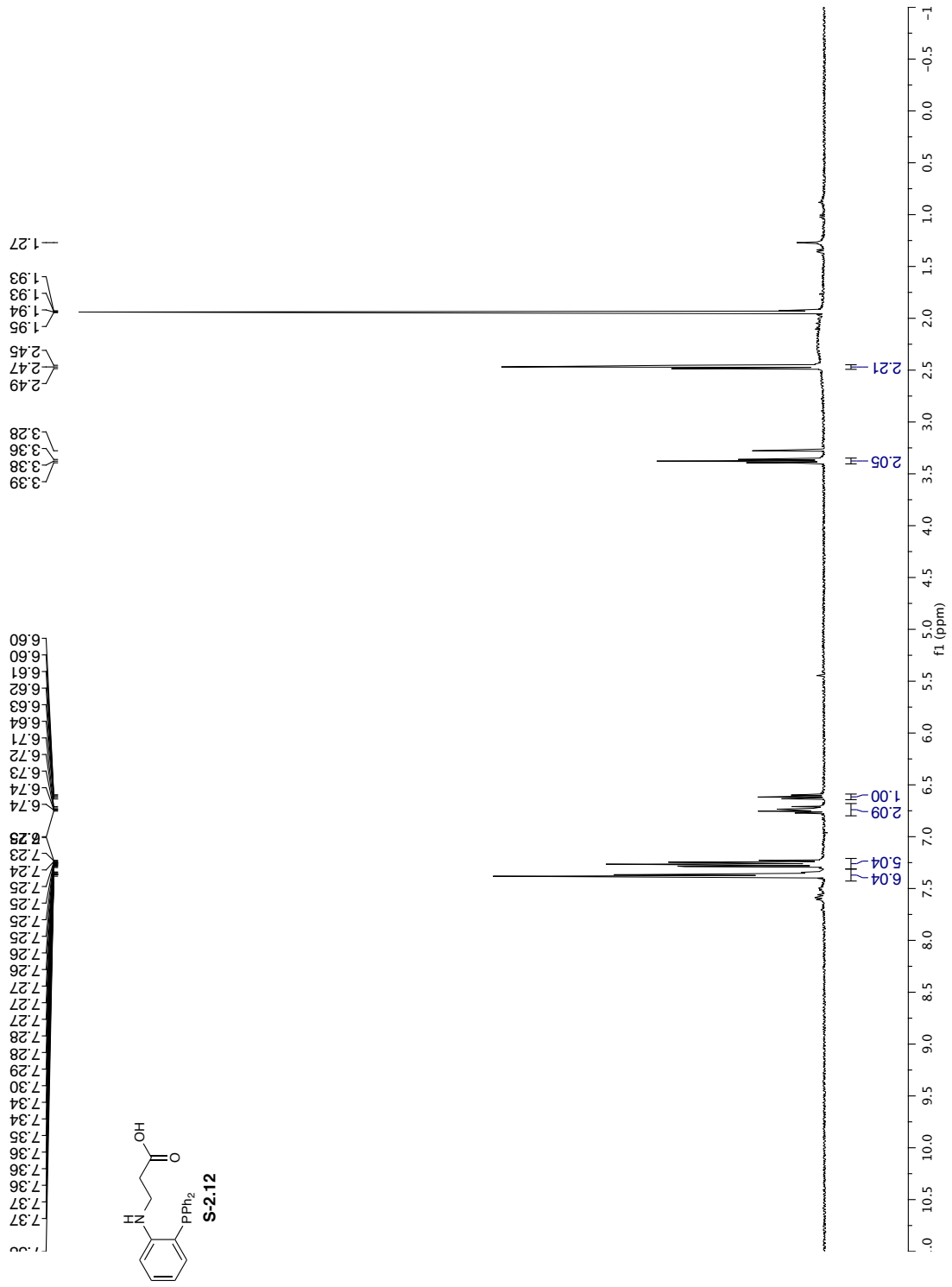


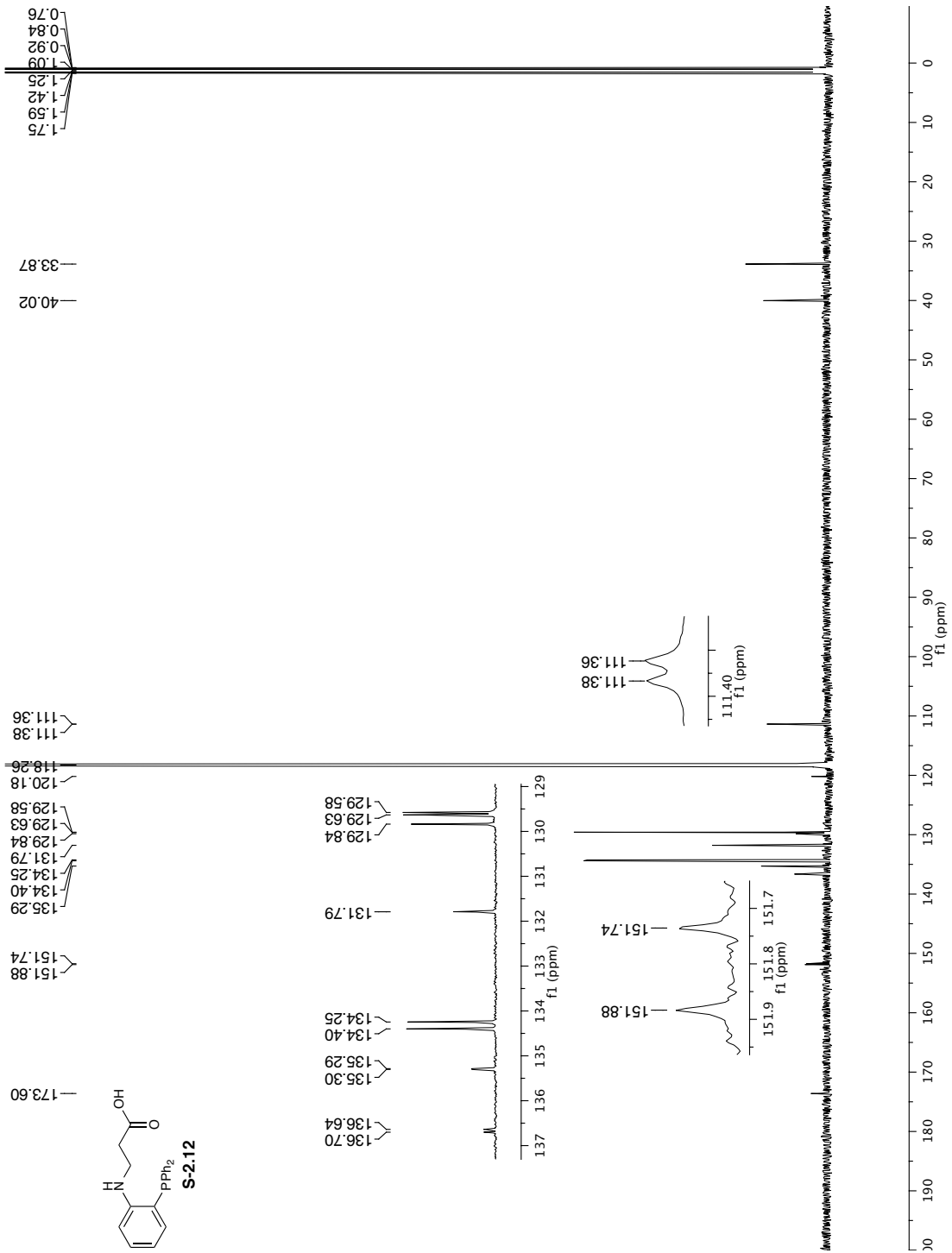
—13.35

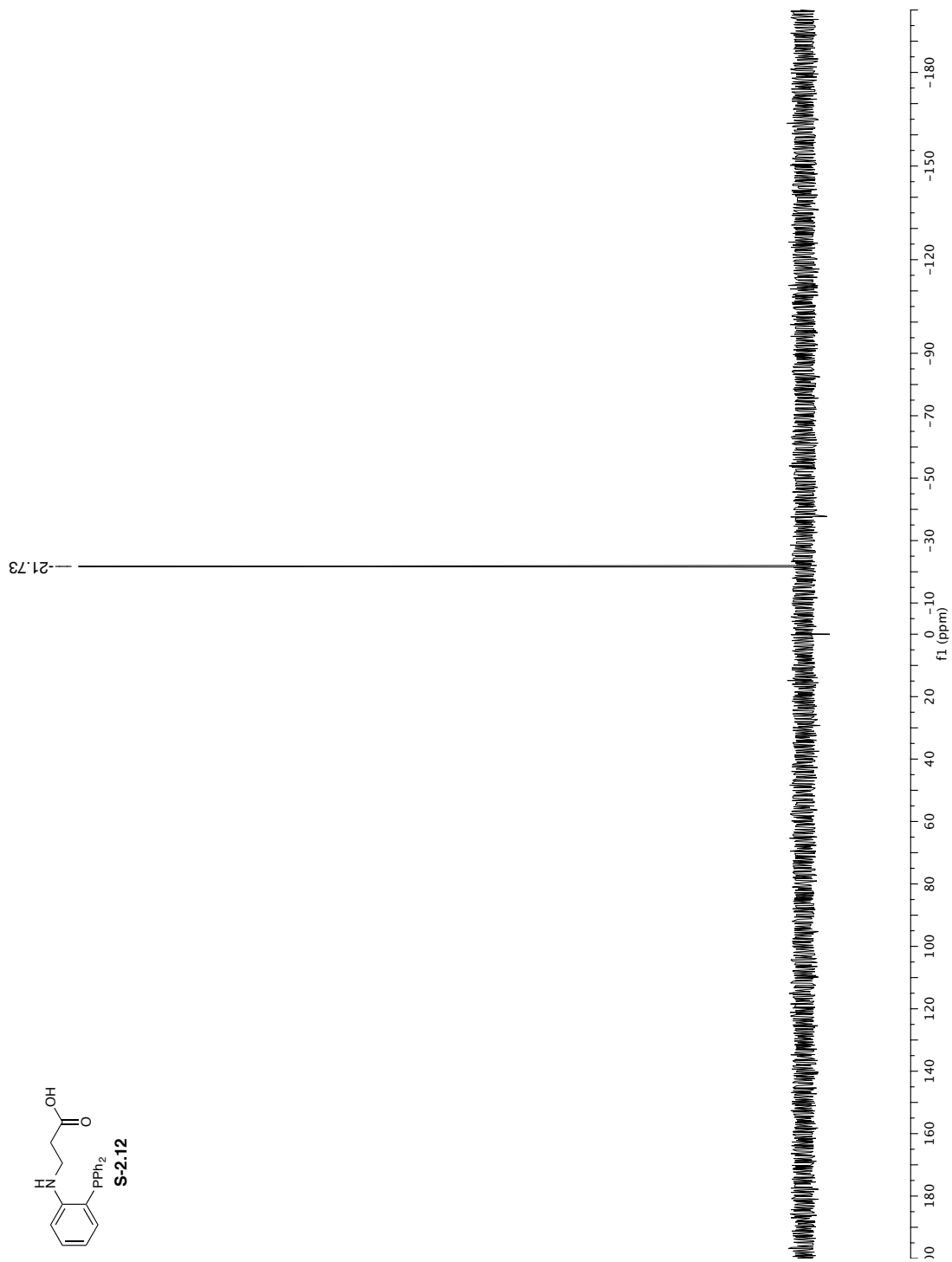
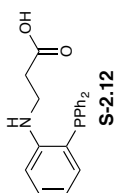










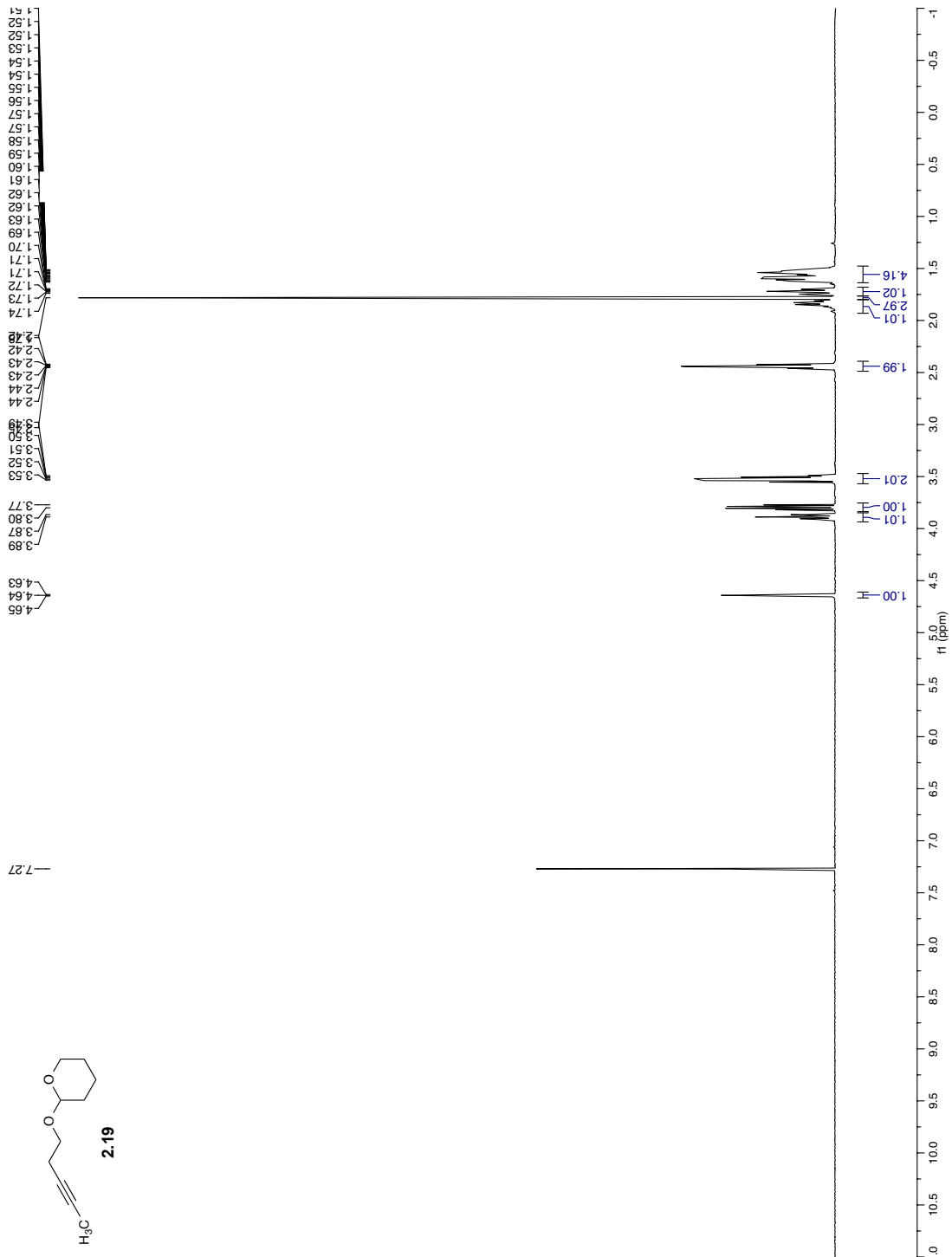


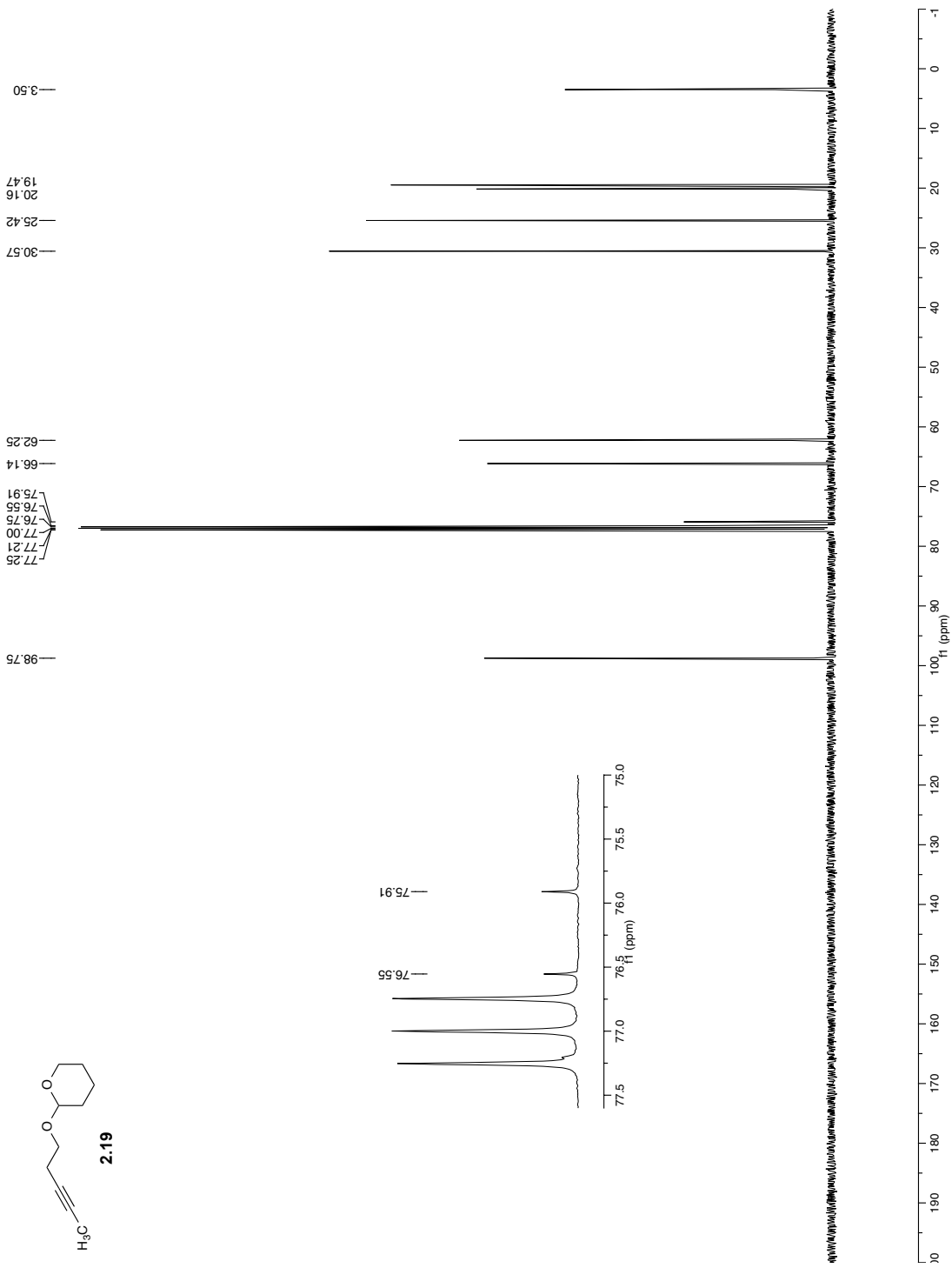


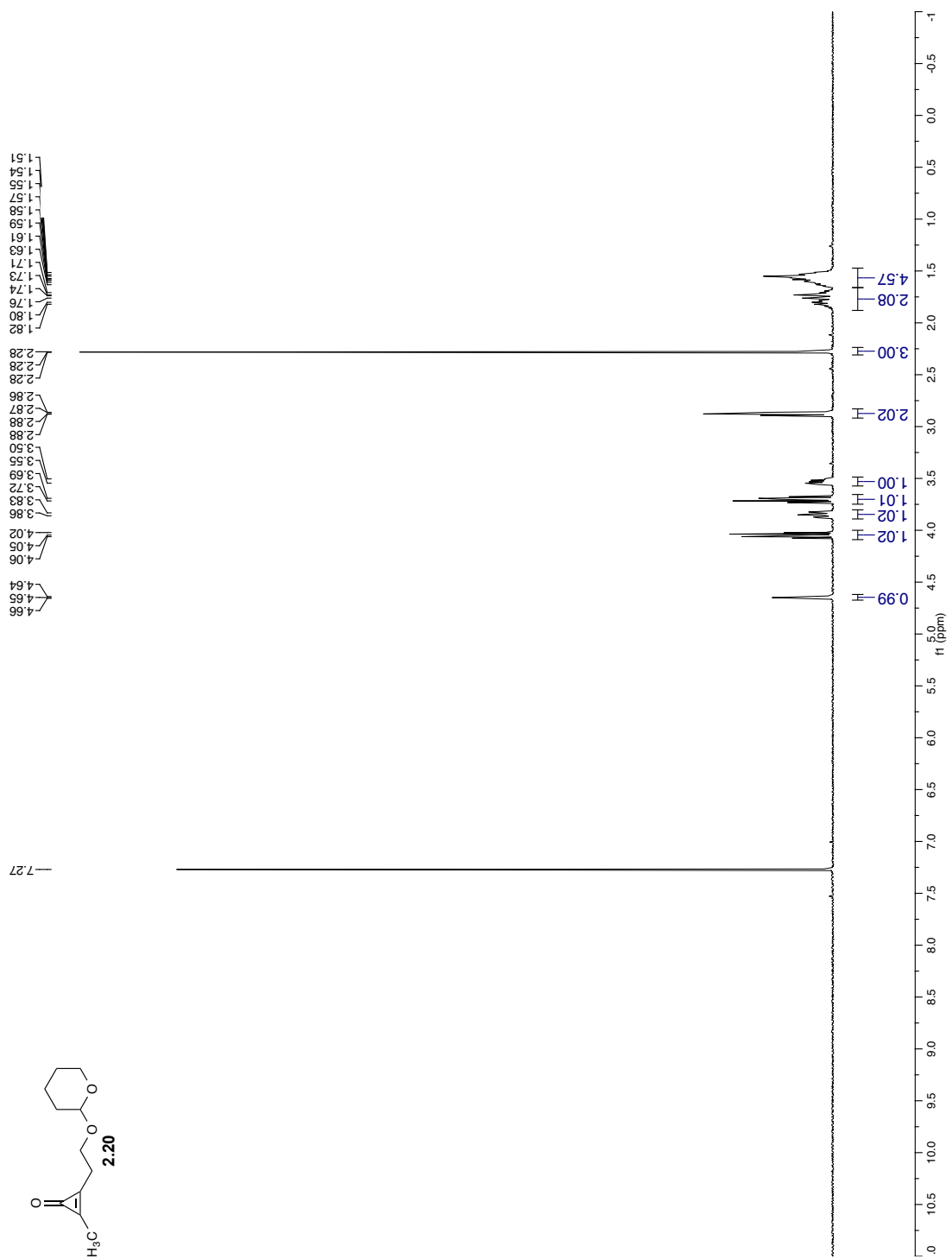


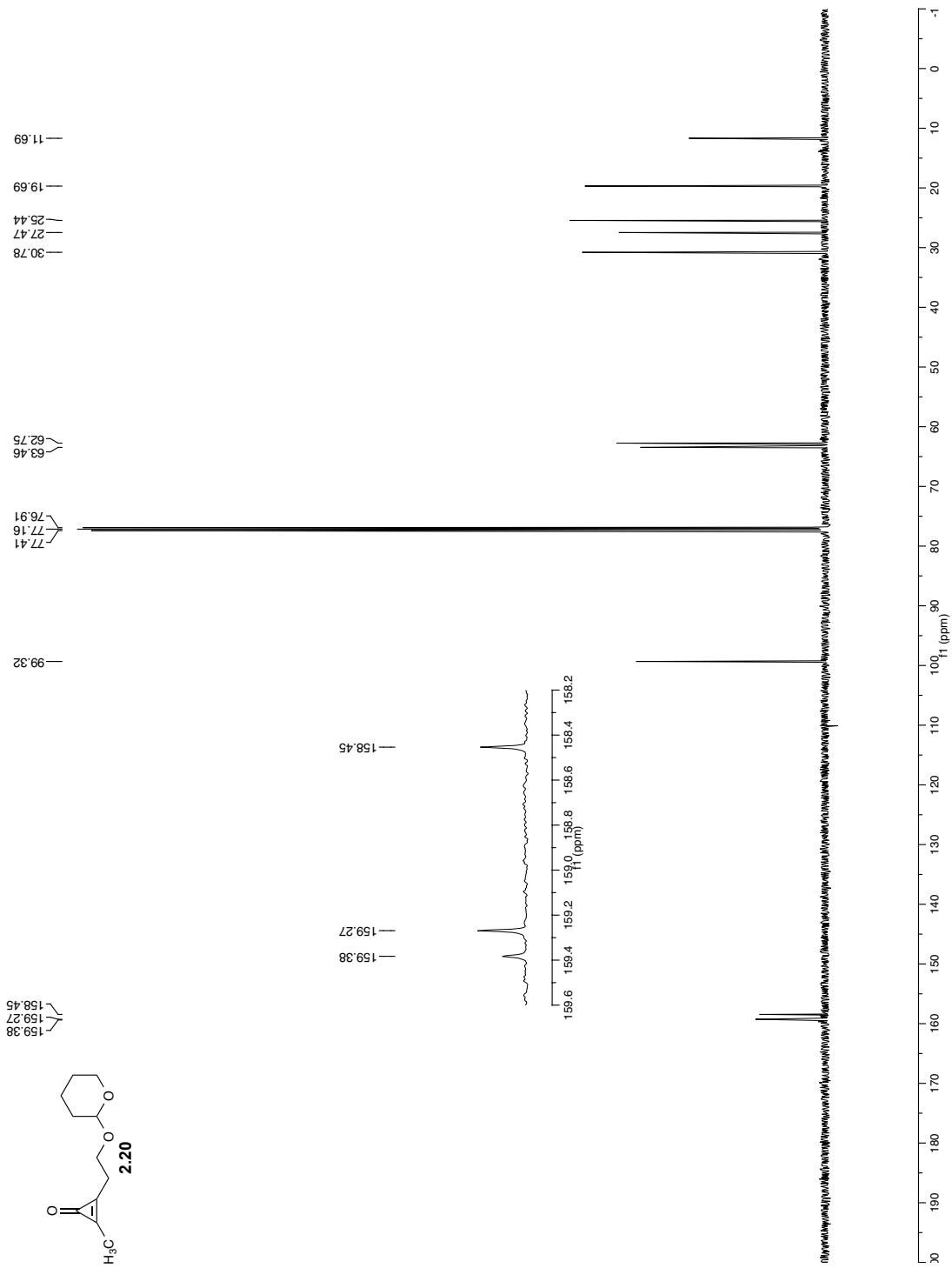


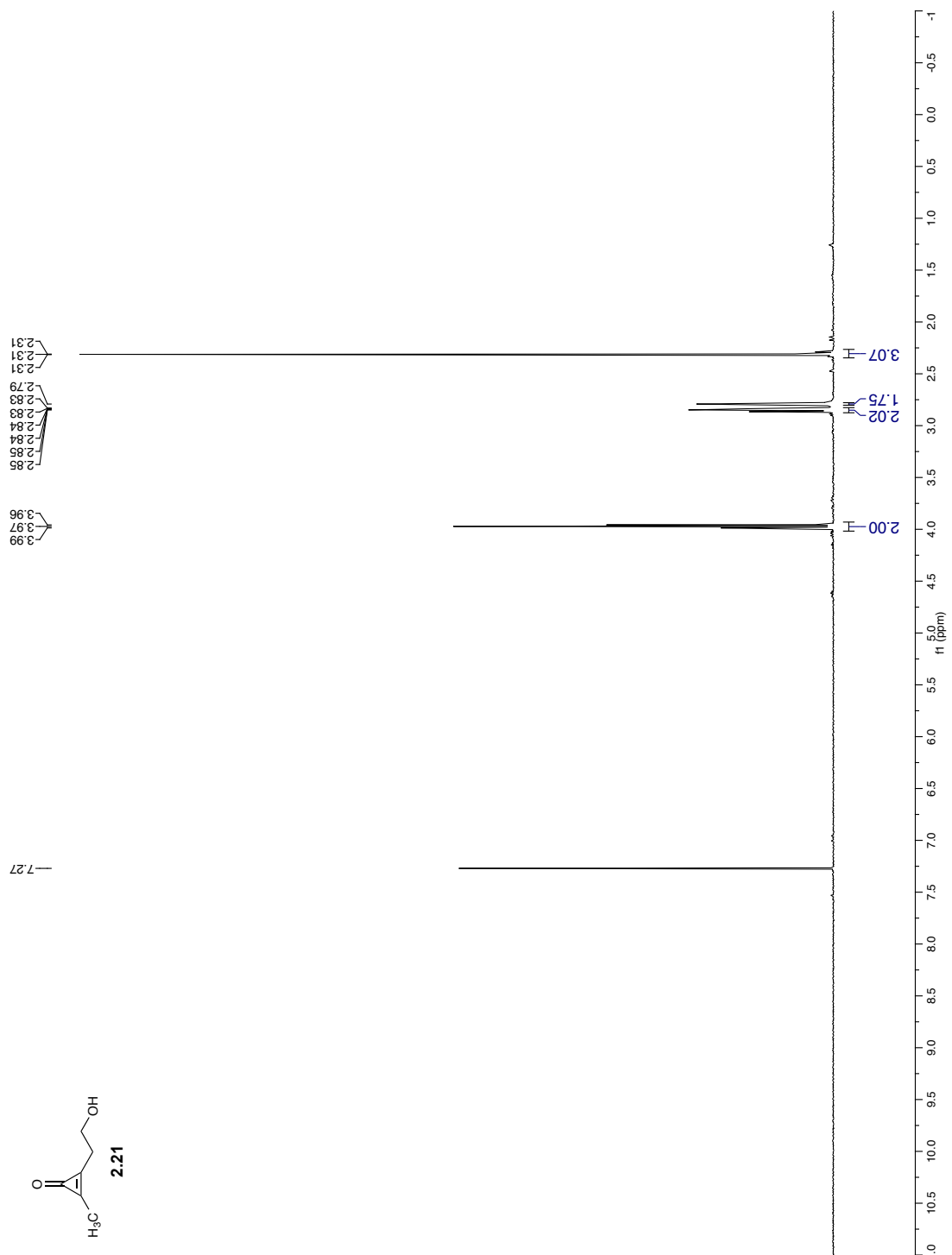


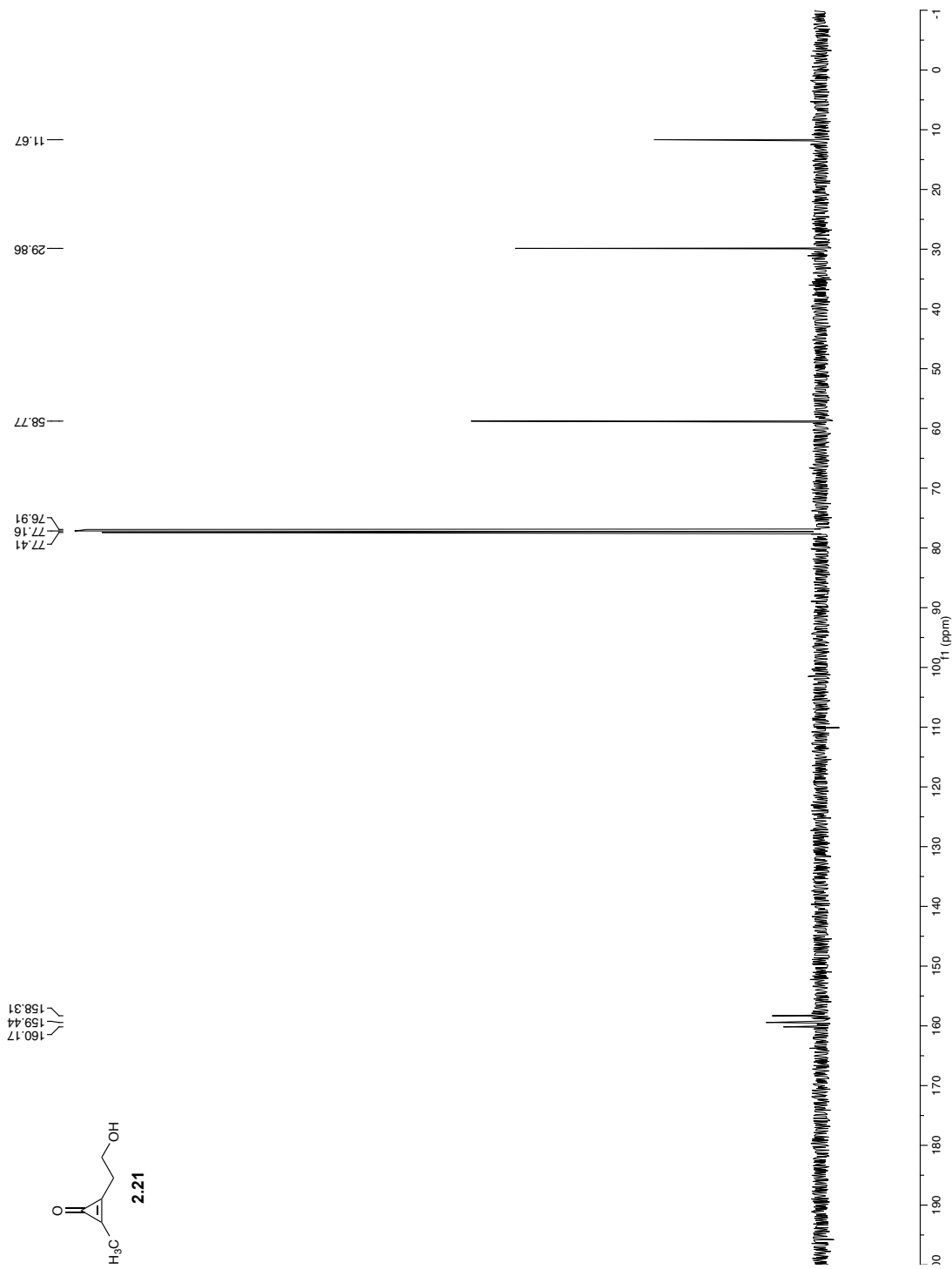


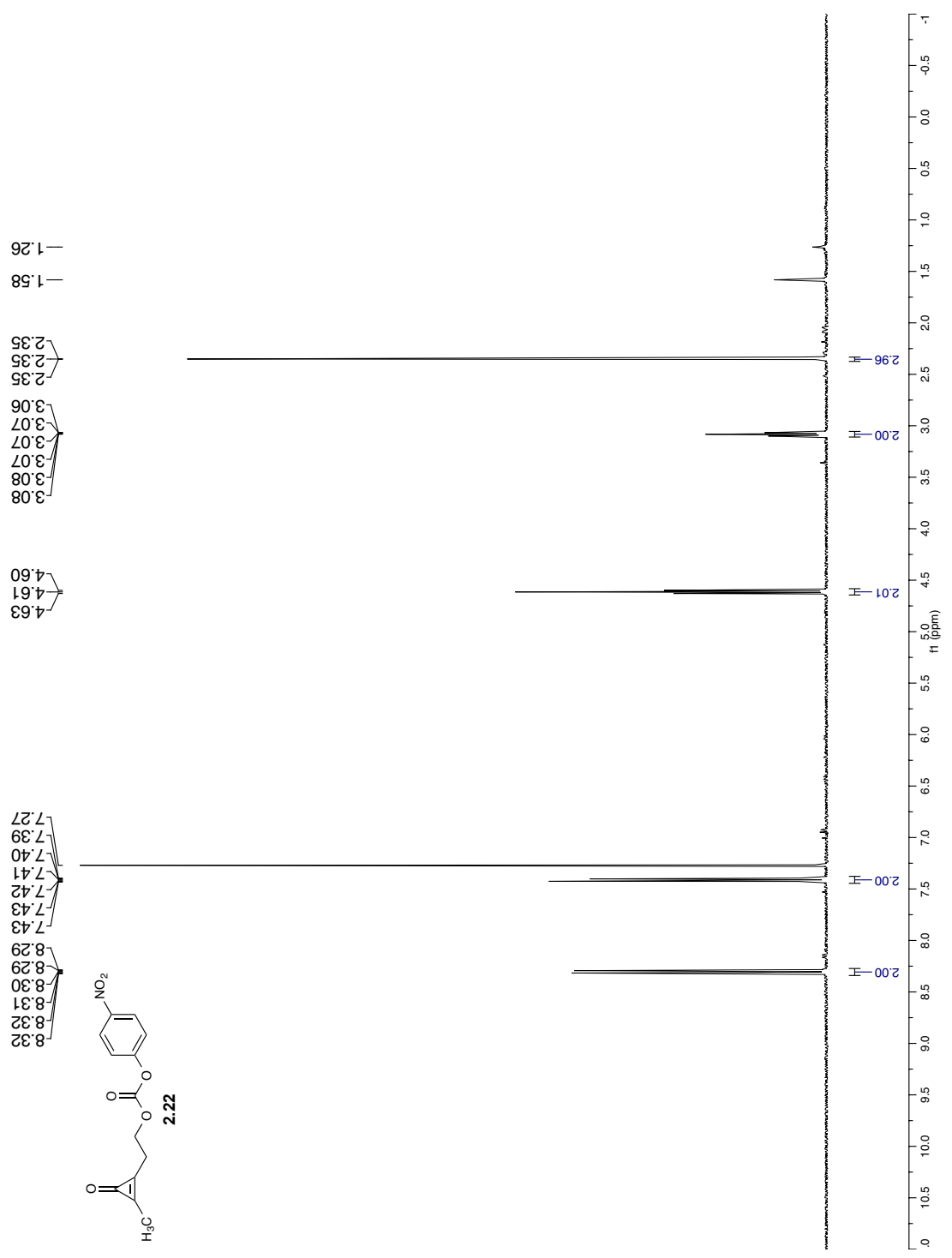




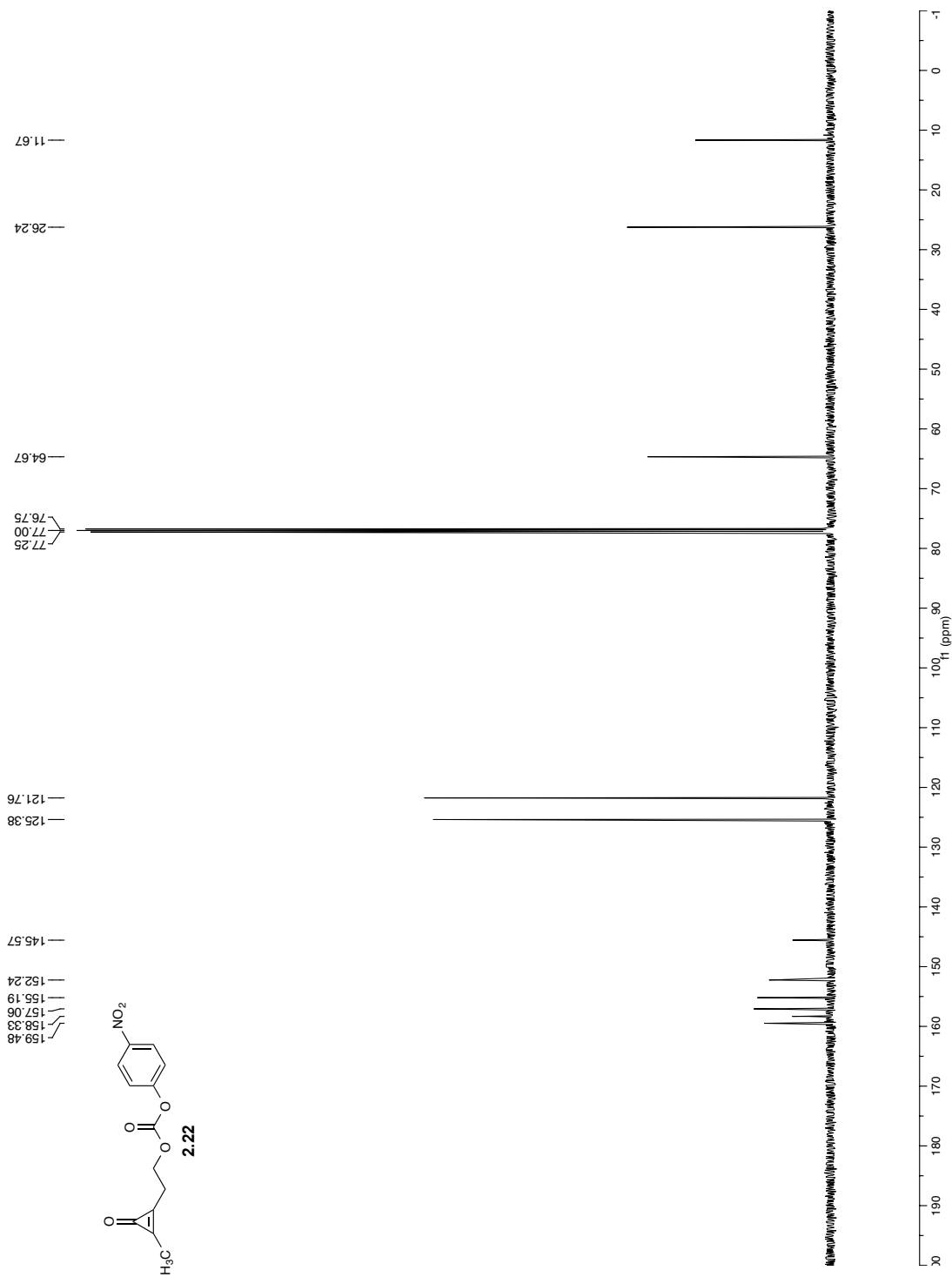




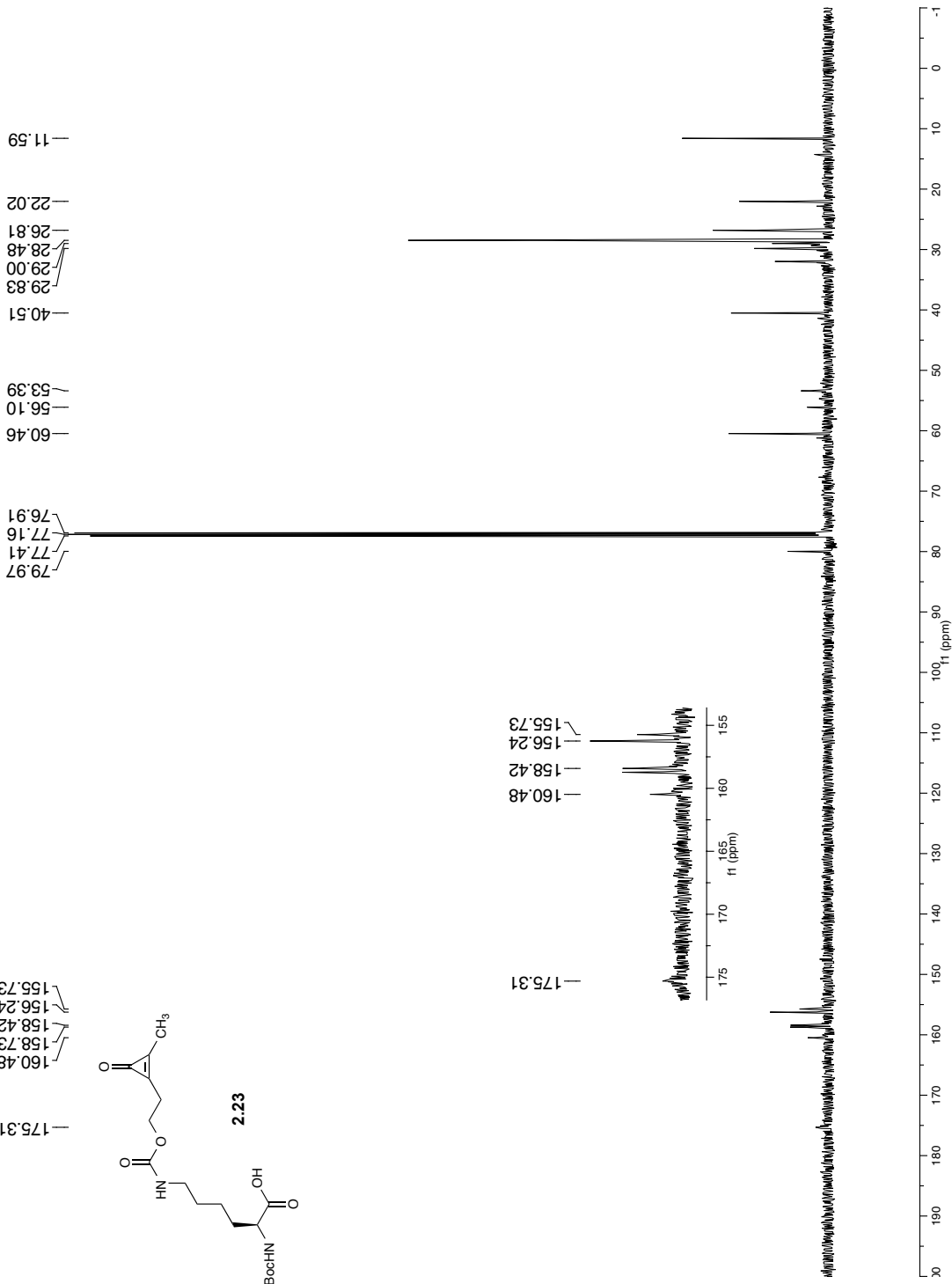


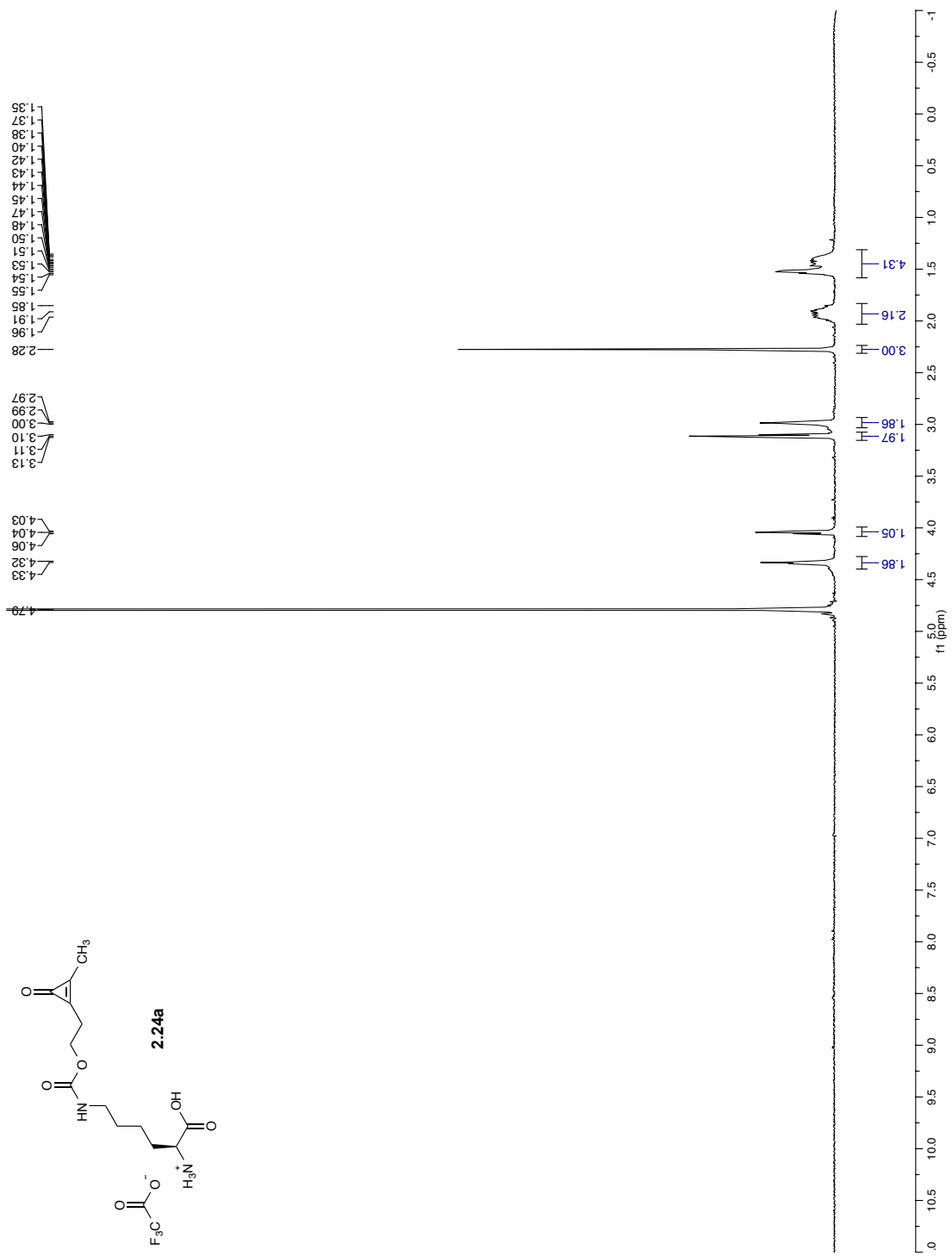


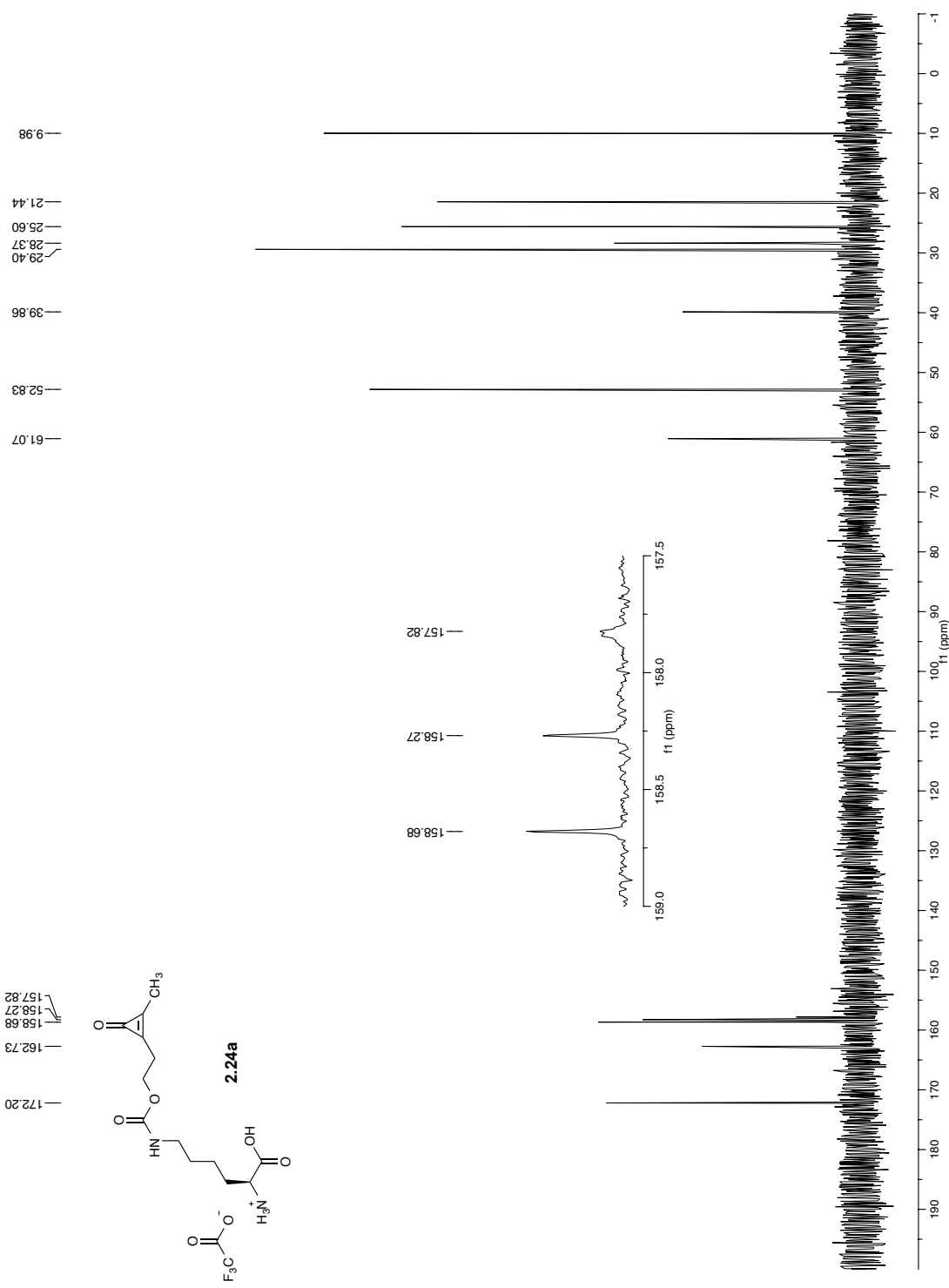


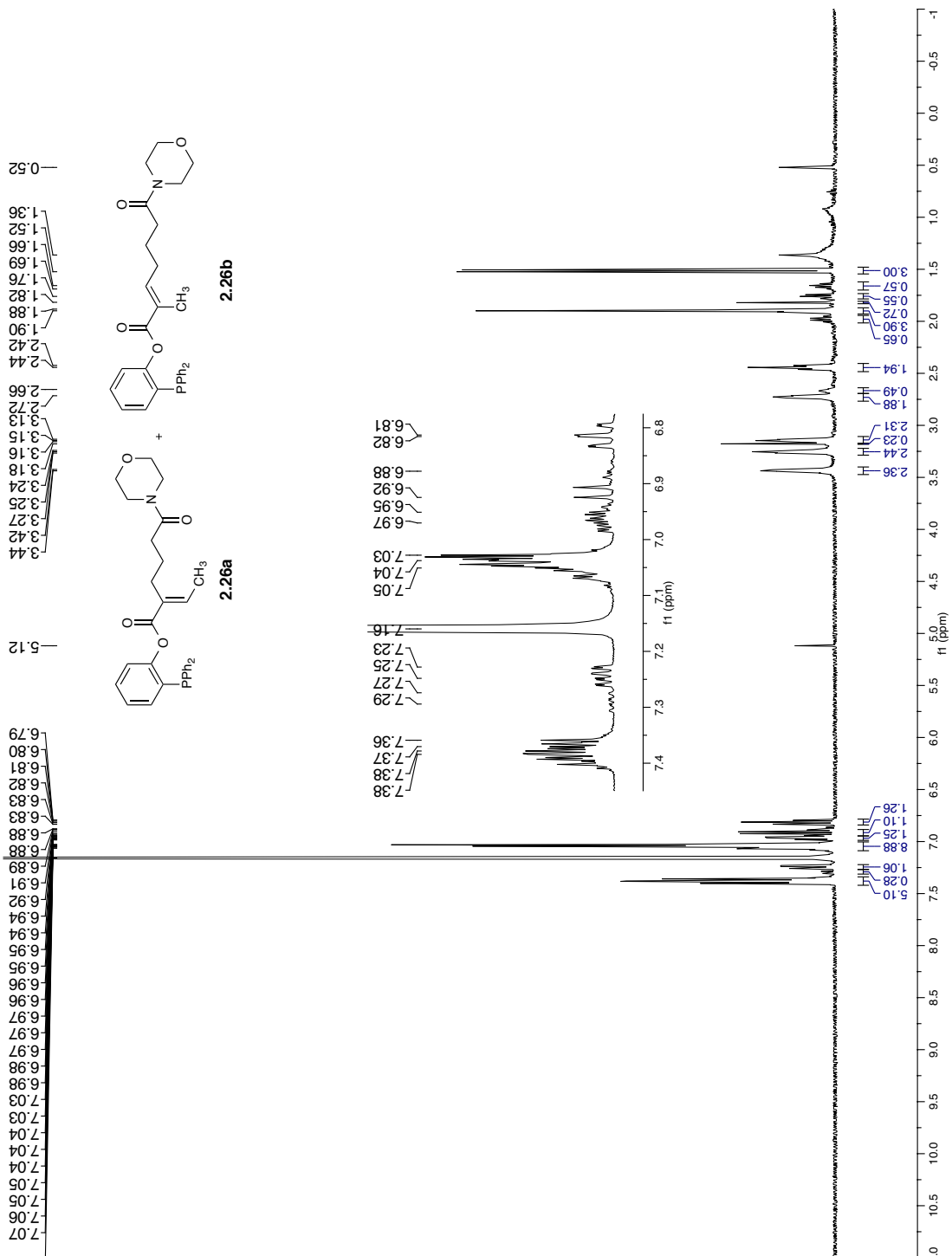


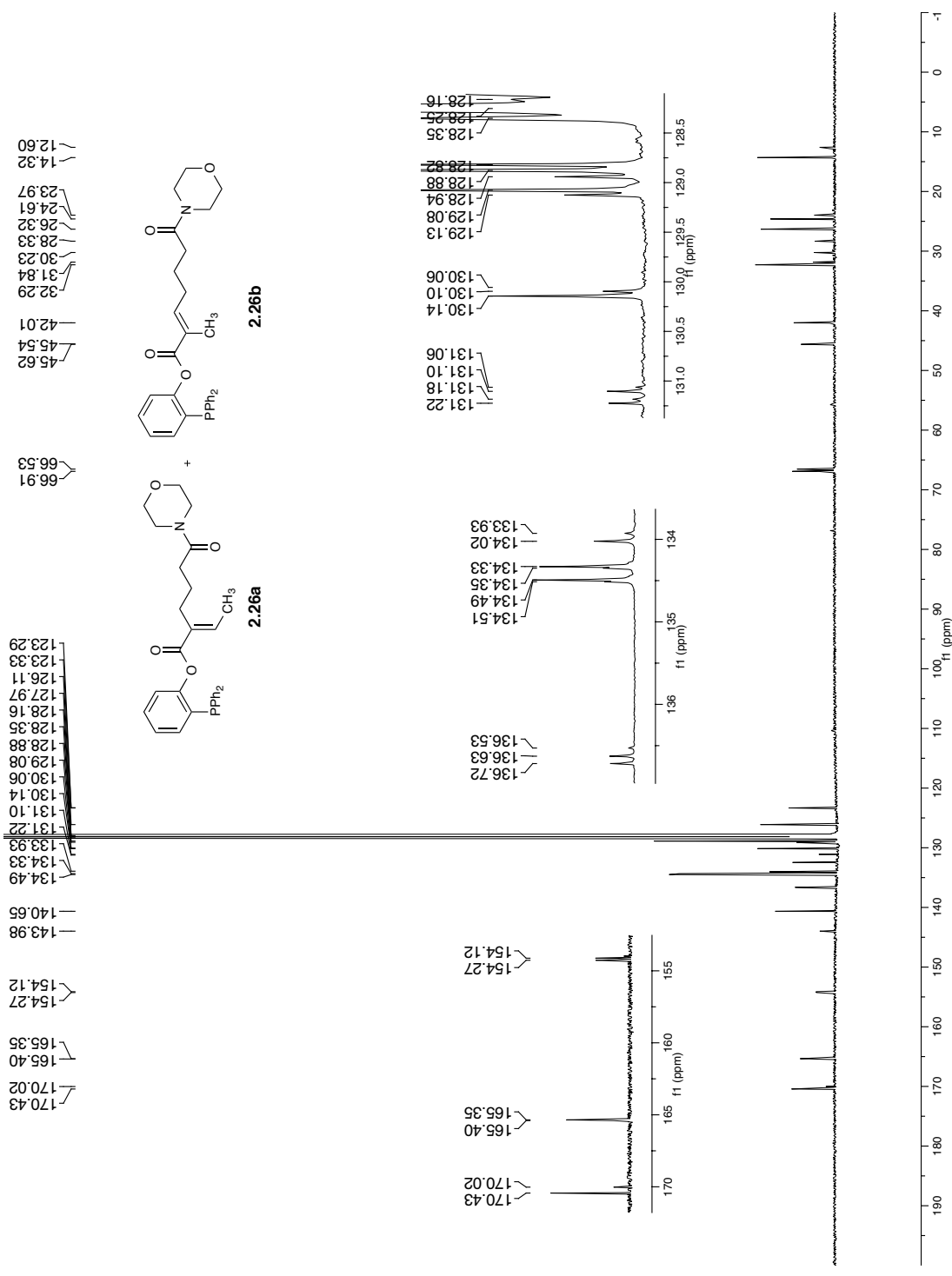




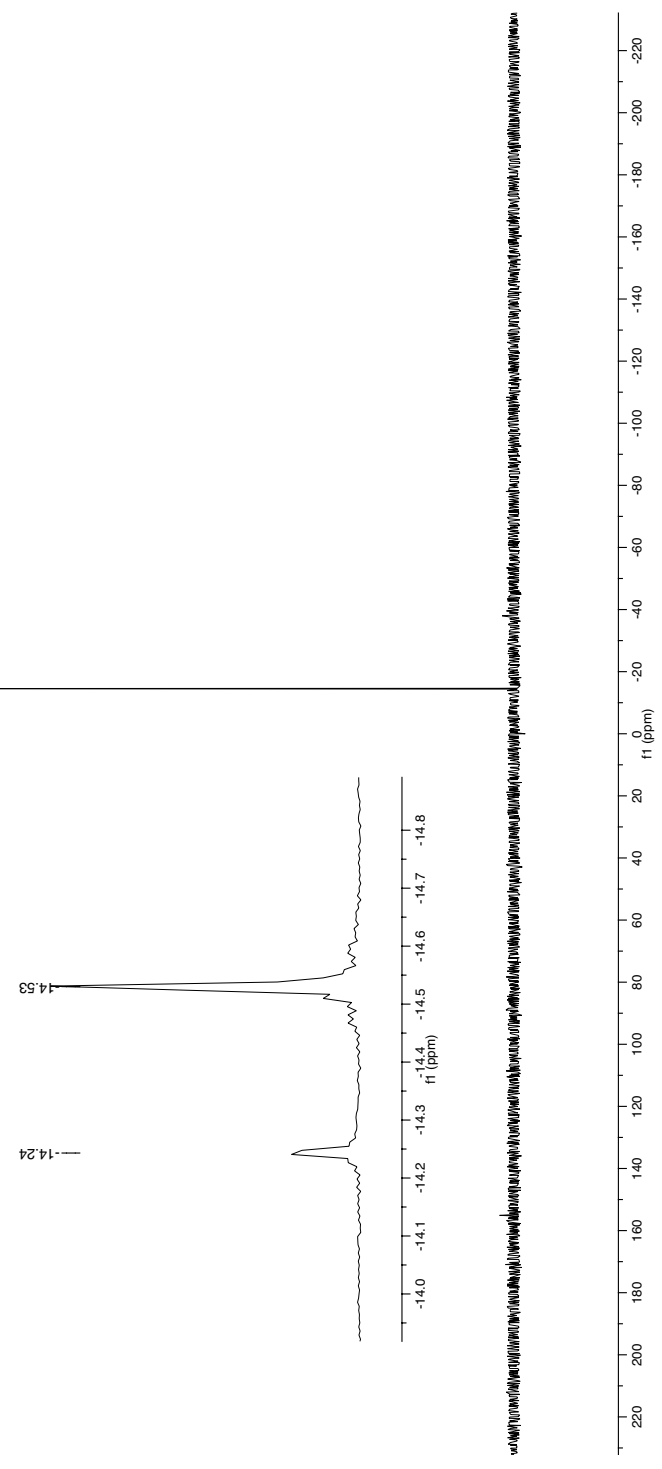
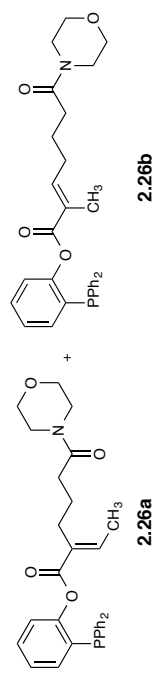




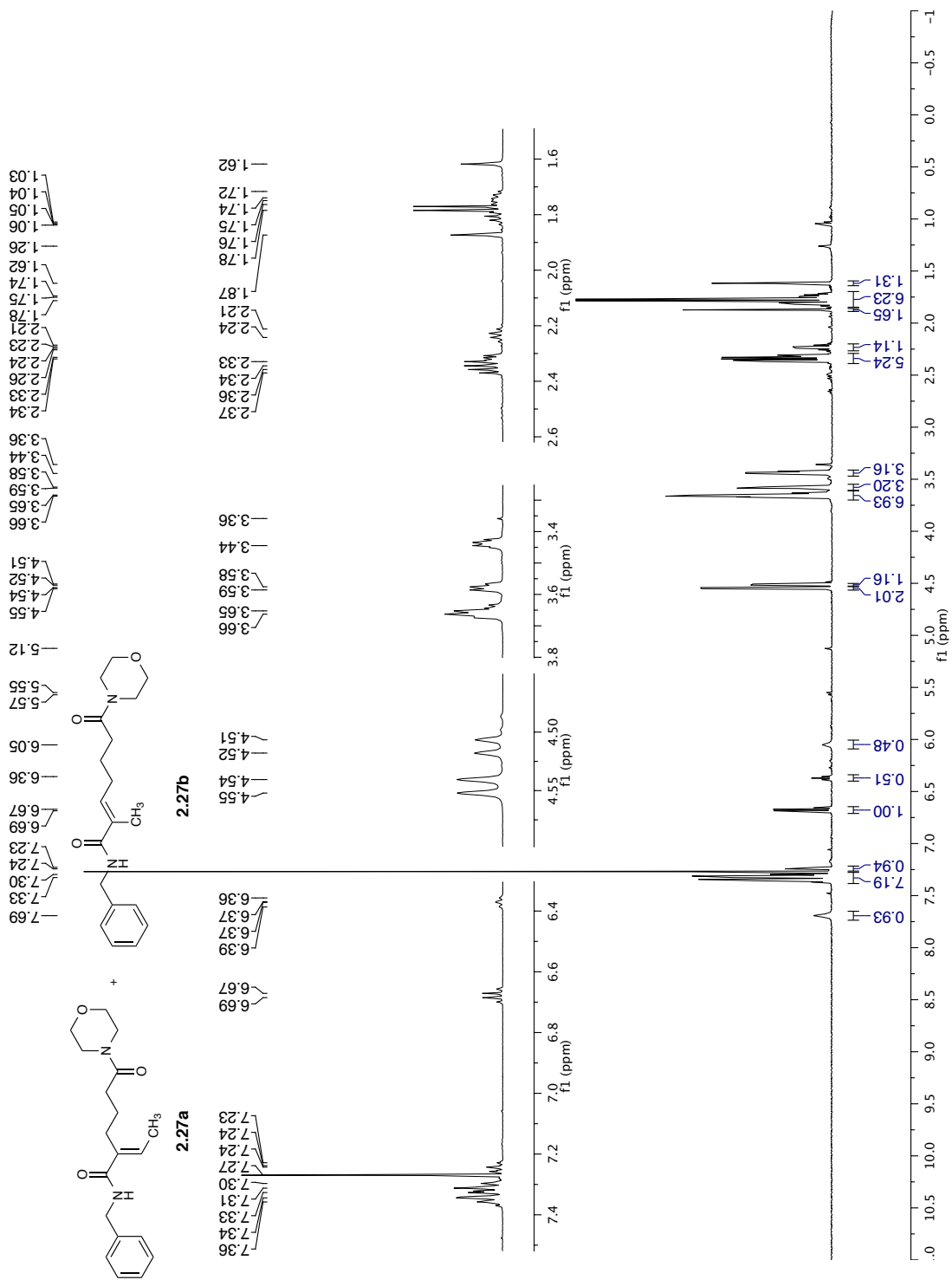


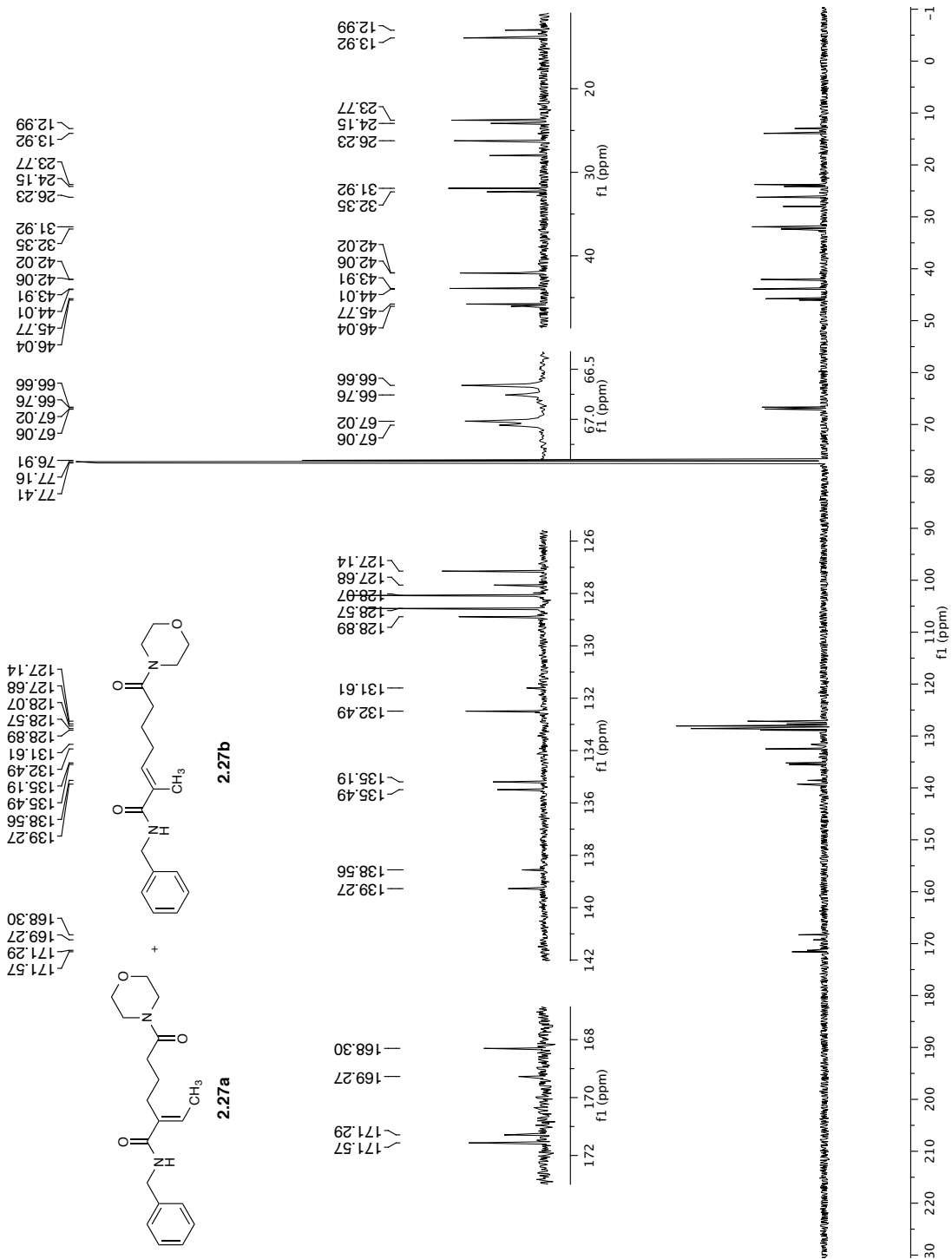


-14.24  
-14.53









## **APPENDIX B: NMR Spectra for Chapters 3 and 4**

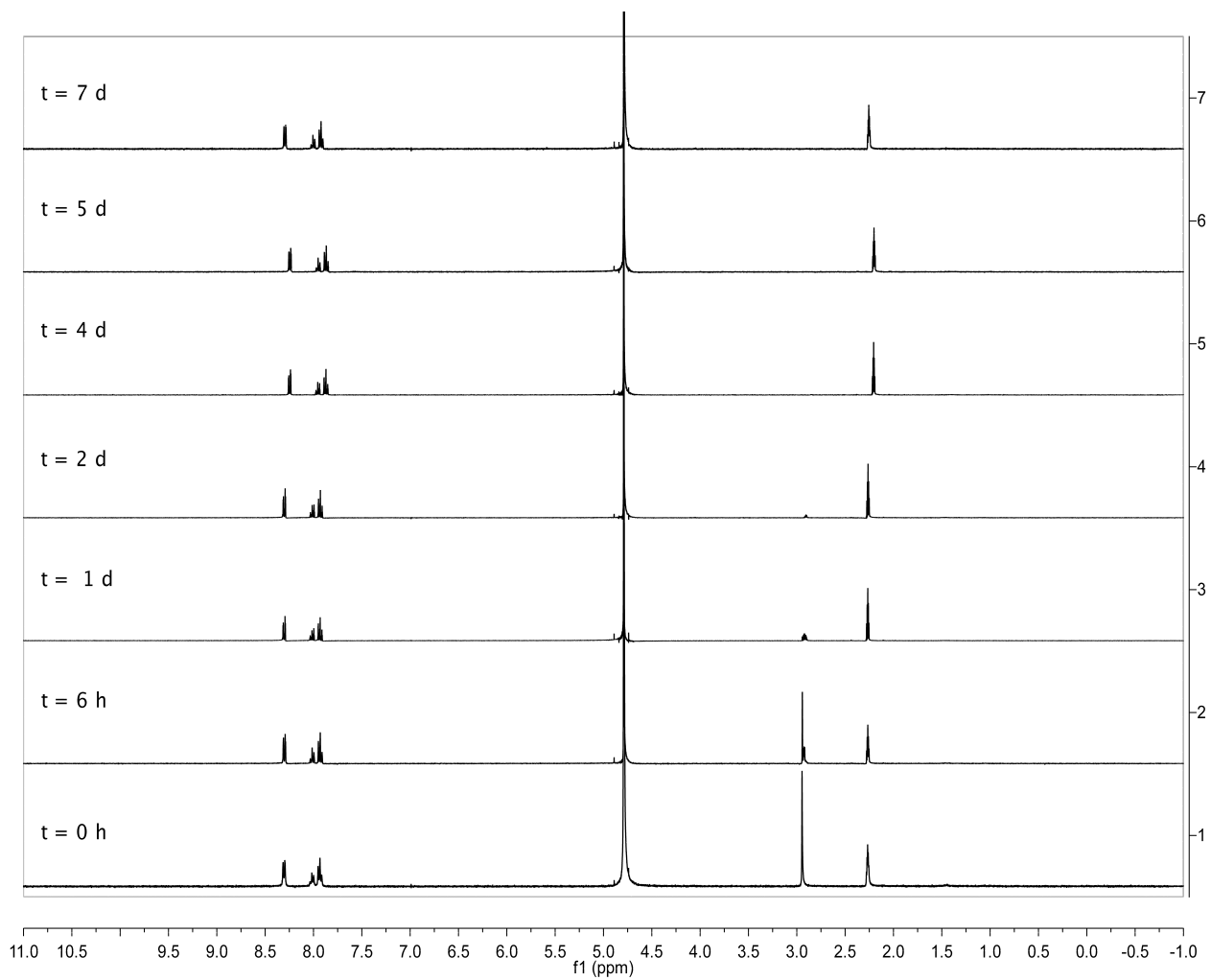
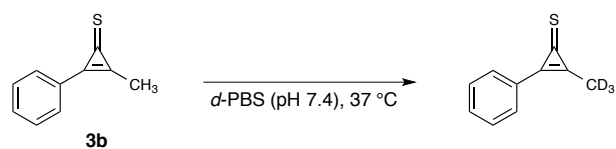


**Figure S3-1.** Cyclopropenethione **3.3b** is stable in *d*-PBS. Compound **3.3b** (10 mM) was incubated in *d*-PBS (50 mM, pH 7.4) at 37 °C and monitored via <sup>1</sup>H NMR spectroscopy.  
 \*Allylic protons exchanged with deuterium.

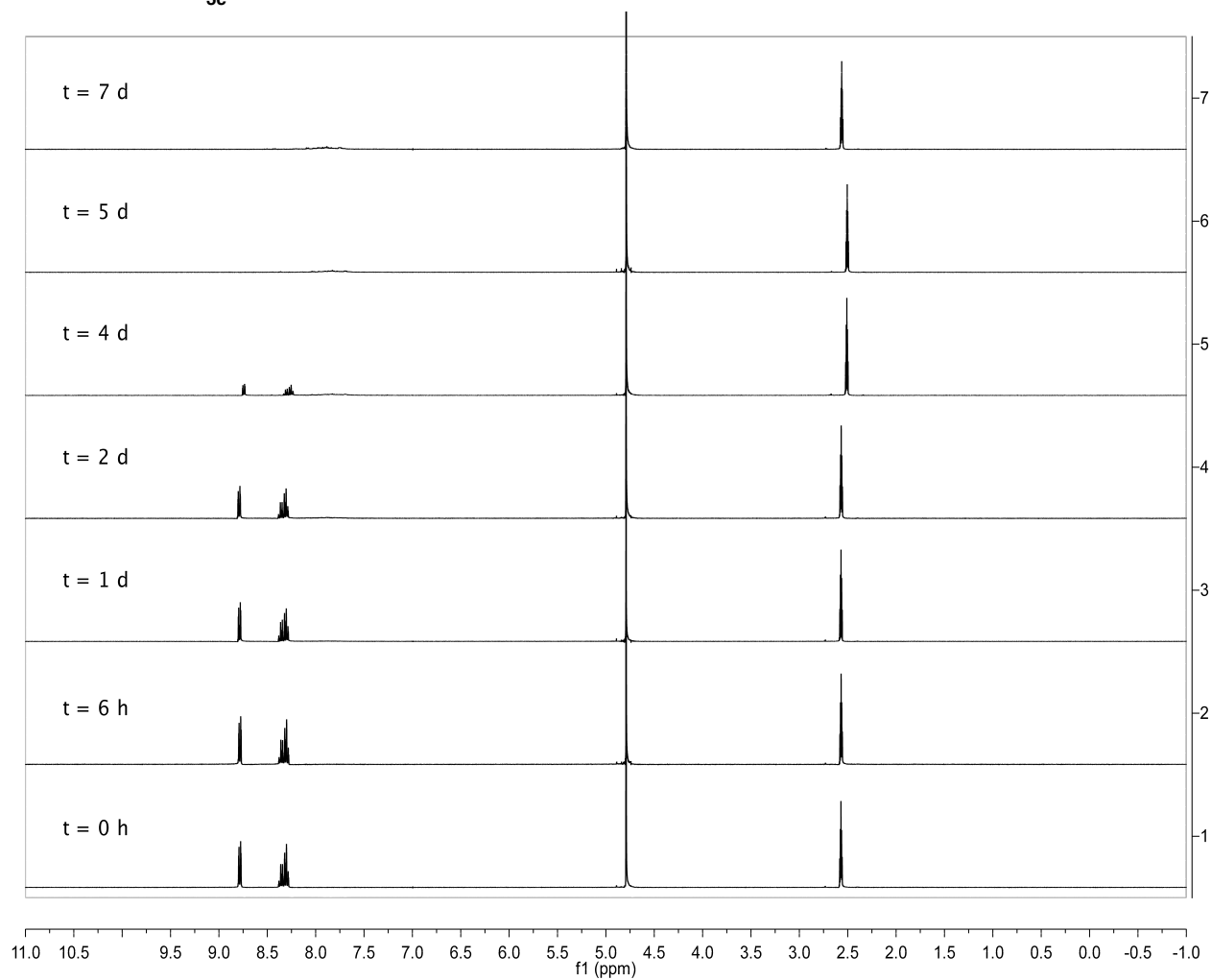
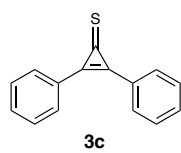


**Figure S3-2.** Cyclopropenethione **3.3c** is stable for ~24 h in *d*-PBS. Compound **3.3c** (10 mM) was incubated in *d*-PBS (50 mM, pH 7.4) at 37 °C and monitored via <sup>1</sup>H NMR spectroscopy.

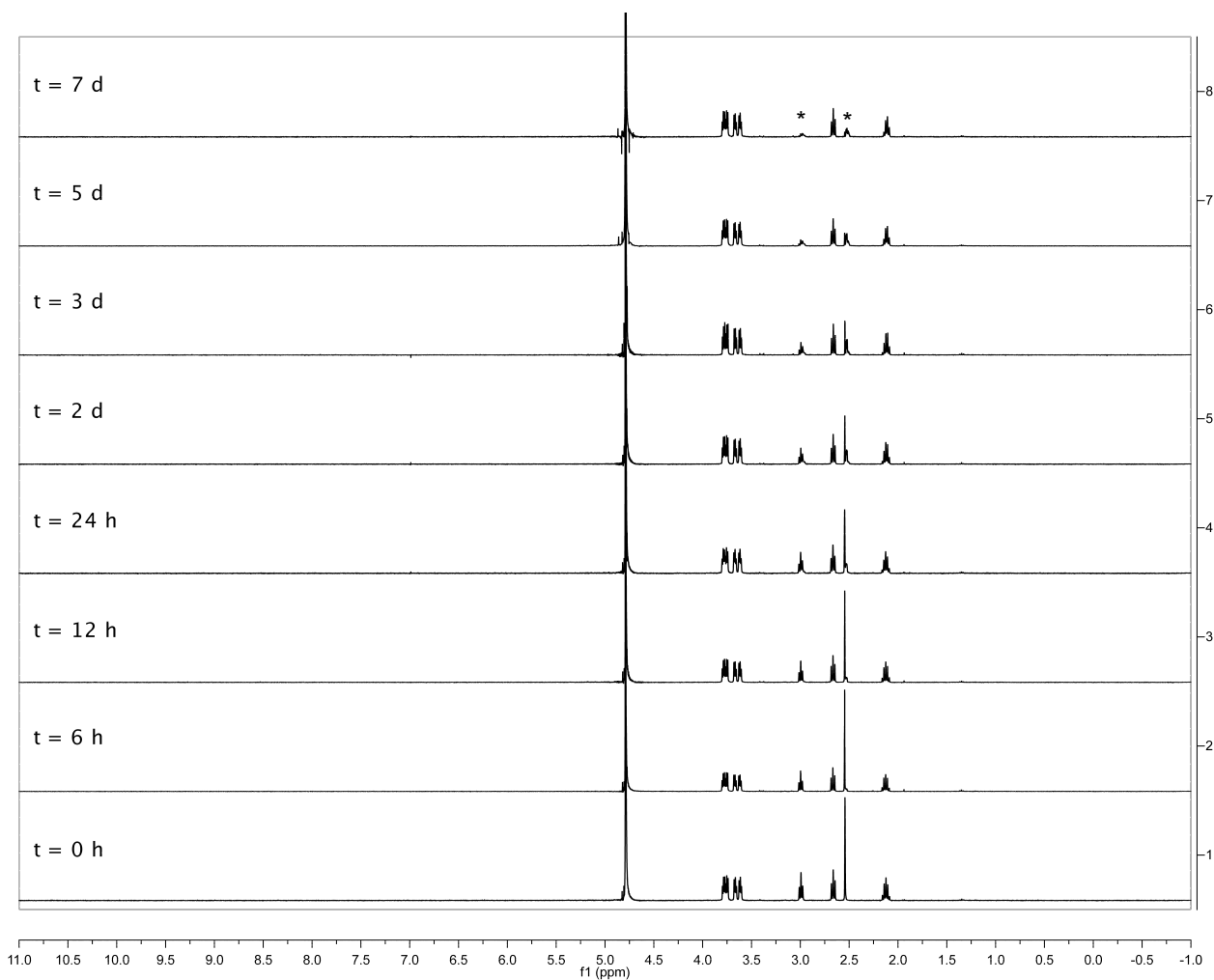
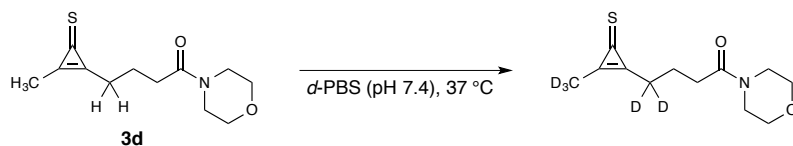


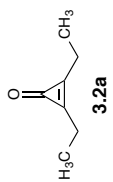
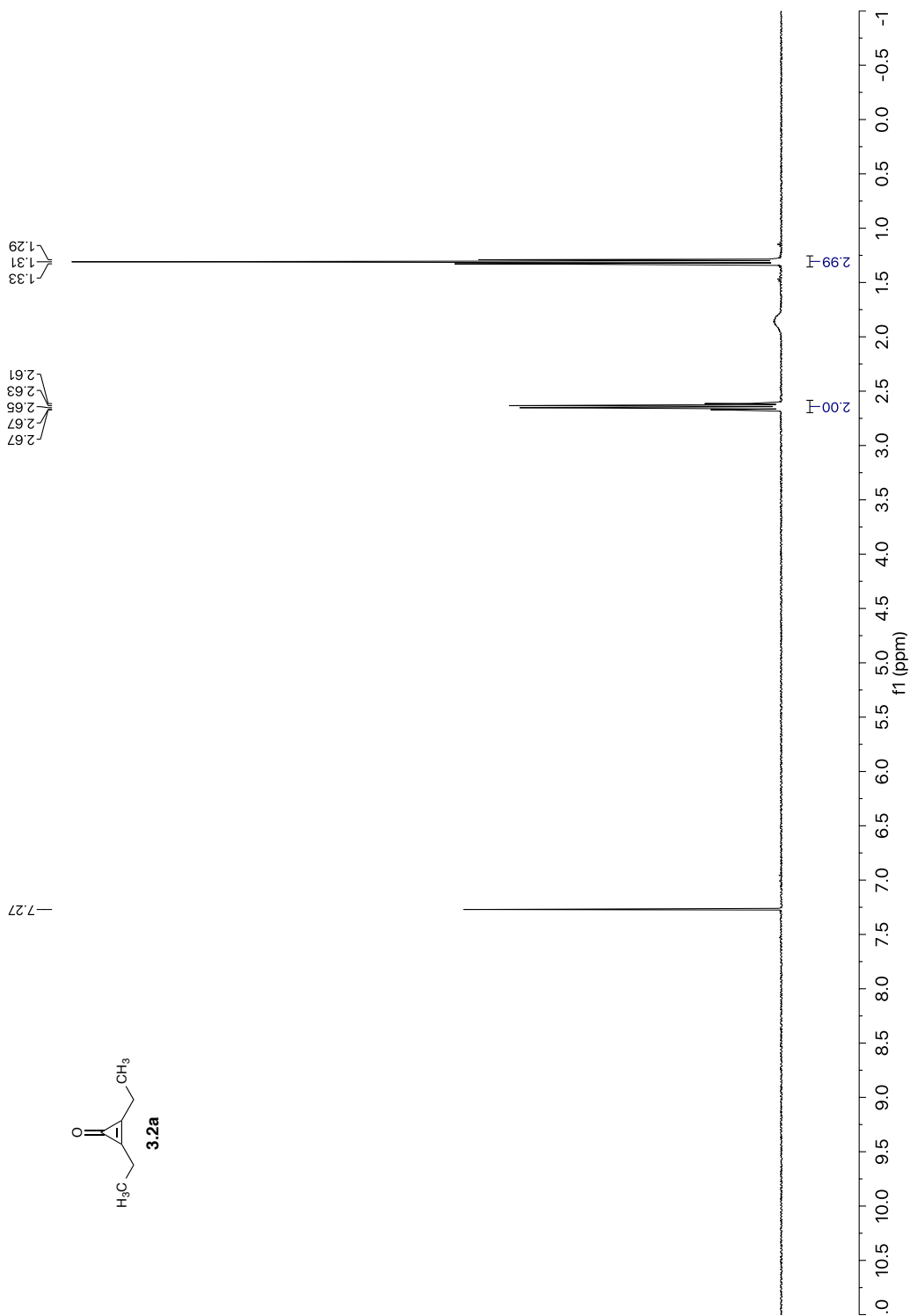
**Figure S3-3.** Cyclopropenethione **3.3d** is stable in *d*-PBS. Compound **3.3d** (10 mM) was incubated in *d*-PBS (pH 7.4) at 37 °C and monitored via <sup>1</sup>H NMR spectroscopy over 7d.

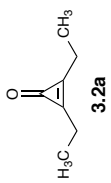
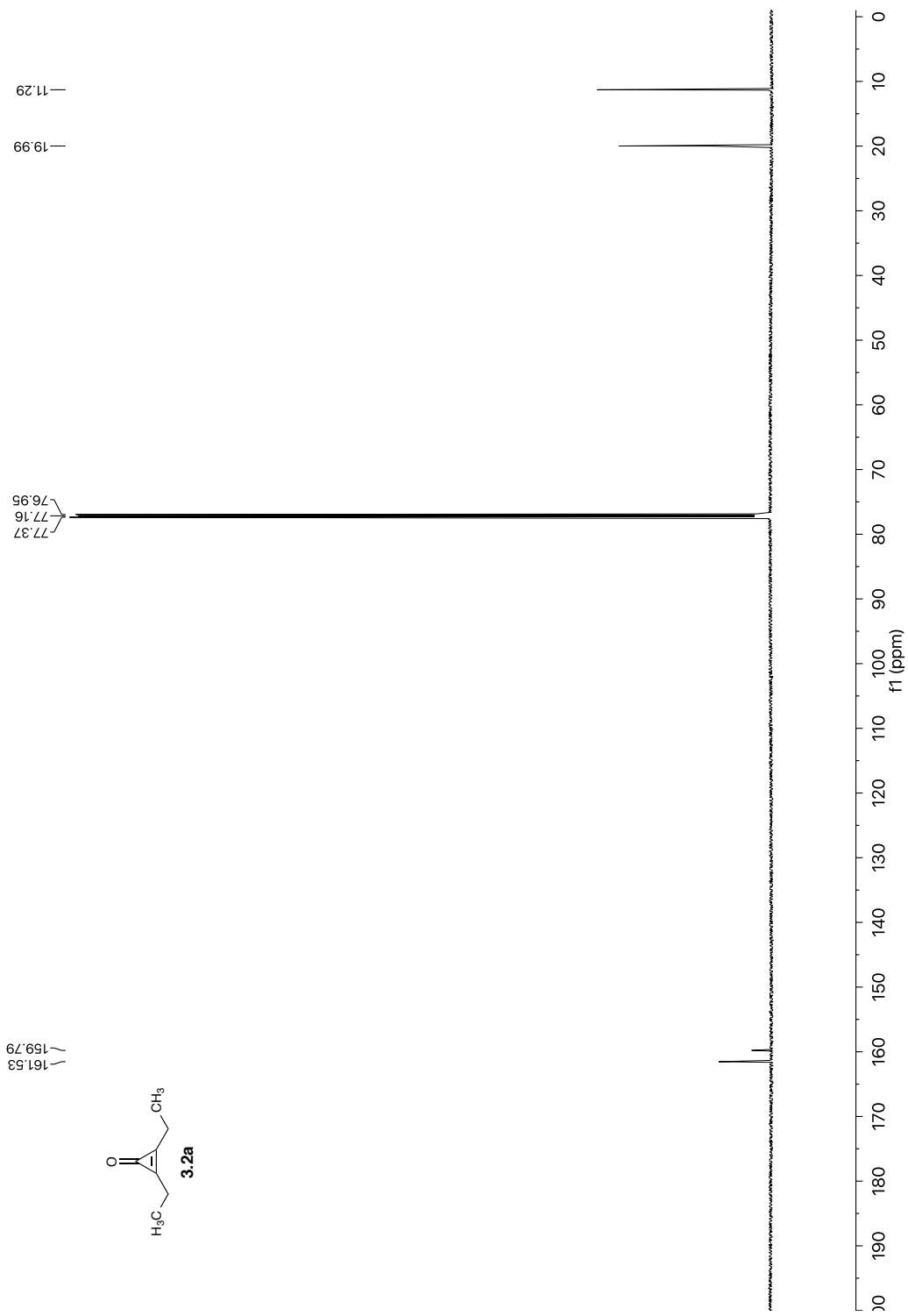
\*Allylic protons exchanged with deuterium.

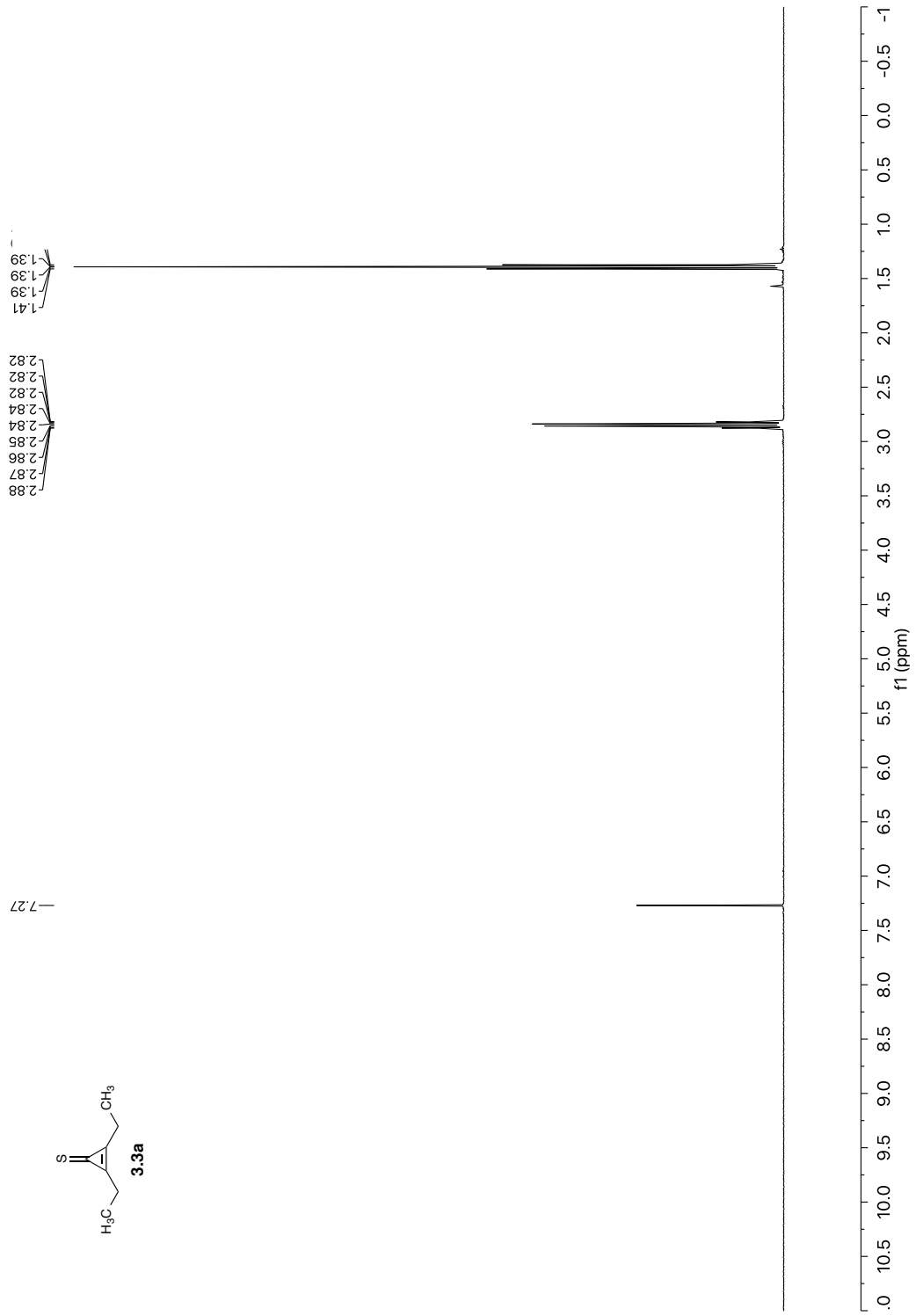


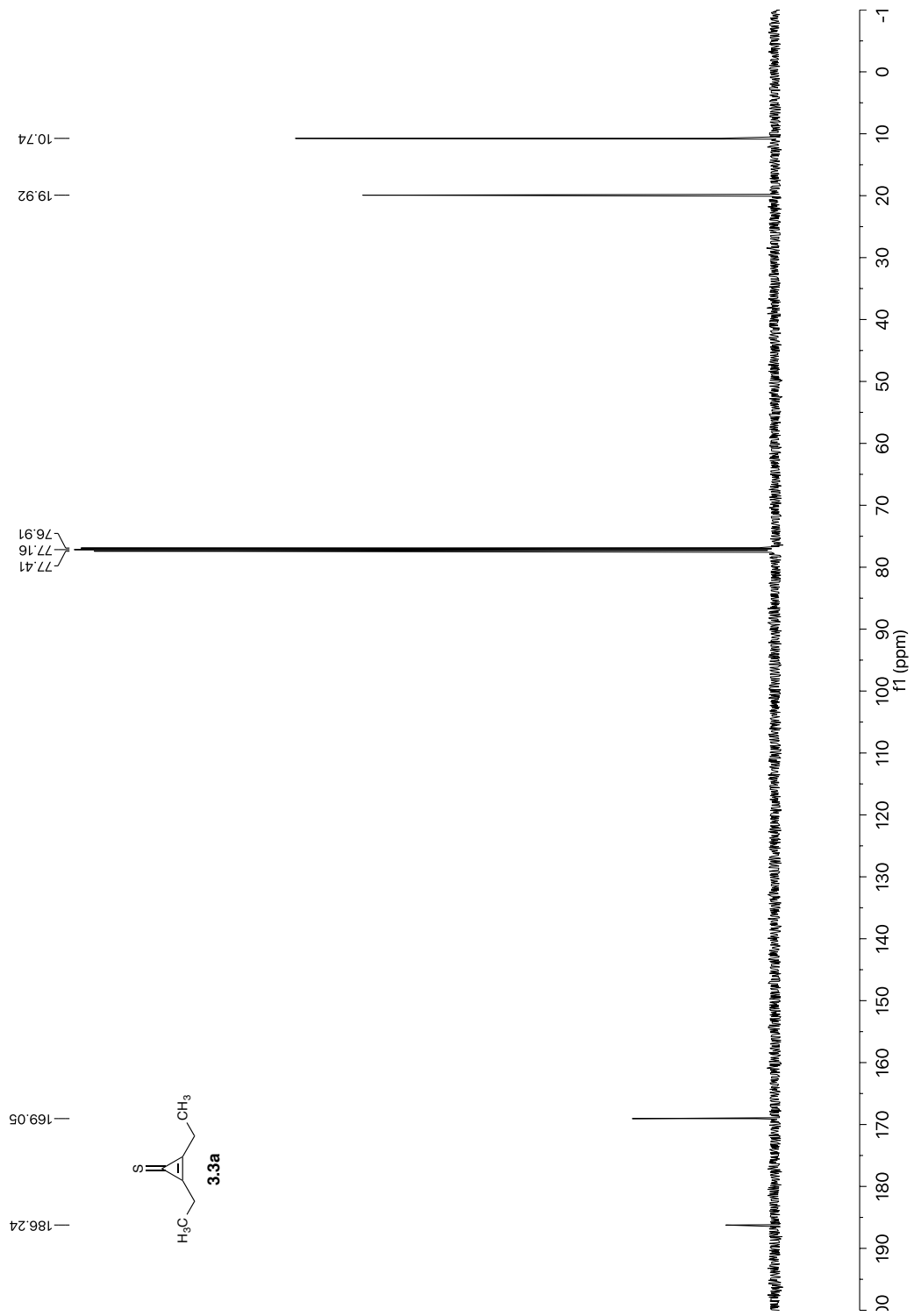


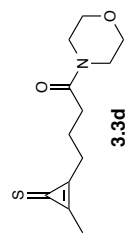
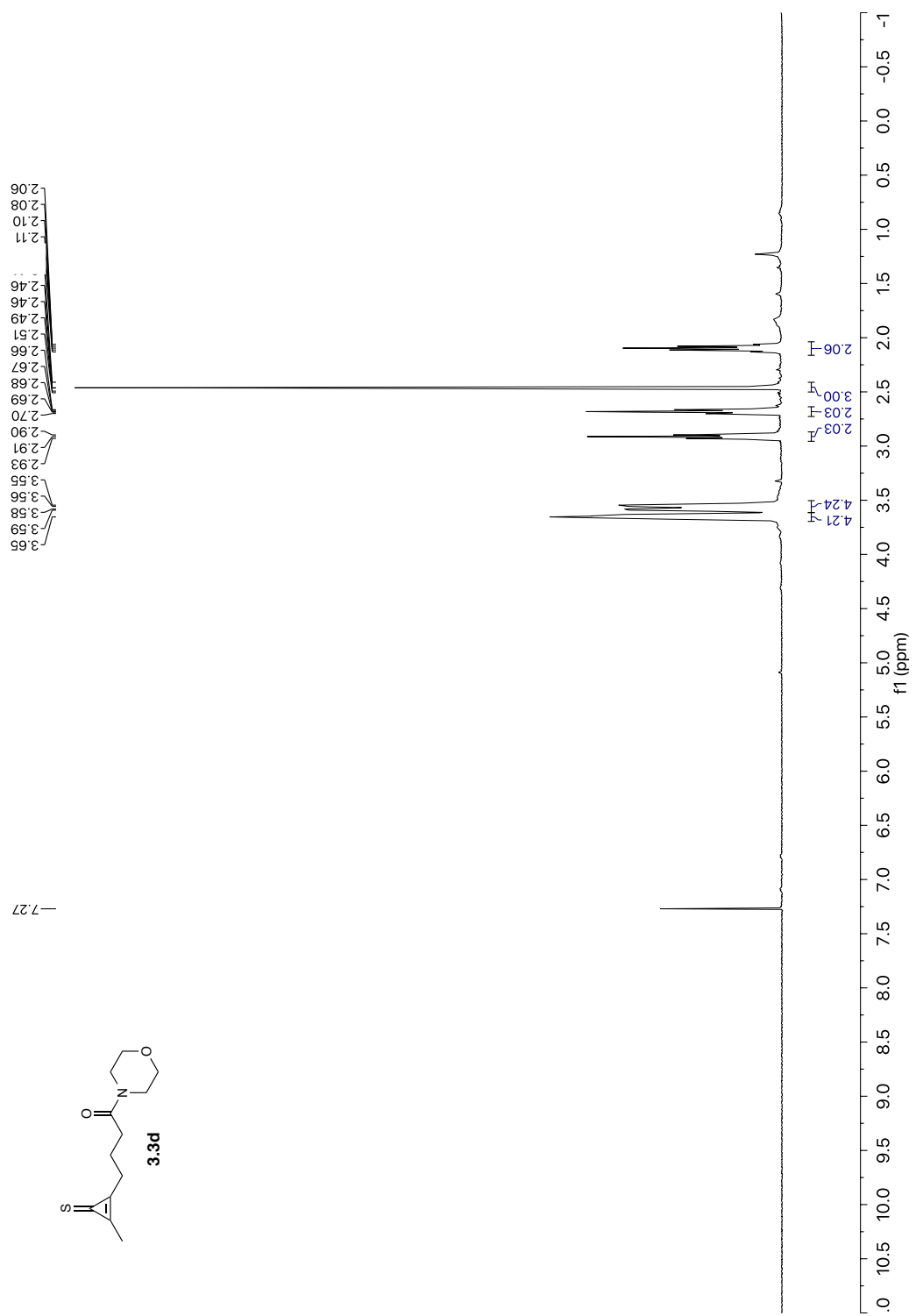


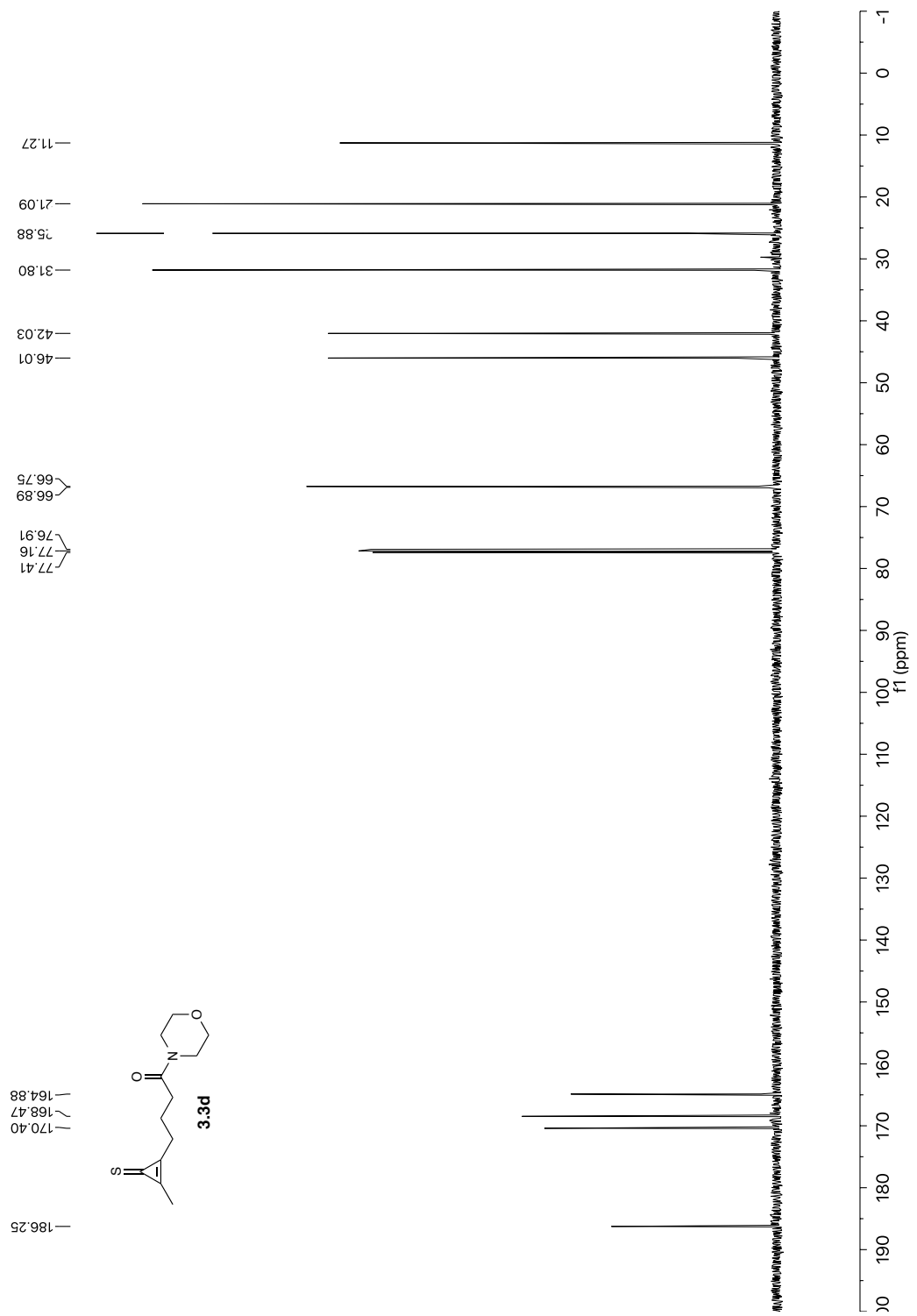


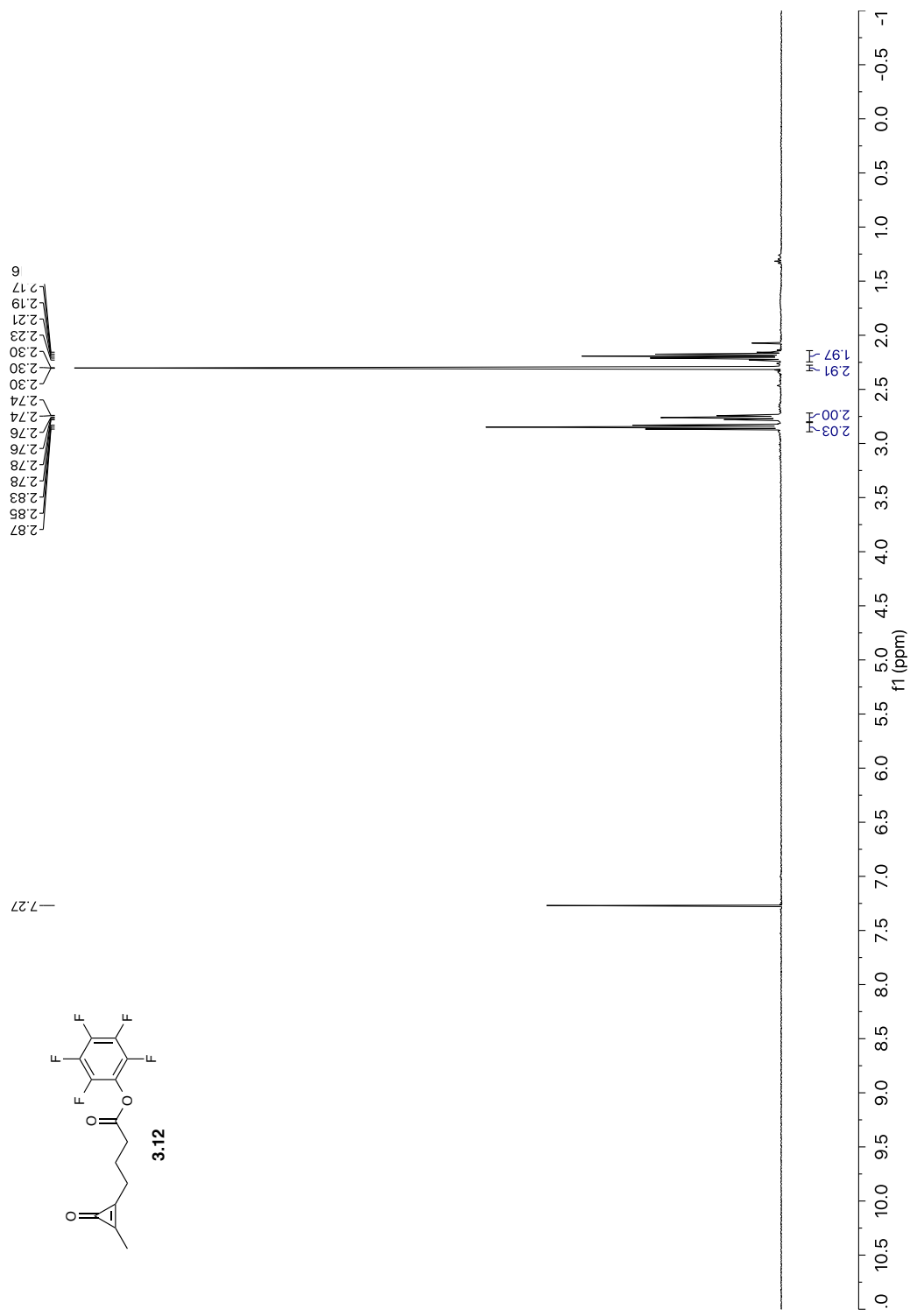


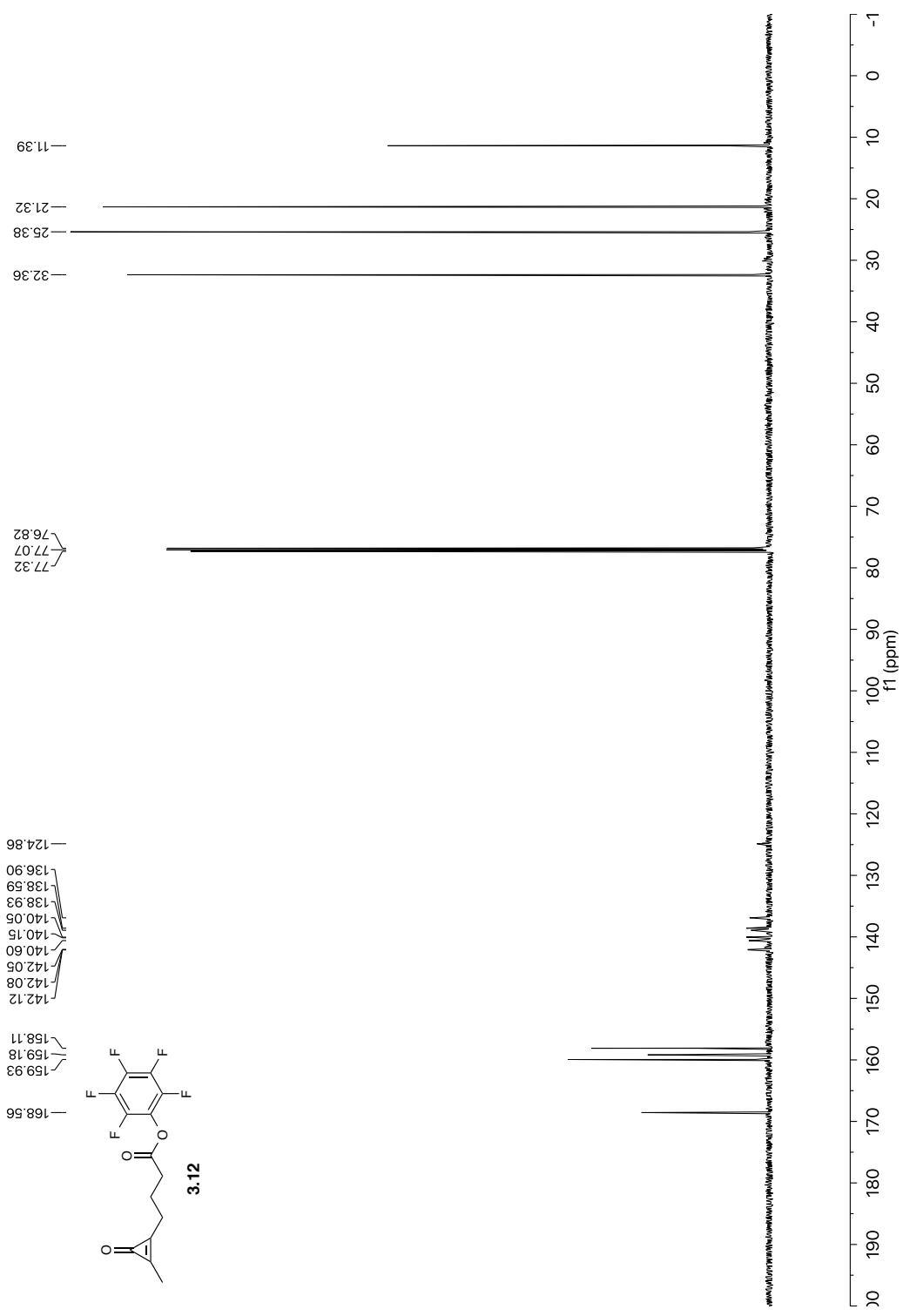




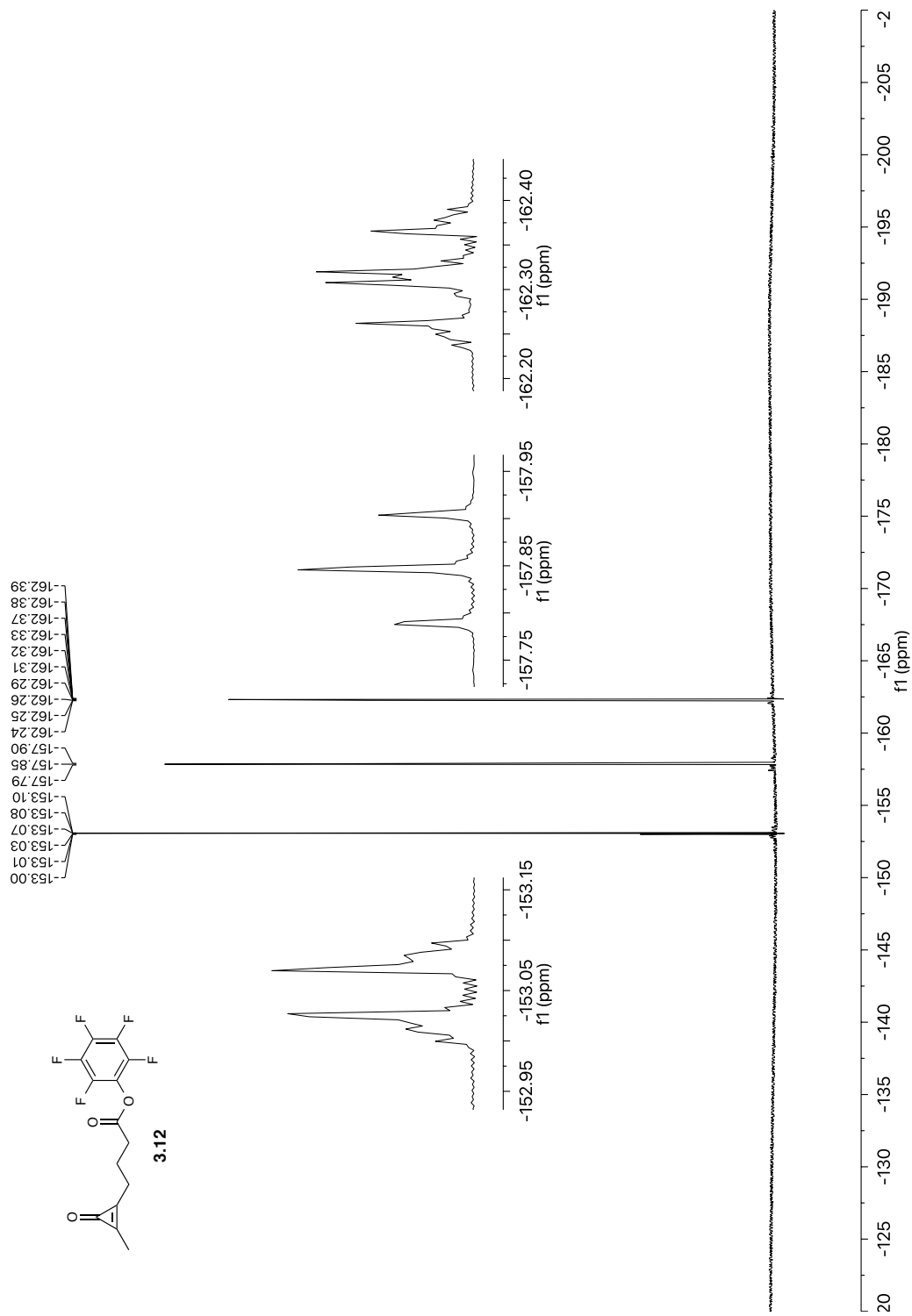


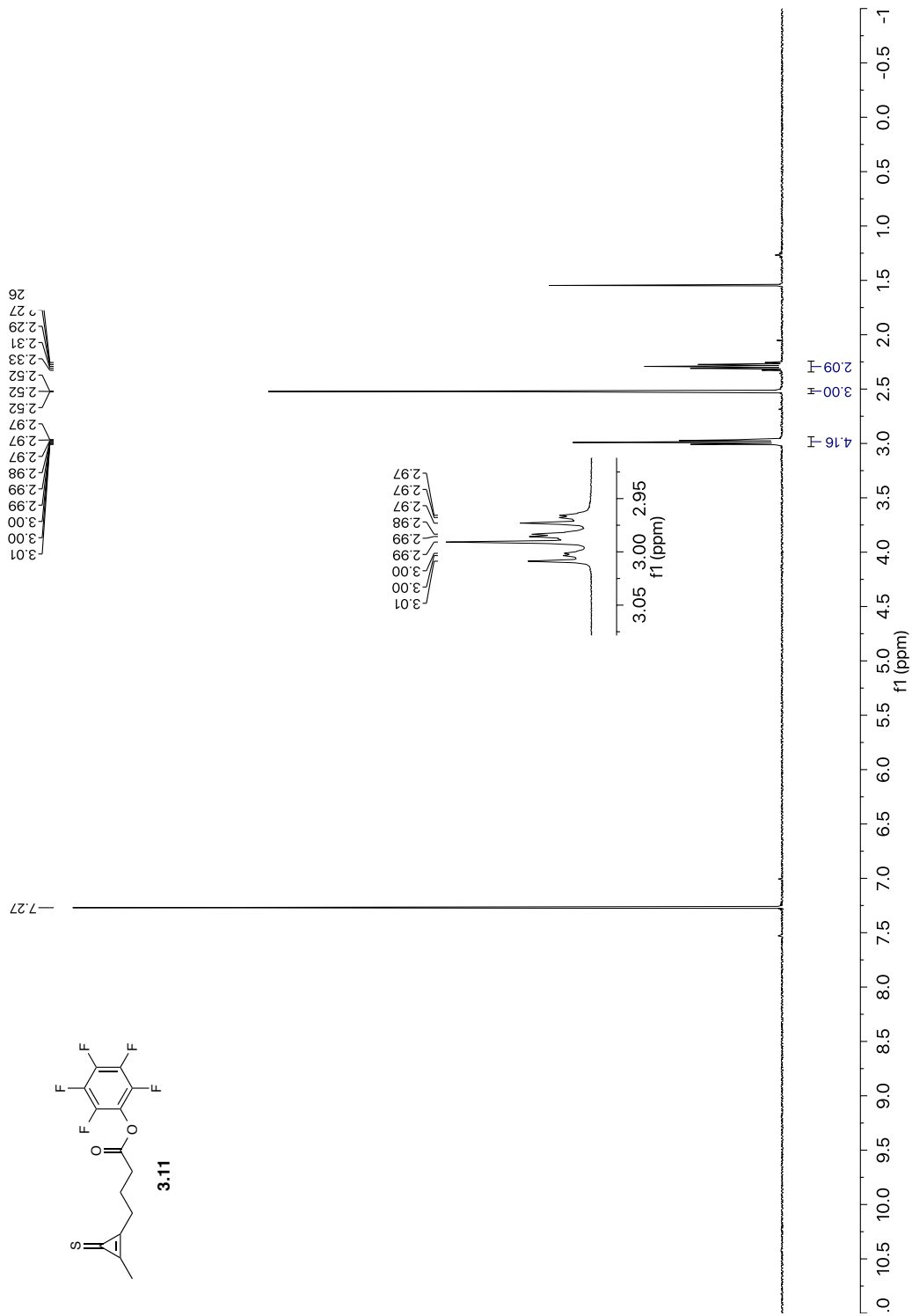


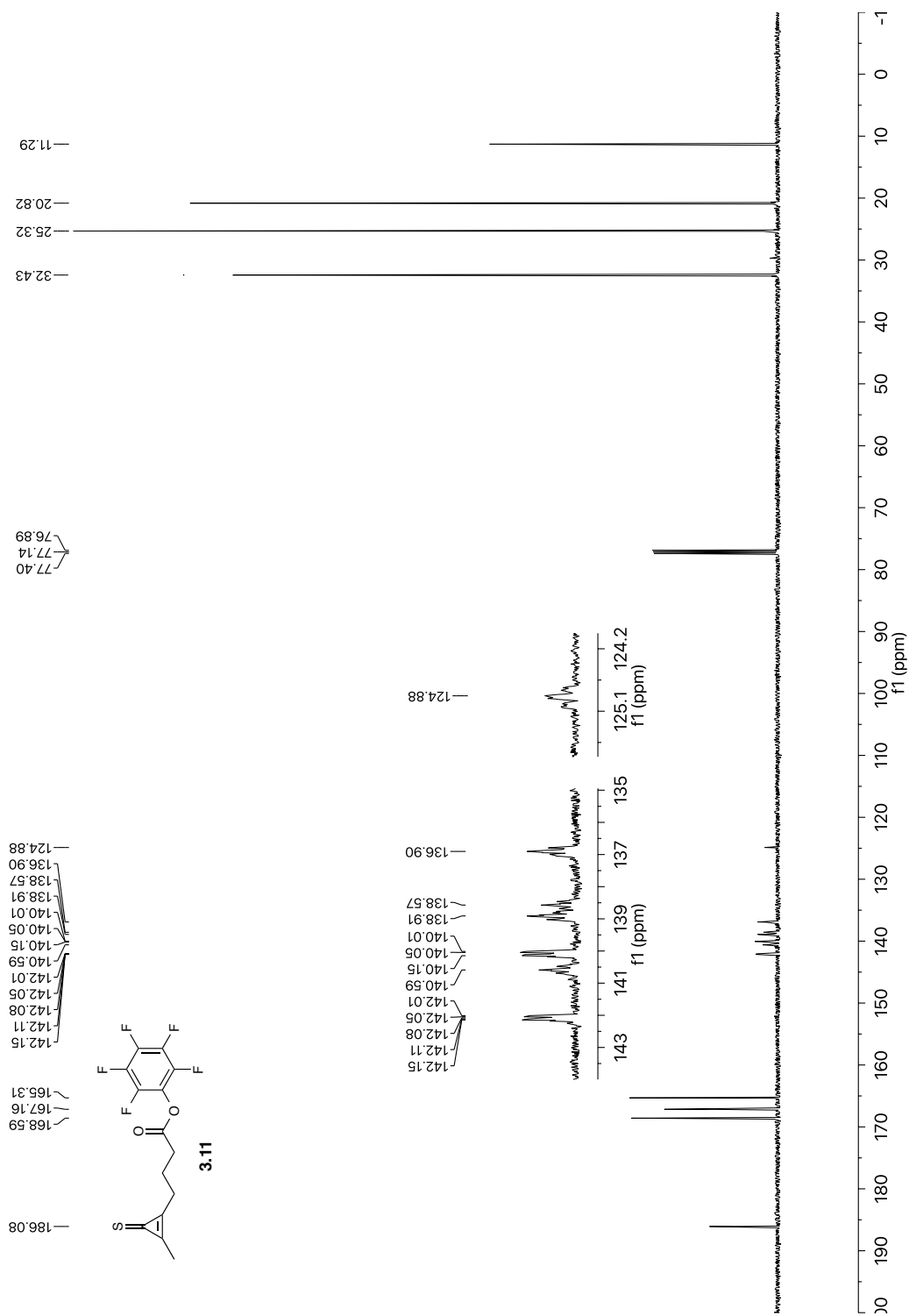


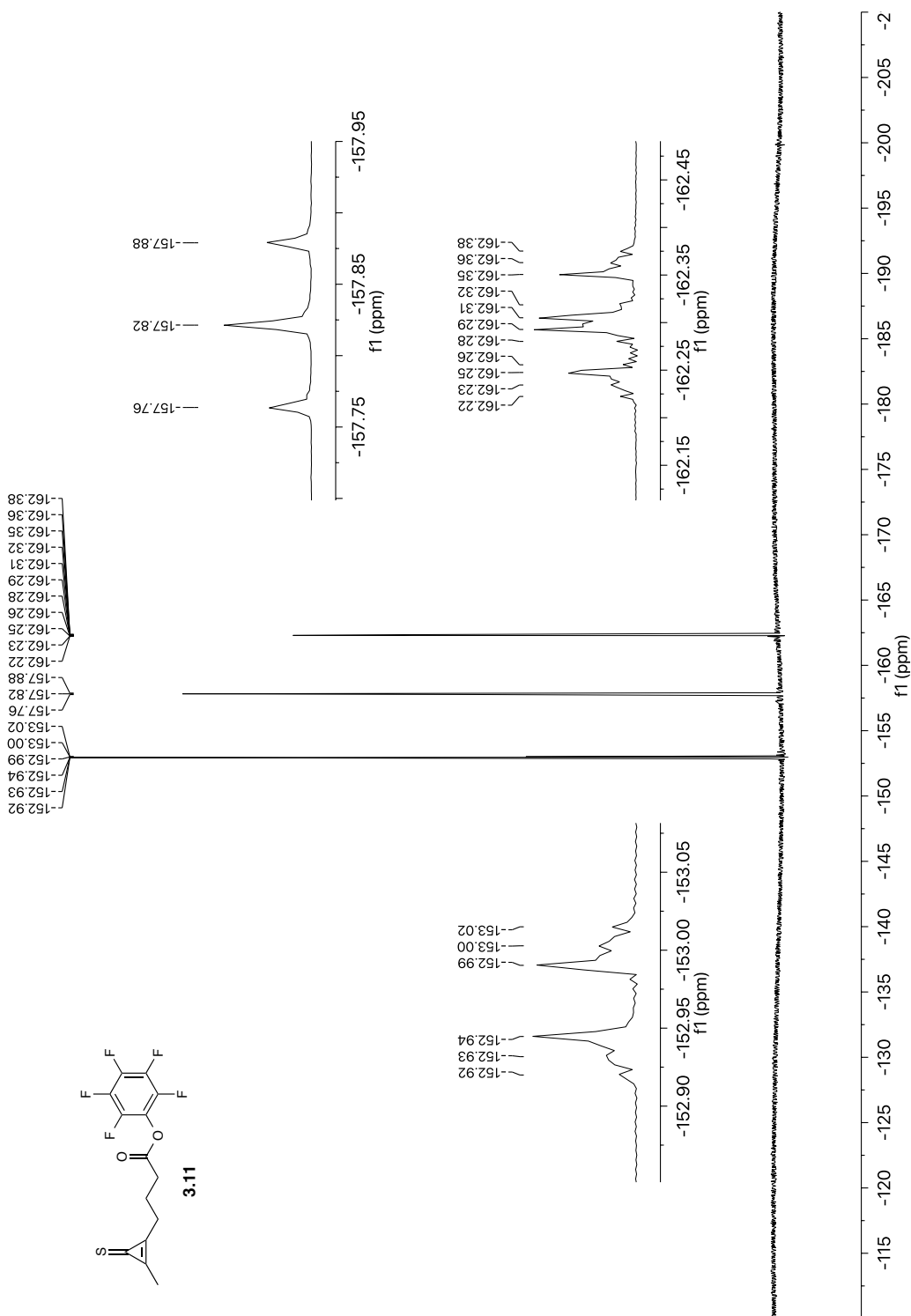
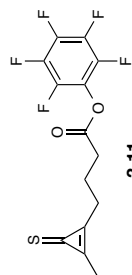






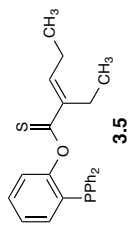












15.31  
16.54

